Lessons in Particle Physics

Luis Anchordoqui and Francis Halzen

University of Wisconsin

Contents

4

Acknowledgments

Chapter 1

General Principles

1.1   Particle Zoo

High energy physics seeks to understand, at the deepest level, the structure of matter and the forces by which it interacts. In the past half-century colossal strides were made in bringing Quantum Field Theory (QFT) to bear upon a wide variety of phenomena. The Large Hadron Collider (LHC) promises to take the next leap in this direction. Counter-circulating proton beams into head-on collisions at a center-of-mass energy $\sqrt{s} = 14$ TeV, the LHC will probe deeply into the sub-fermi distances, opening a new territory where groundbreaking discoveries are expected. In this spirit then, it seems opportune to review our present understanding of particle interactions.

Today, the accepted model for elementary particle physics views quarks and leptons as the basic constituents of ordinary matter. These particles interact via four known basic forces – gravitational, electromagnetic, strong, and weak – that can be characterized on the basis of the following four criteria: the types of particles that experience the force, the relative strength of the force, the range over which the force is effective, and the nature of the particles that mediate the force. The electromagnetic force is carried by the photon, the strong force is mediated by gluons, the $W^{\pm}$ and Z^0 bosons transmit the weak force, and the quantum of the gravitational force is called the graviton. A comparison of the (approximate) relative force strengths is given in Table 1.1. Though gravity is the most obvious force in daily life, on

Table 1.1: *Relative strength of the four forces for two protons inside a nucleus.*

Type	Relative Strength	Field Particle
Strong	1	gluons
Electromagnetic	10^{-2}	photon
Weak	10^{-6}	$W^{\pm}\ Z^0$
Gravitational	10^{-38}	graviton

Table 1.2: *Quark quantum numbers: charge Q, baryon number B, strangeness S, charm c, "beauty" or bottomness b, and "truth" or topness t.*

name	symbol	Q	B	S	c	b	t
up	u	$\frac{2}{3}$	$\frac{1}{3}$	0	0	0	0
down	d	$-\frac{1}{3}$	$\frac{1}{3}$	0	0	0	0
strange	s	$-\frac{1}{3}$	$\frac{1}{3}$	-1	0	0	0
charm	c	$\frac{2}{3}$	$\frac{1}{3}$	0	1	0	0
bottom	b	$-\frac{1}{3}$	$\frac{1}{3}$	0	0	-1	0
top	t	$-\frac{1}{3}$	$\frac{1}{3}$	0	0	0	1

a nuclear scale it is the weakest of the four forces and its effect at the particle level can nearly always be ignored.

The quarks are fractionally charged spin-$\frac{1}{2}$ strongly interacting objects which are known to form the composites collectively called hadrons:

$$\begin{cases} q\bar{q} \text{ (quark + antiquark) mesons} & \text{integral spin} \rightarrow \text{Bose statistics} \\ qqq \text{ (three quarks) baryons} & \text{half-integral spin} \rightarrow \text{Fermi statistics} \end{cases}.$$

There are six different types of quarks, known as flavors: up (symbol: u), down (d), strange (s), charm (c), bottom (b), and top (t); their properties are given in Table 1.2. (Antiquarks have opposite signs of electric charge, baryon number, strangeness, charm, bottomness, and topness.)

Quarks are fermions with spin-$\frac{1}{2}$ and therefore should obey the exclusion principle. Yet for three particular baryons ($\Delta^{++} = uuu$, $\Delta^{-} = ddd$, and $\Omega^{-} = sss$), all three quarks would have the same quantum numbers, and at least two quarks have their spin in the same direction because there are only

two choices, spin up ($\uparrow$) or spin down ($\downarrow$). This would seem to violate the exclusion principle!

Not long after the quark theory was proposed, it was suggested that quarks possess another "charge" which enables them to interact strongly with one another. This "charge" is a three-fold degree of freedom which has come to be known as color,[1] and so the field theory has taken on the name of quantum chromodynamics, or QCD. Each quark flavor can have three colors usually designated red, green, and blue. The antiquarks are colored antired, antigreen, and antiblue. Baryons are made up of three quarks, one with each color. Mesons consist of a quark-antiquark pair of a particular color and its anticolor. Both baryons and mesons are thus colorless or white. Because the color is different for each quark, it serves to distinguish them and allows the exclusion principle to hold. Even though quark color was originally an *ad hoc* idea, it soon became the central feature of the theory determining the force binding quarks together in a hadron.

One may wonder what would happen if we try to see a single quark with color by reaching deep inside a hadron. Quarks are so tightly bound to other quarks that extracting one would require a tremendous amount of energy, so much that it would be sufficient to create more quarks. Indeed, such experiments are done at modern particle colliders and all we get is not an isolated quark, but more hadrons (quark-antiquark pairs or triplets). This property of quarks, that they are always bound in groups that are colorless, is called confinement. Moreover, the color force has the interesting property that, as two quarks approach each other very closely (or equivalently have high energy), the force between them becomes small. This aspect is referred to as asymptotic freedom.[2] When probed at small distances compared to the size of a hadron (i.e., about 1 fm $= 10^{-15}$ m) the "bare" masses of the quarks are: $m_u = 1.5 - 3.3$ MeV, $m_d = 3.5 - 6.0$ MeV, $m_s = 104^{+26}_{-34}$ MeV, $m_c = 1.27^{+0.07}_{-0.11}$ GeV, $m_b = 4.20^{+0.17}_{-0.07}$ GeV and $m_t = 171.2 \pm 2.1$ GeV.[3]

---

[1] H. Fritzsch, M. Gell-Mann and H. Leutwyler, Phys. Lett. B **47**, 365 (1973).

[2] D. J. Gross and F. Wilczek, Phys. Rev. Lett. **30**, 1343 (1973); H. D. Politzer, Phys. Rev. Lett. **30**, 1346 (1973).

[3] We work in natural units, where $\hbar$ is one unit of action and c is one unit of velocity. This implies that [length] = [time] = [energy]$^{-1}$ = [mass]$^{-1}$. Masses are as quoted in C. Amsler *et al.* [Particle Data Group], Phys. Lett. B **667**, 1 (2008).

However, the effective quark masses in composite hadrons are significantly larger; namely, 0.3 GeV, 0.3 GeV, 0.5 GeV, 1.5 GeV and 4.9 GeV, for u, d, s, c, and b; respectively. The lightest flavors are generally stable and are very common in the universe as they are the constituents of protons (uud) and neutrons (ddu). More massive quarks are unstable and rapidly decay; these can only be produced as quark-pairs under high energy conditions, such as in particle accelerators and in cosmic rays.

Leptons are fractionally spin-$\frac{1}{2}$ particles which do not strongly interact. They come in three flavors: electron (e), muon (μ), and tau (τ), with masses $m_e = 0.510998910 \pm 0.0000000013$ MeV, $m_\mu = 105.658367 \pm 0.000004$ MeV, and $m_\tau = 1776.84 \pm 0.17$ MeV. Each flavor has an associated neutrino: ν_e, ν_μ, and ν_τ. It was Fermi who first proposed a kinematic search for the neutrino mass from the hard part of the spectra in Tritium beta decay. In the presence of non-vanishing leptonic mixing, this search sets an upper limit on the absolute mass of any of the neutrinos, $m_\nu < 2.2$ eV at 95% CL. However, at present, WMAP data provides the nominally strongest constraint on the sum of the neutrino masses, $\sum m_\nu < 0.67$ eV at 95%CL.[4]

One important aspect of on-going research is the attempt to find a unified basis for the different forces. For example, the weak and electromagnetic forces are indeed two different manifestations of a single, more fundamental *electroweak* interaction.[5] The electroweak theory has had many notable successes, culminating in the discovery of the predicted $W^\pm$ and Z^0 bosons ($m_W = 80.403 \pm 0.029$ GeV and $m_Z = 91.1876 \pm 0.0021$ GeV). However, the favored electroweak symmetry breaking mechanism requires the existance of a scalar *Higgs boson*, as yet unseen.

Nowadays physical phenomena can be discussed concisely and elegantly in terms of quantum field theories. So far as we know, the veritable "zoo" of subatomic particles is composed of composites of quarks and leptons that interact by exchanging force carriers. To understand the subtleties of our present-day view, we need to begin with the ideas leading up to its formulation. In these lectures, we will provide an elementary introduction to quan-

---

[4] E. Komatsu *et al.* [WMAP Collaboration], Astrophys. J. Suppl. **180**, 330 (2009).

[5] S. L. Glashow, Nucl. Phys. **22**, 579 (1961); S. Weinberg, Phys. Rev. Lett. **19**, 1264 (1967); A. Salam, *Elementary Particle Physics,* ed. N. Svartholm (Nobel Symposium No. 8, Almqvist and Wiksell, Stockholm, 1968) p.367.

tum electrodynamics (QED), quantum chromodynamics, electroweak theory, and physics of the Higgs boson. The course will cover the major theoretical predictions and experimental tests, and is suitable as a starting point for beginning theory students, a review for more advanced theory students, and as an introduction to the field for experimentalists. These lectures will build upon the content of many excellent textbooks.[6]

1.2 Canonical Quantization

The state of a physical system consisting of a collection of N discrete point particles can be specified by a set of $3N$ generalized coordinates q_i. The action of such a physical system, $S = \int L(q_i, \dot{q}_i) \, dt$, is an integral of the so-called Lagrangian function from which the system's behavior can be determined by the principle of least action. (We adopt the standard notation $\dot{q}_i \equiv \partial_t q_i$.) In a local field theory the Lagrangian can be written as the spatial integral of a Lagrangian density, $S = \int \mathscr{L}(\phi, \partial_\mu \phi) \, d^4x$, where the field ϕ itself is a function of the continuous parameters x^μ. Minimization condition on δS yields

$$
\begin{aligned}
0 &= \delta S \\
&= \int d^4x \left[\partial_\phi \mathscr{L} \ \delta\phi + \partial_{\partial_\mu \phi} \mathscr{L} \ \delta(\partial_\mu \phi) \right].
\end{aligned} \tag{1.2.1}
$$

The second term in the integrand can be integrated by parts,

$$
0 = \int d^4x [\partial_\phi \mathscr{L} \ \delta\phi - \partial_\mu (\partial_{\partial_\mu \phi} \mathscr{L}) \ \delta\phi + \partial_\mu (\partial_{\partial_\mu \phi} \mathscr{L} \ \delta\phi)], \tag{1.2.2}
$$

with $\delta(\partial_\mu \phi) = \partial_\mu(\phi + \delta\phi) - \partial_\mu \phi = \partial_\mu(\delta\phi)$. Using Gauss theorem, the last term in Eq. (1.2.2) can be written as a surface integral over the boundary of the four dimensional spacetime region of integration. As in the particle

---

[6]F. Halzen and A. D. Martin, *Quarks and Leptons: An Introductory Course in Modern Particle Physics*, (Wiley, New York, 1984); J. D. Bjorken and S. D. Drell, *Relativistic Quantum Fields*, (McGraw-Hill, New York, 1965); C. Quigg, *Gauge Theories of the Strong, Weak and Electromagnetic Interactions*, Front. Phys. **56**, 1 (1983); J. L. Rosner, *An Introduction to Standard Model Physics*, in The Santa Fe TASI-87 (eds. R. Slansky and G. West, World Scientific, Singapore, 1988), p.3.

mechanics case, the initial and final configurations are assumed given, and so $\delta\phi$ is zero at the temporal beginning and end of this region. Hereafter, we restrict our consideration to deformations $\delta\phi$ that also vanish on the spatial boundary of the integration region. Hence, for arbitrary variations $\delta\phi$, Eq. (1.2.2) leads to the Euler-Lagrange equation of motion for a field:

$$\partial_\mu(\partial_{\partial_\mu\phi}\mathscr{L}) - \partial_\phi\mathscr{L} = 0 \,. \tag{1.2.3}$$

For example, one can obtain Maxwell equations,

$$\epsilon^{\mu\nu\rho\sigma}\partial_\nu F_{\rho\sigma} = 0, \qquad \partial_\mu F^{\mu\nu} = e\,j^\nu \tag{1.2.4}$$

by substituting the Lagrangian

$$\mathscr{L}_{\text{Maxwell}} = -\frac{1}{4}\,F_{\mu\nu}F^{\mu\nu} + eA_\mu j^\mu \tag{1.2.5}$$

into (1.2.3), where $A^\mu = (\phi, \vec{A})$ is the four-vector potential (related to to the electric and magnetic fields by $\vec{E} = -\partial_t\vec{A} - \vec{\nabla}\phi$ and $\vec{B} = \vec{\nabla}\times\vec{A}$, respectively), $F^{\mu\nu} = \partial^\mu A^\nu - \partial^\nu A^\mu$ is the antisymmetric field strength tensor, and we have extracted the electron charge $e \equiv -|e|$ from the four-vector current density j^μ.[7] In the interaction term, the four-current should be understood as an abbreviation of many terms expressing the electric currents of other charged fields in terms of their variables; the four current is not itself a fundamental field.

The canonical momentum for the particle system is $p_i = \partial_{\dot{q}_i}L$ and the corresponding quantity for a field, $\pi(x) = \partial_{\dot\phi}\mathscr{L}$, is called the momentum density conjugate to $\phi(x)$. The Hamiltonian is defined by

$$H = \sum_{i=1}^{3N} p_i\,\dot{q}_i - L(q_i, \dot{q}_i) \tag{1.2.6}$$

and so we can write

$$H = \int d^3x\,\mathscr{H}(x)\,, \tag{1.2.7}$$

---

[7]We adopt Heaviside-Lorentz rationalized units, in which the factors of 4π appear in Coulomb's law and the fine structure constant ($\alpha = \frac{e^2}{4\pi} \approx \frac{1}{137}$) rather than in Maxwell's equations.

where

$$\mathscr{H}(x) = \pi(x)\ \dot{\phi}(x) - \mathscr{L}(\phi, \partial_\mu \phi)\,. \qquad (1.2.8)$$

The Heisenberg commutation relations $[p_i, q_j] = -i\delta_{ij}$, $[p_i, p_j] = [q_i, q_j] = 0$ have as their field counterparts

$$[\pi(\vec{x}, t), \phi(\vec{y}, t)] = -i\delta^{(3)}(\vec{x} - \vec{y})\,, \qquad (1.2.9)$$

with all other pairs of operators commuting. If there are various classical fields to be quantized, e.g. $\phi(x)$ and $\phi^\star(x)$, the equation $\partial_\mu[\partial_{\partial_\mu \phi^\star} \mathscr{L}] - \partial_{\phi^\star} \mathscr{L} = 0$ will too be satisfied, and the field $\phi^\star$ will have its canonically conjugate momentum, $\pi^\star = \partial_{\dot{\phi}^\star} \mathscr{L}$. The Hamiltonian density will be

$$\mathscr{H} = \pi(x)\ \dot{\phi} + \pi^\star(x)\ \dot{\phi}^\star - \mathscr{L}(\phi, \phi^\star, \partial_\mu \phi, \partial_\mu \phi^\star) \qquad (1.2.10)$$

and the additional commutation relation

$$[\pi^\star(\vec{x}, t), \phi^\star(\vec{y}, t)] = -i\delta^{(3)}(\vec{x} - \vec{y}) \qquad (1.2.11)$$

will be assumed to hold. All commutators involving starred with unstarred fields vanish at equal times, since these are independent fields. It is noteworthy that the commutation relations are only defined at equal times. Once these are given, their values at different times are determined by the equations of motion. In the commutation relations, however, the times were set equal but not otherwise specified, and therefore a change in the origin of time has no physical consequences.

1.3 Lorentz Group

One paramount prerequisite to be imposed on a theory describing the behavior of particles at high energies is that it be consistent with the special theory of relativity.[8] This can be achieved by demanding covariance of the equations under Lorentz-Poincaré transformations. A Lorentz-Poincaré change of referencial is a real, linear transformation of the coordinates conserving the norm of the intervals between different points of spacetime. For such

---

[8]A. Einstein, Annalen Phys. **17**, 891 (1905) [Annalen Phys. **14**, 194 (2005)].

transformation, the new spacetime coordinates x'^μ are obtained from the old ones x^μ according to $x'^\mu = \Lambda^\mu{}_\nu\, x^\nu + a^\mu$, satisfying $x'_\mu x'^\mu = x_\mu x^\mu$. Hereafter, we treat the translation of spacetime axes separately, and give the name of Lorentz transformation to the homogenous transformations with $a^\mu = 0$. The condition of reality leads to $(\Lambda_{\mu\nu})^* = \Lambda_{\mu\nu}$ and invariance of the norm yields

$$g_{\mu\nu}\, x^\mu\, x^\nu = g_{\mu\nu}\, x'^\mu\, x'^\nu = g_{\mu\nu}\Lambda^\mu{}_\alpha\, \Lambda^\nu{}_\beta\, x^\alpha\, x^\beta\, , \qquad (1.3.12)$$

i.e.,

$$g_{\mu\nu}\, \Lambda^\mu{}_\alpha\, \Lambda^\nu{}_\beta = g_{\alpha\beta}\, . \qquad (1.3.13)$$

where $g_{\mu\nu} \equiv \mathrm{diag}(1, -1, -1, -1)$ is the metric tensor. In addition, there is a transformation law for the field $\phi(x)$, so that transformed fields $\phi'(x')$ satisfy the same equations in the new spacetime coordinates. The quantized theory will then also be Lorentz invariant if (as indeed is the case) the commutation relations transform covariantly.

Actually, in QFT, it is possible to discuss Lorentz invariance in a way divorced from the specific form of the equations of motion. To this end, consider a system to be fixed and some apparatus that serves to prepare a physical state $|\psi_A\rangle$. Consider now another, similar, apparatus related to the first one by a Lorentz transformation, which prepares the physical state $|\psi_{A'}\rangle$. Apparatus A may, for example, be a black box that emits electrons through an aperture; aparatus A' will be the same source, rotated through an angle θ about some axis and moving with some fixed velocity relative to the apparatus A. Consider, similarly, a measuring apparatus M, which is being used to make measurements on the state $|\psi_A\rangle$ and another measuring apparatus M', which differs from M only in that it is shifted relative to M by the same Lorentz transformation that connects A' with A. The statement of relativistic invariance is that the measurements made by M on the state $|\psi_A\rangle$ yield the same results as those made by M' on the state $|\psi_{A'}\rangle$.

To obtain the formal consequences of this statement, we recall that in a quantum mechanical measurement we generally determine the probability that the physical system is in some state $|\phi\rangle$; e.g., we may ask for the probability that the electrons emitted have momentum p. The probability of that happening will be $|\langle\phi_p|\psi_A\rangle|^2$, where $|\phi_p\rangle$ describes the state in which just this particular momentum is found for the electron. For the transform source and measuring apparatus, the corresponding probability is

$|\langle\phi_{p'}|\psi_{A'}\rangle|^2$, where $|\phi_{p'}\rangle$ is the state for which the electron has the momentum p' connected to p by the same Lorentz transformation that connects A and A'. Because the vector space of states contains all possible physical states, $|\psi_A\rangle$ and $|\psi_{A'}\rangle$ must be related by some transformation $U(\Lambda)$ that depends on the Lorentz transformation Λ. Because the measuring apparatus M and M' are connected by the same Lorentz transformation, we must have both $|\psi_{A'}\rangle = U(\Lambda)|\psi_A\rangle$ and $|\phi_{p'}\rangle = U(\Lambda)|\phi_p\rangle$. The invariance requirement implies that $|\langle\phi_{p'}|\psi_{A'}\rangle|^2 = |\langle\phi_p|\psi_A\rangle|^2$. From this we can deduce that $U(\Lambda)$ must be an unitary (or antiunitary) transformation. Time-reversal invariance is the only symmetry requiring an antiunitary operator,[9] and so here we take U to be unitary.

Now, consider the measurement of the expectation value of the scalar field $\phi(x)$. For a state $|\psi_A\rangle$, this will be $\langle\psi_A|\phi(x)|\psi_A\rangle$, and for the state $\psi_{A'}$ it will be the measurement of the expectation value of the field at the transformed point, i.e., $\langle\psi_{A'}|\phi(x')|\psi_{A'}\rangle$. We thus have

$$\langle\psi_A|\phi(x)|\psi_A\rangle = \langle\psi_A U^\dagger(\Lambda)|\phi(x')|U(\Lambda)\psi_A\rangle. \tag{1.3.14}$$

Therefore the scalar field in a Lorentz invariant theory would transform according to

$$\phi(x') = U(\Lambda)\phi(x)U^\dagger(\Lambda) \tag{1.3.15}$$

with $x' = \Lambda x$.

If $\Lambda^{00} > 0$, the transformation is called orthochronous because it conserves the sense of timelike vectors. Additionally, if $\det(\Lambda^\mu{}_\nu) = 1$, the transformation also conserves the sense of Cartesian systems in ordinary space. The ensemble of these transformations forms a group dubbed proper Lorentz group $SO(3,1)$. The proper Lorentz group is a Lie group. The crucial property here is that all transformations can be expressed as a succession of infinitesimal transformations

$$x^\mu \to x'^\mu = \Lambda^\mu{}_\nu\, x^\nu = (\delta^\mu{}_\nu + \omega^\mu{}_\nu)x^\nu\,, \tag{1.3.16}$$

(arbitrarily close to the identity), where the quantities $\omega^\mu{}_\nu$ are infinitesimals and thus we only keep terms linear in $\omega^\mu{}_\nu$.

---

[9]see, for example, S. Gasiorowicz, *Elementary Particle Physics*, (John Wiley & Sons, Inc., New York, 1966) p.26.

For any continuous group, the transformations that lie infinitesimally close to the identity define a vector space, called the *Lie algebra* of the group. The basis vectors for this vector space are called generators of the Lie algebra. For example, each rotation can be labeled by a set of continuosly varying parameters $(\theta_1, \theta_2, \theta_3)$ that can be regarded as the component of a vector directed along the axis of rotation with magnitude given by the angle of rotation; the generators of the Lie algebra are the angular momentum J^k, which satisfy the commutation relations $[J_i, J_j] = i\epsilon_{ijk}J_k$, where $\epsilon_{ijk} = +1(-1)$ if ijk are a cyclic (anticyclic) permutation of 1 2 3 and $\epsilon_{ijk} = 0$ otherwise. In the lowest-dimension non-trivial representation of the rotation group, the generators may be written $J_i = \frac{1}{2}\sigma_i$, where σ_i are the Pauli matrices[10]

$$\sigma_1 = \begin{pmatrix} 0 & 1 \\ 1 & 0 \end{pmatrix}, \quad \sigma_2 = \begin{pmatrix} 0 & -i \\ i & 0 \end{pmatrix}, \quad \sigma_3 = \begin{pmatrix} 1 & 0 \\ 0 & -1 \end{pmatrix}. \qquad (1.3.17)$$

The basis (or set of base states) for this representation is conventionally chosen to be the eigenvectors of σ_3, that is the column vectors $\binom{1}{0}$ and $\binom{0}{1}$, describing a spin-$\frac{1}{2}$ particle of spin projection up ($m = \frac{1}{2}$ or $\uparrow$) and spin projection down ($m = -\frac{1}{2}$ or $\downarrow$) along the 3-axis, respectively.

For an infinitesimal transformation, the condition (1.3.13) implies

$$g_{\mu\beta}\omega^\mu{}_\sigma + g_{\sigma\nu}\omega^\nu{}_\beta = 0 , \qquad (1.3.18)$$

i.e., the infinitesimals are real antisymmetric tensors, $\omega_{\mu\nu} + \omega_{\nu\mu} = 0$. Note that an antisymmetric 4×4 matrix has $4 \times 3/2 = 6$ independent components,

$$\omega_{\mu\nu} = \sum_{\alpha < \beta} \omega_{\alpha\beta} \left(\mathscr{M}^{\alpha\beta} \right)_{\mu\nu} , \qquad (1.3.19)$$

which define the 6 transformations of the proper Lorentz group: 3 rotations and 3 boosts. A 4-dimensional representation for the 6 $SO(3,1)$ generators is

$$(\mathscr{M}^{\alpha\beta})^\mu{}_\nu = i(g^{\mu\beta}\delta^\alpha{}_\nu - g^{\alpha\mu}\delta^\beta{}_\nu) . \qquad (1.3.20)$$

The following commutation relations result after a little algebra

$$[\mathscr{M}^{\mu\nu}, \mathscr{M}^{\rho\sigma}] = i(g^{\nu\rho}\mathscr{M}^{\mu\sigma} - g^{\mu\rho}\mathscr{M}^{\nu\sigma} - g^{\nu\sigma}\mathscr{M}^{\mu\rho} + g^{\mu\sigma}\mathscr{M}^{\nu\rho}) . \qquad (1.3.21)$$

---

[10] W. Pauli, Z. Phys. **36**, 336 (1926).

Any matrices that are to represent the Lorentz algebra must obey these same commutation rules.

Locally, we have a correspondence: $S0(3,1) \cong SU(2) \oplus SU(2)$. The generators J_i of rotations and K_i of Lorentz boosts can be expressed as

$$J_i = \tfrac{1}{2}\epsilon_{ijk}\mathcal{M}_{jk}, \qquad K_i = \mathcal{M}_{0i}, \tag{1.3.22}$$

and the linear combinations (which are neither hermitian nor antihermitian),

$$A_i = \frac{1}{2}(J_i + iK_i) \quad \text{and} \quad B_i = \frac{1}{2}(J_i - iK_i) \tag{1.3.23}$$

satisfy the $SU(2)$ commutation relations,

$$[A_i, A_j] = i\epsilon_{ijk}A_k, \quad [B_i, B_j] = i\epsilon_{ijk}B_k, \quad [A_i, B_j] = 0\,; \tag{1.3.24}$$

following from

$$[J_i, J_j] = i\epsilon_{ijk}J_k\,, \quad [J_i, K_j] = i\epsilon_{ijk}K_k\,, \quad [K_i, K_j] = -i\epsilon_{ijk}J_k\,. \tag{1.3.25}$$

Under parity $P(x^0 \mapsto x^0 \text{ and } \vec{x} \mapsto -\vec{x})$ we have

$$J_i \mapsto J_i \quad \text{and} \quad K_i \mapsto -K_i \Rightarrow A_i \leftrightarrow B_i\,. \tag{1.3.26}$$

If we now write $U(\Lambda) = e^{i\eta}$, where η is hermitian and reduces to zero for the identity transformation, for an infinitesimal transformation (1.3.15) becomes

$$\phi(x) + i[\eta, \phi(x)] + \cdots = \phi(x^\mu + \omega^\mu{}_\nu x^\nu) \ldots\,. \tag{1.3.27}$$

Expanding the right hand side in terms of ω, we obtain

$$
\begin{aligned}
i[\eta, \phi(x)] &\simeq \phi(x) + \omega^\mu{}_\nu x^\nu \partial_\mu \phi - \phi(x) \\
&\simeq \omega^\mu{}_\nu x^\nu \partial_\mu \phi \\
&\simeq \tfrac{1}{2}\omega^{\mu\nu}(x_\nu \partial_\mu - x_\mu \partial_\nu)\phi(x)\,,
\end{aligned}
\tag{1.3.28}
$$

where in the last line we have used the antisymmetry of $\omega^{\mu\nu}$. Now, identifying $\eta = -\tfrac{1}{2}\omega^{\mu\nu}\mathcal{M}_{\mu\nu}$, we obtain

$$i[\mathcal{M}_{\mu\nu}, \phi(x)] = (x_\mu \partial_\nu - x_\nu \partial_\mu)\phi(x) \equiv L_{\mu\nu}\,\phi(x)\,. \tag{1.3.29}$$

17

Note that for $\mu, \nu = 1, 2, 3$ the quantities $L_1 = L_{23}$, $L_2 = L_{13}$, and $L_3 = L_{12}$ are the differential operators representing the orbital angular momentum.

For a displacement, the analog of (1.3.15) is

$$\phi(x + a) = U(a)\phi(x)U^\dagger(a) \tag{1.3.30}$$

If we write $U(a) = e^{i\zeta}$, then for an infinitesimal a_μ (1.3.30) becomes

$$\phi(x) + a_\mu \partial^\mu \phi(x) \simeq \phi(x) + i[\zeta, \phi], \tag{1.3.31}$$

or

$$ia_\mu[P^\mu, \phi(x)] = i[\zeta, \phi(x)] \tag{1.3.32}$$

so that we can make the identification $\zeta = a_\mu P^\mu$ and write the unitary operator $U(a)$ for arbitrary displacements in the form

$$U(a) = e^{ia_\mu P^\mu}. \tag{1.3.33}$$

The Hamiltonian generates displacements in time, and the operator $\boldsymbol{P}$, which will be seen as the operator representing the momentum of the field, generates spatial displacements. A little computation leads to the commutation relations of the Lorentz-Poincaré algebra

$$[\mathcal{M}^{\mu\nu}, P^\sigma] = i[P^\mu g^{\nu\sigma} - P^\nu g^{\mu\sigma}] \tag{1.3.34}$$

and

$$[P^\mu, P^\nu] = 0. \tag{1.3.35}$$

In closing, we note there is a homeomorphism (not an isomorphism) $SO(3, 1) \cong SL(2, \mathbb{C})$. To see this, take a 4 vector

$$X = x_\mu e^\mu = (x_0, x_1, x_2, x_3) \tag{1.3.36}$$

and a corresponding 2×2 matrix

$$\tilde{X} = x_\mu \sigma^\mu = \begin{pmatrix} x_0 + x_3 & x_1 - ix_2 \\ x_1 + ix_2 & x_0 - x_3 \end{pmatrix}, \tag{1.3.37}$$

where $\sigma^\mu = (\mathbb{1}, \sigma^i)$ is the 4 vector of Pauli matrices. Transformations $X \mapsto \Lambda X$ under $SO(3, 1)$ leave the square

$$|X|^2 = x_0^2 - x_1^2 - x_2^2 - x_3^2 \tag{1.3.38}$$

18

invariant, whereas the action of $SL(2, \mathbb{C})$ mapping $\tilde{X} \mapsto N\tilde{X}N^\dagger$, with $N \in SL(2, \mathbb{C})$ preserves the determinant

$$\det \tilde{X} = x_0^2 - x_1^2 - x_2^2 - x_3^2 \,. \tag{1.3.39}$$

The map between $SL(2, \mathbb{C})$ is 2-1, since $N = \pm\mathbb{1}$ both correspond to $\Lambda = \mathbb{1}$, but $SL(2, \mathbb{C})$ has the advantage to be simply connected, so $SL(2, \mathbb{C})$ is the universal covering group.

1.4   Klein-Gordon Equation

The Lagrangian formulation is particularly suited to relativistic dynamics because provided our choice of $\mathscr{L}$ is a Lorentz scalar, the equation of motion resulting from (1.2.3) will be Lorentz invariant. For example, substituting the Lagrangian

$$\mathscr{L} = \frac{1}{2}\partial_\mu\phi \, \partial^\mu\phi - \frac{1}{2}m^2\phi^2 \tag{1.4.40}$$

into (1.2.3) yields the Klein-Gordon equation

$$\partial_\mu\partial^\mu\phi + m^2\phi \equiv (\Box^2 + m^2)\phi = 0 \,. \tag{1.4.41}$$

By recalling that a prescription for obtaining Schrödinger equation for a free particle of mass m is to substitute the classical energy momentum relation $E = \vec{p}^{\,2}/2m$ by the differential operators $E \to i\hbar\partial_t$ and $\vec{p} \to -i\hbar\vec{\nabla}$, we can see that (for $\hbar = 1$) Klein-Gordon equation satisfies the relativistic energy-momentum relation

$$E^2 = \vec{p}^{\,2} + m^2 \,. \tag{1.4.42}$$

Consequently, Eq. (1.4.41) could otherwise have been called the relativistic Schrödinger equation.

Multiplying Eq. (1.4.41) by $-i\phi^*$ and the complex conjugate equation by $-i\phi$, and substracting, leads the continuty equation

$$\partial_t \underbrace{[i(\phi^* \, \partial_t\phi - \phi \, \partial_t\phi^*)]}_{\rho} + \vec{\nabla} \cdot \underbrace{[-i(\phi^* \, \vec{\nabla}\phi - \phi \, \vec{\nabla}\phi^*)]}_{\vec{j}} = 0 \tag{1.4.43}$$

where ρ is the probability density ($|\phi|^2 \, d^3x$ gives the probability of finding the particle in a volume element d^3x), and $\vec{j}$ is the density flux of a beam of particles.

Considering the motion a free particle of energy E and momentum p, described by Klein-Gordon solution,

$$\phi = N\, e^{i(\vec{p}.\vec{x}-Et)} \;, \tag{1.4.44}$$

from Eq. (1.4.43) we find $\rho = 2\,E\,|N|^2$ and $\vec{j} = 2\,\vec{p}\,|N|^2$. We note that the probability density ρ is the timelike component of a four-vector

$$\rho \propto E = \pm(\vec{p}^{\,2} + m^2)^{1/2}\;. \tag{1.4.45}$$

Thus, in addition to the acceptable $E > 0$ solutions, we have negative energy solutions which have associated a negative probability density. We cannot simply discard the negative energy solutions as we have to work with a complete set of states, and this set inevitably includes the unwanted states.

Pauli and Weisskopf gave a natural interpretation to positive and negative probability densies by inserting the charge e into (1.4.43),

$$ej^\mu = i\,e\,(\phi^*\,\partial^\mu\phi - \phi\,\partial^\mu\phi^*)\,, \tag{1.4.46}$$

and interpreting it as the electromagnetic charge-current density.[11] With this in mind, ej^0 represents a charge density, not a probability density, and so the fact that it can be negative is no longer objectable. In some sense, which we will make clear in a moment, the $E < 0$ solutions may then be regarded as $E > 0$ solutions for particles of opposite charge (antiparticles).

The prescription for handling negative energy configurations was put forward by Stückelberg and by Feynman.[12] Expressed most simply, the idea is that a negative energy solution describes a particle which propagates backwards in time or, equivalently, a positive energy *antiparticle* propagating forward in time. It is crucial to master this idea, as it lies at the heart of our approach to Feynamn diagrams.

Consider a spin-0 particle of energy E, three-momentum $\vec{p}$, and charge e, generally referred to as the "spinless electron." From (1.4.44) and (1.4.46), we know that the electromagnetic four vector current is

$$ej^\mu(e^-) = 2e|N|^2(E,\; \vec{p})\,. \tag{1.4.47}$$

[11] W. Pauli and V. Weisskopf, Helv. Phys. Acta **7**, 709 (1934).

[12] E. C. G. Stückelberg, Helv. Phys. Acta. **14**, 322 (1941); **14**, 558 (1941); **15**, 23 (1942); R. P. Feynman, Phys. Rev. **74**, 939 (1948); **76**, 749 (1949).

Now, taking its antiparticle e^+ of the same $(E, \vec{p})$, because its charge is $-e$, we obtain

$$\begin{aligned} -ej^\mu(e^+) &= -2e|N|^2(E, \vec{p}) \\ &= 2e|N|^2(-E, -p), \end{aligned} \quad (1.4.48)$$

which is exactly the same as the current of the original particle with $-E, -\vec{p}$. Hence, as far as a system is concerned, the emission of an antiparticle with energy E is the same as the absorption of a particle of energy $-E$. Pictorially, we have
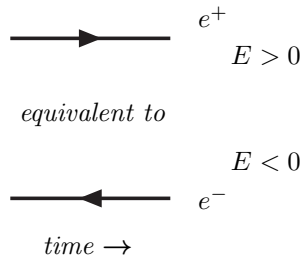
In other words, negative-energy particle solutions going backward in time describe positive-energy antiparticle solutions going forward in time. Of course the reason why this identification can be made is simply because $e^{-i(-E)(-t)} = e^{-iEt}$.

The particle-antiparticle conjugation C constitutes a finite symmetry group containing only two elements, the identity I and an element g, satisfying $g^2 = I$. Invariance of a system under the symmetry operation g means that if the system is in an eigenstate of C, then transitions can only occur to eigenstates with the same eigenvalue.

1.5   Dirac Equation

Let us now attempt to construct a wave equation for spin-$\frac{1}{2}$ relativistic particles of mass m. Following Dirac[13] we proceed by analogy with non-relativistic quantum mechanics and write an equation which, unlike the Klein-Gordon

---

[13]P. A. M. Dirac, Proc. Roy. Soc. Lond. A **117**, 610 (1928); **118**, 351 (1928); **126**, 360 (1930); **133**, 60 (1931).

equation, is linear in ∂_t. In order to be covariant, it must also be linear in $\vec{\nabla}$, and therefore the Hamiltonian has the general form

$$H \ \psi(x) = (\vec{\alpha} \cdot \vec{p} + \beta \, m) \ \psi(x) \,, \qquad (1.5.49)$$

where the four coefficients β and α_1, α_2, and α_3 are determined by the requirement that a free particle must satisfy the relativistic energy-momentum relation (1.4.42)

$$
\begin{aligned}
H^2 \psi &= (\alpha_i p_i + \beta m)(\alpha_j p_j + \beta m)\psi \\
&= (\ \underbrace{\alpha_i^2}_{1} \ p_i^2 + \underbrace{(\alpha_i \alpha_j + \alpha_j \alpha_i)}_{0} \ p_i p_j + \underbrace{(\alpha_i \beta + \beta \alpha_i)}_{0} \ p_i \, m + \underbrace{\beta^2}_{1} \ m^2) \ \psi \,.
\end{aligned}
$$
$$(1.5.50)$$

Here we sum over repeated indices, with the condition $i > j$ on the second term. From Eq. (1.5.50) we see that all the coefficients α_i and β anticommute with each other, and hence they cannot simply be numbers. We are lead to consider matrices α^k $(k = 1, 2, 3)$ and β , which are required to satisfy the conditions

$$\alpha^k \alpha^l + \alpha^l \alpha^k \equiv \{\alpha^k, \alpha^l\} = 2\delta^{kl}, \ \{\alpha^k, \beta\} = 0, \ \text{and} \ \beta^2 = \mathbb{1} \,, \qquad (1.5.51)$$

where $\mathbb{1}$ is the unit matrix. It turns out that the lowest dimensionality matrices, which guarantee that the relativistic energy momentum relation also holds true, are 4×4.

A four-component quantity $\psi_\alpha(x)$ which satisfies the Dirac equation,

$$i \, \partial_t \, \psi_\rho(x) = -i \, [\alpha_{\rho\sigma}]^k \, \partial_{x^k} \, \psi_\sigma(x) + m \, \beta_{\rho\sigma} \, \psi_\sigma(x) \,, \qquad (1.5.52)$$

is called a spinor. Its transformation properties are different from that of a four-vector and we will study them later in this section. Hereafter we omit the spinor subscripts whenever there is no danger of confusion: $\psi(x)$ will always stand for a column to the right of the 4×4 matrices, and $\psi^\dagger(x)$ for a row to the left of the matrices.

It is actually never necessary to have specific representation of the matrices α^k and β; nevertheless some calculations become more transparent by

the choice of a canonical form. The Dirac-Pauli representation is the most frequently used:

$$\vec{\alpha} \equiv \boldsymbol{\alpha} = \begin{pmatrix} 0 & \boldsymbol{\sigma} \\ \boldsymbol{\sigma} & 0 \end{pmatrix} \qquad \text{and} \qquad \beta = \begin{pmatrix} \mathbb{1} & 0 \\ 0 & -\mathbb{1} \end{pmatrix} , \qquad (1.5.53)$$

where the submatrices $\boldsymbol{\sigma}$ are the Pauli spin matrices (1.3.17). Another possible representation in a 2×2 block form is

$$\boldsymbol{\alpha} = \begin{pmatrix} -\boldsymbol{\sigma} & 0 \\ 0 & \boldsymbol{\sigma} \end{pmatrix} \qquad \text{and} \qquad \beta = \begin{pmatrix} 0 & \mathbb{1} \\ \mathbb{1} & 0 \end{pmatrix} . \qquad (1.5.54)$$

This representation is called the Weyl or chiral representation. Unless stated otherwise, we will always use the Dirac-Pauli representation.

On multiplying Dirac's equation by β from the left, we obtain

$$i \beta \, \partial_t \psi = -i \beta \, \boldsymbol{\alpha} . \vec{\nabla} \, \psi + m\psi , \qquad (1.5.55)$$

which can be rewritten as

$$i\gamma^0 \partial_t \psi + i\gamma^k \partial_{x^k} \psi - m\psi = 0 , \qquad (1.5.56)$$

or equivalently,

$$(i\gamma^\mu \partial_\mu - m) \, \psi = 0 . \qquad (1.5.57)$$

Here, we have introduced four Dirac γ-matrices, $\gamma^\mu \equiv (\beta, \beta\boldsymbol{\alpha})$, which satisfy the anticommutation relations

$$\{\gamma^\mu, \gamma^\nu\} = 2g^{\mu\nu} . \qquad (1.5.58)$$

This means that $\gamma^\mu\gamma^\nu = -\gamma^\nu\gamma^\mu$ when $\mu \neq \nu$, $(\gamma^0)^2 = \mathbb{1}$, and $(\gamma^k)^2 = -\mathbb{1}$. We can now unequivocally see that Dirac's equation is actually four differential equations,

$$\sum_{\sigma=1}^{4} \left\{ \sum_\mu i \, [\gamma_{\rho\sigma}]^\mu \, \partial_\mu - m \, \delta_{\rho\sigma} \right\} \psi_\sigma = 0 , \qquad (1.5.59)$$

which couple the four components of a single Dirac spinor ψ.

We want the Dirac equation to preserve its form under Lorentz transformations. We know that the 4-vectors get their components mixed up by

23

Lorentz transformations, so we expect that the components of ψ might get mixed up too. Because both the Dirac equation and Lorentz transformation of the coordinates are themselves linear, we ask that the transformation between ψ and ψ' be linear, i.e.,

$$\psi'^\alpha(x') = \psi'^\alpha(\Lambda x) = S(\Lambda)^\alpha{}_\beta \psi^\beta(x) = S(\Lambda)^\alpha{}_\beta \psi^\beta(\Lambda^{-1}x'), \qquad (1.5.60)$$

where $S(\Lambda)$ is a 4×4 matrix which operates on the spinor index of ψ.

We need to figure out what S is. The requirement is that the Dirac equation has the same form in any inertial frame. If we make a Lorentz transformation from our original frame into another (primed) frame we demand

$$(i\gamma^\mu \partial_\mu' - m)\psi'(x') = 0, \qquad (1.5.61)$$

or equivalently

$$(i\gamma^\mu \Lambda_\mu{}^\nu \partial_\nu - m)S(\Lambda)\,\psi(x) = 0 . \qquad (1.5.62)$$

If we multiply by $S^{-1}(\Lambda)$ from the left we get

$$(i\,S^{-1}\,\gamma^\mu\,S\,\Lambda_\mu{}^\nu\,\partial_\nu - m)\,\psi(x) = 0 . \qquad (1.5.63)$$

The equation therefore is form-invariant, provided we can find $S(\Lambda)$ such that

$$S^{-1}(\Lambda)\,\gamma^\mu\,S(\Lambda)\,\Lambda_\mu{}^\nu = \gamma^\nu, \qquad (1.5.64)$$

or equivalently

$$\Lambda^\nu{}_\mu \gamma^\mu = S^{-1}(\Lambda)\gamma^\nu S(\Lambda). \qquad (1.5.65)$$

To find $S(\Lambda)$ we resort to the trick of considering an infinitesimal Lorentz transformation. Let

$$S(\Lambda) = 1 - \frac{i}{2}\omega_{\mu\nu}\Sigma^{\mu\nu}, \qquad (1.5.66)$$

after a bit of algebra (1.5.64) reduces to the condition

$$[\Sigma^{\mu\nu}, \gamma^\beta] = -i(g^{\mu\beta}\gamma^\nu - g^{\nu\beta}\gamma^\mu). \qquad (1.5.67)$$

A solution is seen to be

$$\Sigma^{\mu\nu} \equiv \frac{1}{2}\sigma^{\mu\nu} = \frac{i}{4}[\gamma^\mu, \gamma^\nu] = \frac{i}{2}\left\{ \begin{array}{cc} 0 & \mu = \nu \\ \gamma^\mu\gamma^\nu & \mu \neq \nu \end{array} \right\} = \frac{i}{2}(\gamma^\mu\gamma^\nu - g^{\mu\nu}). \quad (1.5.68)$$

24

Note that when $\mu \neq \nu$ we have

$$
\begin{aligned}
[\Sigma^{\mu\nu}, \gamma^\beta] &= \frac{i}{2}[\gamma^\mu\gamma^\nu, \gamma^\beta] \\
&= \frac{i}{2}\gamma^\mu\gamma^\nu\gamma^\beta - \frac{i}{2}\gamma^\beta\gamma^\mu\gamma^\nu \\
&= \frac{i}{2}\gamma^\mu\{\gamma^\nu, \gamma^\beta\} - \frac{i}{2}\gamma^\mu\gamma^\beta\gamma^\nu - \frac{i}{2}\{\gamma^\beta, \gamma^\mu\}\gamma^\nu + \frac{i}{2}\gamma^\mu\gamma^\beta\gamma^\nu \\
&= i(\gamma^\mu g^{\nu\beta} - g^{\beta\mu}\gamma^\nu) . \tag{1.5.69}
\end{aligned}
$$

By repeated use of (1.5.58), it is easily seen that (1.5.68) satisfies the commutation relations (1.3.21) of the Lorentz algebra, i.e,

$$
\begin{aligned}
[\Sigma^{\mu\nu}, \Sigma^{\rho\sigma}] &= \frac{i}{2}[\Sigma^{\mu\nu}, \gamma^\rho\gamma^\sigma] \\
&= \frac{i}{2}[\Sigma^{\mu\nu}, \gamma^\rho]\gamma^\sigma + \frac{i}{2}\gamma^\rho[\Sigma^{\mu\nu}, \gamma^\sigma] \\
&= \frac{i}{2}\left(\gamma^\mu\gamma^\sigma g^{\nu\rho} - \gamma^\nu\gamma^\sigma g^{\rho\mu} + \gamma^\rho\gamma^\mu g^{\nu\sigma} - \gamma^\rho\gamma^\nu g^{\sigma\mu}\right) ; \tag{1.5.70}
\end{aligned}
$$

using (1.5.68) to write $i\gamma^\mu\gamma^\sigma = 2\Sigma^{\mu\nu} + g^{\mu\nu}$, we have

$$
[\Sigma^{\mu\nu}, \Sigma^{\rho\sigma}] = i(g^{\nu\rho}\Sigma^{\mu\sigma} - g^{\mu\rho}\Sigma^{\nu\sigma} - g^{\nu\sigma}\Sigma^{\mu\rho} + g^{\mu\sigma}\Sigma^{\nu\rho}) . \tag{1.5.71}
$$

Incidentally $S^\dagger(\Lambda) = \gamma^0 \, S^{-1}(\Lambda) \, \gamma^0$. When the Lorentz transformation is not infinitesimal the form for $S(\Lambda)$ becomes

$$
S(\Lambda) = e^{-(i/2)\,\omega_{\mu\nu}\,\Sigma^{\mu\nu}} . \tag{1.5.72}
$$

For a rotation $\omega_{0i} = 0$ and $\omega_{ij} = \theta_k$, and because $\Sigma^{ij} = \frac{1}{2}\epsilon^{ijk}\,\sigma^k$ we get

$$
S(\Lambda) = e^{-(i/2)\,\boldsymbol{\theta}\,.\,\boldsymbol{\sigma}} , \tag{1.5.73}
$$

which shows the connection between ω_{ij} and the parameters characterizing the rotation (i, j, $k = 1$, 2, 3). For a pure Lorentz transformation $\omega_{ij} = 0$ and $\omega_{0i} = \vartheta_i$, and because $\Sigma^{0i} = \frac{i}{2}\alpha^i$ we have

$$
\begin{aligned}
S(\Lambda) &= e^{(1/2)\,\boldsymbol{\vartheta}\,.\,\boldsymbol{\alpha}} \\
&= 1 + \frac{1}{2}\boldsymbol{\vartheta}\,.\,\boldsymbol{\alpha} + \frac{1}{2!}\left(\frac{\vartheta^2}{4}\right) + \frac{1}{3!}\left(\frac{\vartheta^2}{4}\right)\frac{\boldsymbol{\vartheta}\,.\,\boldsymbol{\alpha}}{2} + \dots \\
&= \cosh\frac{\vartheta}{2} + \hat{\vartheta}\,.\,\boldsymbol{\alpha}\sinh\frac{\vartheta}{2} . \tag{1.5.74}
\end{aligned}
$$

For a special case, we may find the connection between ϑ and the velocity $\vec{v}$ characterizing the pure Lorentz transformation by looking at (1.5.64). For example, consider a Lorentz transformation in which the new frame (prime coordinates) moves with velocity v along the x_3 axis of the original frame (unprimed coordinates). We will leave it to the reader to convince themselves that

$$
\begin{aligned}
t' &= \cosh(\vartheta_3)\ t - \sinh(\vartheta_3)\ x_3 \\
x_3' &= -\sinh(\vartheta_3)\ t + \cosh(\vartheta_3)\ x_3
\end{aligned}
\tag{1.5.75}
$$

with x and y unchanged; here,

$$
\cosh(\vartheta_3) = \frac{1}{\sqrt{1-v^2}} \qquad \text{and} \qquad \hat{\vartheta} \equiv \frac{\vec{v}}{v} = \hat{k}\ .
\tag{1.5.76}
$$

Because $\cos(i\vartheta_3) = \cosh(\vartheta_3)$ and $\sin(i\vartheta_3) = \sinh(\vartheta_3)$, we see that the Lorentz transformation may be regarded as a rotation through an imaginary angle $i\vartheta_3$ in the it-x_3 plane.

To construct the currents, we duplicate the calculation of the previous section taking into account that Dirac's equation is a matrix equation and thus we must consider the hermitian, rather than the complex, conjugate equation. The Dirac's equation hermitian conjugate is

$$
-i\psi^\dagger \gamma^0 \partial_t - i\partial_{x^k}\psi^\dagger(-\gamma^k) - m\psi^\dagger = 0\ .
\tag{1.5.77}
$$

To restore the covariant form we need to flip the plus sign in the second term while leaving the first term unchanged. Since $\gamma^0\gamma^k = -\gamma^k\gamma^0$, this can be accomplished by multiplying (1.5.77) from the right by γ^0. Introducing the adjoint (row) spinor $\bar{\psi} \equiv \psi^\dagger\gamma^0$, we obtain

$$
i\partial_\mu\bar{\psi}\gamma^\mu + m\bar{\psi} = 0\ .
\tag{1.5.78}
$$

Before proceeding, we pause to discuss the transformation properties of $\bar{\psi}(x)\,\gamma^\mu\,\psi(x)$. We have

$$
\begin{aligned}
\bar{\psi}'(x')\,\gamma^\mu\,\psi'(x') &= \bar{\psi}(x)\,S^{-1}(\Lambda)\,\gamma^\mu\,S(\Lambda)\,\psi(x) \\
&= \Lambda^\mu{}_\alpha\,\bar{\psi}(x)\,\gamma^\alpha\,\psi(x)\ .
\end{aligned}
\tag{1.5.79}
$$

This implies that under a Lorentz transformation, the bilinear combination $\bar{\psi}(x)\,\gamma^\mu\,\psi(x)$ transforms like a contravariant four-vector. Along these lines, we can write down a Lagrangian describing the behavior of spin-$\frac{1}{2}$ relativistic particles of mass m

$$\mathscr{L}_{\text{Dirac}} = \bar{\psi}(i\gamma^\mu\partial_\mu - m)\psi \ . \tag{1.5.80}$$

Let us now resume the derivation of the continuity equation, $\partial_\mu j^\mu = 0$. By multiplying (1.5.56) from the left by $\bar{\psi}$ and (1.5.77) from the right by ψ, and adding, we obtain

$$\bar{\psi}\,\gamma^\mu\,\partial_\mu\psi + (\partial_\mu\bar{\psi})\gamma^\mu\psi = \partial_\mu(\bar{\psi}\gamma^\mu\psi) = 0\,, \tag{1.5.81}$$

showing that the probability and flux densities, $j^\mu = \bar{\psi}\gamma^\mu\psi$, satisfy the continuity equation. Moreover,

$$\rho \equiv j^0 = \bar{\psi}\gamma^0\psi = \psi^\dagger\psi = \sum_{i=1}^{4}|\psi_i|^2 \tag{1.5.82}$$

is now positive definite. In this respect, the quantity $\psi(x)$ resembles the Schrödinger wave function, and the Dirac equation may serve as a one particle equation. In that role, however, the coefficient of $-ix^0$ in the decomposition

$$\psi(x) = \int dp\,\psi(p)\,e^{-ip\cdot x} \tag{1.5.83}$$

plays the role of the energy, and there is no reason why negative energies should be excluded.

Next, we discuss the plane wave solutions of the Dirac equation. We will treat positive and negative frequency terms separately and therefore write

$$\psi(x) = u(p)e^{-ipx} + v(p)\,e^{ipx} \ . \tag{1.5.84}$$

Since ψ also satisfies Klein Gordon equation, it is necessary that $p^\mu p_\mu = m^2$ so that $p^0 = +\sqrt{\vec{p}^{\,2} + m^2} \equiv E$. Conventionally, we will call the term with e^{-iEx_0} the positive frequency solution. From the Dirac equation it follows that

$$[i\gamma^\mu(-ip_\mu) - m]\,u(p)\,e^{-ipx} + [i\gamma^\mu(ip_\mu) - m]\,v(p)\,e^{ipx} = 0 \tag{1.5.85}$$

27

or equivalently

$$
\begin{aligned}
(\gamma^\mu p_\mu - m)\, u(p) &= 0 \\
(\gamma^\mu p_\mu + m)\, v(p) &= 0 \ ,
\end{aligned}
\tag{1.5.86}
$$

because the positive and negative frequency solutions are independent.

A point worth noting at this juncture. The two negative energy solutions $u^{(3,4)}$ are to be associated with an antiparticle, say the positron. Using the antiparticle prescription from the previous section: a positron of energy E and momentum $\vec{p}$ is described by one of the $-E$ and $-\vec{p}$ electron solutions, i.e.,

$$
u^{(3,4)}(-p)\, e^{-i[-p]\cdot x} \equiv v^{(2,1)}(p) e^{ip\cdot x} \ ,
\tag{1.5.87}
$$

where $p^0 \equiv E > 0$. The "positron" spinors v are defined just for notational convenience.

It is useful to introduce the notation $\gamma^\mu p_\mu = \gamma_\mu p^\mu = \not{p}$. The "slash" quantities satisfy $\{\not{a}, \not{b}\} = a_\mu b_\nu \{\gamma^\mu, \gamma^\nu\} = 2a_\mu b^\mu \equiv 2a.b$. The Dirac equation for a plane wave solution may thus be written as

$$
\begin{aligned}
(\not{p} - m)\, u(p) &= 0 \\
(\not{p} + m)\, v(p) &= 0 \ .
\end{aligned}
\tag{1.5.88}
$$

It is easily seen that

$$
\begin{aligned}
\bar{u}(p)\, (\not{p} - m) &= 0 \\
\bar{v}(p)\, (\not{p} + m) &= 0 \ .
\end{aligned}
\tag{1.5.89}
$$

When $\vec{p} = 0$, $p_0 = m$ the equations take the form

$$
\begin{aligned}
(\gamma^0 - 1)\, m\, u(0) &= 0 \\
(\gamma^0 + 1)\, m\, v(0) &= 0 \ .
\end{aligned}
\tag{1.5.90}
$$

There are, therefore, two positive and two negative frequency solutions, which – identifying $u^{(3)}(0) \equiv v^{(2)}(0)$ and $u^{(4)}(0) \equiv v^{(1)}(0)$ – we take to be

$$
u^{(1)}(0) = \begin{pmatrix} 1 \\ 0 \\ 0 \\ 0 \end{pmatrix} \quad
u^{(2)}(0) = \begin{pmatrix} 0 \\ 1 \\ 0 \\ 0 \end{pmatrix} \quad
v^{(2)}(0) = \begin{pmatrix} 0 \\ 0 \\ 1 \\ 0 \end{pmatrix} \quad
v^{(1)}(0) = \begin{pmatrix} 0 \\ 0 \\ 0 \\ 1 \end{pmatrix} .
\tag{1.5.91}
$$

28

Since
$$(\not{p} + m)(\not{p} - m) = p^2 - m^2 = 0 \qquad (1.5.92)$$

we may write the solution for arbitrary p in the form

$$
\begin{aligned}
u^{(r)}(p) &= C\,(m + \not{p})\,u^{(r)}(0) \\
v^{(r)}(p) &= C'\,(m - \not{p})\,v^{(r)}(0)\,,
\end{aligned}
\qquad (1.5.93)
$$

where $r = 1, 2$, and C and C' are normalization constants. For fermions, we choose the covariant normalization in which we have $2E$ particles/unit volume, just as we did for bosons

$$\int_{\text{unit vol.}} \rho\,dV = \int \psi^\dagger \psi\,dV = u^\dagger(p)\,u(p) = 2E\,, \qquad (1.5.94)$$

where we have used (1.5.82) and (1.5.84). This leads to the orthogonality relations

$$u^{(r)\dagger}(p)\,u^{(s)}(p) = 2E\delta_{rs}\,, \qquad v^{(r)\dagger}(p)\,v^{(s)}(p) = 2E\delta_{rs}\,. \qquad (1.5.95)$$

By summing $\bar{u}(p)\,\gamma^0(\gamma^\mu p_\mu - m)\,u(p) = 0$ and $\bar{u}(p)\,(\gamma^\mu p_\mu - m)\,\gamma^0\,u(p) = 0$, we obtain

$$2\,\bar{u}(p)\,p_0\,u(p) - 2\,m\,u^\dagger(p)\,u(p) = 0\,, \qquad (1.5.96)$$

where we have used the relation $\gamma^0\gamma^k = -\gamma^k\gamma^0$. The orthogonality relations then become

$$\bar{u}^{(r)}(p)\,u^{(s)}(p) = \frac{m}{E}\,u^{(r)\dagger}(p)\,u^{(s)}(p) = 2m\delta_{rs} \qquad (1.5.97)$$

and

$$\bar{v}^{(r)}(p)\,v^{(s)}(p) = -\frac{m}{E}\,v^{(r)\dagger}(p)\,v^{(s)}(p) = -2m\delta_{rs}\,. \qquad (1.5.98)$$

Finally, using $\not{p}\not{p} = p^2$ we obtain

$$
\begin{aligned}
\bar{u}^{(r)}(p)\,u^{(s)}(p) &= |C|^2\,\bar{u}^{(r)}(0)\,(m + \not{p})(m + \not{p})\,u^{(s)}(0) \\
&= 2m\,|C|^2\,\bar{u}^{(r)}(0)\,(m + \not{p})\,u^{(s)}(0) \\
&= 2m\,|C|^2\,\bar{u}^{(r)}(0)\,(m + \gamma^0 p_0 + \alpha^k p_k \beta)\,u^{(s)}(0) \\
&= 2m\,|C|^2\,(m + E)\,\bar{u}^{(r)}(0)\,u^{(s)}(0) \\
&= 2m\,|C|^2\,(m + E)\,\delta_{rs}\,,
\end{aligned}
\qquad (1.5.99)
$$

29

and determine the normalization constant

$$C = \frac{1}{\sqrt{m + E}} \ . \tag{1.5.100}$$

A straightforward calculation leads to

$$C' = \frac{1}{\sqrt{m + E}} \ . \tag{1.5.101}$$

Introducing two-component spinors $\chi^{(r)}$, where $\chi^1 = \binom{1}{0}$ and $\chi^2 = \binom{0}{1}$, we may examine the explicit form of the solution of the Dirac equation in the Pauli-Dirac representation. For $E > 0$ we have

$$
\begin{aligned}
u^{(r)}(p) &= \frac{m + \not{p}}{\sqrt{m + E}} \ \chi^{(r)} \\
&= \frac{m + \sigma_3 E - i\sigma_2 \boldsymbol{\sigma} \cdot \vec{p}}{\sqrt{m + E}} \ \chi^{(r)} \\
&= \frac{1}{\sqrt{m + E}} \begin{pmatrix} m + E & -\boldsymbol{\sigma} \cdot \vec{p} \\ \boldsymbol{\sigma} \cdot \vec{p} & m - E \end{pmatrix} \begin{pmatrix} \chi^{(r)} \\ 0 \end{pmatrix} \\
&= \sqrt{E + m} \begin{pmatrix} \chi^{(r)} \\ (E + m)^{-1} \ \boldsymbol{\sigma} \cdot \vec{p} \ \chi^{(r)} \end{pmatrix} , \tag{1.5.102}
\end{aligned}
$$

and so the positive-energy four spinor solutions of Dirac's equation are

$$u_1(E, \vec{p}) = \sqrt{m + E} \begin{pmatrix} \begin{pmatrix} 1 \\ 0 \end{pmatrix} \\ (m + E)^{-1} \ \boldsymbol{\sigma} \cdot \vec{p} \begin{pmatrix} 1 \\ 0 \end{pmatrix} \end{pmatrix} , \tag{1.5.103}$$

and

$$u_2(E, \vec{p}) = \sqrt{m + E} \begin{pmatrix} \begin{pmatrix} 0 \\ 1 \end{pmatrix} \\ (m + E)^{-1} \ \boldsymbol{\sigma} \cdot \vec{p} \begin{pmatrix} 0 \\ 1 \end{pmatrix} \end{pmatrix} . \tag{1.5.104}$$

For low momenta, the upper two components are a great deal larger than the lower ones. For the $E < 0$ solutions,

$$u^{(r+2)}(p) = \frac{1}{\sqrt{m+E}} \begin{pmatrix} m+E & -\boldsymbol{\sigma}.\vec{p} \\ \boldsymbol{\sigma}.\vec{p} & m-E \end{pmatrix} \begin{pmatrix} 0 \\ \chi^{(r)} \end{pmatrix}, \qquad (1.5.105)$$

hence the four spinor solutions of Dirac equation are

$$u_3(E,\vec{p}) = \sqrt{m-E} \begin{pmatrix} -(m-E)^{-1} \boldsymbol{\sigma}.\vec{p} \begin{pmatrix} 1 \\ 0 \end{pmatrix} \\ \begin{pmatrix} 1 \\ 0 \end{pmatrix} \end{pmatrix}, \qquad (1.5.106)$$

and

$$u_4(E,\vec{p}) = \sqrt{m-E} \begin{pmatrix} -(m-E)^{-1} \boldsymbol{\sigma}.\vec{p} \begin{pmatrix} 0 \\ 1 \end{pmatrix} \\ \begin{pmatrix} 0 \\ 1 \end{pmatrix} \end{pmatrix}. \qquad (1.5.107)$$

To obtain the completness properties of the solutions, we consider the positive and negative solutions separately. We use the explicit solutions already obtained,

$$\begin{aligned}
(\Lambda_+)_{\alpha\beta} &\equiv \frac{1}{2m} \sum_{r=1}^{2} u_\alpha^{(r)}(p)\, \bar{u}_\beta^{(r)}(p) \\
&= \frac{1}{2m\,(m+E)} \left[\sum_r (\slashed{p}+m)u^{(r)}(0)\,\bar{u}^{(r)}(0)(\slashed{p}+m) \right]_{\alpha\beta} \\
&= \frac{1}{2m\,(m+E)} \left[(m+\slashed{p})\frac{1+\gamma^0}{2}(m+\slashed{p}) \right]_{\alpha\beta} \\
&= \frac{1}{2m\,(m+E)} \left\{ m(\slashed{p}+m) + \frac{1}{2}(\slashed{p}+m)[(m-\slashed{p})\gamma^0 + 2E] \right\}_{\alpha\beta} \\
&= \frac{1}{2m}(\slashed{p}+m)_{\alpha\beta}. \qquad (1.5.108)
\end{aligned}$$

31

Similarly, if we define Λ_- by

$$(\Lambda_-)_{\alpha\beta} = -\frac{1}{2m} \sum_{r=1}^{2} v_\alpha^{(r)}(p) \, \bar{v}_\beta^{(r)}(p) \qquad (1.5.109)$$

we get

$$(\Lambda_-)_{\alpha\beta} = \frac{1}{2m} (m - \not{p})_{\alpha\beta} . \qquad (1.5.110)$$

The completness relation is that

$$\Lambda_+ + \Lambda_- = \frac{1}{2m} \sum_{r=1}^{2} [u_\alpha^{(r)}(p) \, \bar{u}_\beta^{(r)}(p) - v_\alpha^{(r)}(p) \, \bar{v}_\beta^{(r)}(p)] = \mathbb{1} . \qquad (1.5.111)$$

The separate matrices, Λ_+ and Λ_-, have the properties of projection operators, because $\Lambda_\pm^2 = \Lambda_\pm$ and $\Lambda_+\Lambda_- = \Lambda_-\Lambda_+ = 0$. The operators $\Lambda_\pm$ project positive and negative frequency solutions, but because there are four soultions, there must still be another projector operator, which separates the $r = 1, 2$ solutions. This projector operator h must be such that

$$h^{(r)} h^{(s)} = \delta_{rs} h^{(r)} \quad \text{and} \quad [h^{(r)}, \Lambda_\pm] = 0 . \qquad (1.5.112)$$

Since the two solutions have something to do with the two possible polarization directions of a spin-$\frac{1}{2}$ particle, we may expect the operator to be some sort of generalization of the non-relativistic operator which projects out the state polarized in a given direction for a two component spinor. On inspection, we see that the helicity operator,

$$h \equiv \hat{p} . \mathbf{\Sigma} = \frac{1}{2} \hat{p}_k \begin{pmatrix} \sigma^k & 0 \\ 0 & \sigma^k \end{pmatrix} , \qquad (1.5.113)$$

satisfies (1.5.112), where $\hat{p} \equiv \vec{p}/|\vec{p}|$ is the unit vector pointing in the direction of momentum. It follows from (1.5.49) that the helicity operator commutes with H and therefore it shares its eigenstates with H and its eigenvalues are conserved. To find the eigenvalues of the helicity operator we calculate[14]

$$h^2 = \frac{1}{4} \begin{pmatrix} (\mathbf{\sigma}.\hat{p})^2 & 0 \\ 0 & (\mathbf{\sigma}.\hat{p})^2 \end{pmatrix} = \frac{1}{4} \begin{pmatrix} \hat{p}^2 & 0 \\ 0 & \hat{p}^2 \end{pmatrix} . \qquad (1.5.114)$$

---

[14]Note that $\sigma_i \, \sigma_j = \delta_{ij} + i\epsilon_{ijk}\sigma_k$, and so $(\mathbf{\sigma}.\vec{p})^2 = \sigma_i \, p^i \, \sigma_j \, p^j = (\delta_{ij} + \epsilon_{ijk}\sigma_k)p^i p^j = \vec{p}^{\,2}$.

Thus, the eigenvalues of the helicity operator are

$$h = \begin{cases} +\frac{1}{2} \ \text{positive helicity}, & \Longrightarrow \\ -\frac{1}{2} \ \text{negative helicity}, & \Longleftrightarrow \end{cases} \qquad (1.5.115)$$

The "spin" component in the direction of motion, $\frac{1}{2}\hat{p}.\boldsymbol{\sigma}$, is thus a "good" quantum number and can be used to label the solutions.

Assuming a particle has momentum $\vec{p}$ and choosing the x_3-axis along the direction of $\vec{p}$, we can determine which of the four spinors u_1, u_2, v_1, and v_2 have spin up and spin down. With these assumptions, $\boldsymbol{\sigma}.\vec{p} = \sigma_3 p_3$, $|\vec{p}| = p_3$ and the helicity operator (1.5.113) simplifies to

$$h = \frac{1}{2}\begin{pmatrix} \sigma_3 \hat{p}_3 & 0 \\ 0 & \sigma_3 \hat{p}_3 \end{pmatrix} = \frac{1}{2}\begin{pmatrix} \sigma_3 & 0 \\ 0 & \sigma_3 \end{pmatrix}. \qquad (1.5.116)$$

We then find

$$\begin{aligned}
hu_1 &= \frac{\sqrt{E+m}}{2}\begin{pmatrix} 1 & & & \\ & -1 & & \\ & & 1 & \\ & & & -1 \end{pmatrix}\begin{pmatrix} \begin{pmatrix} 1 \\ 0 \end{pmatrix} \\ (E+m)^{-1}\,\boldsymbol{\sigma}.\vec{p}\begin{pmatrix} 1 \\ 0 \end{pmatrix} \end{pmatrix} \\
&= \frac{\sqrt{E+m}}{2}\begin{pmatrix} \begin{pmatrix} 1 \\ 0 \end{pmatrix} \\ (E+m)^{-1}\,\boldsymbol{\sigma}.\vec{p}\begin{pmatrix} 1 \\ 0 \end{pmatrix} \end{pmatrix} = \frac{1}{2}u_1 \qquad (1.5.117)
\end{aligned}$$

and

$$\begin{aligned}
hu_2 &= \frac{\sqrt{E+m}}{2}\begin{pmatrix} 1 & & & \\ & -1 & & \\ & & 1 & \\ & & & -1 \end{pmatrix}\begin{pmatrix} \begin{pmatrix} 0 \\ 1 \end{pmatrix} \\ (E+m)^{-1}\,\boldsymbol{\sigma}.\vec{p}\begin{pmatrix} 0 \\ 1 \end{pmatrix} \end{pmatrix} \\
&= \frac{\sqrt{E+m}}{2}\begin{pmatrix} \begin{pmatrix} 0 \\ -1 \end{pmatrix} \\ (E+m)^{-1}\,\boldsymbol{\sigma}.\vec{p}\begin{pmatrix} 0 \\ -1 \end{pmatrix} \end{pmatrix} = -\frac{1}{2}u_2. \qquad (1.5.118)
\end{aligned}$$

33

For antiparticles with negative energy and momentum $-\vec{p}$, $\boldsymbol{\sigma}.\vec{p} = \sigma_3(-p_3)$ and the helicity operator simplifies to

$$h = \frac{1}{2}\begin{pmatrix} -\sigma_3\hat{p}_3 & 0 \\ 0 & -\sigma_3\hat{p}_3 \end{pmatrix} = \frac{1}{2}\begin{pmatrix} -\sigma_3 & 0 \\ 0 & -\sigma_3 \end{pmatrix}. \tag{1.5.119}$$

We then find

$$hv_1 = \frac{\sqrt{E+m}}{2}\begin{pmatrix} -1 & & & \\ & 1 & & \\ & & -1 & \\ & & & 1 \end{pmatrix}\begin{pmatrix} (E+m)^{-1}\,\boldsymbol{\sigma}.\vec{p}\,\begin{pmatrix} 0 \\ 1 \end{pmatrix} \\ \begin{pmatrix} 0 \\ 1 \end{pmatrix} \end{pmatrix}$$

$$= \frac{\sqrt{E+m}}{2}\begin{pmatrix} (E+m)^{-1}\,\boldsymbol{\sigma}.\vec{p}\,\begin{pmatrix} 0 \\ 1 \end{pmatrix} \\ \begin{pmatrix} 0 \\ 1 \end{pmatrix} \end{pmatrix} = \frac{1}{2}v_1 \tag{1.5.120}$$

and

$$hv_2 = \frac{\sqrt{E+m}}{2}\begin{pmatrix} -1 & & & \\ & 1 & & \\ & & -1 & \\ & & & 1 \end{pmatrix}\begin{pmatrix} (E+m)^{-1}\,\boldsymbol{\sigma}.\vec{p}\,\begin{pmatrix} 1 \\ 0 \end{pmatrix} \\ \begin{pmatrix} 1 \\ 0 \end{pmatrix} \end{pmatrix}$$

$$= \frac{\sqrt{E+m}}{2}\begin{pmatrix} (E+m)^{-1}\,\boldsymbol{\sigma}.\vec{p}\,\begin{pmatrix} -1 \\ 0 \end{pmatrix} \\ \begin{pmatrix} -1 \\ 0 \end{pmatrix} \end{pmatrix} = -\frac{1}{2}v_2. \tag{1.5.121}$$

For space invertion, or the parity operation, $\Lambda^\nu{}_\mu = \mathrm{diag}(1, -1, -1, -1)$. Then, (1.5.64) becomes $S_\mathrm{P}^{-1}\gamma^0 S_\mathrm{P} = \gamma^0$ and $S_\mathrm{P}^{-1}\gamma^k S_\mathrm{P} = -\gamma^k$ (for $k = 1, 2, 3$), which is satisfied by $S_\mathrm{P} = \gamma^0$. In the Dirac-Pauli representation of γ^0, the behavior of the four components of ψ under parity is therefore $\psi'_{1,2} = \psi_{1,2}$ and $\psi'_{3,4} = -\psi_{3,4}$. The "at rest" states (1.5.91) are thus eigenstates of parity, with the positive and negative energy states (that is, the electron and positron) having opposite intrinsic parities.

Table 1.3: Bilinear covariants. The list is arranged in increasing order of the number of γ^μ matrices that are sandwiched between $\bar\psi$ and ψ. The pseudoscalar is the product of four matrices. If five matrices were used, at least two would be the same, in which case the product will be reduced to three and be already included in the axial vector.

		No. of Compts.	Space Inversion, P
Scalar	$\bar\psi\psi$	1	$+$ under P
Vector	$\bar\psi\gamma^\mu\psi$	4	Space compts. $-$ under P
Tensor	$\bar\psi\sigma^{\mu\nu}\psi$	6	
Axial vector	$\bar\psi\gamma^5\gamma^\mu\psi$	4	Space compts. $+$ under P
Pseudoscalar	$\bar\psi\gamma^5\psi$	1	$-$ under P

To construct the most general form of currents consistent with Lorentz covariance, we need to tabulate bilinear quantities of the form $(\bar\Psi)(4 \times 4)(\psi)$, which have definite properties under Lorentz transformations, where the 4×4 matrix is a product of γ-matrices. To simplify the notation, we introduce

$$\gamma^5 \equiv i\gamma^0\gamma^1\gamma^2\gamma^3 \, . \tag{1.5.122}$$

It follows that

$$\gamma^{5\dagger} = \gamma^5, \quad (\gamma^5)^2 = \mathbb{1}, \quad \gamma^5\gamma^\mu + \gamma^\mu\gamma^5 = 0 \, . \tag{1.5.123}$$

In the Dirac-Pauli representation

$$\gamma^5 = \begin{pmatrix} 0 & \mathbb{1} \\ \mathbb{1} & 0 \end{pmatrix} . \tag{1.5.124}$$

We are interested in the behavior of bilinear quantities under proper Lorentz transformations (that is rotations and boosts), and under space invertion (the parity operation). An exhaustive list of the possibilities is given in Table 1.3. Because of the anticommutation relations, (1.5.58), the tensor is antisymmetric

$$\sigma^{\mu\nu} = \frac{i}{2} \left(\gamma^\mu\gamma^\nu - \gamma^\nu\gamma^\mu \right) . \tag{1.5.125}$$

From (1.5.79), it follows immediately that $\bar{\psi}\psi$ is a Lorentz scalar. The probability density $\rho = \psi^\dagger\psi$ is not a scalar, but is the timelike component of the four vector $\bar{\psi}\gamma^\mu\psi$. Because $\gamma^5 S_P = -S_P\gamma^5$, the presence of γ^5 gives rise to the pseudo-nature of the axial vector and pseudoscalar. For example, a pseudoscalar is a scalar under proper Lorentz transformations but, unlike a scalar, changes sign under parity.

In the Weyl representation, the boost and rotation generators can be written as

$$\Sigma^{0j} = \frac{i}{4}[\gamma^0, \gamma^j] = -\frac{i}{2}\begin{pmatrix} \sigma^j & 0 \\ 0 & -\sigma^j \end{pmatrix}, \qquad (1.5.126)$$

and

$$\Sigma^{jk} = \frac{i}{4}[\gamma^j, \gamma^k] = \frac{i}{2}\epsilon^{jkl}\begin{pmatrix} \sigma^l & 0 \\ 0 & \sigma^l \end{pmatrix}. \qquad (1.5.127)$$

From the block-diagonal form of the Lorentz generators, it is evident that the Dirac representation of the Lorentz group is reducible. We can form two 2-dimensional representations by considering each block separately and writing $\psi\begin{pmatrix}\psi_L \\ \psi_R\end{pmatrix}$. The two-component objects ψ_L and ψ_R are called left-handed and right-handed Weyl spinors. In terms of ψ_L and ψ_R, the *massless* Dirac equation

$$i\gamma^\mu\partial_\mu\,\psi(x) = \begin{pmatrix} 0 & i(\partial_0 + \boldsymbol{\sigma}\cdot\vec{\nabla}) \\ i(\partial_0 - \boldsymbol{\sigma}\cdot\vec{\nabla}) & 0 \end{pmatrix}\begin{pmatrix} \psi_L(x) \\ \psi_R(x) \end{pmatrix} = 0 \quad (1.5.128)$$

divides into two decoupled equations,

$$i(\partial_0 - \boldsymbol{\sigma}\cdot\vec{\nabla})\psi_L = 0 \;\longmapsto\; Eu_L = -\boldsymbol{\sigma}\cdot\vec{p}\,u_L, \qquad (1.5.129)$$

$$i(\partial_0 + \boldsymbol{\sigma}\cdot\vec{\nabla})\psi_R = 0 \;\longmapsto\; Eu_R = \boldsymbol{\sigma}\cdot\vec{p}\,u_R, \qquad (1.5.130)$$

for two component spinors $u_L(\vec{p})$ and $u_R(\vec{p})$. Translating these results to four-component form $u = \begin{pmatrix}u_L \\ u_R\end{pmatrix}$, with $\psi(x) = u(p)e^{-ipx}$. Each solution is based on the relativistic energy-momentum relation, $E^2 = \vec{p}^{\,2}$, and so has one positive and one negative solution.

Assume (1.5.129) is the wave equation for a "massless" fermion, a neutrino. The positive energy solution has $E = |\vec{p}|$ and so satisfies

$$\boldsymbol{\sigma}\cdot\hat{p}\,u_L = -u_L. \qquad (1.5.131)$$

This means that u_L describes a left-handed ($h = -\frac{1}{2}$) neutrino of energy E and momentum $\vec{p}$. The remaining solution has negative energy. To interpret this, we consider a neutrino solution with energy $-E$ and momentum $-\vec{p}$. It satisfies

$$\boldsymbol{\sigma} \cdot (-\hat{p}) \ u_L = u_L \,, \qquad (1.5.132)$$

with positive helicity, and hence describes a right-handed ($h = +\frac{1}{2}$) antineutrino of energy E and momentum $\vec{p}$. Symbolically, we say (1.5.129) describes ν_L and $\bar{\nu}_R$. These solutions break invariance under the parity operation P, which takes $\nu_L \rightarrow \nu_R$. For massless neutrinos this is not a censure, because weak interactions do not respect parity conservation. The second equation, (1.5.130) describes the other helicity states ν_R and $\bar{\nu}_L$.

In the Weyl representation,

$$\gamma^5 = \begin{pmatrix} -\mathbb{1} & 0 \\ 0 & \mathbb{1} \end{pmatrix}, \qquad (1.5.133)$$

thus, we can project a Dirac spinor to a left- or right-handed spinor

$$\frac{\mathbb{1} - \gamma^5}{2} u = \begin{pmatrix} \mathbb{1} & 0 \\ 0 & 0 \end{pmatrix} \begin{pmatrix} u_L \\ u_R \end{pmatrix} = \begin{pmatrix} u_L \\ 0 \end{pmatrix},$$

$$\frac{\mathbb{1} + \gamma^5}{2} u = \begin{pmatrix} 0 & 0 \\ 0 & \mathbb{1} \end{pmatrix} \begin{pmatrix} u_L \\ u_R \end{pmatrix} = \begin{pmatrix} 0 \\ u_R \end{pmatrix}. \qquad (1.5.134)$$

Of course, the fact that $\frac{1}{2}(\mathbb{1} - \gamma^5)$ projects out negative helicity fermions at high energy does not depend on the choice of representation. Working in the Dirac-Pauli representation of γ-matrices, with $E \gg m$ and $E \simeq |p|$, we have

$$\gamma^5 \begin{pmatrix} \chi^{(s)} \\ \frac{\boldsymbol{\sigma} \cdot \vec{p}}{m+E} \chi^{(s)} \end{pmatrix} \simeq \begin{pmatrix} \boldsymbol{\sigma} \cdot \hat{p} \, \chi^{(s)} \\ \chi^{(s)} \end{pmatrix} \simeq \boldsymbol{\sigma} \cdot \hat{p} \begin{pmatrix} \chi^{(s)} \\ \frac{\boldsymbol{\sigma} \cdot \vec{p}}{m+E} \chi^{(s)} \end{pmatrix}, \qquad (1.5.135)$$

which implies

$$\gamma^5 u^{(s)} = \begin{pmatrix} \boldsymbol{\sigma} \cdot \hat{p} & 0 \\ 0 & \boldsymbol{\sigma} \cdot \hat{p} \end{pmatrix} u^{(s)}, \qquad (1.5.136)$$

where $u^{(s)}$ is the electron spinor of 1.5.102. This shows that in the extreme relativistic limit, the chirality operator (γ^5) is equal to the helicity operator;

and so for example, $\frac{1}{2}(\mathbb{1} - \gamma^5)u = u_L$ corresponds to an electron of negative helicity. We need only choose a representation if we wish to show explicit spinors. The particular advantage of the Dirac-Pauli representation is that it diagonalizes the energy in the non-relativistic limit (γ^0 is diagonal), whereas the Weyl representation diagonalizes the helicity in the extreme relativistic limit (γ^5 is diagonal).

In closing, it is appropriate to peep ahead at weak interactions, which are discussed in Chapter 5. A vast number of experimental evidence attest that leptons enter the "charged-current" weak interactions in a special combination of two bilinear covariants. For example, for the electron and its neutrino, the weak current

$$J^\mu = \bar{u}_e \gamma^\mu \tfrac{1}{2}(\mathbb{1} - \gamma^5)\, u_\nu \qquad (1.5.137)$$

has a $V - A$ form. Because of the presence of the $\frac{1}{2}(\mathbb{1} - \gamma^5)$, the mixture of vector (V) and axial vector (A) ensures that parity is violated. Indeed, parity is maximally violated, because only left-handed neutrinos (and right-handed antineutrinos) are coupled to charge leptons by the weak interactions. Namely, (1.5.134) can be rewritten as,

$$u = u_L + u_R \equiv \tfrac{1}{2}(\mathbb{1} - \gamma^5)u + \tfrac{1}{2}(\mathbb{1} + \gamma^5)u\,, \qquad (1.5.138)$$

and so (1.5.137) becomes

$$J^\mu = \bar{u}_e \tfrac{1}{2}(\mathbb{1} + \gamma^5)\gamma^\mu \tfrac{1}{2}(\mathbb{1} - \gamma^5)u_\nu + \bar{u}_e \tfrac{1}{2}(\mathbb{1} - \gamma^5)\gamma^\mu \tfrac{1}{2}(\mathbb{1} - \gamma^5)u_\nu\,. \qquad (1.5.139)$$

However, since $(\mathbb{1} + \gamma^5)(\mathbb{1} - \gamma^5) = 0$ and $\gamma^\mu\gamma^5 = -\gamma^5\gamma^\mu$, the second term in (1.5.139) vanishes, yielding

$$J^\mu = \bar{u}_e \tfrac{1}{2}(\mathbb{1} + \gamma^5)\gamma^\mu \tfrac{1}{2}(\mathbb{1} - \gamma^5)u_\nu = \bar{u}_{eL}\gamma^\mu \tfrac{1}{2}(\mathbb{1} - \gamma^5)u_\nu\,. \qquad (1.5.140)$$

Note that, $\bar{u}_L = u_L^\dagger\gamma^0 = u^\dagger\tfrac{1}{2}(\mathbb{1} - \gamma^5)\gamma^0 = \bar{u}\tfrac{1}{2}(\mathbb{1} + \gamma^5)$, because $\gamma^5 = \gamma^{5\dagger}$ and $\gamma^0\gamma^5 = -\gamma^5\gamma^0$. In summary, the $\frac{1}{2}(\mathbb{1} - \gamma^5)$ in (1.5.137) automatically selects a left-handed neutrino (or a right-handed antineutrino).

1.6 Nonrelativistic Perturbation Theory

So far, free-particle states have been eigenstates of the Hamiltonian. In other words, we have seen no interactions and no scattering. There is no known

method, other than perturbation theory, that could be used to include non-linear terms in the Hamiltonian (or Lagrangian) that will couple different Fourier modes (and the particles that occupy them) to one another. Therefore, in order to obtain a closer description of the real world, inevitably we are forced to resort to some form of approximation methods.

In perturbation theory we divide the Hamiltonian into two parts H_0 and $V(\vec{x}, t)$, where H_0 is a Hamiltonian for which we know how to solve the equations of motion,

$$H_0|\phi_n\rangle = E_n|\phi_n\rangle \quad \text{with} \quad \langle\phi_m|\phi_n\rangle = \int_V \phi_m^* \, \phi_n \, d^3x = \delta_{mn} \,, \quad (1.6.141)$$

and $V(\vec{x}, t)$ is a perturbing interaction. For simplicity we have normalized the solution to one particle in a box of volume V. Since the only soluble field theory is the free-field theory, we take for H_0 the sum of all free particle Hamiltonians, *with the physical masses appearing in them*.[15] In the formal development we consider, for the sake of simplicity, a theory involving one scalar field. The objective is to solve Schrödinger equation

$$[H_0 + V(\vec{x}, t)]\psi = i\partial_t\psi \quad (1.6.142)$$

for such a scalar particle moving in the presence of an iteraction potential $V(\vec{x}, t)$. Any solution of (1.6.142) can be expressed in the form

$$|\psi\rangle = \sum_n c_n(t)|n\rangle e^{-iE_n t} = \sum_n c_n(t) \, \phi_n(\vec{x}) \, e^{-iE_n t} \,. \quad (1.6.143)$$

When this expression is substituted in the Schrödinger equation we get an equation for the coefficients $c_n(t)$

$$\sum_n c_n(t)V(\vec{x}, t)|n\rangle e^{-iE_n t} = i \sum_n \dot{c}_n(t)|n\rangle e^{-iE_n t} \,, \quad (1.6.144)$$

or equivalently

$$\sum_n c_n(t)V(\vec{x}, t)\phi_n(\vec{x})e^{-iE_n t} = i \sum_n \dot{c}_n(t)\phi_n(\vec{x})e^{-iE_n t} \,. \quad (1.6.145)$$

---

[15]A point worth noting a this juncture: the quantities which in the free Lagrangians play the role of the masses of the free particles, are no longer equal to the masses when interactions are present because of the possibility of self-interaction.

Multiplying by ϕ_f^*, integrating over the volume and using the orthogonality relation (1.6.141), we obtain the following coupled linear differential equations for the coefficients

$$\dot{c}_f = -i \sum_n c_n(t) \int \phi_f^* V \phi_n \, d^3x \, e^{i(E_f - E_n)t} \,. \tag{1.6.146}$$

Assume that before the potential V acts, the particle is in an eigenstate i of the unperturbed Hamiltonian. We therefore set at time $t = -T/2$ all the $c_n(-T/2) = 0$, for $n \neq i$, and $c_i(-T/2) = 1$. The relation

$$|\psi\rangle = \sum_n c_n(t)|n\rangle \tag{1.6.147}$$

shows that the system state $|\psi\rangle = |i\rangle$, as desired. Replacing the initial condition into (1.6.146) we get

$$\dot{c}_f = -i \int d^3x \, \phi_f^* V \phi_i \, e^{i(E_f - E_i)t} \,. \tag{1.6.148}$$

Next, provided that the potential is small and transient, we can, as a first approximation, assume that these initial conditions remain true at all times. To find the amplitude for the system to be in the state $|f\rangle$ at t, we project out the eigenstate $|f\rangle$ from $|\psi\rangle$ by calculating

$$c_f(t) = -i \int_{-T/2}^t dt' \int d^3x \, \phi_f^* V \phi_i \, e^{i(E_f - E_i)t'} \tag{1.6.149}$$

and, in particular, at time $T/2$ after the interaction has ceased,

$$T_{fi} \equiv c_f(T/2) = -i \int_{-T/2}^{T/2} dt \int d^3x \, \left[\phi_f(\vec{x})e^{-iE_f t}\right]^* V(\vec{x}, t)[\phi_i(\vec{x})e^{-iE_i t}] \,, \tag{1.6.150}$$

which can be rewritten in a covariant form as follows

$$T_{fi} = -i \int d^4x \, \phi_f^*(x) \, V(x) \, \phi_i(x) \,. \tag{1.6.151}$$

Certainly, the expression for $c_f(t)$ is only a good approximation if $c_f(t) \ll 1$, as this has been assumed in obtaining the result.

It is tempting to identify $|T_{fi}|^2$ with the probability that the particle is scattered from an initial state $|i\rangle$ to a final state $|f\rangle$. To see whether this identification is possible, we consider the case in which $V(\vec{x}, t) = V(\vec{x})$ is time independent; then using

$$\frac{1}{2\pi} \int_{-\infty}^{\infty} dq \, e^{iqp} = \delta(p) \tag{1.6.152}$$

(1.6.150) becomes

$$
\begin{aligned}
T_{fi} &= -iV_{fi} \int_{-\infty}^{\infty} dt \, e^{i(E_f - E_i)t} \\
&= -2\pi i \, V_{fi} \, \delta(E_f - E_i), \tag{1.6.153}
\end{aligned}
$$

with

$$V_{fi} \equiv \int d^3x \, \phi_f^*(\vec{x}) \, V(\vec{x}) \, \phi_i(x) . \tag{1.6.154}$$

The δ-funtion in (1.6.153) expresses the fact that the energy of the particle is conserved in the transition $i \to f$. By the uncertainty principle, this means that an infinite time separates the states i and f, and $|T_{fi}|^2$ is therefore not a meaningful quantity. We define instead a transition probability per unit time

$$W = \lim_{T \to \infty} \frac{|T_{fi}|^2}{T} . \tag{1.6.155}$$

Squaring (1.6.153)

$$
\begin{aligned}
W &= \lim_{T \to \infty} 2\pi \frac{|V_{fi}|^2}{T} \delta(E_f - E_i) \int_{-T/2}^{+T/2} dt \, e^{i(E_f - E_i)t} \\
&= \lim_{T \to \infty} 2\pi \frac{|V_{fi}|^2}{T} \delta(E_f - E_i) \int_{-T/2}^{+T/2} dt \\
&= 2\pi |V_{fi}|^2 \delta(E_f - E_i) . \tag{1.6.156}
\end{aligned}
$$

This equation can only be given physical meaning after integration over a set of initial and final states. In particle physics, we usually deal with situations where we begin with a specified initial state and end up in one set of final states. We denote with $\rho(E_f)$ the density of final states, i.e., $\rho(E_f)dE_f$ is

the number of states in the energy interval $(E_f, E_f + dE_f)$. Integration over this density, imposing energy conservation leads to the transition rate

$$
\begin{aligned}
W_{fi} &= 2\pi \int dE_f \; \rho(E_f) \; |V_{fi}|^2 \; \delta(E_f - E_i) \\
&= 2\pi |V_{fi}|^2 \; \rho(E_i) \,.
\end{aligned}
\tag{1.6.157}
$$

This formula, of great practical importance, is known as Fermi's golden rule.[16]

Clearly we can improve on the above approximation by inserting the result for $c_n(t)$, (1.6.149), in the right-hand side of (1.6.146)

$$
\dot{c}_f(t) = \cdots + (-i)^2 \left[\sum_n V_{ni} \int_{-T/2}^{t} dt' \, e^{i(E_n - E_i)t'} \right] V_{fn} \, e^{i(E_f - E_n)t}
\tag{1.6.158}
$$

where the dots represent the first order result. The correction to T_{fi} is

$$
T_{fi} = \cdots - \sum_n V_{fn} \, V_{ni} \int_{-\infty}^{\infty} dt \, e^{i(E_f - E_n)t} \int_{-\infty}^{t} dt' \, e^{i(E_n - E_i)t'} \,.
\tag{1.6.159}
$$

To make the integral over dt' meaningful, we must include a term in the exponent involving a small positive quantity ϵ which we let go to zero after integration

$$
\int_{-\infty}^{t} dt' \, e^{i(E_n - E_i - i\epsilon)t'} = i \frac{e^{i(E_n - E_i - i\epsilon)t}}{E_i - E_n + i\epsilon} \,.
\tag{1.6.160}
$$

The second order correction to T_{fi} is given by

$$
T_{fi} = \cdots - 2\pi i \sum_n \frac{V_{fn} V_{ni}}{E_i - E_n + i\epsilon} \delta(E_f - E_i) \,,
\tag{1.6.161}
$$

and the rate for the $i \to f$ transition is given by (1.6.157) with the replacement

$$
V_{fi} \to V_{fi} + \sum_n V_{fn} \frac{1}{E_i - E_n + i\epsilon} V_{ni} + \dots \,.
\tag{1.6.162}
$$

Equation (1.6.162) is the perturbation series for the amplitude with terms to first, second, ... order in V.

---

[16]E. Fermi, *Nuclear Physics*, (Chicago: University of Chicago Press, 1950).

Chapter 2

Symmetries and Invariants

2.1 Noether Theorem

The remarkable connection between symmetries and conservation laws are summarized in Noether's theorem: *any differentiable symmetry of the action of a physical system has a corresponding conservation law.*[1] This theorem grants observed selection rules in nature to be expressed directly in terms of symmetry requirements in the Lagrangian density. Under an infinitesimal displacement $x'_\mu = x_\mu + \epsilon_\mu$, the Lagrangian changes by the amount

$$\delta\mathscr{L} = \mathscr{L}' - \mathscr{L} = \epsilon_\mu\ \partial^\mu\mathscr{L}\ . \tag{2.1.1}$$

On the other hand, if $\mathscr{L}$ is translationally invariant, it has no explicit coordinate dependence, i.e., for systems described by n independent fields $\mathscr{L}(\phi_r, \partial^\mu\phi_r)$, where $r = 1, \ldots, n$. Hence,

$$\delta\mathscr{L} = \sum_r \left[\partial_{\phi_r}\mathscr{L}(\phi_r, \partial^\mu\phi_r)\ \delta\phi_r + \partial_{\partial^\mu\phi_r}\mathscr{L}(\phi_r, \partial^\mu\phi_r)\ \ \delta(\partial^\mu\phi_r)\right]\ , \tag{2.1.2}$$

where

$$\delta\phi_r = \phi_r(x + \epsilon) - \phi_r(x) = \epsilon_\nu\ \partial^\nu\phi_r(x)\ . \tag{2.1.3}$$

---

[1] E. Noether, Nachr. d. König. Gesellsch. d. Wiss. zu Göttingen, Math-phys. Klasse, 235 (1918) [arXiv:physics/0503066]. For a detailed discussion of this theorem, see e.g., E. L. Hill, Rev. Mod. Phys. **23**, 253 (1957).

Equating these two expressions and using Euler-Lagrange equation (1.2.3) gives

$$\epsilon_\mu \, \partial^\mu \mathscr{L}(\phi_r, \partial^\mu \phi_r) = \partial^\mu \left[\sum_r \partial_{\partial^\mu \phi_r} \mathscr{L}(\phi_r, \partial^\mu \phi_r) \, \epsilon_\nu \, \partial^\nu \phi_r \right] . \qquad (2.1.4)$$

Because this holds for arbitrary displacements ϵ_μ, we can write $\partial^\mu \mathfrak{J}_{\mu\nu} = 0$, where the energy-momentum stress tensor $\mathfrak{J}_{\mu\nu}$ is defined by

$$\mathfrak{J}_{\mu\nu} = -g_{\mu\nu} \, \mathscr{L} + \sum_r \partial_{\partial^\mu \phi_r} \mathscr{L} \, \partial_\nu \phi_r . \qquad (2.1.5)$$

From this differential conservation law one finds

$$P_\nu = \int d^3x \, \mathfrak{J}_{0\nu} = \int d^3x \left[\sum_r \pi_r \partial_\nu \phi_r - g_{0\nu} \, \mathscr{L} \right] \qquad (2.1.6)$$

and so $\partial^t P_\nu = 0$. We have already seen that $\mathfrak{J}_{00}$ is the Hamiltonian density

$$\mathfrak{J}_{00} = \sum_r \pi_r \, \dot{\phi}_r - \mathscr{L} = \mathscr{H} \qquad (2.1.7)$$

and

$$\int d^3x \, \mathfrak{J}_{00} = H . \qquad (2.1.8)$$

Thus, we can identify the operator P_ν as the conserved energy-momentum four-vector.

Similarly, we may construct the angular momentum constant of motion by considering an infinitesimal Lorentz transformation, (1.3.16). The practical test of Lorentz invariance is to make the replacement

$$\phi_r(x) \to S_{rs}^{-1}(\Lambda) \, \phi_s(x') \qquad (2.1.9)$$

in the equations of motion and to determine whether they take the same form in the prime coordinate system as they did in the unprimed system. Here, $S_{rs}(\Lambda)$ is a transformation matrix for the fields ϕ_r under the infinitesimal Lorentz transformation (1.3.16). We have already seen an example of this for the Dirac equation, where we recall from (1.5.66) and (1.5.68) that

$$S_{rs}(\Lambda) = \delta_{rs} + \frac{1}{8}[\gamma^\mu, \gamma^\nu]_{rs}\omega_{\mu\nu} . \qquad (2.1.10)$$

We now take over the test (2.1.10) into the Lagrangian theory and demand that the Lagrangian density be a Lorentz scalar and hence remain form invariant under the replacement (2.1.10), i.e.,

$$\mathscr{L}\left(S_{sr}^{-1}\phi_s(x'), \partial^\mu S_{rs}^{-1}\phi_s(x')\right) = \mathscr{L}\left(\phi_r(x'), \partial^{\mu'}\phi_r(x')\right) . \qquad (2.1.11)$$

This will guarantee the form invariance of the equations of motion, which are derived from $\mathscr{L}$ by an invariant action principle. For an infinitesimal transformation, we write

$$
\begin{aligned}
\delta\phi_r(x) &= S_{rs}^{-1}(\Lambda)\phi_s(x') - \phi_r(x) \\
&= \phi_r(x') - \phi_r(x) + \frac{i}{2}\omega_{\mu\nu}\Sigma_{rs}^{\mu\nu}\phi_s .
\end{aligned}
\qquad (2.1.12)
$$

Expanding (2.1.11) about x we find, using the Euler-Lagrange equation,

$$\mathscr{L}(x') - \mathscr{L}(x) = \omega^{\mu\nu}x_\nu\,\partial_\mu\mathscr{L} = \partial_\mu[\partial_{\partial_\mu\phi_r}\mathscr{L}\,\delta\phi_r] , \qquad (2.1.13)$$

Eqs. (2.1.12) and (2.1.13) lead to the conservation law $\partial_\mu\mathfrak{M}^{\mu\nu\lambda} = 0$, where

$$
\begin{aligned}
\partial_\mu\mathfrak{M}^{\mu\nu\lambda} &= \partial_\mu\left\{\left(x^\lambda g^{\mu\nu} - x^\nu g^{\mu\lambda}\right)\mathscr{L} + \partial_{\partial_\mu\phi_r}\mathscr{L}\left[\left(x^\nu\partial^\lambda - x^\lambda\partial^\nu\right)\phi_r - i\sigma_{rs}^{\nu\lambda}\phi_s\right]\right\} \\
&= \partial_\mu\left[\left(x^\nu\mathfrak{J}^{\mu\lambda} - x^\lambda\mathfrak{J}^{\mu\nu}\right) - i\partial_{\partial_\mu\phi_r}\mathscr{L}\Sigma_{rs}^{\nu\lambda}\phi_s\right] .
\end{aligned}
\qquad (2.1.14)
$$

The conserved angular momentum is

$$
\begin{aligned}
\mathscr{M}^{\nu\lambda} &= \int d^3x\,\mathfrak{M}^{0\nu\lambda} \\
&= \int d^3x\,\left[\left(x^\nu\mathfrak{J}^{0\lambda} - x^\lambda\mathfrak{J}^{0\nu}\right) - i\pi_r\,\Sigma_{rs}^{\nu\lambda}\,\phi_s\right] \\
&= i[x^\mu\partial^\nu - \xi^\nu\partial^\mu]\phi_r + \Sigma_{rs}^{\mu\nu}\,\phi_s(x)
\end{aligned}
\qquad (2.1.15)
$$

so that $\partial_t\mathscr{M}^{\nu\lambda} = 0$.

Going over now to the QFT, we must ask whether we may still apply the classical result that, a scalar $\mathscr{L}$ guarantees Lorentz invariance of the theory and, via the Noether theorem, leads to the energy-momentum and angular-momentum constants of motion. In QFT the field amplitudes $\phi(r)$ become operators upon state functions, or vectors, in a Hilbert space. If we impose the requirements of Lorentz covariance on the *matrix elements* of

45

these operators, which represent physical observables as viewed in two different Lorentz frames, we come to certain operator restrictions on the $\phi_r(x)$. For a QFT a scalar $\mathscr{L}$ is not sufficient to guarantee relativistic invariance, but we must also verify that the fields obey these operator requirements. For most field theories generally discussed in physics the Lagrangian approach and Noether's theorem can be carried over directly to the quantum domain without difficulty. In particular, the P_μ and $\mathscr{M}_{\mu\nu}$ obtained through Noether's procedure in (2.1.6) and (2.1.15) are found to be satisfactory.

2.2   Gauge Invariance

The importance of the connection between *symmetry* properties and the invariance of physical quantities can hardly be overemphasized. Homogeneity and isotropy of spacetime imply the Lagrangian is invariant under time displacements, is unaffected by the translation of the entire system, and does not change if the system is rotated an infinitesimal angle. We have seen that these particular measurable properties of spacetime lead to the conservation of energy, momentum, and angular momentum. These, however, are only three of various invariant symmetries in nature which are regarded as cornerstones of particle physics. In this section, we will focus attention on conservation laws associated with "internal" symmetry transformations that do not mix fields with internal spacetime properties, i.e., transformations that commute with the spacetime components of the wave function.

2.2.1   Maxwell-Dirac Lagrangian

We have seen that a free fermion of mass m is described by a complex field $\psi(x)$. Inspection of Dirac's Lagrangian (1.5.80) shows that $\psi(x)$ is invariant under the global phase transformation

$$\psi(x) \rightarrow \exp(i\alpha)\ \psi(x), \tag{2.2.16}$$

where the single parameter α could run continuously over real numbers. Now, Noether's theorem implies the existance of a conserved current. To see this, we need to study the invariance of $\mathscr{L}$ under infinitesimal $U(1)$

transformations $\psi \to (1 + i\alpha)\psi$. Invariance requires the Lagrangian to be unchanged, that is,

$$
\begin{aligned}
\delta\mathscr{L} &= \partial_\psi\mathscr{L}\ \delta\psi + \partial_{\partial_\mu\psi}\mathscr{L}\ \delta(\partial_\mu\psi) + \delta\bar{\psi}\ \partial_{\bar{\psi}}\mathscr{L} + \delta(\partial_\mu\bar{\psi})\ \partial_{\partial_\mu\bar{\psi}}\mathscr{L} \\
&= \partial_\psi\mathscr{L}\ (i\alpha\psi) + \partial_{\partial_\mu\psi}\mathscr{L}\ (i\alpha\partial_\mu\psi) + \ldots \\
&= i\alpha\left[\partial_\psi\mathscr{L} - \partial_\mu(\partial_{\partial_\mu\psi}\mathscr{L})\right]\psi + i\alpha\partial_\mu(\partial_{\partial_\mu\psi}\mathscr{L}\ \psi) + \ldots \\
&= 0\ .
\end{aligned}
\tag{2.2.17}
$$

The term in square brackets vanishes by virtue of the Euler-Lagrange equation, (1.2.3), for ψ (and similarly for $\bar{\psi}$) and so (2.2.17) reduces to the form of an equation for a conserved current $\partial_\mu j^\mu = 0$, where

$$
j^\mu = -\frac{i}{2}\left(\partial_{\partial_\mu\psi}\mathscr{L}\ \psi - \bar{\psi}\ \partial_{\partial_\mu\bar{\psi}}\mathscr{L}\right) = \bar{\psi}\gamma^\mu\psi\ ,
\tag{2.2.18}
$$

using (1.5.80). It follows that the charge $Q = \int d^3x\ j^0$ must be a conserved quantity because of the $U(1)$ phase invariance.[2]

A global phase transformation is surely not the most general invariance, for it would be more convenient to have independent phase changes at each point. We thus generalize Eq. (2.2.16) to include local phase transformations

$$
\psi \to \psi' \equiv \exp[i\alpha(x)]\ \psi\ .
\tag{2.2.19}
$$

The derivative $\partial_\mu\alpha(x)$ breaks the invariance of Dirac's Lagrangian, which acquires an additional phase change at each point

$$
\delta\mathscr{L}_{\text{Dirac}} = \overline{\psi}\ i\gamma^\mu\left[i\partial_\mu\alpha(x)\right]\psi\ .
\tag{2.2.20}
$$

The Lagrangian (1.5.80) is not invariant under *local gauge transformations*, but if we seek a modified derivative, $\partial_\mu \to D_\mu \equiv \partial_\mu + ieA_\mu$, which transforms covariantly under phase transformations, $D_\mu\psi \to e^{i\alpha(x)}D_\mu\psi$, then local gauge invariance can be restored

$$
\begin{aligned}
\mathscr{L} &= \overline{\psi}\ (i\,\slashed{D} - m)\ \psi \\
&= \overline{\psi}\ (i\,\slashed{\partial} - m)\ \psi - e\,\overline{\psi}\ \slashed{A}(x)\ \psi\ .
\end{aligned}
\tag{2.2.21}
$$

---

[2]The spinor operators ψ and $\psi^\dagger$ satisfy the equal-time anticommutation relations $\{\psi_a(x), \psi_b^\dagger(y)\} = \delta^3(x - y)\ \delta_{ab}$; $\{\psi_a(x), \psi_b(y)\} = \{\psi_a^\dagger(x), \psi_b^\dagger(y)\} = 0$.

Namely, if $\psi \to \psi'$ and $A \to A'$, we have

$$
\begin{aligned}
\mathscr{L}' &= \overline{\psi}' \, (i \, \slashed{\partial} - m) \, \psi' - e \, \overline{\psi}' \, \slashed{A}' \, \psi' \\
&= \overline{\psi} \, (i \, \slashed{\partial} - m) \, \psi - \overline{\psi} \, [\slashed{\partial}\alpha(x)] \, \psi - e \, \overline{\psi}\slashed{A}' \, \psi \,,
\end{aligned}
\qquad (2.2.22)
$$

and we can ensure $\mathscr{L} = \mathscr{L}'$ if we demand the *vector potential* A_μ to change by a total divergence

$$
A'_\mu(x) = A_\mu(x) - \frac{1}{e}\partial_\mu\alpha(x)\,,
\qquad (2.2.23)
$$

which does not change the electromagnetic field strength, $F_{\mu\nu}$. In other words, by demanding local phase invariance in ψ, we must introduce a gauge field A_μ that couples to fermions of charge e in exactly the same way as the photon field.

An alternative approach to visualize the consequences of local gauge invariance is as follows. The wave function of a particle (of charge e) as it moves in spacetime from point A to point B undergoes a phase change

$$
\Phi_{AB} = \exp\left(-ie \int_A^B A_\mu(x)dx^\mu\right)\,,
\qquad (2.2.24)
$$

where $-eA_\mu(x)$ parametrizes the infinitesimal phase change in $(x^\mu, x^\mu + dx^\mu)$.[3] The integral in (2.2.24) for points at finite separation is known as a Wilson line.[4] A crucial property of the Wilson line is that it depends on the path taken and therefore Φ_{AB} is not uniquely defined. However, if C is a closed path that returns to A (i.e., a Wilson loop)

$$
\Phi_C = \exp\left(-ie \oint A_\mu(x)dx^\mu\right)\,,
\qquad (2.2.25)
$$

the phase becomes a nontrivial function of A_μ, that is by construction locally gauge invariant. (Note that for a Wilson loop, any change in the contribution to Φ_C from the integral up to a given point x^0_μ will be compensated by an

---

[3]C. N. Yang, Phys. Rev. Lett. **33**, 445 (1974).

[4]K. G. Wilson, Phys. Rev. D **10**, 2445 (1974). This path-dependent phase was used long before Wilson's work, in Schwinger's early papers of QED, and in Y. Aharonov and D. Bohm, Phys. Rev. **115**, 485 (1959).

equal and opposite contribution from the integral departing from x_μ^0.) To verify this claim, we express the closed path integral (2.2.25) as a surface integral via Stokes' theorem

$$\oint A_\mu(x) dx^\mu = \int F_{\mu\nu}(x) d\sigma^{\mu\nu} \quad , \tag{2.2.26}$$

where $d\sigma^{\mu\nu}$ is an element of surface area. One can now check by inspection that the Wilson loop is invariant under changes (2.2.23) of $A_\mu(x)$ by a total divergence.[5]

To obtain the QED Lagrangian we need to include the kinetic term (1.2.5), which accounts for the energy and momentum of free electromagnetic fields.

$$\mathscr{L} = -\frac{1}{4} F_{\mu\nu} F^{\mu\nu} + \overline{\psi}(i \not\partial - m)\psi - e\overline{\psi} \not A \psi \ . \tag{2.2.27}$$

If the electromagnetic current is defined as $ej_\mu \equiv e\overline{\psi}\gamma_\mu\psi$, this Lagrangian leads to Maxwell's equations (1.2.4). The local phase changes (2.2.19) form a $U(1)$ group of transformations. Since such transformations commute with one another, the group is said to be *Abelian*. Electrodynamics is thus an *Abelian gauge theory*.

2.2.2   Yang-Mills Lagrangian

If by imposing local phase invariance on Dirac's Lagrangian we are lead to the interacting theory of QED, then in an analogous way one can hope to infer the structure of other interesting theories by starting from more general fundamental symmetries. Pioneer work by Yang and Mills considered that a charged particle moving along in spacetime could undergo not only phase changes, but also changes of identity (say, a quark can change its color from red to blue or change its flavor from u to d).[6] Such a kind of transformation requires a generalization of local phase rotation invariance to invariance under any continuous symmetry group. The coefficient eA_μ of the infinitesimal displacement dx_μ should be replaced by a $n \times n$ matrix

---

[5]The gauge invariance of $F_{\mu\nu}$ can also be seen through the commutator of the covariant derivative, $[D_\mu, D_\nu] = ieF_{\mu\nu}$.

[6]C. N. Yang and R. L. Mills, Phys. Rev. **96**, 191 (1954).

$-g\mathbf{A}_\mu(x) \equiv -gA^a_\mu(x)\mathbf{t}_a$ acting in the n-dimensional space of the particle's degrees of freedom, where g is the coupling constant. Here, the $\mathbf{t}_a$ define a linearly independent basis set of matrices for such transformations, whereas the A^a_μ are their coefficients.

Both the Wilson line and the Wilson loop can be generalized to Yang-Mills transformations. However, careful must be taken as some subtleties arise because the integral in the exponent now contains the matrices $\mathbf{A}_\mu(x)$ which do not necessarily commute with one another at different points of spacetime, and consequently a *path-ordering* $(P\{\})$ is needed. Hence, we introuce a parameter s of the path P, which runs from 0 at $x = A$ to 1 at $x = B$. The Wilson line is then defined as the power series expansion of the exponential with the matrices in each term ordered so that higher values of s stand to the left

$$\mathbf{\Phi}_{AB} = P\left\{\exp\left(ig\int_0^1 ds\, \frac{dx^\mu}{ds}\, \mathbf{A}_\mu(x)\right)\right\} \ . \tag{2.2.28}$$

If the basis matrices $\mathbf{t}_a$ do not commute with one another, the theory is said to be *non-Abelian*.

Now, to ensure that changes in phase or identity conserve probability, we demand $\mathbf{\Phi}_{AB}$ be a unitary matrix, i.e., $\mathbf{\Phi}^\dagger_{AB}\mathbf{\Phi}_{AB} = \mathbb{I}$. If we wish to separate out pure phase changes (in which $\mathbf{A}_\mu(x)$ is a multiple of the unit matrix) from the remaining transformations, one may consider only transformations such that $\det(\mathbf{\Phi}_{AB}) = 1$. The last condition becomes evident if we note that near the identity any unitary matrix can be expanded in terms of Hermitian generators of $SU(N)$, and hence for infinitesimal separation between A and B we can write

$$\mathbf{\Phi}_{AB} = \mathbb{I} + i\epsilon(gA^a_\mu\mathbf{t}_a) + \mathcal{O}(\epsilon^2) \ , \tag{2.2.29}$$

or equivalently

$$\begin{aligned}\mathbb{I} &= \mathbf{\Phi}^\dagger_{AB}\mathbf{\Phi}_{AB} \\ &= \mathbb{I} + ig\epsilon[\mathbf{A}_\mu(x)^\dagger - \mathbf{A}_\mu(x)] + \mathcal{O}(\epsilon^2)\,. \end{aligned} \tag{2.2.30}$$

This shows that we must consider only transformations such that

$$\begin{aligned}\det\left(e^{ig\,A^a_\mu\,\mathbf{t}_a}\right) &= e^{ig\,A^a_\mu\,\mathrm{Tr}(\mathbf{t}_a)} \\ &= 1\,, \end{aligned} \tag{2.2.31}$$

50

corresponding to *traceless* $\mathbf{A}_\mu(x)$. All in all, the $n \times n$ basis matrices $\mathbf{t}_a$ must be Hermitian and traceless. There are $n^2 - 1$ of them, corresponding to the number of independent $SU(N)$ generators. The basis matrices satisfy the commutation relations

$$[\mathbf{t}_i, \mathbf{t}_j] = ic_{ijk}\mathbf{t}_k \ , \qquad (2.2.32)$$

where the c_{ijk} are *structure constants* characterizing the group. In the fundamental representation of $SU(2)$, the generators are proportional to Pauli matrices ($\mathbf{t}_i = \sigma_i/2$), and the structure constants are defined by the Levi-Civita symbol ($c_{ijk} = \epsilon_{ijk}$). The generators of $SU(3)$ in the fundamental representation are $\mathbf{t}_i = \lambda_i/2$, where $\lambda_i/2$ are the Gell-Mann matrices normalized such that Tr $(\lambda_i \lambda_j) = 2\delta_{ij}$.[7] The $SU(3)$ structure constants $c_{ijk} = f_{ijk}$ are fully antisymmetric under interchange of any pair of indices and the non-vanishing values are permutations of $f_{123} = 1$, $f_{458} = f_{678} = \frac{\sqrt{3}}{2}$, $f_{147} = f_{165} = f_{246} = f_{257} = f_{345} = f_{376} = \frac{1}{2}$. (In the fundamental representation Tr $\mathbf{t}_i \mathbf{t}_j = \delta_{ij}/2$.)

Next, by considering an infinitesimal closed-path transformation analogous to (2.2.25), but for matrices $\mathbf{A}_\mu(x)$ that do not commute with one another, we write the field-strength tensor, $\mathbf{F}_{\mu\nu} = F^a_{\mu\nu}\mathbf{t}_a$, for a non-abelian transformation:

$$\mathbf{F}_{\mu\nu} = \partial_\mu \mathbf{A}_\nu - \partial_\nu \mathbf{A}_\nu - ig[\mathbf{A}_\mu, \mathbf{A}_\nu] \, , \qquad (2.2.33)$$

or equivalently,

$$F^i_{\mu\nu} = \partial_\mu A^i_\nu - \partial_\nu A^i_\mu + gc_{ijk}A^j_\mu A^k_\nu \ . \qquad (2.2.34)$$

An alternative way to introduce non-Abelian gauge fields is to demand that, by analogy with (2.2.16), a theory involving fermions ψ be invariant under local transformations,

$$\psi(x) \to \psi'(x) = V(x)\psi(x) \equiv \exp\left[i\alpha_a(x)\boldsymbol{t}^a\right]\psi(x) \, , \qquad (2.2.35)$$

where V is an arbitrary unitary matrix ($V^\dagger V = \mathbb{1}$) which we show parametrized by its general form. A summation over the repeated suffix a is implied.

Duplicating the preceding discussion for $U(1)$ gauge group, we demand

---

[7]M. Gell-Mann, Phys. Rev. **125**, 1067 (1962).

$\mathscr{L} \to \mathscr{L}'$, where

$$
\begin{aligned}
\mathscr{L}' &\equiv \overline{\psi}'(i\,\not{\partial} - m)\psi' \\
&= \overline{\psi}V^{\dagger}(i\,\not{\partial} - m)V\psi \\
&= \overline{\psi}(i\,\not{\partial} - m)\psi + i\psi V^{\dagger}\gamma^{\mu}(\partial_{\mu}V)\psi \ .
\end{aligned} \tag{2.2.36}
$$

The last term, as in the abelian case, spoils the invariance of $\mathscr{L}$. As before, it can be compensated if we replace $\partial_{\mu} \to \mathbf{D}_{\mu} \equiv \partial_{\mu} - ig\mathbf{A}_{\mu}(x)$. Namely, under the transformation (2.2.35) the Lagrangian

$$
\mathscr{L} = \overline{\psi}(i\,\not{\mathbf{D}} - m)\psi \tag{2.2.37}
$$

becomes

$$
\begin{aligned}
\mathscr{L}' &\equiv \overline{\psi}'(i\,\not{\mathbf{D}}' - m)\psi' \\
&= \overline{\psi}V^{\dagger}(i\,\not{\partial} + g\,\not{\mathbf{A}}' - m)V\psi \\
&= \mathscr{L} + \overline{\psi}[g(V^{\dagger}\,\not{\mathbf{A}}'V - \not{\mathbf{A}}) + iV^{\dagger}(\not{\partial}V)]\psi \ ,
\end{aligned} \tag{2.2.38}
$$

which is equal to $\mathscr{L}$ if we take

$$
\mathbf{A}'_{\mu} = V\mathbf{A}_{\mu}V^{\dagger} - \frac{i}{g}(\partial_{\mu}V)V^{\dagger} \ . \tag{2.2.39}
$$

The covariant derivative acting on ψ transforms in the same way as ψ itself under a gauge transformation: $\mathbf{D}_{\mu}\psi \to \mathbf{D}'_{\mu}\psi' = V\mathbf{D}_{\mu}\psi$. The field strength $\mathbf{F}_{\mu\nu}$ transforms as $\mathbf{F}_{\mu\nu} \to \mathbf{F}'_{\mu\nu} = V\mathbf{F}_{\mu\nu}V^{\dagger}$. As in the abelian case, it can be computed via $[\boldsymbol{D}_{\mu}, \boldsymbol{D}_{\nu}] = -ig\mathbf{F}_{\mu\nu}$; both sides transform as $V(\ )V^{\dagger}$ under a local gauge transformation.

To obtain propagating gauge fields, we follow the steps of QED and add a kinetic term, $-(1/4)F^{i}_{\mu\nu}F^{i\mu\nu}$ to the Lagrangian. After reminding the reader the representation $\mathbf{F}_{\mu\nu} = F^{i}_{\mu\nu}$ written for gauge group generators normalized such that $\text{Tr}(\mathbf{t}_{i}\mathbf{t}_{j}) = \delta_{ij}/2$, we are ready to write down the full Yang-Mills Lagrangian for gauge fields interacting with matter fields

$$
\mathscr{L} = -\tfrac{1}{2}\text{Tr}(\mathbf{F}_{\mu\nu}\mathbf{F}^{\mu\nu}) + \overline{\psi}(i\,\not{\mathbf{D}} - m)\psi \ . \tag{2.2.40}
$$

The interaction of a gauge field with fermions corresponds to a term in the interaction Lagrangian $\Delta\mathscr{L} = g\overline{\psi}(x)\gamma^{\mu}\mathbf{A}_{\mu}(x)\psi(x)$. The $[\mathbf{A}_{\mu}, \mathbf{A}_{\nu}]$ term in

$\mathbf{F}_{\mu\nu}$ leads to self-interactions of non-Abelian gauge fields, arising solely from the kinetic term. They have no analogue in QED and arise on account of the non-abelian character of the gauge group, yielding three- and four-field vertices of the form

$$\Delta\mathscr{L}_K^{(3)} = (\partial_\mu A_\nu^i)gc_{ijk}A^{\mu j}A^{\nu k} \tag{2.2.41}$$

and

$$\Delta\mathscr{L}_K^{(4)} = -\tfrac{g^2}{4}c_{ijk}c_{imn}A^{\mu j}A^{\nu k}A_\mu^m A_\nu^n \ , \tag{2.2.42}$$

respectively. These self-interactions are a paramount property of non-Abelian gauge theories and drive the remarkable *asymptotic freedom* of QCD, which leads to its becoming weaker at short distances allowing the application of perturbation theory.

2.2.3 Isospin

Isospin arises because the nucleon may be view as having an internal degree of freedom with two allowed states, the proton and the neutron, which the nuclear interaction does not distinguish.[8] Consider the description of the two-nucleon system. Each nucleon has spin $\frac{1}{2}$ (with spin states $\uparrow$ and $\downarrow$), and so following the rules for the addition of angular momenta, the composite system may have total spin $S = 1$ or $S = 0$. The composition of these spin triplet and spin singlet states is

$$\begin{cases} |S = 1, M_s = 1\rangle = \uparrow\uparrow \\ |S = 1, M_s = 0\rangle = \sqrt{\tfrac{1}{2}}(\uparrow\downarrow + \downarrow\uparrow) \\ |S = 1, M_s = -1\rangle = \downarrow\downarrow \\ |S = 0, M_S = 0\rangle = \sqrt{\tfrac{1}{2}}(\uparrow\downarrow - \downarrow\uparrow) \ . \end{cases} \tag{2.2.43}$$

Each nucleon is similarly postulated to have isospin $T = \frac{1}{2}$, with $T_3 = \pm\frac{1}{2}$ for protons and neutrons respectively. The $T = 1$ and $T = 0$ states of the

---

[8]J. M. Blatt and V. F. Weisskopf, *Theoretical Nuclear Physics*, (Wiley, New York, 1952)

nucleon-nucleon system can be constructed in exact analogy to spin

$$
\left\{
\begin{aligned}
|T = 1, T_3 = 1\rangle &= \psi_p^{(1)} \psi_p^{(2)} \\
|T = 1, T_3 = 0\rangle &= \sqrt{\tfrac{1}{2}}(\psi_p^{(1)} \psi_n^{(2)} + \psi_n^{(1)} \psi_p^{(2)}) \\
|T = 1, T_3 = -1\rangle &= \psi_n^{(1)} \psi_n^{(2)}
\end{aligned}
\right. \tag{2.2.44}
$$

$$
|T = 0, T_3 = 0\rangle = \sqrt{\tfrac{1}{2}}(\psi_p^{(1)} \psi_n^{(2)} - \psi_n^{(1)} \psi_p^{(2)}) \, .
$$

In general, the most positively charged particle is chosen to have the maximum value of T_3. The nucleon field operators will transform according to

$$
U \begin{pmatrix} \psi_p(x) \\ \psi_n(x) \end{pmatrix} U^{-1} = \begin{pmatrix} u_{11} & u_{12} \\ u_{21} & u_{22} \end{pmatrix} \begin{pmatrix} \psi_p(x) \\ \psi_n(x) \end{pmatrix} \equiv \mathscr{U} \begin{pmatrix} \psi_p(x) \\ \psi_n(x) \end{pmatrix} . \tag{2.2.45}
$$

The preservation of the commutation relations requires that the 2×2 matrix $\mathscr{U}$ be unitary. Such a 2×2 unitary matrix is characterized by four parameters; when the common phase factor is taken out, we have three parameters, and a conventional way of writing a general form for U is (ommiting the phase factor)

$$
\mathscr{U} = e^{(i/2)\boldsymbol{\alpha} \cdot \boldsymbol{\tau}} \tag{2.2.46}
$$

where the three traceless hermitian canonical 2×2 matrices

$$
\tau_1 = \begin{pmatrix} 0 & 1 \\ 1 & 0 \end{pmatrix}, \quad \tau_2 = \begin{pmatrix} 0 & -i \\ i & 0 \end{pmatrix}, \quad \tau_3 = \begin{pmatrix} 1 & 0 \\ 0 & -1 \end{pmatrix} \tag{2.2.47}
$$

are just the Pauli spin matrices. The close similarity between (2.2.45) and the way in which we would express rotational invariance[9] suggests a way of characterizing the invariance. We will speak of an invariance under rotations in an "internal" space.

The isospin T is the analog of the angular momentum

$$
U = e^{i\boldsymbol{\alpha} \cdot \boldsymbol{T}} \, . \tag{2.2.48}
$$

The rotational invariance implies that the isospin is conserved. For an infinitesimal rotation, (2.2.45) reads

$$
\psi(x) + i\alpha_i[T_i, \psi(x)] = \psi(x) + \tfrac{1}{2}i\alpha_i \tau_i \, \psi(x) \, ,
$$

---

[9]The major difference is that in (2.2.45) the spatial coordinates are not involved.

i.e.,

$$[T_i, \psi(x)] = \frac{1}{2}\tau_i\psi(x) \tag{2.2.49}$$

where we represent $\begin{pmatrix} \psi_p(x) \\ \psi_n(x) \end{pmatrix}$ by $\psi(x)$. It is easily seen that these relations are satisfied by

$$\boldsymbol{T} = \frac{1}{2}\int d^3x\,\psi^\dagger(x)\,\boldsymbol{\tau}\,\psi(x)\,. \tag{2.2.50}$$

Note that

$$T_3 = \frac{1}{2}\int d^3x\,[\psi_p^\dagger(x)\,\psi_p(x) - \psi_n^\dagger(x)\,\psi_n(x)]\,. \tag{2.2.51}$$

Hence, the charge operator for nucleons Q may be written as

$$Q = \int d^3x\,\psi_p^\dagger(x)\,\psi_p(x) = \int d^3x\,\psi^\dagger(x)\,\tfrac{1+\tau_3}{2}\,\psi(x)\,. \tag{2.2.52}$$

We may introduce the baryon-number operator N_B by the definition

$$N_B = \int d^3x\,[\psi_p^\dagger(x)\psi_p(x) + \psi_n^\dagger(x)\psi_n(x) + \ldots]\,, \tag{2.2.53}$$

where the extra terms, not written down, are similar contributions from other fields carrying baryon number. Therefore, if we consider only protons and neutrons,

$$Q = \tfrac{1}{2}N_B + T_3\,. \tag{2.2.54}$$

It follows from the easily derived commutation relations

$$[T_i,\ T_j] = i\epsilon_{ijk}T_k \tag{2.2.55}$$

that

$$[Q,\ T_i] \neq 0 \quad i = 1, 2 \tag{2.2.56}$$

so that charge violates isospin conservation.

The construction of antiparticle isospin multiplets requires care. It is well illustrated by a simple example. Consider a particular isospin transformation of the nucleon doublet, a rotation through π about the 2-axis. We obtain

$$\begin{pmatrix} \psi_p' \\ \psi_n' \end{pmatrix} = e^{-i\pi(\tau_2/2)}\begin{pmatrix} \psi_p \\ \psi_n \end{pmatrix} = -i\tau_2\begin{pmatrix} \psi_p \\ \psi_n \end{pmatrix} = \begin{pmatrix} 0 & -1 \\ 1 & 0 \end{pmatrix}\begin{pmatrix} \psi_p \\ \psi_n \end{pmatrix}\,. \tag{2.2.57}$$

We define antinucleon states using the particle-antiparticle conjugation operator C, $C\psi_p = \psi_{\bar{p}}$, $C\psi_n = \psi_{\bar{n}}$. Applying C to (2.2.57) therefore gives

$$\begin{pmatrix} \psi'_{\bar{p}} \\ \psi'_{\bar{n}} \end{pmatrix} = \begin{pmatrix} 0 & -1 \\ 1 & 0 \end{pmatrix} \begin{pmatrix} \psi_{\bar{p}} \\ \psi_{\bar{n}} \end{pmatrix}. \tag{2.2.58}$$

However, we want the antiparticle doublet to transform in exactly the same way as the particle doublet. We must therefore make two changes. First we must reorder the doublet so that the most positively chargeed particle has $T_3 = +\frac{1}{2}$ and then we must introduce a minus sign to keep the matrix transformation identical to (2.2.57). We obtain

$$\begin{pmatrix} -\psi'_{\bar{n}} \\ \psi'_{\bar{p}} \end{pmatrix} = \begin{pmatrix} 0 & -1 \\ 1 & 0 \end{pmatrix} \begin{pmatrix} -\psi_{\bar{n}} \\ \psi_{\bar{p}} \end{pmatrix}. \tag{2.2.59}$$

That is, the antiparticle doublet $(-\psi_{\bar{n}}, \psi_{\bar{p}})$ transforms exactly as the particle doublet (ψ_p, ψ_n). This is a special property of $SU(2)$; it is not possible, for example, to arrange an $SU(3)$ triplet of antiparticles so that it transforms as the particle triplet. A composite system of a nucleon-antinucleon pair has isospin states

$$\begin{cases} |T = 1, T_3 = 1\rangle = -\psi_p \psi_{\bar{n}} \\ |T = 1, T_3 = 0\rangle = \sqrt{\frac{1}{2}}(\psi_p \psi_{\bar{p}} - \psi_n \psi_{\bar{n}}) \\ |T = 1, T_3 = -1\rangle = \psi_n \psi_{\bar{p}} \end{cases} \tag{2.2.60}$$
$$|T = 0, T_3 = 0\rangle = \sqrt{\frac{1}{2}}(\psi_p \psi_{\bar{p}} + \psi_n \psi_{\bar{n}}) \ .$$

2.3 Higgs Mechanism

In the preceding sections much importance has been attached to symmetry principles. We have discussed the connection between exact symmetries and conservation laws and have found that the proviso of a local gauge invariance can serve as a dynamical principle to captain the assembly of interacting field theories. However, in several areas we are still far from where we need to be. For example, the gauge principle has lead us to theories in which all the interactions are mediated by massless bosons, while we have already mentioned

that the carriers of the weak force are massive. Moreover, there are many situations in physics in which the exact symmetry of an interaction is hidden by the circumstances. The canonical example is that of a Heisenberg ferromagnet, an infinite crystalline array of spin-$\frac{1}{2}$ magnetic dipoles. Below the Curie temperature T_C the ground state is a completely ordered configuration in which all dipoles are aligned in some arbitrary direction, belying the rotation invariance of the underlying interaction. It is thus of interest to learn how to deal with symmetries that are not manifest, perhaps in the hope of evading the conclusion that interactions must be mediated by massless gauge bosons.

Let us first elaborate on an intuitive description of *hidden symmetry*. In the infinite ferromagnet mentioned above, the nearest-neighbor interaction between spins (or magnetic dipole moments) is invariant under the group of spatial rotations $SO(3)$. In the disordered paramagnetic phase, which exists above T_C, the medium displays an exact symmetry in the absence of an external field. The spontaneous magnetization of the system is zero and there is no preferred direction in space. This means the $SO(3)$ invariance is manifest. A priviliged direction may be selected by imposing an external magnetic field, which tends to align the spins in the material. The $SO(3)$ symmetry is hence broken down to an axial $SO(2)$ symmetry of rotations around the external field direction. The full symmetry is restored when the external field is turned off. For temperatures below T_C, when the system is in the ordered ferromagnetic phase, the situation is rather different. In the absence of an external field, the configuration of lowest energy has non-zero spontaneous magnetization, because the nearest-neighbor force favors the parallel alignment of spins. In these circumstances the $SO(3)$ symmetry is said to be spontaneously broken down to $SO(2)$. The fact that the direction of the spontaneous magnetization is random and the fact that the measurable properties of the infinite ferromagnet do not depend upon its orientation are vestiges of the original $SO(3)$ symmetry. The ground state is thus infinitely degenerate. A particular direction for the spontaneous magnetization may be chosen by imposing an external field which breaks the $SO(3)$ symmetry explicitely. However, in contrast to the paramagnetic case the spontaneous magnetization does not return to zero when the external field is turned off. For the rotational invariance to be broken spontaneously, it is crucial that

the ferromagnet be infinite in extent, so that rotation from one degenerate ground state to another would require the impossible task of rotating an infinite number of elementary dipoles. All in all, spontaneous symmetry breaking can arise when the Lagrangian of a system possesses symmetries which do not however hold for the ground state of the system. The Higgs mechanism is a gauge theoretic realization of such spontaneous symmetry breaking.[10]

To deeply fathom the situation, let us now consider a simple world consisting just of scalar particles described by the Lagrangian

$$\mathscr{L} = \tfrac{1}{2} \left(\partial_\mu \phi \right) \left(\partial^\mu \phi \right) - V(\phi) \tag{2.3.61}$$

and study how the particle spectrum depends upon the effective potential $V(\phi)$. If the potential is an even functional of the scalar field, $V(\phi) = V(-\phi)$, then the Lagrangian (2.3.61) is invariant under the symmetry operation which replaces ϕ by $-\phi$. To explore possibilities, it is convenient to consider an explicit potential,

$$V(\phi) = \tfrac{1}{2} \mu^2 \phi^2 + \tfrac{1}{4} \lambda \phi^4 \ , \tag{2.3.62}$$

where λ is required to be positive so that the energy is bounded from below. Two qualitatively different cases, corresponding to manifest or spontaneously broken symmetry, may be distingusihed depending on the sign of the coefficient μ^2. If $\mu^2 > 0$, the potential has a unique minimum at $\phi = 0$ that corresponds to the ground state, i.e., the vacuum. This identification is perhaps most easily seen in the Hamiltonian formalism. Substituting (2.3.61) into (1.2.8) we obtain

$$\mathscr{H} = \frac{1}{2} \left[(\partial_0 \phi)^2 + \left(\vec{\nabla} \phi \right)^2 \right] + V(\phi) \, . \tag{2.3.63}$$

The state of lowest energy is thus seen to be one for which the value of the field ϕ is constant, which we denote by $\langle \phi \rangle_0$. The value of this constant is determined by the dynamics of the theory; it corresponds to the absolute minimum (or minima) of the potential $V(\phi)$. (We usually refer to $\langle \phi \rangle_0$ as the vacuum expectation value of the field ϕ.) For $\mu > 0$, the vacuum obeys

---

[10] P. W. Higgs, Phys. Rev. Lett. **13**, 508 (1964).

the reflection symmetry of the Lagrangian, with $\langle\phi\rangle_0 = 0$. The approximate form of the Lagrangian appropriate to study small oscillations around this minimum is that of a free particle with mass μ,

$$\mathscr{L} = \tfrac{1}{2}[(\partial_\mu\phi)(\partial^\mu\phi) - \mu^2\phi^2]\,. \tag{2.3.64}$$

The ϕ^4 term shows that the field is self-interacting, because the four-particle vertex exists with coupling λ. If $\mu^2 < 0$, the Lagrangian has a mass term of the wrong sign for the field ϕ and the potential has two minima. These minima satisfy $\phi(\mu^2 + \lambda\phi^2) = 0$, and are therefore at $\langle\phi\rangle_0 = \pm v$, with $v = \sqrt{-\mu^2/\lambda}$. (The extremum $\phi = 0$ does not correspond to the energy minimum.) The potential has two degenerate lowest energy states, either of which may be chosen to be the vacuum. Because of the parity invariance of the Lagrangian, the ensuing physical consequences must be independent of this choice. Nevertheless, we will see that whatever is our choice the symmetry of the theory is spontaneously broken: *the parity transformation $\phi \to -\phi$ is an invariant of the Lagrangian, but not of the vacuum state.* To this end, let us choose $\langle\phi\rangle_0 = +v$. Perturbative calculations should involve expansions around the classical minimum, we therefore write

$$\phi(x) = v + \eta(x)\,, \tag{2.3.65}$$

where $\eta(x)$ represents the quantum fluctuations about this minimum. Substituting (2.3.65) into (2.3.61), we obtain

$$\mathscr{L}' = \tfrac{1}{2}(\partial_\mu\eta)(\partial^\mu\eta) - \lambda v^2\eta^2 - \lambda v\eta^3 - \tfrac{1}{4}\lambda\eta^4 + \text{const.} \tag{2.3.66}$$

The field η has a mass term of the correct sign. Indeed, the relative sign of the η^2 term and the kinetic energy is negative. Identifying the first two terms of $\mathscr{L}'$ with (1.4.40) gives $m_\eta = \sqrt{2\lambda v^2} = \sqrt{-2\mu^2}$. The higher-order terms in η represent the interaction of the η field with itself.

Before proceeding, we pause to stress that the Lagrangian $\mathscr{L}$ of (2.3.61) [with (2.3.62)] and $\mathscr{L}'$ of (2.3.66) are completely equivalent. A transformation of the type (2.3.65) cannot change the physics. If we could solve the two Lagrangians exactly, they must yield identical physics. However, in QFT we are not able to perform such a calculation. Instead, we do perturbation theory and calculate the fluctuations around the minimum energy. Using $\mathscr{L}$, we

find out that the perturbation series does not converge because we are trying to expand about the unstable point $\phi = 0$. The correct way to proceed is to adopt $\mathscr{L}'$ and expand in η around the stable vacuum $\langle\phi\rangle_0 = +v$. In perturbation theory, $\mathscr{L}'$ provides the correct physical framework, whereas $\mathscr{L}$ does not. Therefore, the scalar particle (described by the in-principle-equivalent Lagrangians $\mathscr{L}$ and $\mathscr{L}'$) is massive.

To approach our destination of generating a mass for the gauge bosons, we duplicate the above procedure for a complex scalar field, $\phi = \frac{1}{\sqrt{2}}(\phi_1 + i\phi_2)$, with Lagrangian density

$$\mathscr{L} = (\partial_\mu\phi)^*(\partial^\mu\phi) - \mu^2\phi^*\phi - \lambda(\phi^*\phi)^2 \,, \tag{2.3.67}$$

which is invariant under the transformation $\phi \to e^{i\alpha}\phi$. That is $\mathscr{L}$ possesses a $U(1)$ global gauge symmetry. By considering $\lambda > 0$ and $\mu^2 < 0$, we rewrite (2.3.67) as

$$\mathscr{L} = \tfrac{1}{2}\left(\partial_\mu\phi_1\right)\left(\partial^\mu\phi_1\right) + \tfrac{1}{2}\left(\partial_\mu\phi_2\right)\left(\partial^\mu\phi_2\right) - \tfrac{1}{2}\mu^2(\phi_1^2+\phi_2^2) - \tfrac{1}{4}\lambda(\phi_1^2+\phi_2^2)^2 \,. \tag{2.3.68}$$

In this case, there is a circle of minima of the potential $V(\phi)$ in the ϕ_1-ϕ_2 plane of radius v such that $\phi_1^2 + \phi_2^2 = v^2$ with $v^2 = -\mu^2/\lambda$. As before, we translate the field ϕ to a minimum energy position, which without loss of generality we may take as the point $\phi_1 = v$ and $\phi_2 = 0$. We expand $\mathscr{L}$ around the vacuum in terms of fields η and ξ by substituting

$$\phi(x) = \sqrt{\tfrac{1}{2}}[v + \eta(x) + i\xi(x)] \tag{2.3.69}$$

into (2.3.67) and obtain

$$\mathscr{L}' = \tfrac{1}{2}(\partial_\mu\xi)^2 + \tfrac{1}{2}(\partial_\mu\eta)^2 + \mu^2\eta^2 + \text{const.} + \mathcal{O}(\eta^3, \xi^3) + \mathcal{O}(\eta^4, \xi^4)\,. \tag{2.3.70}$$

The third term has the form of a mass term $(-\tfrac{1}{2}m_\eta^2\eta^2)$ for the η field. Therefore, the η-mass is again $m_\eta = \sqrt{-2\mu^2}$. The first term in $\mathscr{L}'$ stands for the kinetic energy of ξ, but there is no corresponding mass term for the ξ field. In other words, the theory contains a massless scalar, so-called "Goldstone boson." Therefore, in attempting to generate a massive gauge boson we have encountered a problem: the spontaneously broken gauge theory seems to be plagued with its own massless scalar particle. Intuitively, it is easily seen
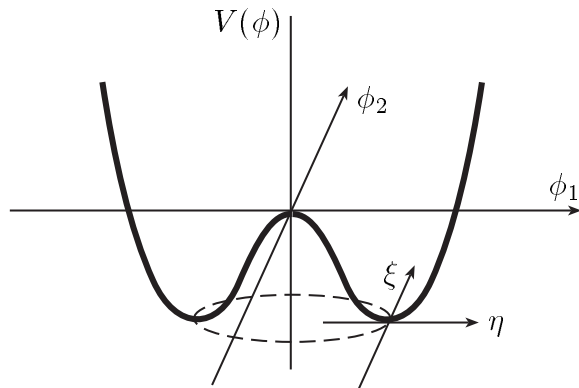
Figure 2.1: *The potential $V(\phi)$ for a complex scalar field, for the case $\mu^2 < 0$ and $\lambda > 0$.*

the reason for its presence. As shown in Fig. 2.1, the potential in the tangent ξ direction is flat, implying a massless mode; there is no resistance to excitations along the ξ-direction.

The Lagrangian (2.3.70) is a simple example of the Goldstone theorem, which states that in a spontaneous symmetry breaking the original symmetry is still present, but nature manages to camouflage the symmetry in such a way that its presence can be viewed only indirectly.[11] In the ferromagnet example, the analogue of our Goldstone boson is the long-range spin waves which are oscillations of the spin alignment.

The final step of this section is to study spontaneous symmetry breaking of a local $U(1)$ gauge symmetry. To this end, we must start with a Lagrangian that is invariant under a local $U(1)$ transformation $\phi(x) \to e^{i\alpha(x)}\phi(x)$. This is accomplished by replacing ∂_μ by a covariant derivative $D_\mu = \partial_\mu + ieA_\mu$, where the gauge field transforms as $A_\mu(x) \to A_\mu(x) - \partial_\mu\alpha(x)/e$. The gauge invariant Lagrangian is thus

$$\mathcal{L} = (\partial^\mu - ieA^\mu)\phi^*(\partial_\mu + ieA_\mu)\phi - \mu^2\phi^*\phi - \lambda(\phi^*\phi)^2 - \tfrac{1}{4}F_{\mu\nu}F^{\mu\nu}. \quad (2.3.71)$$

As usual there are two cases, depending upon the parameters of the effective potential. If $\mu^2 > 0$, (aside from the ϕ^4 self-interaction term) this is just

---

[11]J. Goldstone, Nuovo Cim. **19**, 154 (1961); J. Goldstone, A. Salam and S. Weinberg, Phys. Rev. **127**, 965 (1962).

the QED Lagrangian for a charged scalar particle of mass μ. The situation when $\mu^2 < 0$ is that of spontaneously broken symmetry and demands a closer analysis. On substituting (2.3.69), the Lagrangian (2.3.71) becomes

$$
\begin{aligned}
\mathscr{L}' \;=\;& \tfrac{1}{2}(\partial_\mu \xi)^2 + \tfrac{1}{2}(\partial_\mu \eta)^2 - v^2\lambda\eta^2 + \tfrac{1}{2}e^2 v^2 A_\mu A^\mu + ev A_\mu \partial^\mu \xi - \tfrac{1}{4}F_{\mu\nu}^2 \\
&+ \;\; \text{interaction terms} \; .
\end{aligned}
\tag{2.3.72}
$$

The particle spectrum of $\mathscr{L}'$ appears to be a massless Goldstone boson ξ, a massive scalar η, and a massive vector A_μ. Namely, from (2.3.72) we have $m_\xi = 0$, $m_\eta = \sqrt{2\lambda v^2}$, and $m_A = ev$. This implies that we have generated a mass for the gauge field, but we still are facing the problem of the ocurrence of the Goldstone boson. However, because of the presence of a term off-diagonal in the fields $A_\mu \partial^\mu \xi$, this time care must be taken in interpreting the Lagrangian (2.3.72). Actually, the particle spectrum we assigned before to $\mathscr{L}'$ must be incorrect. By giving mass to A_μ, we have clearly raised the polarization degrees of freedom from 2 to 3, because it can now have a longitudinal polarization. We deduce that the fields in $\mathscr{L}'$ do not all correspond to distinct particles. To find a gauge transformation which eliminates a field from the Lagrangian, we first note that to lowest order in ξ (2.3.69) can be rewritten as

$$
\phi \simeq \sqrt{\tfrac{1}{2}}(v + \eta)\, e^{i\xi/v} \; .
\tag{2.3.73}
$$

This suggests that we should substitute a different set of real fields H, θ, A_μ, where

$$
\phi \to \sqrt{\tfrac{1}{2}}\,[v + H(x)]e^{i\theta(x)/v} \;, \qquad A_\mu \to A_\mu - \frac{1}{ev}\,\partial_\mu \theta
$$

into the original Lagrangian (2.3.71). This is a particular choice of gauge, with $\theta(x)$ chosen that H is real. We therefore anticipate that the theory will be independent of θ. Actually, we have

$$
\begin{aligned}
\mathscr{L}'' \;=\;& \tfrac{1}{2}(\partial_\mu H)^2 - \lambda v^2 H^2 + \tfrac{1}{2}e^2 v^2 A_\mu^2 - \lambda v H^3 - \tfrac{1}{4}\lambda H^4 \\
&+ \;\; \tfrac{1}{2}e^2 A_\mu^2 H^2 + v e^2 A_\mu^2 H - \tfrac{1}{4}F_{\mu\nu}F^{\mu\nu} \; .
\end{aligned}
\tag{2.3.74}
$$

The Goldstone bosson is not actually present in the theory. In other words, the apparent extra degree of freedom is actually spurious, because it corresponds only to the freedom to make a gauge transformation. The Lagrangian

describes just two interacting massive particles, a vector gauge boson A_μ and a massive scalar H, usually referred to as a Higgs particle. The unwanted massless Goldstone boson has been turned into the longitudinal polarization of A_μ. This is known as the "Higgs mechanism."

2.4   Standard Model of Particle Physics

The standard model of weak, electromagnetic, and strong interactions is based on the gauge group $SU(3)_C \times SU(2)_L \times U(1)_Y$, with three fermion generations. A single generation of quarks and leptons consists of five different representations of the gauge group $Q_L(3, \, 2)_{1/6}$, $U_R(3, \, 1)_{2/3}$, $D_R(3, \, 1)_{-1/3}$, $L_L(1, \, 2)_{-1/2}$, $E_R(1, \, 1)_{-1}$, where the sub-indeces L and R indicate the fermion chirality. Our notation here means that, for example, a left-handed lepton field L_L is a singlet of the $SU(3)$ color group, a doublet of the $SU(2)$ weak isospin, and carries hypercharge $-1/2$ under the $U(1)$ group. The model contains a single higgs boson doublet, $\phi(1, \, 2)_{1/2}$, whose vacuum expectation value breaks the gauge symmetry into $SU(3)_C \times U(1)_{\rm EM}$. The gauge interactions are mediated by eight $SU(3)$ color gluons $G_\mu^a(8, \, 1)_0$, three $SU(2)$ left chiral gauge bosons $A_\mu^i(1, \, 3)_0$, and one $U(1)$ hypercharge gauge field $B_\mu(1, \, 1)_0$. All the above gauge bosons are realized in the adjoint representations of their corresponding gauge groups, and the strength of the interactions are described by their coupling constants g_s, g, and g'. The gauge interactions arise through the covariant derivative

$$\boldsymbol{D}_\mu = \partial_\mu - i \left[g_s \sum_{a=1}^{8} G_\mu^a \, \boldsymbol{t}_a^C + g \sum_{i=1}^{3} A_\mu^i \, \boldsymbol{t}_i^L + \tfrac{1}{2} g' B_\mu \right], \qquad (2.4.75)$$

where $\boldsymbol{t}_C^a = (\lambda^a/2; 0)$ for (quarks; lepton, Higgs) and $\boldsymbol{t}_L^i = (\tau^i/2; 0)$ for $SU(2)$ (doublets; singlets).

We first focus attention on the electroweak sector. Proceeding in the same spirit of (1.5.137) and anticipating a possible $SU(2)$ structure for the weak currents, we are led to construct an "isospin" triplet of "weak currents"

$$J_\mu^i(x) = \tfrac{1}{2} \, \bar{u}_L \, \gamma_\mu \tau_i \, u_L, \qquad \text{with } i = 1, \, 2, \, 3, \qquad (2.4.76)$$

for the *spinor operators*,

$$u_L = L_L = \begin{pmatrix} \nu_{eL} \\ e_L^- \end{pmatrix}, \qquad u_L = Q_L = \begin{pmatrix} u_L \\ d_L \end{pmatrix}, \qquad (2.4.77)$$

whose corresponding charges $T^i = \int J_0^i(x)\, d^3x$ generate an $SU(2)_L$ algebra, see (2.2.55).

The presence of mass terms for A_μ^i destroy the gauge invariance of the Lagrangian. Therefore, to approach the goal of generating a mass for the gauge bosons, we entertain the mechanism of spontaneous symmetry breaking. Consider the complex scalar Higgs boson field, which, if you recall, is in the spinor representation of the $SU(2)_L$ group and has a charge $1/2$ under $U(1)_Y$, i.e.,

$$\phi = \begin{pmatrix} \phi^+ \\ \phi^0 \end{pmatrix} = \sqrt{\tfrac{1}{2}} \begin{pmatrix} \phi_1 + i\phi_2 \\ \phi_3 + i\phi_4 \end{pmatrix} . \qquad (2.4.78)$$

The gauge invariant Lagrangian is thus

$$\mathscr{L}_\phi = (\partial_\mu \phi)^\dagger (\partial^\mu \phi) - \mu^2\, \phi^\dagger \phi - \lambda (\phi^\dagger \phi)^2 \ . \qquad (2.4.79)$$

We repeat the by now familiar procedure of translating the field ϕ to a true ground state. The vacuum expectation value is obtained by looking at the stationary points of $\mathscr{L}_\phi$,

$$\frac{\partial \mathscr{L}_\phi}{\partial(\phi^\dagger \phi)} = 0 \Rightarrow \phi^\dagger \phi \equiv \frac{1}{2}(\phi_1^2 + \phi_2^2 + \phi_3^2 + \phi_4^2) = -\frac{\mu^2}{2\lambda} \ . \qquad (2.4.80)$$

The values of $(\mathrm{Re}\ \phi^+,\ \mathrm{Im}\ \phi^+,\ \mathrm{Re}\ \phi^0,\ \mathrm{Im}\ \phi^0)$ can range over the surface of a 4-dimensional sphere of radius v, such that $v^2 = -\mu^2/\lambda$ and $\phi^\dagger \phi = |\phi^+|^2 + |\phi^0|^2$. This implies that Lagrangian of ϕ is invariant under rotations of this 4-dimensional sphere, i.e., a group $SO(4)$ isomorphic to $SU(2) \times U(1)$. We must expand $\phi(x)$ about a particular minimum. Without loss of generality, we *define* the vacuum expectation value of ϕ to be a real parameter in the ϕ^0 direction, i.e., $\phi_1 = \phi_2 = \phi_4 = 0$, $\phi_3^2 = -\mu^2/\lambda$. We can now expand $\phi(x)$ about this particular vacuum

$$\langle \phi \rangle = \frac{1}{\sqrt{2}} \begin{pmatrix} 0 \\ v \end{pmatrix} . \qquad (2.4.81)$$

64

To introduce electroweak interactions with ϕ, we replace ∂_μ by the covariant derivative (2.4.75) in the Lagrangian (2.4.79), and evaluate the resulting kinetic term $(D_\mu\phi)^\dagger(D^\mu\phi)$, at the vacuum expectation value $\langle\phi\rangle$. The relevant terms are:

$$
\begin{aligned}
\Delta\mathscr{L} &= \frac{1}{2}(0 \; v)\left(\frac{1}{2}gA_\mu^j\tau_j + \frac{1}{2}g'B_\mu\right)\left(\frac{1}{2}gA^{k\mu}\tau_k + \frac{1}{2}g'B^\mu\right)\begin{pmatrix}0\\v\end{pmatrix} \\[2mm]
&= \frac{1}{8}(0 \; v)\begin{pmatrix} gA_\mu^3 + g'B_\mu & g(A_\mu^1 - iA_\mu^2) \\[2mm] g(A_\mu^1 + iA_\mu^2) & -gA_\mu^3 + g'B_\mu \end{pmatrix}^2\begin{pmatrix}0\\v\end{pmatrix} \\[2mm]
&= \frac{1}{8}v^2[g^2(A_\mu^1)^2 + g^2(A_\mu^2)^2 + (-gA_\mu^3 + g'B_\mu)^2]. \qquad (2.4.82)
\end{aligned}
$$

Note that

$$
\begin{aligned}
\frac{1}{8}v^2[g^2(A_\mu^3)^2 - 2gg'A_\mu^3 B^\mu + g'^2 B_\mu^2] &= \frac{1}{8}v^2[gA_\mu^3 - g'B_\mu]^2 + 0[g'A_\mu^3 + gB_\mu]^2 \\[2mm]
&= \frac{1}{2}m_z^2 Z_\mu^2 + \frac{1}{2}m_A A_\mu^2. \qquad (2.4.83)
\end{aligned}
$$

Therefore, there are three massive vector bosons:

$$
W_\mu^\pm = \frac{1}{\sqrt{2}}(A_\mu^1 \mp iA_\mu^2) \qquad (2.4.84)
$$

and

$$
Z_\mu^0 = \frac{1}{\sqrt{g^2 + g'^2}}(gA_\mu^3 - g'B_\mu). \qquad (2.4.85)
$$

The fourth vector field, orthogonal to Z_μ^0,

$$
A_\mu = \frac{1}{\sqrt{g^2 + g'^2}}(g'A_\mu^3 + gB_\mu), \qquad (2.4.86)
$$

remains massless. We identify this field with the electromagnetic vector potential.

The gauge fields have "eaten up" the Goldstone bosons and become massive. The scalar degrees of freedom become the longitudinal polarizations of the massive vector bosons. The spontaneous symmetry breaking rotates

the four $SU(2)_L \times U(1)_Y$ gauge bosons to their mass eigenstates by means of the gauge interaction term of the Higgs fields, $\{A_\mu^1,\ A_\mu^2\} \to \{W_\mu^+,\ W_\mu^-\}$ and $\{A_\mu^3,\ B_\mu\} \to A_\mu,\ Z_\mu^0$. In terms of the weak mixing angle, θ_w (defined by $\tan \theta_w = g'/g$), the photon and Z^0-boson fields read

$$
\begin{pmatrix} Z_\mu^0 \\ A_\mu \end{pmatrix} = \begin{pmatrix} \cos\theta_w & -\sin\theta_w \\ \sin\theta_w & \cos\theta_w \end{pmatrix} \begin{pmatrix} A_\mu^3 \\ B_\mu \end{pmatrix}. \tag{2.4.87}
$$

The $W^\pm$ and the Z^0 boson masses, at lowest order in perturbation theory, can be rewritten as

$$
m_W = \frac{g\,v}{2} = \frac{g}{2\sqrt{2\,\lambda}} m_H \quad \text{and} \quad m_Z = \frac{m_W}{\cos\theta_w}, \tag{2.4.88}
$$

showing that the Higgs mass m_H sets the electroweak mass scale.

In terms of the mass eigenstates the covariant derivative (2.4.75) becomes

$$
\begin{aligned}
D_\mu &= \partial_\mu - i\frac{g}{\sqrt{2}}(W_\mu^+ T^+ + W_\mu^- T^-) - i\frac{1}{\sqrt{g^2 + g'^2}} Z_\mu (g^2 T^3 - g'^2 Y) \\
&\quad - i\frac{gg'}{\sqrt{g^2 + g'^2}} A_\mu (T^3 + Y),
\end{aligned} \tag{2.4.89}
$$

where $T^\pm = T^1 \pm iT^2$. The normalization is chosen so that, in the spinor representation of $SU(2)$

$$
T^\pm = \tfrac{1}{2}(\sigma^1 \pm i\sigma^2) = \sigma^\pm. \tag{2.4.90}
$$

After identifying the coefficient of the electromagnetic interaction

$$
e = \frac{gg'}{\sqrt{g^2 + g'^2}} = g\sin\theta_w, \tag{2.4.91}
$$

with the electron charge, it becomes evident that the electromagnetic interaction (a $U(1)$ gauge symmetry with coupling e) "sits across" weak isospin (an $SU(2)_L$ symmetry with coupling g and weak hypercharge (a $U(1)$ symmetry with coupling g'). Note that the two couplings g and g' can be replaced by e and θ_w, where the parameter θ_w is to be determined by the experiment. After we identify the electric charge quantum number in (2.4.89) with $Q = T^3 + Y$, with the manipulation in the Z^0 coupling

$$
g^2 T^3 - g'^2 Y = (g^2 + g'^2)T^3 - g'^2 Q, \tag{2.4.92}
$$

Table 2.1: *Weak isospin, and hypercharge quantum numbers.*

Lepton	T	T^3	Q	Y	Quark	T	T^3	Q	Y
ν_e	$\frac{1}{2}$	$\frac{1}{2}$	0	$-\frac{1}{2}$	u_L	$\frac{1}{2}$	$\frac{1}{2}$	$\frac{2}{3}$	$\frac{1}{6}$
e_L^-	$\frac{1}{2}$	$-\frac{1}{2}$	-1	$-\frac{1}{2}$	d_L	$\frac{1}{2}$	$-\frac{1}{2}$	$-\frac{1}{3}$	$\frac{1}{6}$
					u_R	0	0	$\frac{2}{3}$	$\frac{2}{3}$
e_R^-	0	0	-1	-1	d_R	0	0	$-\frac{1}{3}$	$-\frac{1}{3}$

we can rewrite the covariant derivative (2.4.89) as follows

$$D_\mu = \partial_\mu - i\frac{g}{\sqrt{2}}(W_\mu^+ T^+ + W_\mu^- T^-) - i\frac{g}{\cos\theta_w}Z_\mu(T^3 - \sin^2\theta_w Q) - ieA_\mu Q \,.$$

(2.4.93)

The covariant derivative (2.4.93) uniquely determines the coupling of the $W^\pm$ and Z^0 fields to fermions, once the quantum numbers of the fermion fields are specified. For the right-handed fields, $T^3 = 0$ and hence $Y = Q$. For the left-handed fields, L_L and Q_L, the assignments $Y = -1/2$ and $Y = +1/6$, respectively, combine with $T^3 = \pm 1/2$ to give the correct electric charge assignments. The weak isospin and hypercharge quantum numbers of leptons and quarks are given in Table 2.1.

If we ignore fermion masses, the Lagrangian for the weak interactions of quarks and leptons follows directly from the charge assignments given above. The fermion kinetic energy terms are

$$\mathscr{L} = \overline{L}_L(i\,\slashed{D})L_L + \overline{E}_R(i\,\slashed{D})E_R + \overline{Q}_L(i\,\slashed{D})Q_L + \overline{U}_R(i\,\slashed{D})U_R + \overline{D}_R(i\,\slashed{D})D_R.$$

(2.4.94)

To work out the physical consequences of the fermion-vector boson couplings, we should write (2.4.94) in terms of the vector boson mass eigenstates. Using the form of the covariant deivative (2.4.93) we can rewrite (2.4.94) as

$$\begin{aligned}
\mathscr{L} &= \overline{L}_L(i\slashed{\partial})L_L + \overline{E}_R(i\slashed{\partial})E_R + \overline{Q}_L(i\slashed{\partial})Q_L + \overline{U}_R(i\slashed{\partial})U_R + \overline{D}_R(i\slashed{\partial})D_R \\
&+ g(W_\mu^+ J_W^{+\mu} + W_\mu^- J_W^{-\mu} + Z_\mu^0 J_Z^\mu) + eA_\mu j^\mu,
\end{aligned}$$

(2.4.95)

where

$$J_W^{+\mu} = \frac{1}{\sqrt{2}}(\bar{\nu}_L\,\gamma^\mu e_L + \bar{u}_L\,\gamma^\mu d_L),$$

$$J_W^{-\mu} = \frac{1}{\sqrt{2}}(\bar{e}_L\,\gamma^\mu \nu_L + \bar{d}_L\,\gamma^\mu u_L),$$

$$
\begin{aligned}
J_Z^\mu &= \left[\bar\nu_L \, \gamma^\mu \left(\frac{1}{2} \right) \nu_L + \bar e_L \, \gamma^\mu \left(-\frac{1}{2} + \sin^2 \theta_w \right) e_L + \bar e_R \, \gamma^\mu \left(\sin^2 \theta_w \right) e_R \right. \\
&\quad + \; \bar u_L \, \gamma^\mu \left(\frac{1}{2} - \frac{2}{3} \sin^2 \theta_w \right) u_L + \bar u_R \, \gamma^\mu \left(-\frac{2}{3} \sin^2 \theta_w \right) u_R \\
&\quad + \; \left. \bar d_L \, \gamma^\mu \left(-\frac{1}{2} + \frac{1}{3} \sin^2 \theta_w \right) d_L + \bar d_R \, \gamma^\mu \left(\frac{1}{3} \sin^2 \theta_w \right) d_R \right] \frac{1}{\cos \theta_w}, \\
j^\mu &= \; \bar e \, \gamma^\mu (-1) e + \bar u \, \gamma^\mu \left(+\frac{2}{3} \right) u + \bar d \, \gamma^\mu \left(-\frac{1}{3} \right) d \qquad\qquad (2.4.96)
\end{aligned}
$$

and equivalent expressions hold for the other two generations.

The gauge invariant QCD Lagrangian for interacting colored quarks q and vector gluons G_μ, with coupling specified by g_s, follows simply from demanding that the Lagrangian be invariant under local phase transformations to the quark fields. Using (2.2.40) we obtain

$$
\mathscr{L}_{\mathrm{QCD}} = \bar q_j (i \gamma^\mu \partial_\mu - m) q_j + g_s (\bar q_j \gamma^\mu t_a q_j) G_\mu^a - \tfrac{1}{4} G_{\mu\nu}^a G_a^{\mu\nu} \;, \qquad (2.4.97)
$$

where q_1, q_2, and q_3 denote the three color fields and, for simplicity, we show just one quark flavor. Because we can arbitrarily vary the phase of the three quark color fields, it is not surprising that eight vector gluon fields are needed to compensate all possible phase changes. Just as for the photon, local invariance requires the gluons to be massless.

As we anticipated in Sec. 2.2.2, the field strength tensor $G_{\mu\nu}^a$ has a remarkable new property on account of the $[\boldsymbol{G}_\mu, \boldsymbol{G}_\nu]$ term. Imposing the gauge symmetry has required that the kinetic energy term in $\mathscr{L}_{\mathrm{QCD}}$ is not purely kinetic but includes an induced self-interaction between the gauge bosons. This becomes clear if we rewrite Lagrangian (2.4.97) in the symbolic form

$$
\mathscr{L}_{\mathrm{QCD}} = "\bar q q" + "G^2" + g_s \, "\bar q q G" + g_s \, "G^3" + g_s^2 \, "G^4" . \qquad (2.4.98)
$$

The first three terms have QED analogues. They describe the free propagation of quarks and gluons and the quark-gluon interaction. The remaining two terms show the presence of three- and four-gluon vertices in QCD and reflect the fact that gluons themselves carry color charge. They have no analogue in QED and arise on account of the non-Abelian character of the gauge group.

Since explicit fermion mass terms violate the gauge symmetries, the masses of the chiral fields arise from the Yukawa interactions which couple a right-handed fermion with its left handed doublet and the Higgs field after spontaneous symmetry breaking.[12] For example, to generate the electron mass, we include the following $SU(2) \times U(1)$ gauge invariant term in the Lagrangian

$$\mathscr{L}_e^{\text{Yukawa}} = -Y_e \left[(\bar{\nu}_e, \bar{e})_L \begin{pmatrix} \phi^+ \\ \phi_0 \end{pmatrix} e_R + \bar{e}_R (\phi^-, \bar{\phi}^0) \begin{pmatrix} \nu_e \\ e \end{pmatrix}_L \right] , \qquad (2.4.99)$$

where Y_e is the Yukawa coupling constant of the electron. The Higgs doublet has exactly the required $SU(2) \times U(1)$ quantum numbers to couple to $\bar{e}_L e_R$. We spontaneously break the symmetry and substitute

$$\phi = \sqrt{\tfrac{1}{2}} \begin{pmatrix} 0 \\ v + H(x) \end{pmatrix} \qquad (2.4.100)$$

into (2.4.99). The neutral Higgs field $H(x)$ is the only remnant of the Higgs doublet, (2.4.78), after spontaneous symmetry breaking has taken place. The other three fields can be gauged away. On substitution of ϕ, the Lagrangian becomes

$$\mathscr{L}_e^{\text{Yukawa}} = -\frac{Y_e}{\sqrt{2}} v (\bar{e}_L e_R + \bar{e}_R e_L) - \frac{Y_e}{\sqrt{2}} (\bar{e}_L e_R + \bar{e}_R e_L) H . \qquad (2.4.101)$$

We choose Y_e so that

$$m_e = \frac{Y_e \, v}{\sqrt{2}} \qquad (2.4.102)$$

and thus generate the required electron mass,

$$\mathscr{L}_e^{\text{Yukawa}} = -m_e \bar{e}e - \frac{m_e}{v} \bar{e}e H . \qquad (2.4.103)$$

Note however, that because Y_e is arbitrary, the actual mass of the electron is not predicted. Besides the mass term, the Lagrangian contains an interaction term coupling the Higgs scalar to the electron.

The quark masses are generated in the same way. The only novel feature is that to generate a mass for the upper member of the quark doublet, we

---

[12]H. Yukawa, Proc. Phys. Math. Soc. Jap. **17**, 48 (1935).

must construct the complex conjugate of the Higgs doublet

$$\tilde{\phi} = -i\tau_2\phi^* = \begin{pmatrix} -\bar{\phi}^0 \\ \phi^- \end{pmatrix} \underset{\text{breaking}}{\longrightarrow} \sqrt{\tfrac{1}{2}} \begin{pmatrix} v+H \\ 0 \end{pmatrix} . \qquad (2.4.104)$$

Because of the special properties of $SU(2)$, $\bar{\phi}$ transforms identically to ϕ (but has opposite weak hypercharge to ϕ, namely, $Y = -1/2$). Therefore, it can be used to construct a gauge invariant contribution to the Lagrangian

$$\begin{aligned} \mathscr{L}_q^{\text{Yukawa}} &= -Y_d(\bar{u}, \bar{d})_L \begin{pmatrix} \phi^+ \\ \phi_0 \end{pmatrix} d_R + Y_u(\bar{u}, \bar{d})_L \begin{pmatrix} -\bar{\phi}^0 \\ \phi^- \end{pmatrix} u_R + \text{h.c.} \\ &= -m_d\bar{d}d - m_u\bar{u}u - \tfrac{m_d}{v}\bar{d}dH - \tfrac{m_u}{v}\bar{u}uH . \qquad (2.4.105) \end{aligned}$$

All in all, the Yukawa Lagrangian then takes the form

$$-\mathscr{L}^{\text{Yukawa}} = Y_d{}^{ij}\,\overline{Q}_{L_i}\,\phi\,D_{R_j} + Y_u{}^{ij}\,\overline{Q}_{L_i}\,\tilde{\phi}\,U_{R_j} + Y_e{}^{ij}\,\overline{L}_{L_i}\,\phi\,E_{R_j} + \text{h.c.}, \quad (2.4.106)$$

where ij are the generation indices.

It is important to note that the standard model also comprises an accidental global symmetry $U(1)_B \times U(1)_e \times U(1)_\mu \times U(1)_\tau$, where $U(1)_B$ is the baryon number symmetry and $U(1)_{e,\mu,\tau}$ are three lepton flavor symmetries, with total lepton number given by $L = L_e + L_\mu + L_\tau$. It is an accidental symmetry because we do not impose it. It is a consequence of the gauge symmetries and the low energy particle content. It is possible (but not necessary), however, that effective interaction operators induced by the high energy content of the underlying theory may violate sectors of the global symmetry.

Up to now we have "concocted" a standard model of particle physics from general group-theory considerations of principles of symmetry and invariants. Of course, in real life a model of nature is usually uncovered in a less pristine fashion. To convey an impression of how the theories developed, and how the standard model has successfully confronted experiment, we will describe a number of the most important theoretical results. We will start from the most precisely tested theory in physics, QED, and carry on to QCD and the electroweak theory, both offspring of QED.

Chapter 3

QED

3.1   Invariant Amplitude

In Maxwell's theory of electromagnetism, charged particles, such as electrons, interact through their electromagnetic fields. However, for many years it was difficult to conceive how such action-at-a-distance between charges came about. In QFT, we have such a tangible connection. The quantum field theory approach visualizes the force between electrons as an interaction arising in the exchange of "virtual" photons, which can only travel a distance allowed by the uncertainty principle. These virtual photons, of course, cannot live an existence independent of the charges that emit or absorb them.

When calculating scattering cross sections, the interaction between particles can be described by starting from a free field which describes the incoming and outgoing particles, and including an interaction Hamiltonian to describe how the particles deflect one another. The amplitude for scattering is the sum of each possible interaction history over all possible intermediate particle states. The number of times the interaction Hamiltonian acts is the order of the perturbation expansion. The perturbative series can be written as a sum over Feynman diagrams; e.g., the lowest order (tree level) diagrams for Bhabha scattering ($e^+e^- \to e^+e^-$) are shown in Fig. 3.1, and the various virtual contributions containing one-loop and two-loops (with a closed electron loop) are shown in Figs. 3.2 and 3.3.

In the non-relativistic limit of perturbation theory, we have introduced
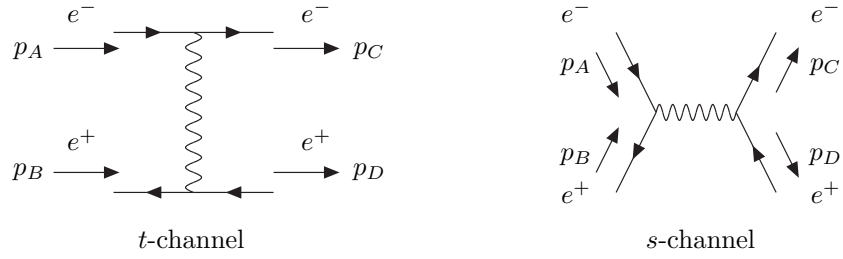
Figure 3.1: *Bhabha scattering tree-level diagrams.*

a factor like V_{ni} for each interaction vertex and for the propagation of each intermediate state we have introduced a "propagator" factor like $1/(E_i - E_n)$. [For details, we refer the reader to Eq. (1.6.162).] The intermediate states are virtual in the sense that the energy is not conserved, $E_n \neq E_i$, but there is energy conservation between the initial and final states as indicated by the delta function $\delta(E_f - E_i)$. Throughout this chapter we generalize the perturbative scheme to handle relativistic particles, including their antiparticles.
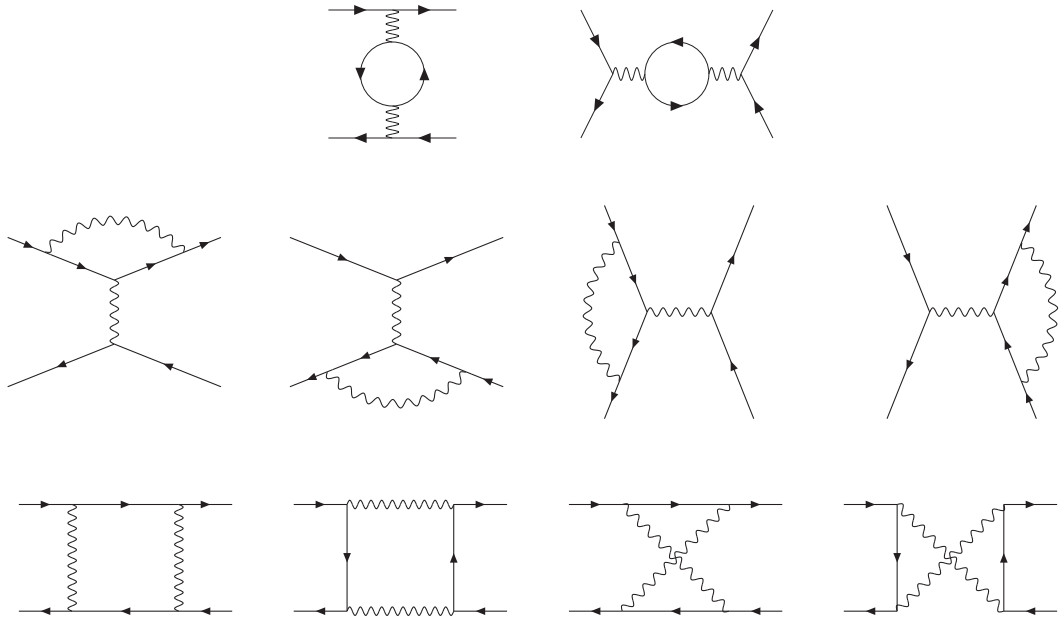
Figure 3.2: *Bhabha scattering one-loop diagrams.*
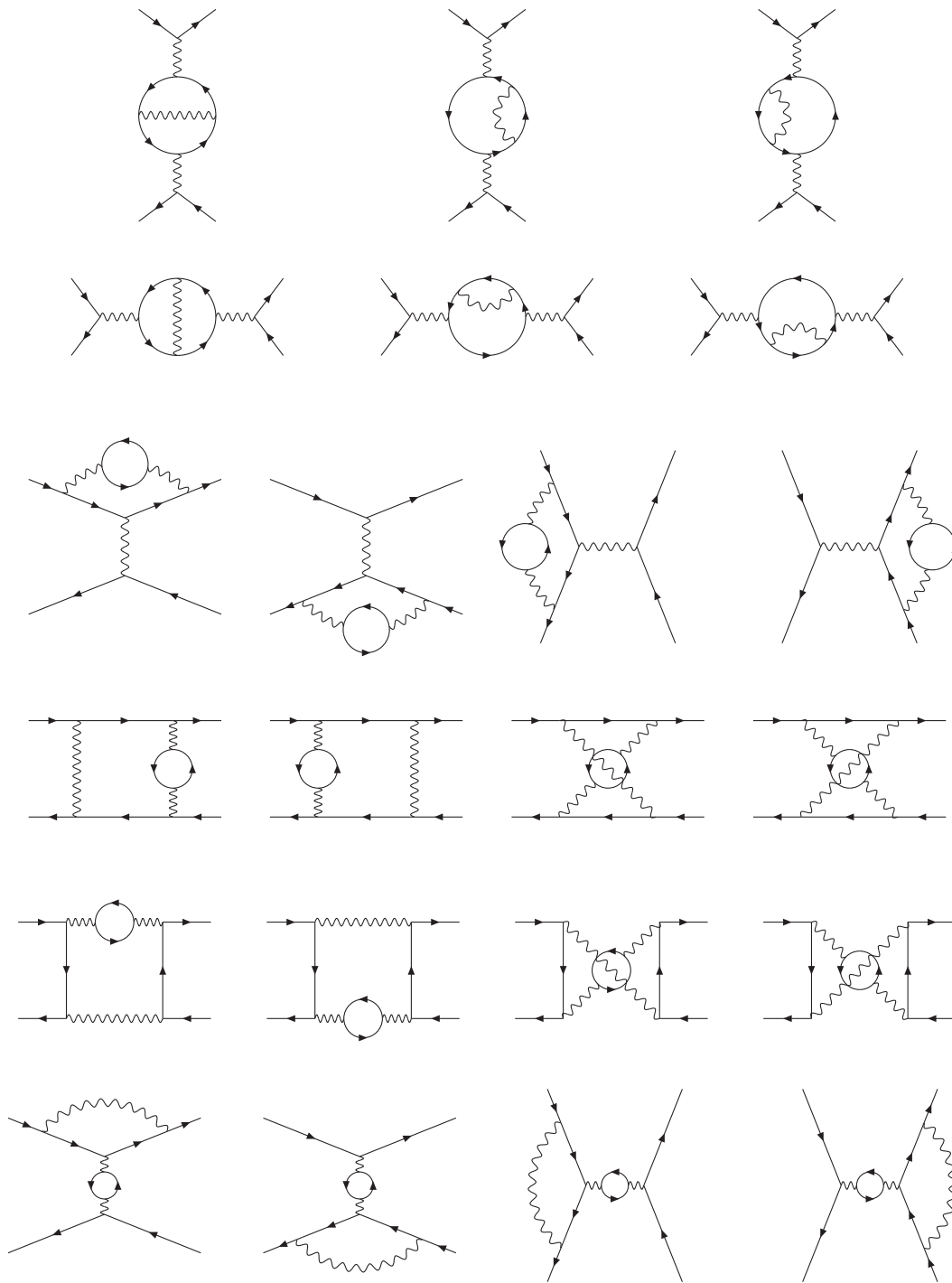
Figure 3.3: *Bhabha scattering two-loop diagrams with a closed electron loop.*

73
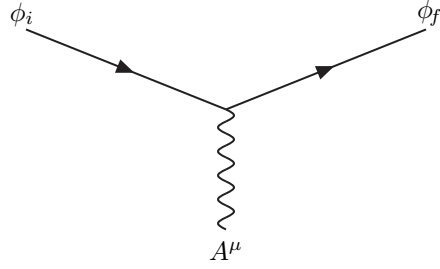
Figure 3.4: *A "spinless" electron interacting with A^μ.*

We first have to figure out how to use perturbation theory in a covariant way. We illustrate this, by choosing the interacting particles to be "spinless" charged leptons, as it is desirable to begin by avoiding the complications of their spin. This choice requires some explanation. No spinless quark or lepton has ever been observed in an experiment. Spinless hadrons exist (e.g., the π-meson), but they are complicated composite structures of spin-$\frac{1}{2}$ quarks and spin-1 gluons. The spin-0 leptons (that is leptons satisfying the Klein-Gordon equation) are completely fictitious objects.

Consider the scattering of a spinless electron in an electromagnetic potential, shown in Fig. 3.4. In classical electrodynamics, the motion of a particle of charge e in an electromagnetic potential $A^\mu = (\phi, \vec{A})$ is obtained by the substitution $p^\mu \to p^\mu - eA^\mu$. The corresponding quantum mechanical substitution is therefore $i\partial^\mu \to i\partial^\mu - eA^\mu$. The Klein-Gordon equation becomes

$$(\partial_\mu \partial^\mu + m^2)\phi = -V\phi \tag{3.1.1}$$

where

$$V = ie(\partial_\mu A^\mu + A^\mu \partial_\mu) - e^2 A^2 \tag{3.1.2}$$

is the (electromagnetic) perturbation. Working to lowest order, we neglect the $e^2 A^2$ term in (3.1.2). The amplitude for the scattering of e^- from a state ϕ_i to ϕ_f of an electromagnetic potential A_μ is

$$
\begin{aligned}
T_{fi} &= -i \int \phi_f^*(x)\, V(x)\, \phi_i(x)\, d^4x \\
&= -i \int \phi_f^*\, ie(A^\mu \partial_\mu + \partial_\mu A^\mu)\, \phi_i\, d^4x\,. \tag{3.1.3}
\end{aligned}
$$

The derivative in the second term, which acts on both A^μ and ϕ_i, can be

74

e^-
p_A e^- p_C
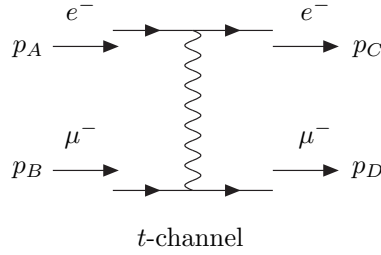
μ^-
p_B μ^- p_D

t-channel

Figure 3.5: *Tree level diagram for electron-muon scattering.*

turned around by integration by parts, so that it acts on ϕ_f^*

$$\int \phi_f^* \, \partial_\mu(A^\mu \phi_i) \, d^4x = - \int \partial_\mu(\phi_f^*) \, A^\mu \, \phi_i \, d^4x \qquad (3.1.4)$$

where the surface term has been omitted as the potential is taken to vanish as $|\vec{x}|, t \to \pm\infty$. We can now rewrite the amplitude in a very suggestive form

$$T_{fi} = -i \int j_\mu^{fi} e A^\mu \, d^4x \qquad (3.1.5)$$

where

$$e j_\mu^{fi}(x) = ie[\phi_f^*(\partial_\mu \phi_i) - (\partial_\mu \phi_f^*)\phi_i] \qquad (3.1.6)$$

which, by comparison with (1.4.46), can be regarded as the electromagnetic current for the $i \to f$ electron transition. If the incoming e^- has four momentum p_i, we have $\phi_i(x) = N_i e^{-ip_i \cdot x}$, where N_i is the normalization constant. Using an analogous expression, for ϕ_f it follows that

$$e j_\mu^{fi} = e N_i N_f (p_i + p_f)_\mu \, e^{i(p_f - p_i) \cdot x} \, . \qquad (3.1.7)$$

Next, using the results for the scattering of the "spinless" electron off an electromagnetic potential, we can calculate the scattering of the same electron off another charged particle, say a "spinless" muon. The Feynman diagram of such a process is shown in Fig. 3.5. The calculation is a straightforward extension of the previous one; we just have to identify the electromagnetic potential A^μ with its source, the charged "spinless" muon. This is done with the help of Maxwell's equations, $\Box^2 A^\mu = j_{(2)}^\mu$, which determine the electromagnetic field A^μ associated with the current

$$e j_{(2)}^\mu = e N_B N_D (p_D + p_B)^\mu \, e^{i(p_D - p_B) \cdot x} \, , \qquad (3.1.8)$$

75

where the momenta are defined in Fig. 3.5. Now, using $\Box^2 e^{iq.x} = -q^2 \, e^{iq.x}$ we obtain

$$A^\mu = -\frac{1}{q^2} \, j^\mu_{(2)} \; , \tag{3.1.9}$$

with $q = p_D - p_B$. Inserting this field due to the muon into (3.1.5), we find the tree level amplitude for electron muon scattering

$$T_{fi} = -ie^2 \int j^{(1)}_\mu(x) \left(\frac{-1}{q^2}\right) j^\mu_{(2)} \, d^4x \; . \tag{3.1.10}$$

Substituting (3.1.8) and (3.1.7), and carrying out the x integration we find,

$$T_{fi} = -iN_A \, N_B \, N_C \, N_D \, (2\pi)^4 \, \delta^{(4)}(p_D + p_C - p_B - p_A) \, \mathfrak{M} \tag{3.1.11}$$

where

$$-i\mathfrak{M} = [-ie(p_A + p_C)^\mu] \left(-i\frac{g_{\mu\nu}}{q^2}\right) [-ie(p_B + p_D)^\nu] \, . \tag{3.1.12}$$

A consistency check on (3.1.12) shows that we would have obtained the same amplitude considering the muon scattering off the electromagnetic field A^μ produced by the electron. Consequently, $\mathfrak{M}$, as defined by (3.1.11), is called the *invariant amplitude*. The delta function expresses energy-momentum conservation for the process. It is noteworthy that the photon propagator carries Lorentz indices because it is a spin-1 particle. The four-momentum q of the photon is determined by four-momentum conservation at the vertices. We see that $q^2 \neq 0$, and we say the photon is "virtual" or "off-mass shell." Each vertex factor contains the electromagnetic coupling e and a four-vector index to connect with the photon index. The particular distribution of the minus signs and factors i has been made up to give the correct result for higher order diagrams. Note that the multiplicative of the three factors gives $-i\mathfrak{M}$. Whenever the same vertex or internal line occurs in a Feynman diagram the corresponding factor will contribute multiplicatively to the amplitude $-i\mathfrak{M}$ for that diagram.

To relate these calculations to experimental observables, we must set the normalization N of the free particle wave functions (1.4.44). Recall that the probability density of particles described by ϕ is $\rho = 2E|N|^2$. The proportionality of ρ to E was just what we needed to compensate for the

Lorentz contraction of the volume element d^3x and to keep the number of particles ρd^3x unchanged. We then work with a volume V and normalize to $2E$ particles within that volume, $\int_V \rho\, dV = 2E$. This leads to the covariant normalization

$$N = \frac{1}{\sqrt{V}}. \qquad (3.1.13)$$

The transition rate per unit volume of the process $A + B \to C + D$ is

$$W_{fi} = \frac{|T_{fi}|^2}{TV}, \qquad (3.1.14)$$

where T is the time interval of the interaction and the transition amplitude is given in (3.1.11). Upon squaring, one delta function remains, and $(2\pi)^4$ times the other gives TV. Therefore, making use of (3.1.13) we obtain

$$W_{fi} = (2\pi)^4 \frac{\delta^{(4)}(p_A + p_B - p_C - p_D)|\mathfrak{M}|^2}{V^4}. \qquad (3.1.15)$$

Experimental results on $AB \to CD$ scattering are quoted in the form of a "cross section," which is related to the transition rate according to

$$\text{cross section} = \frac{W_{fi}}{(\text{initial flux})}\,(\text{number of final states}), \qquad (3.1.16)$$

where the factors in brackets allow for the "density" of incoming and outgoing states. (The derivation of the formula for particle decay rates proceeds along similar lines, see Appendix A.)

For a single particle, quantum physics restricts the number of final states in a volume V with momenta in element d^3p to be $V d^3p/(2\pi)^3$, but we have $2E$ particles in V, yielding

$$\text{No. of final states/particle} = \frac{V\, d^3p}{(2\pi)^3\, 2E}. \qquad (3.1.17)$$

Therefore, for particles C, D scattered into momentum elements d^3p_C, d^3p_D,

$$\text{No. of available final states} = \frac{V\, d^3p_C}{(2\pi)^3 2E_C} \frac{V\, d^3p_D}{(2\pi)^3 2E_D}. \qquad (3.1.18)$$

It is easiest to calculate the initial flux in the lab frame. The number of beam particles passing through unit area per unit time is $|\vec{v}_A| 2E_A/V$, and

the number of target particles per unit volume is $2E_B/V$. Therefore, we obtain the normalization-independent measure of the ingoing "density" by taking

$$\text{Initial flux} = |\vec{v}_A| \frac{2E_A}{V} \frac{2E_B}{V} . \qquad (3.1.19)$$

Substituting (3.1.15), (3.1.18), and (3.1.19) into (3.1.16) we obtain the differential cross section $d\sigma$ for scattering into $d^3p_C \, d^3p_D$

$$d\sigma = \frac{V^4}{|\vec{v}_A| 2E_A \, 2E_B} \frac{1}{V^4} |\mathfrak{M}|^2 \frac{(2\pi)^4}{(2\pi)^6} \delta^{(4)}(p_A + p_B - p_C - p_D) \frac{d^3p_C}{2E_C} \frac{d^3p_D}{2E_D} . \qquad (3.1.20)$$

Note that the arbitrary normalization volume cancels. Consequently, hereafter we drop V and work in unit volume, i.e., we normalize to $2E$ particles/unit volume, and the normalization factor (3.1.13) of the wave function is $N = 1$.

For reactions symmetric about the collision axis, we can simplify the Lorentz invariant phase space factor

$$dQ = (2\pi)^4 \, \delta^{(4)}(p_A + p_B - p_C - p_D) \frac{d^3p_C}{(2\pi)^3 \, 2E_C} \frac{d^3p_D}{(2\pi)^3 \, 2E_D} , \qquad (3.1.21)$$

by partially evaluating the phase-space integrals in the center-of-mass frame. We first choose to integrate all three components of p_D over the delta functions enforcing 3-momentum conservation. This sets $\vec{p}_C = -\vec{p}_D$ and converts the Lorentz invariant phase space factor to the form

$$
\begin{aligned}
dQ &= \frac{1}{4\pi^2} \frac{d^3p_C}{2E_C} \frac{1}{2E_D} \delta(E_A + E_B - E_C - E_D) \\
&= \frac{1}{4\pi^2} \frac{p_C^2 \, dp_C \, d\Omega}{4E_C E_D} \delta(W - E_C - E_D) , \qquad (3.1.22)
\end{aligned}
$$

where $d\Omega$ is the element of solid angle about $\vec{p}_C$ and $\sqrt{s} \equiv W = E_A + E_B$. Now, using $W = E_C + E_D = (p_f^2 + m_C^2)^{1/2} + (p_f^2 + m_D^2)^{1/2}$, we obtain

$$\frac{dW}{dp_f} = p_f \left(\frac{1}{E_C} + \frac{1}{E_D} \right) , \qquad (3.1.23)$$

and rewrite Eq. (3.1.22) as

$$
\begin{aligned}
dQ &= \frac{1}{4\pi^2} \frac{p_f}{4} \left(\frac{1}{E_C + E_D} \right) dW \, d\Omega \, \delta(W - E_C - E_D) \\
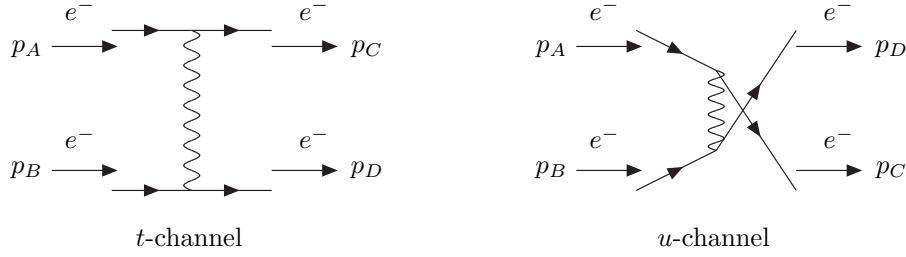&= \frac{1}{4\pi^2} \frac{p_f}{4\sqrt{s}} \, d\Omega , \qquad (3.1.24)
\end{aligned}
$$

78

Figure 3.6: *Lowest-order Feynman diagrams for Møller scattering.*

where $|\vec{p}_C| = |\vec{p}_D| = p_f$.

On the other hand, the incident flux for a general collinear collision between A and B reads,

$$
\begin{aligned}
F & = |\vec{v}_A - \vec{v}_B| \, 2E_A \, 2E_B \\
& = 4(|\vec{p}_A|E_B + |\vec{p}_B|E_A) \\
& = 4[(p_A.p_B)^2 - m_A^2 m_B^2]^{1/2} ,
\end{aligned}
\tag{3.1.25}
$$

and hence the differential cross section in the center-of-mass is

$$
\left.\frac{d\sigma}{d\Omega}\right|_{\text{c.m.}} = \frac{1}{64\pi^2 s} \frac{p_f}{p_i} |\mathfrak{M}|^2
\tag{3.1.26}
$$

where $|\vec{p}_A| = |\vec{p}_B| = p_i$. In the special case where all four particles have identical masses (including the commonly seen limit $m \to 0$), Eq. (3.1.26) reduces to

$$
\left.\frac{d\sigma}{d\Omega}\right|_{\text{c.m.}} = \frac{|\mathfrak{M}|^2}{64\pi^2 s} .
\tag{3.1.27}
$$

In closing we note that for electron-electron scattering we need to take into account that we have identical particles in the initial and final states, and hence the amplitude should be symmetric under the interchange of particle labels $C \leftrightarrow D$ and $A \leftrightarrow B$. Therefore, we have two Feynman diagrams shown in Fig. 3.6. The tree level invariant amplitude for the scattering of a spinless electron is then

$$
-i\mathfrak{M} = -i\left(-\frac{e^2(p_A + p_C)_\mu (p_B + p_D)^\mu}{(p_D - p_B)^2} - \frac{e^2(p_A + p_D)_\mu (p_B + p_C)^\mu}{(p_C - p_B)^2} \right) .
\tag{3.1.28}
$$

Note that the symmetry under $p_C \leftrightarrow p_D$ ensures that $\mathfrak{M}$ is also symmetric under $p_A \leftrightarrow p_B$.

3.2 Unpolarized Cross Section

We have seen that a free electron of four-momentum p^μ is described by a spinor, $\psi = u(p)e^{-ip.x}$, which satisfies the Dirac equation $(\gamma_\mu p^\mu - m)\psi = 0$. The equation for an electron in an electromagnetic field A^μ is obtained by the substitution $p^\mu \to p^\mu - eA^\mu$, where we have again taken e to be the charge of the electron. We find

$$(\gamma_\mu p^\mu - m)\psi = \gamma^0 V \, \psi, \qquad (3.2.29)$$

where the perturbation is given by $\gamma^0 V = e\gamma_\mu A^\mu$. The introduction of γ^0 is to make (3.2.29) of the form $(E + \dots)\psi = V\psi$, so that the potential energy enters in the same way as in the Schrödinger equation.

Using first-order perturbation theory (1.6.151), the amplitude for the scattering of an electron from state ψ_i to state ψ_f is

$$
\begin{aligned}
T_{fi} &= -i \int \psi_f^\dagger(x) \, V(x) \, \psi_i(x) \, d^4x \\
&= -ie \int \overline{\psi}_f \, \gamma_\mu \, A^\mu \, \psi_i \, d^4x \\
&= ie \int j_\mu^{fi} \, A^\mu \, d^4x \qquad (3.2.30)
\end{aligned}
$$

where

$$
\begin{aligned}
e\, j_\mu^{fi} &\equiv e\,\overline{\psi}_f \, \gamma_\mu \, \psi_i \\
&= e\,\overline{u}_f \, \gamma_\mu \, u_i \, e^{i(p_f - p_i).x} \qquad (3.2.31)
\end{aligned}
$$

can be regarded as the electromagnetic transition current between states i and f.

Repeating the steps of the preceding section, the tree level transition amplitude for electron-muon scattering is

$$
\begin{aligned}
T_{fi} &= -ie^2 \int j_\mu^{(1)}(x) \, \left(\frac{-1}{q^2}\right) j_{(2)}^\mu \, d^4x \\
&= -i(e\overline{u}_C \gamma_\mu u_A) \left(\frac{-1}{q^2}\right) (e\overline{u}_D \gamma^\mu u_B) \, (2\pi)^4 \, \delta^{(4)}(p_A + p_B - p_C - p_D),
\end{aligned}
$$

$$(3.2.32)$$

where $q = p_A - p_C$, and the factor $(2\pi)^4$ times the delta function arises from the integration over the x dependence of the currents. Recall that the invariant amplitude $\mathfrak{M}$ is defined by

$$T_{fi} = -i(2\pi)^4 \delta^{(4)}(p_A + p_B - p_C - p_D)\,\mathfrak{M}\,, \qquad (3.2.33)$$

and so we have

$$-i\mathfrak{M} = (-ie\overline{u}_C\gamma^\mu u_A)\left(\frac{-ig_{\mu\nu}}{q^2}\right)(-ie\overline{u}_D\gamma^\nu u_B)\,. \qquad (3.2.34)$$

To calculate the unpolarized cross section, we must amend the cross section formulae of Sec. 3.1. By unpolarized we mean that no information about the electron spins is recorded in the experiment. To allow for scattering in all possible spin configurations, we therefore have to make the replacement

$$|\mathfrak{M}|^2 \to \overline{|\mathfrak{M}|^2} \equiv \frac{1}{(2s_A + 1)(2s_B + 1)}\sum_{\text{spins}}|\mathfrak{M}|^2\,, \qquad (3.2.35)$$

where s_A, s_B are the spins of the incoming particles. That is, we average over the spins of the incoming particles and sum over the spins of the particles in the final state.

To obtain the (unpolarized) cross section, we have to take the square of the modulus of

$$\mathfrak{M} = -e^2\overline{u}(k')\,\gamma^\mu\,u(k)\left(\frac{1}{q^2}\right)\overline{u}(p')\,\gamma^\nu\,u(p) \qquad (3.2.36)$$

and then carry out the spin sums (the momenta are defined in Fig. 3.5, with $p_A = k$, $p_B = p$, $p_C = k'$, $p_D = p'$, and $q = k - k'$). It is convenient to separate the sums over the electron and muon spins by writing (3.2.35) as

$$\overline{|\mathfrak{M}|^2} = \frac{e^4}{q^4}L_{(e)}^{\mu\nu}L_{\mu\nu}^{(\mu)} \qquad (3.2.37)$$

where the tensor associated with the electron vertex is

$$L_{(e)}^{\mu\nu} \equiv \frac{1}{2}\sum_{e-\text{spins}}[\overline{u}(k')\gamma^\mu u(k)][\overline{u}(k')\gamma^\nu u(k)]^*\,, \qquad (3.2.38)$$

and with a similar expression for $L_{\mu\nu}^{(\mu)}$.

The spin summations look like a forbidding task. Fortunately, well-established trace techniques considerably simplify such calculations. To begin, we note that the second square bracket of (3.2.38) (a 1×1 matrix for which the complex and hermitian conjugates are the same) is equal to

$$
\begin{aligned}
[u^\dagger(k')\, \gamma^0\, \gamma^\nu\, u(k)]^\dagger &= [u^\dagger(k)\, \gamma^{\nu\dagger}\, \gamma^0\, u(k')] \\
&= [\overline{u}(k)\gamma^\nu u(k')]\,, \tag{3.2.39}
\end{aligned}
$$

where we have used $\gamma^{\nu\dagger}\gamma^0 = \gamma^0\gamma^\nu$. That is, the complex conjugation in (3.2.38) simply reverses the order of the matrix product. We now write the complete product in (3.2.38) explicitly in terms of individual matrix elements (labeled $\alpha, \beta, \ldots$, with summation over repeated indices implied)

$$
L^{\mu\nu}_{(e)} = \frac{1}{2} \sum_{s'} \overline{u}^{(s')}_\alpha(k')\, \gamma^\mu_{\alpha\beta} \underbrace{\sum_s u^{(s)}_\beta(k)\, \overline{u}^{(s)}_\gamma(k)}_{(\slashed{k}+m_e)_{\beta\gamma}}\, \gamma^\nu_{\gamma\delta}\, u^{(s')}_\delta(k')\,, \tag{3.2.40}
$$

where m_e is the mass of the electron. Thus, $L^{\mu\nu}_{(e)}$ becomes the trace of the product of 4×4 matrices

$$
L^{\mu\nu}_{(e)} = \frac{1}{2}\mathrm{Tr}[(\slashed{k}' + m_e)\, \gamma^\mu\, (\slashed{k} + m_e)\, \gamma^\nu]\,. \tag{3.2.41}
$$

A straightforward evaluation of the tensor associated with the electron vertex (3.2.41) using the trace theorems given in Appendix B leads to

$$
\begin{aligned}
L^{\mu\nu}_{(e)} &= \frac{1}{2}\mathrm{Tr}(\slashed{k}'\gamma^\mu\, \slashed{k}\gamma^\nu) + \frac{1}{2}m_e^2\mathrm{Tr}(\gamma^\mu\gamma^\nu) \\
&= 2(k'^\mu k^\nu + k'^\nu k^\mu - (k'.k - m_e^2)g^{\mu\nu})\,. \tag{3.2.42}
\end{aligned}
$$

The evaluation of $L^{\mu\nu}_{(\mu)}$ is identical, yielding

$$
L^{(\mu)}_{\mu\nu} = 2(p'_\mu p_\nu + p'_\nu p_\mu - (p'.p - m_\mu^2)g_{\mu\nu})\,, \tag{3.2.43}
$$

where m_μ is the mass of the muon. Forming the product of (3.2.42) and (3.2.43), we finally arrived at the following "exact" form for the spin average $e^-\mu^- \to e^-\mu^-$ amplitude,

$$
\begin{aligned}
\overline{|\mathfrak{M}|^2} &= \frac{8e^4}{q^4}[(k' . p')(k . p) + (k' . p)(k . p') \\
&\quad + m_e^2 p' . p - m_\mu^2 k' . k + 2m_e^2 m_\mu^2]\,. \tag{3.2.44}
\end{aligned}
$$

In the extreme relativistic limit, we could neglect the terms containing m_e^2 and m_μ^2.

3.3 Mandelstam Variables

In high energy physics, cross sections and decay rates are written using kinematic variables that are relativistic invariants. For any "two particle to two particle" process $(A+B \to C+D)$ we have at our disposal the four-momenta associated with each particle, and thus invariant variables are the scalar products $p_A \cdot p_B$, $p_A \cdot p_C$, $p_A \cdot p_D$. Rather than these, it is conventional to use the related (Mandelstam) variables[1]

$$
\begin{aligned}
s &= (p_A + p_B)^2 = (p_C + p_D)^2 \\
t &= (p_A - p_C)^2 = (p_B - p_D)^2 \\
u &= (p_A - p_D)^2 = (p_B - p_C)^2.
\end{aligned}
\qquad (3.3.45)
$$

However, because $p_i^2 = m_i^2$ (with $i = A, B, C, D$) and $p_A + p_B = p_C + p_D$ due to energy momentum conservation,

$$
\begin{aligned}
s + t + u &= \sum_i m_i^2 + 2p_A^2 + 2p_A \cdot (p_B - p_C - p_D) \\
&= \sum_i m_i^2,
\end{aligned}
\qquad (3.3.46)
$$

i.e., only two of the three variables are independent.

To get a better feel for s, t, and u let us evaluate them explicitly in the center-of-mass frame for particles all of mass m,

$$
\begin{aligned}
s &= (p_A + p_B)^2 = 4(k^2 + m^2), \\
t &= (p_A - p_C)^2 = -(\vec{k}_i - \vec{k}_f)^2 = -2k^2(1 - \cos\theta) \\
u &= (p_A - p_D)^2 = -(\vec{k}_i + \vec{k}_f)^2 = -2k^2(1 + \cos\theta)
\end{aligned}
$$

where, $p_A = (E, \vec{k}_i)$, $p_B = (E, -\vec{k}_i)$, $p_C = (E, \vec{k}_f)$, $p_D = (E, -\vec{k}_f)$, $E = (k^2 + m^2)^{1/2}$, and θ is the center-of-mass scattering angle, i.e., $\vec{k}_i \cdot \vec{k}_f = k^2 \cos\theta$. As $k^2 \geq 0$, we have $s \geq 4m^2$; and since $-1 \leq \cos\theta \leq 1$, we have $t \leq 0$ and $u \leq 0$. Note that $t = 0$ $(u = 0)$ corresponds to forward (backward) scattering.

In the center-of-mass system for the reaction $A+B \to C+D$, s is equal to the square center-of-mass energy E_{cm}^2, where E_{cm} is the sum of the energies of

---

[1]S. Mandelstam, Phys. Rev. **112**, 1344 (1958).

particles A and B, t represents the square of the momentum transfer between particles A and C, and u (which is not an independent variable) represents the square of the momentum transfer between particles A and D. This is called the s-channel process. As we have seen, in the s-channel s is positive, while t and u are negatives.

From this process we can form another process, $A\overline{C} \to \overline{B} + D$, by taking the antiparticle of C to the left-hand side and the antiparticle of B to the right-hand side. The antiparticles have four-momenta which are the negatives of the momenta of the particles: $p_B \to -p_B$ and $p_C \to -p_C$ relative to the s-channel reaction. Hence, here $s = (p_A - p_B)^2$, $t = (p_A + p_C)^2$, and $u = (p_A - p_D)^2$. This is called the t-channel process. In this channel t is positive and represents the square of center-of-mass energy of the $A\overline{C}$ system, whereas $s \leq 0$ and $u \leq 0$ are squares of momentum transfers.

We can form yet another process from the above, $A + \overline{D} \to \overline{B} + C$, by taking the antiparticle of B to the left-hand side and the antiparticle of D to the right-hand side. Correspondingly here, $s = (p_A - p_B)^2$, $t = (p_A - p_C)^2$, and $u = (p_A + p_D)^2$. This is called the u-channel process. In this channel, u is positive and represents the square of center-of-mass energy of the $A\overline{D}$ system, while $s \leq 0$ and $t \leq 0$ are squares of momentum transfers.

In the extreme relativistic limit the Mandelstam variables become

$$
\begin{aligned}
s &\equiv (k+p)^2 &&\simeq 2k \cdot p \simeq 2k' \cdot p' \simeq 4k^2\,, \\
t &\equiv (k-k')^2 &&\simeq -2k \cdot k' \simeq -2p \cdot p' \simeq -2k^2(1-\cos\theta)\,, \quad (3.3.47)\\
u &\equiv (k-p')^2 &&\simeq -2k \cdot p' \simeq -2k' \cdot p \simeq -2k^2(1+\cos\theta)\,,
\end{aligned}
$$

where $p_A \equiv k$, $p_B \equiv p$, $p_C \equiv k'$, and $p_D \equiv p'$. At high energies, the unpolarized $e^-\mu^- \to e^-\mu^-$ scattering amplitude (3.2.44) can be rewritten as

$$
\begin{aligned}
\overline{|\mathfrak{M}|^2} &= \frac{8e^4}{(k-k')^4}[(k' \cdot p')(k \cdot p) + (k' \cdot p)(k \cdot p')] \\
&= 2e^4\frac{s^2+u^2}{t^2}. && (3.3.48)
\end{aligned}
$$

We may also obtain the amplitude for $e^-e^+ \to \mu^+\mu^-$ by "crossing" the result for $e^-\mu^- \to e^-\mu^-$. The required interchange is $k' \leftrightarrow -p$, that is, $s \leftrightarrow t$ in (3.3.48), and we obtain

$$
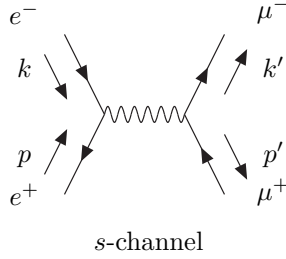\overline{|\mathfrak{M}|^2} = 2e^4\frac{t^2+u^2}{s^2}\,, \qquad (3.3.49)
$$

Figure 3.7: *Feynman diagram for $e^+e^- \to \mu^+\mu^-$.*

where now $e^-e^+ \to \mu^+\mu^-$ is the s-channel process. The corresponding tree level diagram is drawn in Fig. 3.7. This result can be translated into a differential cross section for $e^-e^+ \to \mu^+\mu^-$ scattering using (3.1.27). In the center-of-mass frame we have

$$\frac{d\sigma}{d\Omega}\bigg|_{\text{cm}} = \frac{1}{64\pi^2 s} 2e^4[\tfrac{1}{2}(1 + \cos^2\theta)] , \qquad (3.3.50)$$

where the quantity in square brackets is $(t^2 + u^2)/s^2$. Using $\alpha = e^2/4\pi$, this becomes

$$\frac{d\sigma}{d\Omega}\bigg|_{\text{cm}} = \frac{\alpha^2}{4s}(1 + \cos^2\theta) . \qquad (3.3.51)$$

To obtain the reaction cross section, we integrate over θ and ϕ

$$\sigma_{e^+e^- \to \mu^+\mu^-} = \frac{4\pi\alpha^2}{3s} . \qquad (3.3.52)$$

A comparison of these results with PETRA data[2] is shown in Figs. 3.8 and 3.9. The PETRA accelerator consists of a ring of magnets which simultaneously accelerate an electron and a positron beam circulating in opposite directions. In selected spots these beams are crossed, resulting in e^+e^- interactions with $\sqrt{s} = 2E_{\text{beam}}$, where E_{beam} is the energy of each beam. Equation (3.3.52) can be written in numerical form as

$$\sigma_{e^+e^- \to \mu^+\mu^-} = \frac{20(\text{nb})}{E_{\text{beam}}^2/\text{GeV}^2} . \qquad (3.3.53)$$

---

[2] H. J. Behrend *et al.* [CELLO Collaboration], Z. Phys. C **14**, 283 (1982); Phys. Lett. B **191**, 209 (1987); Phys. Lett. B **222**, 163 (1989); W. Bartel *et al.* [JADE Collaboration], Z. Phys. C **26**, 507 (1985); Phys. Lett. B **161**, 188 (1985).
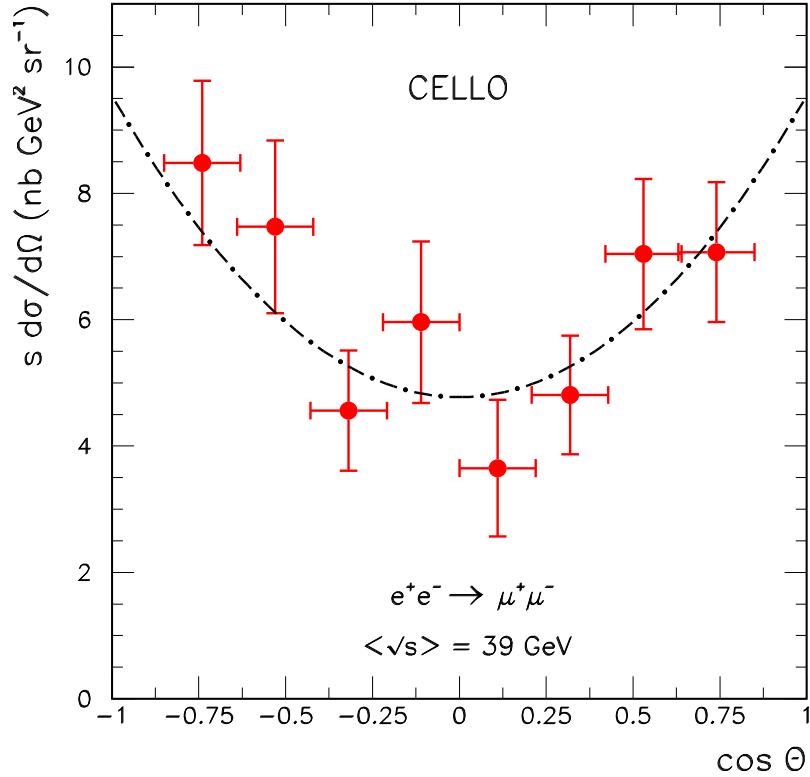
Figure 3.8: *The $e^+e^- \to \mu^+\mu^-$ angular distribution for $\langle\sqrt{s}\rangle = 39$ GeV. The dot-dashed line shows the relativistic limit of lowest order QED prediction.*

There are, of course, corrections to (3.3.53) of order α^3, $\alpha^4, \ldots$, arising due to interference with, or directly from, the amplitudes of higher order diagrams.

We can now use the procedure sketched in Sec. (3.2) to calculate the (lowest-order) amplitude for Møller scattering. As noted in the analysis of spinless electrons, for $e^-e^- \to e^-e^-$, we have identical particles in the initial and final states, and so the amplitude should be symmetric under the interchange of particle labels $C \leftrightarrow D$ (and $A \leftrightarrow B$), i.e., we have to calculate the t- and u-channel diagrams drawn in Fig. 3.6. To obtain the amplitude for $e^-e^+ \to e^-e^+$, we can simply use the antiparticle prescription to "cross" the result for $e^-e^- \to e^-e^-$. Furthermore, one can immediately check by
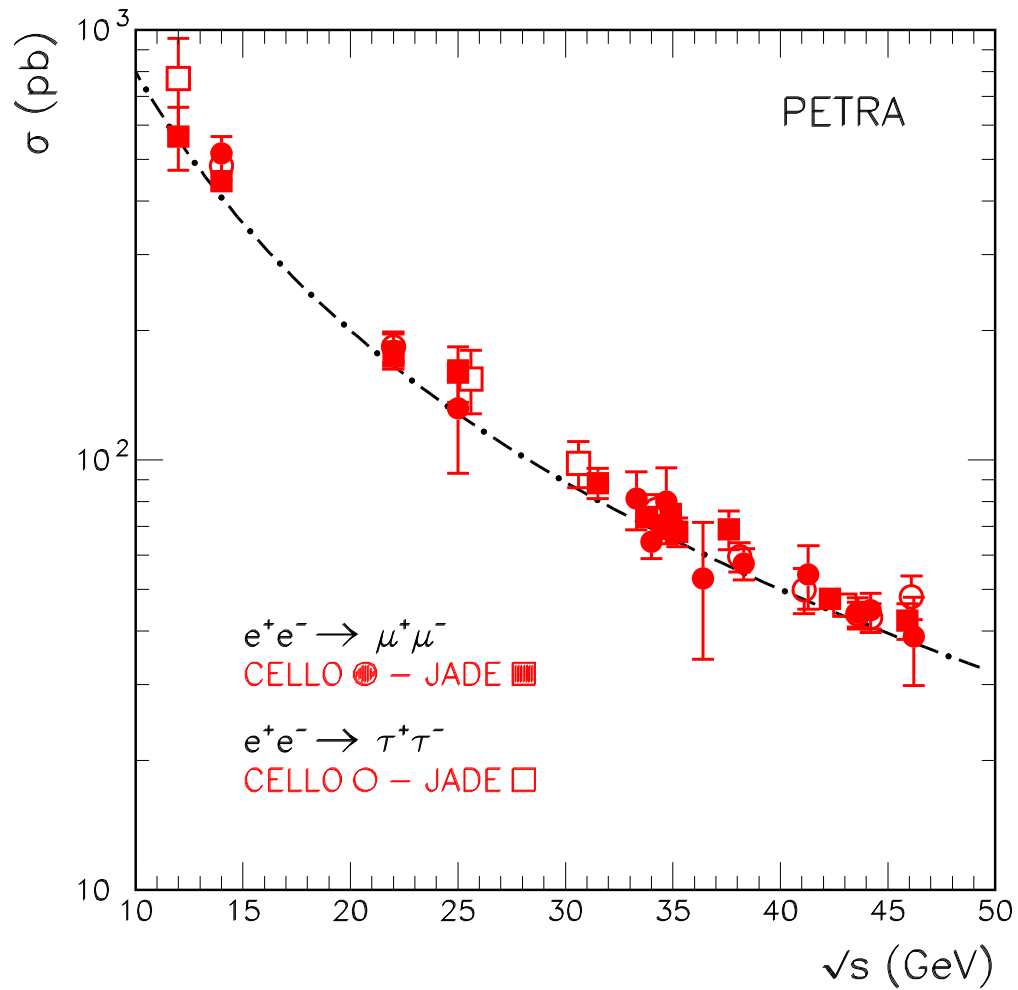
Figure 3.9: *Solid (open) symbols indicate the cross section for $e^+e^- \to \mu^+\mu^-$ ($e^+e^- \to \tau^+\tau^-$) measured at PETRA versus the center-of-mass energy. The dot-dashed line shows the relativistic limit of lowest order QED prediction.*
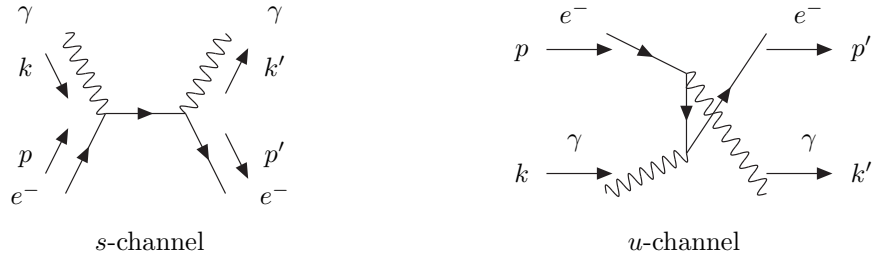
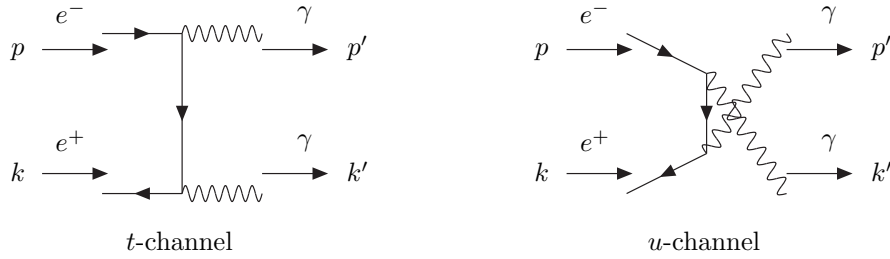Figure 3.10: *Lowest-order Feynman diagrams for Compton scattering.*

Figure 3.11: *Lowest-order Feynman diagrams for pair annihilation.*

inspection of Figs. 3.10 and 3.11 that a similar analysis applies to obtain the amplitude of pair annihilation $e^+e^- \rightarrow \gamma\gamma$ by crossing the amplitude for Compton scattering $e^-\gamma \rightarrow e^-\gamma$. In Table 3.1 we give the amplitudes for all these processes in the extreme relativistic limit. The origin of the forward and backward peaks in the differential cross section is identified; corresponding to t- and u-channel exchanged with photons and electrons being almost on mass shell. Recall that t- and u- are the squares of the three momentum transferred, i.e., the momentum carried by the virtual particle. When the mediator has a very small momentum squared (i.e., almost on its mass shell), then by the uncertainty principle the range of interaction is very large. Interaction with small deflections thus occurs with large cross sections.

Similar results are found in QCD for the strong $qq \rightarrow qq$, $q\bar{q} \rightarrow q\bar{q}$ interactions via single gluon exchange. In fact, the results are identical except that we must average (sum) over the color of the initial (final) quarks, in addition to their spins, and make the replacement $\alpha \rightarrow \alpha_s$, where $\alpha_s = g_s^2/4\pi$ is the quark gluon coupling.

88

Table 3.1: *Leading order contributions of some QED processes.*

Process	$\overline{\lvert\mathfrak{M}\rvert^2}/2e^4$
$\underbrace{\text{Møller scattering}}_{e^-e^-\to e^-e^-}$	$\underbrace{\dfrac{s^2+u^2}{t^2}}_{\text{forward}} + \underbrace{\dfrac{2s^2}{tu}}_{\text{interference}} + \underbrace{\dfrac{s^2+t^2}{u^2}}_{\text{backward}}$
(Crossing $s\leftrightarrow u$)	($u\leftrightarrow t$ symmetric)
$\underbrace{\text{Bhabha scattering}}_{e^-e^+\to e^-e^+}$	$\underbrace{\dfrac{s^2+u^2}{t^2}}_{\text{forward}} + \underbrace{\dfrac{2u^2}{ts}}_{\text{interference}} + \underbrace{\dfrac{u^2+t^2}{s^2}}_{\text{timelike}}$
$e^-\mu^- \to e^-\mu^-$	$\underbrace{\dfrac{s^2+u^2}{t^2}}_{\text{forward}}$
$e^-e^+ \to \mu^-\mu^+$	$\underbrace{\dfrac{u^2+t^2}{s^2}}_{\text{timelike}}$
$\underbrace{\text{Compton scattering}}_{e^-\gamma\to e^-\gamma}$	$-\underbrace{\dfrac{u}{s}}_{\text{timelike}} - \underbrace{\dfrac{s}{u}}_{\text{backward}}$
$\underbrace{\text{pair annihilation}}_{e^+e^-\to\gamma\gamma}$	$\underbrace{\dfrac{u}{t}}_{\text{forward}} + \underbrace{\dfrac{t}{u}}_{\text{backward}}$

3.4 Feynman Rules

This section encompasses a heuristic treatment of QED based on Feynman's intuitive space-time approach.[3] Our primary aim is to motivate Feynman rules and to calculate physical amplitudes. We saw earlier [Eq. (1.6.161)] that the nonrelativistic perturbation expansion of the transition amplitude is

$$T_{fi} = -i2\pi\delta(E_f - E_i) \left[\langle f|V|i \rangle + \sum_{n \neq 1} \langle f|V|n \rangle \frac{1}{E_i - E_n} \langle n|V|i \rangle + \ldots \right],$$
(3.4.54)

where we have associated factors of $\langle f|V|n \rangle$ with the vertices and identified $1/(E_i - E_n)$ as the propagator. The state vectors are eigenstates of the Hamiltonian in the absence of V, i.e., $H_0|n\rangle = E_n|n\rangle$. Formally we may therefore rewrite (3.4.54) as

$$T_{fi} = 2\pi\delta(E_f - E_i)\langle f|(-iV) + (-iV)\frac{i}{E_i - H_0}(-iV) + \ldots |i\rangle, \quad (3.4.55)$$

where we have made use of the completness relation $\sum |n\rangle\langle n| = 1$. It is natural to take $(-iV)$, rather than V, as the perturbation parameter.[4] That is, the vertex factor is $-iV$, and the propagator may thus be regarded as i times the inverse of the Schrödinger operator,

$$-i(E_i - H_0)\psi = -iV\psi \qquad (3.4.56)$$

acting on the intermediate state. We can now apply the same technique to various relativistic wave equations to deduce the form of the propagators for the corresponding particles.

For example, the form of the Klein-Gordon equation corresponding to (3.4.56) is

$$i(\Box^2 + m^2)\phi = -iV\phi, \qquad (3.4.57)$$

see (3.1.1). Guided by the relativistic generalization of (3.4.55), we expect the propagator for a spinless particle to be the inverese of the operator on

---

[3]R. P. Feynman, Rev. Mod. Phys. **20**, 367 (1948); Phys. Rev. **80**, 440 (1950).

[4]The $-i$ arises from the i in $i\partial\psi/\partial t = V\psi$, which leads to a time dependence e^{-iVt} in the interaction picture.

the left-hand side of (3.4.57). For an intermediate state of momentum p, this gives

$$\frac{1}{i(-p^2 + m^2)} = \frac{i}{p^2 - m^2} \,. \tag{3.4.58}$$

In a similar fashion, an electron in an electromagnetic field satisfies

$$(\not{p} - m_e)\psi = e\gamma^\mu A_\mu \psi \,. \tag{3.4.59}$$

As before, we must multiply by $-i$. Hence, the vertex factor is is $-ie\gamma^\mu$. The electron propagator is therefore the inverse of $-i$ times the left-hand side of (3.4.59):

$$\frac{1}{-i(\not{p} - m_e)} = \frac{i}{\not{p} - m_e} = \frac{i(\not{p} + m_e)}{p^2 - m_e^2} = \frac{i}{p^2 - m_e^2} \sum_s u\overline{u} \,, \tag{3.4.60}$$

where we have used $\not{p}\not{p} = p^2$ and the completeness relation (1.5.108). The numerator contains the sum over the spin states of the virtual electron.

In summary, the general form of the propagator of a virtual particle of mass m is

$$\frac{i}{p^2 - m^2} \sum_{\text{spins}} \,. \tag{3.4.61}$$

The spin sum is the completeness relation; we include all possible spin states of the propagating particle. We would also integrate over the different momentum states that propagate. For the diagrams we have considered so far, this momentum is fixed by the momenta of the external particles.

The propagator for the photon is not unique, on account of the freedom in the choice of A^μ. Recall that physics is unchanged by the transformation that is associated with the invariance of QED under phase or gauge transformations of the wavefunctions of charged particles

$$A_\mu \to A'_\mu = A_\mu + \partial_\mu \chi \,, \tag{3.4.62}$$

where χ is any function that satisfies

$$\Box^2 \chi = 0 \,. \tag{3.4.63}$$

The wave equation for a photon (1.2.4) can be written as

$$(g^{\nu\lambda}\Box^2 - \partial^\nu \partial^\lambda)A_\lambda = j^\nu \tag{3.4.64}$$

and, in fact, a photon propagator cannot exist until we remove some of the gauge freedom of A_λ. In our discussion so far, we have chosen to work in the Lorentz class of gauges with $\partial_\lambda A^\lambda = 0$. In such a case, the wavefunction A^μ for a free photon satisfies the equation

$$\Box^2 A^\mu = 0 \,, \tag{3.4.65}$$

which has solutions

$$A^\mu = \epsilon^\mu(q)e^{-iq \cdot x} \,, \tag{3.4.66}$$

where the four vector ϵ^μ is the polarization vector of the photon. With this in mind, the wave equation (3.4.64) simplifies to $g^{\nu\lambda}\Box^2 A_\lambda = j^\nu$, and since $g_{\mu\nu}g^{\nu\lambda} = \delta_\mu^\lambda$ (where δ_μ^λ is the Kronecker delta), the propagator (the inverse of the momentum space operator multiply by $-i$) is

$$i\frac{-g_{\mu\nu}}{q^2} \,. \tag{3.4.67}$$

The wave equation for a spin-1 particle of mass M can be obtained from that for the photon by the replacement $\Box^2 \rightarrow \Box^2 + M^2$. From (3.4.64) we see that the wavefunction B_λ for a free particle satisfies

$$\left[g^{\nu\lambda}(\Box^2 + M^2) - \partial^\nu\partial^\lambda\right] B_\lambda = 0 \,. \tag{3.4.68}$$

Proceeding exactly as before, we determine the inverse of the momentum space operator by solving

$$\left[g^{\nu\lambda}(-p^2 + M^2) - p^\nu p^\lambda)\right]^{-1} = \delta_\lambda^\mu(Ag_{\mu\nu} + Bp_\mu p_\nu) \tag{3.4.69}$$

for A and B. The propagator, which is the quantity in brackets on the right-hand side of (3.4.69) multiplied by i, is found to be

$$\frac{i(-g^{\mu\nu} + p^\mu p^\nu/M^2)}{p^2 - M^2} \,. \tag{3.4.70}$$

We can show that the numerator is the sum over the three spin states of the massive particle when taken on-shell $p^2 = M^2$. We first take the divergence, ∂_ν, of (3.4.68). Two terms cancel and we find

$$M^2\partial^\lambda B_\lambda = 0 \,. \tag{3.4.71}$$

92

Hence for a massive vector particle, we have no choice but to take $\partial^\lambda B_\lambda = 0$; it is not a gauge condition. As a consequence, the wave equation reduces to

$$(\Box^2 + M^2)B_\mu = 0 \tag{3.4.72}$$

with free particle solutions

$$B_\mu = \epsilon_\mu \, e^{-ip \cdot x} \, . \tag{3.4.73}$$

The condition (3.4.71) demands $p^\mu . \epsilon_\mu = 0$ and so reduces the number of independent polarization vectors from four to three in a covariant fashion.

Likewise, the Lorentz condition for photons, $\partial_\mu A^\mu = 0$ gives, $q_\mu . \epsilon^\mu = 0$, reducing the number of independent components of ϵ^μ to three. In this case we can explore the consequences of the additional gauge freedom (3.4.62). Choose a gauge parameter

$$\chi = iae^{-iq.x} \tag{3.4.74}$$

with a constant so that (3.4.63) is satisfied. Substituting this, together with (3.4.66) into (3.4.62) shows that the physics is unchanged by the replacement

$$\epsilon_\mu \to \epsilon'_\mu = \epsilon_\mu + aq_\mu \, . \tag{3.4.75}$$

In other words, two polarization vectors $(\epsilon_\mu, \, \epsilon'_\mu)$ which differ by a multiple of q_μ describe the same photon. We may use this freedom to ensure that the time component of ϵ^μ vanishes, $\epsilon^0 \equiv 0$ and the Lorentz condition reduces to $\vec{\epsilon} . \vec{q} = 0$. This (noncovariant) choice of gauge is known as the Coulomb gauge. This means that there are only *two* independent polarization vectors and they are both transverse to the three-momentum of the photon. For example, for a photon traveling along the z-axis, we may take

$$\epsilon_1 = (1, 0, 0), \quad \epsilon_2 = (0, 1, 0) \, . \tag{3.4.76}$$

A free photon is thus described by its momentum q and a polarization vector $\vec{\epsilon}$. Since $\vec{\epsilon}$ transforms as a vector, we can anticipate that it is associated with a particle of spin-1. Nevertheless, we have associated with a virtual photon the covariant propagator $i(-g_{\mu\nu})/q^2$, where $-g_{\mu\nu}$ implies we are summing over *four* polarization states. The completeness relation (in an obvious notation)

93

is given by

$$
\begin{aligned}
-g_{\mu\nu} &= \sum_{\lambda=1}^{4} \epsilon_\mu^{(\lambda)*}\,\epsilon_\nu^{(\lambda)} = \sum_T \epsilon_\mu^{T*}\epsilon_\nu^T + \sum_L \epsilon_\mu^{L*}\epsilon_\nu^L + \sum_S \epsilon_\mu^{S*}\epsilon_\nu^S \\
&= \underbrace{(\delta_{ij} - \hat{q}_i \hat{q}_j)}_{\text{transverse}} + \underbrace{\hat{q}_i \hat{q}_j}_{\text{longitudinal}} + \underbrace{(-g_{\mu 0} g_{\nu 0})}_{\text{scalar}} \, . \quad (3.4.77)
\end{aligned}
$$

However, in a sense every photon is virtual, being emitted and then sooner or later being absorbed. How can one reconcile the two descriptions? Consider a typical Feynman diagram containing a virtual photon exchanged between charged particles. For such diagrams (e.g., Fig. 3.5) we have found a transition amplitude of the form

$$
\begin{aligned}
T_{fi} &= -ie^2 \int j_\mu^A(x) \left(\frac{-g^{\mu\nu}}{q^2}\right) j_\nu^B(x)\, d^4x \\[6pt]
&= -ie^2 \int \left(\underbrace{\frac{j_1^A j_1^B + j_2^A j_2^B}{q^2}}_{\text{transverse}} + \underbrace{\frac{j_3^A j_3^B - j_0^A j_0^B}{q^2}}_{\text{longitudinal/scalar}} \right) d^4x \,, \quad (3.4.78)
\end{aligned}
$$

where we have taken the photon four-momentum $q^\mu = (q^0, 0, 0, |\vec{q}|)$. That is, we choose the 3-axis to be along $\hat{q}$. Recall that charge conservation gives rise to the continuity equation $\partial^\mu j_\mu = 0$. For both the A and B currents this implies

$$
q^\mu j_\mu = q^0 j_0 - |\vec{q}| j_3 = 0 \,. \tag{3.4.79}
$$

Therefore if the exchange photon is almost real, $q^0 \approx |\vec{q}|$, then $j_3 = j_0$ and the longitudinal and scalar contributions cancel each other, leaving only the two transverse contributions. For a real photon, we can therefore make the replacement

$$
\sum_T = \epsilon_\mu^{T*}\epsilon_\nu^T \to -g_{\mu\nu} \,. \tag{3.4.80}
$$

On the other hand, for a virtual photon the longitudinal and scalar components cannot be neglected.

Now, in the spirit of (3.4.55), we can obtain the invariant amplitude $\mathfrak{M}$ by drawing all (topologically distinct and connected) Feynman diagrams for the process and assigning multiplicative factors (summarized in Table 3.2) with the various elements of each diagram.

Table 3.2: *Feynman rules for* $-i\mathfrak{M}$.

	Multiplicative Factor

• **External Lines**

spin-0 boson (or antiboson)	1
spin-$\frac{1}{2}$ fermion (in, out)	u, $\overline{u}$
spin-$\frac{1}{2}$ antifermion (in, out)	$\overline{v}$, v
spin-1 photon (in, out)	ϵ_μ, ϵ_μ^*

• **Internal Lines − Propagators**

spin-0 boson	$\frac{i}{p^2-m^2}$
spin-$\frac{1}{2}$ fermion	$\frac{i(\not{p}+m)}{p^2-m^2}$
massive spin-1 boson	$\frac{-i(g_{\mu\nu}-p_\mu p_\nu/M^2)}{p^2-M^2}$
massless spin-1 boson (Feynman gauge)	$\frac{-ig_{\mu\nu}}{p^2}$

• **Vertex Factors**

photon−spin-0 (charge e)	$-ie(p+p')^\mu$
photon−spin-$\frac{1}{2}$ (charge e)	$-ie\gamma^\mu$

• *Loops:* $\int d^4k/(2\pi)^4$ over loop momentum; include -1 if fermion loop and take the trace of associated γ-matrices.

• *Identical fermions:* -1 between diagrams which differ only in $e^- \leftrightarrow e^-$ or initial $e^- \leftrightarrow$ final e^+.

95

3.5 Beyond the Trees

In this section, we attempt to provide a glimpse of the rich structure of QFT and expose the reader to the concepts of loops, renormalization, and running couplings in a concise and physical way. Because QFT is not the main subject of this course, the following discussion is rather incomplete and a few results are not explicitly derived. Nonetheless, only unrevealing algebra is omitted, which can be found in most field theory books.[5]

The bulk of hadrons produced in e^-e^+ annihilations are fragments of a quark and antiquark produced by the process $e^-e^+ \to q\bar{q}$. The cross section for the (QED) process $e^-e^+ \to q\bar{q}$ is readily obtained from that for the process drawn in Fig. 3.7,

$$\sigma_{e^+e^- \to \mu^+\mu^-} = \frac{4\pi\alpha^2}{3Q^2} , \tag{3.5.81}$$

a result obtained in (3.3.52). Here, the center-of-mass energy squared is $s = Q^2 = 4E_{\text{beam}}$. The required cross section is

$$\sigma_{e^+e^- \to q\bar{q}} = 3\, e_q^2\, \sigma_{e^+e^- \to \mu^-\mu^+} \tag{3.5.82}$$

where we have taken account of the fractional charge of the quark, e_q. The extra factor of 3 arises because we have a diagram for each quark color and the cross sections have to be added. To obtain the cross section for producing all types of hadrons, we must sum over all quark flavors $q = u, d, s, \ldots$, and hence

$$\begin{aligned}
\sigma_{e^+e^- \to \text{hadrons}} &= \sum_q \sigma_{e^+e^- \to q\bar{q}} \\
&= 3\sum_q e_q^2\, \sigma_{e^+e^- \to \mu^-\mu^+} .
\end{aligned} \tag{3.5.83}$$

This simple calculation leads to the dramatic prediction

$$R \equiv \frac{\sigma_{e^+e^- \to \text{hadrons}}}{\sigma_{e^+e^- \to \mu^-\mu^+}} = 3\sum_q e_q^2 . \tag{3.5.84}$$

---

[5]E.g., M. E. Peskin and D. V. Schroeder, *An Introduction to Quantum Field Theory,* (Addison-Wesley, Reading, 1995); R. K. Ellis, W. J. Stirling and B. R. Webber, *QCD and collider physics,* Camb. Monogr. Part. Phys. Nucl. Phys. Cosmol. **8**, 1 (1996).
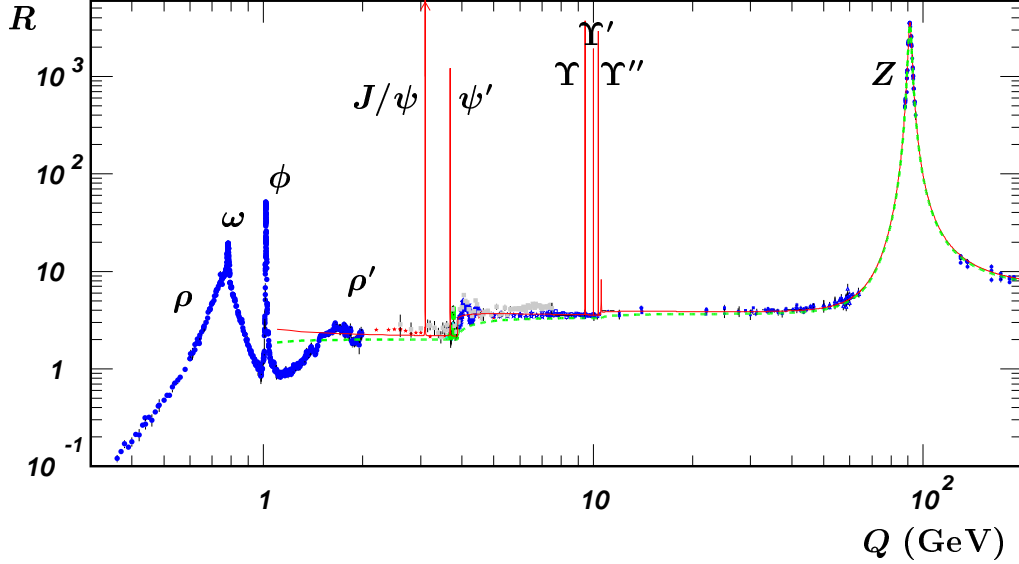
Figure 3.12: *Ratio R of (3.5.84) as a function of the total e^+e^- center-of-mass energy. (The sharp peaks correspond to the production of narrow resonances just below or near the flavor thresholds.)*

Because $\sigma_{e^+e^- \to \mu^-\mu^+}$ is well known (see Fig. 3.9), a measurement of the total e^+e^- annihilation cross section into hadrons therefore directly counts the number of quarks, their flavors, as well as their colors. We have

$$
\begin{aligned}
R &= 3\left[\left(\tfrac{2}{3}\right)^2 + \left(\tfrac{1}{3}\right)^2 + \left(\tfrac{1}{3}\right)^2\right] = 2 && \text{for } u,\, d,\, s, \\
&= 2 + 3\left(\tfrac{2}{3}\right)^2 = \tfrac{10}{3} && \text{for } u,\, d,\, s,\, c, \\
&= \tfrac{10}{3} + 3\left(\tfrac{1}{3}\right)^2 = \tfrac{11}{3} && \text{for } u,\, d,\, s,\, c,\, b. && (3.5.85)
\end{aligned}
$$

In Fig. 3.12 these predictions are compared to the measurements of R.[6] The

---

[6]See e.g., M. Bernardini *et al.*, Phys. Lett. B **51**, 200 (1974); J. Siegrist *et al.*, Phys. Rev. D **26**, 969 (1982); M. Althoff *et al.* [TASSO Collaboration], Z. Phys. C **22**, 307 (1984); D. Besson *et al.* [CLEO Collaboration], Phys. Rev. Lett. **54**, 381 (1985); B. Adeva *et al.* [Mark-J Collaboration], Phys. Rev. D **34**, 681 (1986); T. Kumita *et al.* [AMY Collaboration], Phys. Rev. D **42**, 1339 (1990).

value of $R \simeq 2$ is apparent below the threshold for producing charmed particles at $Q = 2(m_c + m_u) \simeq 3.7$ GeV. Above the threshold for all five quark flavors ($Q > 2m_b \simeq 10$ GeV), $R = \frac{11}{3}$ as predicted. These measurements confirm that there are three colors of quark, because $R = \frac{11}{3}$ would be reduced by a factor of 3 if there was only one color.

These results for R will be modified when interpreted in the context of QCD. Equation (3.5.83) is based on the (leading order) process $e^+e^- \to q\bar{q}$. However, we should also include diagrams where the quark and/or antiquark radiate gluons. In general

$$R(\alpha, s) = \frac{\sigma_{e^+e^- \to q\bar{q}}}{\sigma_{e^+e^- \to \mu^+\mu^-}} \tag{3.5.86}$$

is a function of the electromagnetic coupling α,

$$\alpha = \frac{e^2}{4\pi}\; ; \tag{3.5.87}$$

and the annihilation energy $s = 4E_{\text{beam}}^2$:

$$\tag{3.5.88}$$

As always, in (3.5.88) the antiparticles are drawn using only particle (e^-, μ^-, q) lines, but note that we omit the arrow lines indicating the time direction of the antiparticle's four-momenta. Hereafter we will adopt this simplified notation whenever there is no danger of confusion.

When the annihilation energy far exceeds the light masses m of quarks and leptons, we must expect that for the dimensionless observable R,

$$R(\alpha, s) \xrightarrow[s \gg m^2]{} \text{constant} \tag{3.5.89}$$

because there is no intrinsic scale in theories with massless exchange bosons. This prediction disagrees with experiment and is, in fact, not true in renormalizable QFT. The exchange of a massless photon is ultraviolet divergent,

requiring the introduction of a cutoff Λ. Thus, a scale is introduced into the calculation and the dimensionless observable $R(\alpha, s, \Lambda^2)$ is of the form

$$R = R\left(\alpha, \frac{s}{\Lambda^2}\right) . \tag{3.5.90}$$

This seems ugly; it is not: Λ appears order by order in the perturbative series but not in the final answer.[7] Therefore,

$$\Lambda^2 \frac{dR}{d\Lambda^2} = 0 . \tag{3.5.91}$$

This is the renormalization group equation, which can be written more explicitly:

$$\Lambda^2 \frac{\partial R}{\partial \Lambda^2} + \Lambda^2 \frac{\partial \alpha}{\partial \Lambda^2} \frac{\partial R}{\partial \alpha} = 0 , \tag{3.5.92}$$

which exhibits that R can depend on Λ directly, or via the coupling α. Equation (3.5.92) can be rewritten in the variable $t \equiv \ln(s/\Lambda^2)$. Using $\Lambda^2 \partial/(\partial \Lambda^2) = -\partial/[\partial \ln(s/\Lambda^2)]$, we obtain

$$\left(-\frac{\partial}{\partial t} + \beta \frac{\partial}{\partial \alpha}\right) R\left(\alpha(s), \frac{s}{\Lambda^2}\right) = 0 , \tag{3.5.93}$$

where

$$\beta = \Lambda^2 \frac{\partial \alpha}{\partial \Lambda^2} = \frac{\partial \alpha}{\partial t} . \tag{3.5.94}$$

With the identification $\Lambda^2 = s$, the renormalization group equation has the very simple solution,

$$R\left(\alpha(s), 1\right) , \tag{3.5.95}$$

in which the observable depends on s only via the coupling. Because $\alpha(s)$ is dimensionless, dimensional analysis requires

$$\alpha(s) = F\left(\alpha(\Lambda^2), \frac{s}{\Lambda^2}\right) , \tag{3.5.96}$$

which is consistent with (3.5.94),

$$\Lambda^2 \frac{d\alpha(s)}{d\Lambda^2} = \left[\frac{\partial F}{\partial z}(\alpha(s), z)\right]_{z=1} = \beta(\alpha) . \tag{3.5.97}$$
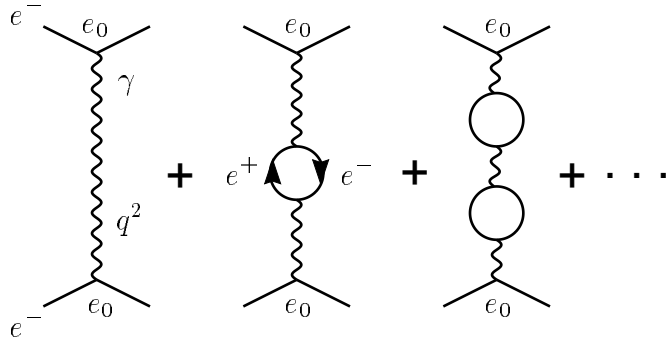
---

[7]In other words, because any Λ-value is arbitrary, physical observables (e.g., R) cannot depend on Λ.

The solution is

$$t = \ln(s/\Lambda) = \int_{\alpha(\Lambda)}^{\alpha(s)} \frac{dx}{\beta(x)} . \qquad (3.5.98)$$
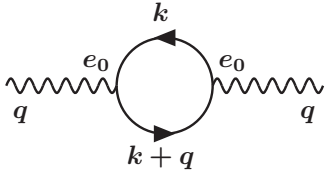
The "running" of the coupling is described by the β-function, which can be computed perturbatively. We discuss this next.

In field theory the interaction of two electrons by the exchange of a virtual photon is described by a perturbative series

$$= e_0^2 - e_0^2\, \Pi(q^2) + e_0^2\, \Pi^2(q^2) - \cdots ,$$
$$= \frac{e_0^2}{1 + \Pi(q^2)} , \qquad (3.5.99)$$

where

$$\Pi(q^2) = \qquad \qquad . \qquad (3.5.100)$$

Note the negative sign associated with the fermion loop, which is made explicit in order to introduce the summation (3.5.99). $\Pi(q^2)$ is ultraviolet divergent as $k \to \infty$; explicit calculation (see Appendix C) confirms this and we therefore write $\Pi(q^2)$ in terms of a divergent and finite part

$$\Pi(q^2) = \frac{e_0^2}{12\pi^2} \int_{m_e^2}^{\Lambda^2} \frac{dk^2}{k^2} - \frac{e_0^2}{12\pi^2} \ln \frac{-q^2}{m_e^2}$$
$$= \frac{e_0^2}{12\pi^2} \ln \left(\frac{\Lambda^2}{-q^2} \right) . \qquad (3.5.101)$$

100

The trick is to introduce a new charge e which is finite:

$$e^2 = e_0^2 \left[1 - \Pi(-q^2 = \mu^2) + \cdots \right] , \qquad (3.5.102)$$

or

$$e = e_0 \left[1 - \frac{1}{2}\Pi(-q^2 = \mu^2) + \cdots \right] . \qquad (3.5.103)$$

We never said what e_0 was. It is, in fact, infinitesimal and combines with the divergent loop Π to yield the finite, physical charge e. This operation is performed at some reference momentum μ, e.g. $e(\mu = 0)$ is the Thomson charge with $\alpha = e^2(\mu = 0)/(4\pi) = 1/137.035999679(94)$. To illustrate how this works we calculate $e^- e^-$ scattering. The amplitude is (ignoring identical particle effects)

$$(3.5.104)$$

where (3.5.104) has been obtained by substituting the renormalized charge e for the bare charge using (3.5.103)

$$(3.5.105)$$

101

In the last term of (3.5.104) we can just replace e_0 by e as the additional terms associated with the substitution (3.5.105) only appear in higher order. Therefore (3.5.104) can be rewritten as:

$$\text{at } -q^2 = \mu^2$$

$$\frac{\alpha}{3\pi} \ln\left(\frac{\Lambda^2}{-q^2}\right) - \frac{\alpha}{3\pi} \ln\left(\frac{\Lambda^2}{\mu^2}\right)$$

$$= \frac{\alpha}{3\pi} \ln\left(\frac{\mu^2}{-q^2}\right) = \text{finite!} \qquad (3.5.106)$$

The divergent parts cancel and we obtain a finite result to $\mathcal{O}(\alpha^2)$. In a renormalizable theory this cancellation happens at every order of perturbation theory. The price we have paid is the introduction of a parameter $\alpha(\mu^2)$ which is fixed by experiment. The electron charge, unfortunately, cannot be calculated.

In summary, by using the substitution (3.5.102) the perturbation series using infinitesimal charges e_0 and infinite loops Π has been reshuffled order by order to obtain finite observables. The running charge (3.5.102) can be written as

$$\alpha = \alpha_0 \left[1 - \Pi(q^2) + \cdots\right] = \frac{\alpha_0}{1 + \Pi(q^2)}. \qquad (3.5.107)$$

For the QED result (3.5.101),

$$\alpha(Q^2 = -q^2) = \frac{\alpha_0}{1 - b\alpha_0 \ln \frac{Q^2}{\Lambda^2}} \qquad (3.5.108)$$

with $b = 1/3\pi$. The ultraviolet cutoff is eliminated by renormalizing the charge to some measured value at $Q^2 = \mu^2$,
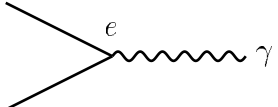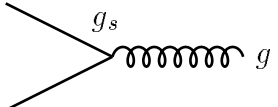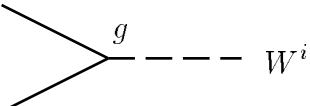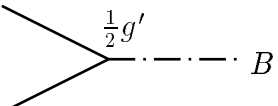
$$\frac{1}{\alpha(Q^2)} - \frac{1}{\alpha(\mu^2)} = -b \ln \frac{Q^2}{\mu^2}. \qquad (3.5.109)$$

One also notices that b determines the β-function to leading order in perturbation theory. We obtain indeed from (3.5.94) and (3.5.108) that

$$\beta(\alpha) = \frac{\partial \alpha(Q^2)}{\partial t} = b\alpha^2 + \mathcal{O}(\alpha^3).$$ (3.5.110)

In Table 3.3 we have listed the b-values determining the running of the other standard model couplings: the weak couplings g, g' and the strong color charge g_s. From Eq. (3.5.95) it is clear that much of the structure of the gauge theory is dictated by identifying the momentum dependence of the couplings.

Table 3.3: *b-values for the running of the coupling constants.*

coupling $\alpha_i \equiv \dfrac{g_i^2}{4\pi}$	b_i-value
$e \;\rangle\!\!\!\sim\!\!\!\sim\; \gamma$	$\dfrac{1}{3\pi}$
$g_s \;\rangle\!\!\!\text{0000000}\; g$	$\dfrac{2n_q - 33}{12\pi}$
$g \;\rangle\!\!- - -\; W^i$	$\dfrac{4n_g + \frac{1}{2}n_d - 22}{12\pi}$
$\frac{1}{2}g' \;\rangle\!\!-\cdot-\cdot\; B$	$\dfrac{\frac{20}{3}n_g + \frac{1}{2}n_d}{12\pi}$

n_q : number of quarks (2–6)
n_g : number of generations (3)
n_d : number of Higgs doublets (1)

The formal arguments have revealed the screening of the electric charge. There is physics associated with Eq. (3.5.99). In quantum field theory a

charge is surrounded by virtual e^+e^- pairs which screen the charge more efficiently at large than at small distances. Therefore $\alpha^{-1}(\mu^2 = 0) \simeq 137$ is smaller than the short-distance value $\alpha^{-1}(\mu^2 = m_Z^2) = 127.925 \pm 0.016.$[8] We note that, qualitatively,

$$\frac{1}{\alpha(0)} - \frac{1}{\alpha(m_Z^2)} \simeq 9 \simeq \frac{1}{3\pi} \ln\left(\frac{m_Z^2}{m_e^2}\right) ; \qquad (3.5.111)$$

see (3.5.109).

For 3 generations of quarks the b-value for QCD is negative. While $q\bar{q}$ pairs screen color charge just like e^+e^- pairs screen electric charge (the $2n_f/12\pi$ term in b), loops with gluons reverse that effect with a larger, negative b-value of $-33/12\pi$. The color charge grows with distance yielding the *asymptotic freedom* property: $\alpha_s \to 0$ as $Q \to \infty$. On the other hand, the theory becomes strongly coupled (infrared slavery) at the energy scale $Q^2 \sim \Lambda_{\mathrm{QCD}}^2$, presumably leading to the confinement of quarks and gluons.

---

[8]J. Erler, Phys. Rev. D **59**, 054008 (1999).

Chapter 4

Hard Scattering Processes

4.1 Deep Inelastic Scattering

Hadrons are composite systems with many internal degrees of freedom. The strongly interacting constituents of these systems, the so-called "partons" are described by QCD. This theory is asymptotically free, that is, it can be treated in a perturbative way for very large values of the four-momentum transfer, $Q^2 \equiv -q^2$. However, the binding forces become increasingly strong if the momentum transfer decreases towards the region $\lesssim 1$ GeV, which is the natural habitat of nucleons and pions. In particular, the "running" of the QCD coupling constant $\alpha_s(Q^2)$, is expected to diverge if Q^2 decreases to values near $\Lambda_{\mathrm{QCD}}^2 \approx (250$ MeV$)^2$, which defines the "Landau pole" of QCD.[1] This behavior is totally different from QED, for which $\alpha(Q^2)$ diverges for huge momentum transfers at the Planck scale, corresponding to $Q \approx M_{\mathrm{Pl}} \approx 1.22 \times 10^{19}$ GeV, or 1.62×10^{-35} m, below any distance ever to be resolved by experiment. Contrariwise, the Landau pole of QCD corresponds to a resolution of nucleon's size (somewhat below 1 fm or 10^{-15} m) and is referred to as the onset of the "deep inelastic regime."[2]

In the late 60s, deep inelastic scattering experiments paved the way for understanding the structure of the nucleon. When trying to deduce the struc-

---

[1] L. D. Landau and I. Y. Pomeranchuk, Dokl. Akad. Nauk Ser. Fiz. **102**, 489 (1955).

[2] R. Devenish and A. Cooper-Sarkar, *Deep Inelastic Scattering*, (Oxford University Press, 2004).
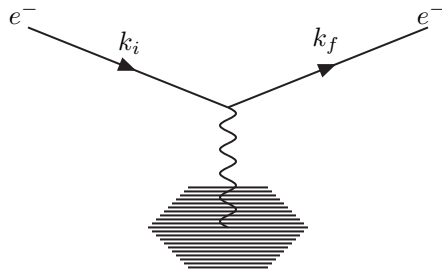
Figure 4.1: *Lowest-order electron scattering by a charge cloud.*

ture of composite objects, like hadrons, the underlying idea is quite simple and straightforward. Suppose we want to determine the charge distribution shown in Fig. 4.1, which could, for example, be the cloud of an atom. The procedure to obatin this information is to scatter electrons on this cloud, measure the angular cross section and compare it with the known cross section for scattering of a point distribution. As the charge cloud certainly is not a point charge, this would give us a form factor $F(q)$, i.e.,

$$\frac{d\sigma}{d\Omega} = \frac{d\sigma}{d\Omega}\bigg|_{\text{point}} |F(q)|^2 \,, \tag{4.1.1}$$

where q is the momentum transfer between the incident electron and the target, $q = k_i - k_f$. We then attempt to deduce the structure of the target from the $F(q)$ so determined.

We can gain insight into this technique by first looking at the scattering of unpolarized electrons of energy E from a static spinless charge distribution $-Ze\rho(\vec{x})$, normalized so that

$$\int \rho(\vec{x}) \, d^3x = 1 \,. \tag{4.1.2}$$

For a static target, it is found that the form factor in (4.1.1) is just the Fourier transform of the charge distribution

$$F(\vec{q}) = \int \rho(\vec{x}) \, e^{i\vec{q}\cdot\vec{x}} \, d^3x \,, \tag{4.1.3}$$

while the reference cross section for a structureless target (see Appendix D) is

$$\frac{d\sigma}{d\Omega}\bigg|_{\text{point}} \equiv \frac{d\sigma}{d\Omega}\bigg|_{\text{Mott}} = \frac{(Z\alpha)^2 E^2}{4k^4 \, \sin^4(\theta/2)} \left[1 - v^2 \, \sin^2(\theta/2)\right] \,, \tag{4.1.4}$$

106

where $k = |\vec{k}_i| = |\vec{k}_f|$, $v = k/E$, and θ is the angle through which the electron is scattered. By virtue of the normalization condition (4.1.2) $F(0) = 1$. If $|\vec{q}|$ is not too large, we can expand the exponential in (4.1.3), yielding

$$
\begin{aligned}
F(\vec{q}) &= \int \left(1 + i\vec{q} \cdot \vec{x} - \frac{(\vec{q} \cdot \vec{x})^2}{2} \dots \right) \rho(\vec{x}) \, d^3x \\
&= \int \left(1 + iq\, r\, \cos\theta - \frac{1}{2} q^2\, r^2\, \cos^2\theta \dots \right) \rho(r) r^2 \, d(\cos\theta) \, d\phi \, dr \\
&= 1 - \frac{1}{6} |\vec{q}|^2 \langle r^2 \rangle + \dots \, ,
\end{aligned}
\tag{4.1.5}
$$

where we have assumed that ρ is spherically symmetric, that is, a function of $r \equiv |\vec{x}|$ alone. The small-angle scattering therefore just measures the mean square radius,

$$
\langle r^2 \rangle = \int r^2 \, \rho(r) \, 4\pi \, r^2 \, dr \, ,
\tag{4.1.6}
$$

of the charge cloud. This is because in the small $|\vec{q}|$ limit the photon in Fig. 4.1 is soft and with its large wavelength can resolve only the size of the charge distribution $\rho(r)$ and is not sensitive to its detailed structure.

The above discussion cannot be applied directly to yield the structure of the proton. First, the proton's magnetic moment is involved in the scattering of the electron, not just its charge. Second, the proton is not static, but will recoil under the electron's bombardment. If, however, the proton were a point charge e with Dirac magnetic moment $e/2M$, then we already know the answer. We can take over the result for electron-muon scattering and simply replace the mass of the muon by that of the proton:

$$
\left. \frac{d\sigma}{d\Omega} \right|_{\text{lab}} = \left(\frac{\alpha^2}{4E^2 \sin^4(\theta/2)} \right) \frac{E'}{E} \left(\cos^2 \frac{\theta}{2} - \frac{q^2}{2M^2} \sin^2 \frac{\theta}{2} \right) \, ,
\tag{4.1.7}
$$

where the factor

$$
\frac{E'}{E} = \left(1 + \frac{2E}{M} \sin^2 \frac{\theta}{2} \right)^{-1}
\tag{4.1.8}
$$

given by (E.0.9), arises from the recoil of the target.

Copying the calculation of the electron muon cross section, the lowest order amplitude for electron proton elastic scattering (shown in Fig. 4.2) is

$$
T_{fi} = -i \int e j_\mu \left(-\frac{1}{q^2} \right) (-e) J^\mu d^4x \, ,
\tag{4.1.9}
$$

107
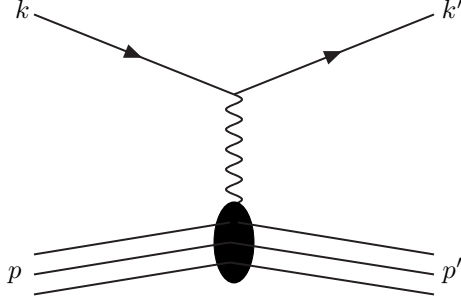
Figure 4.2: *Lowest-order electron-proton elastic scattering.*

where $q = p - p'$ and the electron and proton transition currents are, respectively

$$ej^\mu = e\overline{u}(k')\, \gamma^\mu\, u(k)e^{i(k'-k)\cdot x}\,, \qquad (4.1.10)$$

$$-eJ^\mu = -e\overline{u}(p')\, [\quad]\, u(p)e^{i(p'-p)\cdot x}\,. \qquad (4.1.11)$$

Since the proton is an extended structure, we cannot replace the square brackets in (4.1.11) by γ^μ, as for point spin-$\frac{1}{2}$ particles in (4.1.10). However, we know that J^μ must be a Lorentz four vector, and so we must use the most general four-vector that can be constructed from p, p', q, and the Dirac γ matrices,

$$[\quad] = \left[F_1(q^2)\gamma^\mu + \frac{\kappa}{2M}F_2(q^2)\, i\sigma^{\mu\nu}q_\nu\right] \qquad (4.1.12)$$

where F_1 and F_2 are two independent form factors and κ is the anomalous magnetic moment. (Terms involving γ^5 are ruled out by conservation of parity.)

For $q^2 \to 0$, that is, when we probe with long-wavelength photons, it does not make any difference that the proton has structure at order of 1 fermi. We effectively see a particle of charge e and magnetic moment $(1+\kappa)e/2M$, where κ, the anomalous moment, is measured to be 1.79. The factors in (4.1.12) must therefore be chosen so that in this limit $F_1(0) = 1$ and $F_2(0) = 1$. The corresponding values for the neutron are $F_1(0) = 0$, $F_2(0) = 1$, and experimentally $\kappa_n = -1.91$.

If we use (4.1.12) to calculate the differential cross section for electron-proton elastic scattering, we find an expression similar to (4.1.7),

$$\begin{aligned}
\frac{d\sigma}{d\Omega}\bigg|_{\text{lab}} &= \left(\frac{\alpha^2}{4E^2\sin^4(\theta/2)}\right)\frac{E'}{E}\left\{\left(F_1^2 - \frac{\kappa^2 q^2}{4M^2}F_2^2\right)\cos^2(\theta/2)\right. \\
&\quad \left. - \frac{q^2}{2M^2}(F_1 + \kappa F_2)^2\,\sin^2(\theta/2)\right\}\,, \qquad (4.1.13)
\end{aligned}$$

108

kown as the Rosenbluth formula.[3] The two form factors, $F_{1,2}(q^2)$, parametrize our ignorance of the detailed structure of the proton represented by the blob in Fig. 4.2. These form factors can be determined experimentally by measuring $d\sigma/d\Omega$ as a function of θ and q^2. Note that if the proton were point-like like the muon, then $\kappa = 0$ and $F_1(q^2) = 1$ for all q^2, and (4.1.13) would revert to (4.1.7).

In practice, it is better to use linear combinations of the $F_{1,2}$

$$ G_E \equiv F_1 + \frac{\kappa q^2}{4M^2} F_2, \qquad G_M \equiv F_1 + \kappa F_2 , \qquad (4.1.14) $$

defined so that no interference terms, $G_E G_M$, occur in the cross section. Equation (4.1.13) then becomes

$$ \frac{d\sigma}{d\Omega}\bigg|_{\text{lab}} = \left(\frac{\alpha^2}{4E^2 \sin^4(\theta/2)}\right) \frac{E'}{E} \left(\frac{G_E^2 + \tau G_M^2}{1+\tau} \cos^2 \frac{\theta}{2} + 2\tau G_M^2 \sin^2 \frac{\theta}{2}\right) , $$
$$ (4.1.15) $$

with $\tau \equiv -q^2/4M^2$. Now that interference terms have disappeared, these proton form factors may be regarded as generalizations of the non-relativistic form factor introduced in (4.1.1); G_E and G_M are referred to as the electric and magnetic form factors, respectively. The data on angular dependence of $ep \to ep$ scattering can be used to separate G_E, G_M at different values of q^2. The result for $G_E(q^2)$ is

$$ G_E(q^2) \simeq \left(1 - \frac{q^2}{0.71}\right)^{-2} \qquad \text{(in units of GeV}^2). \qquad (4.1.16) $$

The behavior for small $-q^2$ can be used to determine the residual terms in the expansion of (4.1.5). In particular, the mean square proton charge radius is

$$ \langle r^2 \rangle = 6 \left(\frac{dG_E(q^2)}{dq^2}\right)_{q^2=0} = (0.81 \times 10^{-13} \text{ cm})^2 . \qquad (4.1.17) $$

The same radius of about 0.8 fm is obtained for the magnetic moment distribution.

Having measured the size of the proton, one might like to take a more detailed look at its structure by increasing the $-q^2$ of the photon to give

[3]M. N. Rosenbluth, Phys. Rev. **79**, 615 (1950).
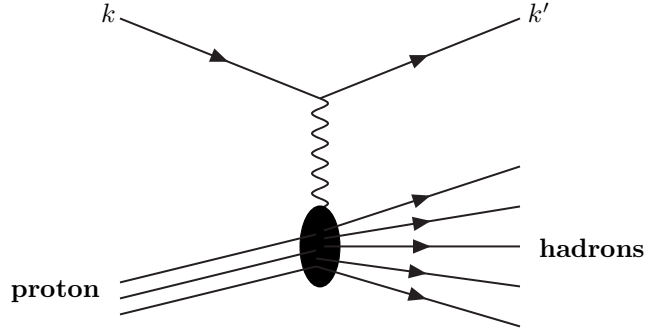
Figure 4.3: *Lowest-order diagram for $ep \to eX$.*

better spatial resolution. This can be done simply by requiring a large energy loss of the bombarding electron. There is, however, a catch: because of the large transfer of energy, the proton will often break up. The picture of Fig. 4.2 would therefore need to be generalized to Fig. 4.3. For modest $-q^2$, one might just excite the proton into a Δ-state and hence produce an extra π-meson, that is $ep \to e\Delta^+ \to ep\pi^0$. In this case, the square of the invariant mass is $W^2 \simeq M_\Delta^2$. When $-q^2$ is very large, however, the debris becomes so messy that the initial state proton loses its identity completely and a new formalism must be devised to extract information from the measurement.

The problem facing us now is illustrated by recalling (4.1.10), (4.1.11), and Fig. 4.2. The switch from a muon to a proton target was made by replacing the lepton current $j^\mu (\sim \overline{u}\gamma^\mu u)$ by a proton current $J^\mu (\sim \overline{u}\Gamma^\mu u)$, and the most general form of Γ^μ was constructed. This is inadequate to describe the inelastic events of Fig. 4.3 because the final state is not a single fermion described by a Dirac $\overline{u}$ entry in the matrix current. Therefore, J^μ must have a more complex structure than (4.1.11). The square of the invariant amplitude (3.2.37) is generalized to

$$\overline{|\mathfrak{M}|^2} \propto L_{\mu\nu}^{(e)} \; W^{\mu\nu}, \tag{4.1.18}$$

where $L_{\mu\nu}^{(e)}$ represents the lepton tensor of (3.2.41), since everything in the leptonic part of the diagram above the photon propagator in Fig. 4.3 is left unchanged. The hadronic tensor $W^{\mu\nu}$ serves to parametrize our ignorance of the form of the current at the end of the propagator. The most general form of the tensor $W^{\mu\nu}$ must now be constructed out of $g^{\mu\nu}$ and the independent momenta p and q (with $p' = p+q$); γ^μ is not included as we are parametrizing

$\overline{|\mathfrak{M}|^2}$ which is already summed and averaged over spins. We write

$$W^{\mu\nu} = -W_1 g^{\mu\nu} + \frac{W_2}{M^2} p^\mu p^\nu + \frac{W_4}{M^2} q^\mu q^\nu + \frac{W_5}{M^2}(p^\mu q^\nu + q^\mu p^\nu). \qquad (4.1.19)$$

We have omitted antisymmetric contributions to $W^{\mu\nu}$, since their contribution to the cross section vanishes after insertion into (4.1.18) because the tensor $L^{(e)}_{\mu\nu}$ is symmetric. Note the omission of W_3 in our notation; this spot is reserved for a parity violating structure function when a neutrino beam is substituted for the electron beam, so that the virtual photon probe is replaced by a weak boson.

The current conservation at the vertex requires $q_\mu W^{\mu\nu} = q_\nu W^{\mu\nu} = 0$; consequently,

$$
\begin{aligned}
0 &= q_\nu W^{\mu\nu} \\
&= -q_\nu W_1 g^{\mu\nu} + \frac{W_2}{M^2}(p \cdot q) p^\mu + \frac{W_4}{M^2} q^2 q^\mu + \frac{W_5}{M^2}[q^2 p^\mu + (p \cdot q) q^\mu].
\end{aligned}
$$
$$(4.1.20)$$

Setting the coefficients of q^μ and p^μ to zero, we find

$$-W_1 + \frac{W_4}{M^2} q^2 + \frac{W_5}{M^2}(p \cdot q) = 0, \qquad (4.1.21)$$

$$\frac{W_2}{M^2}(p \cdot q) + \frac{W_5}{M^2} q^2 = 0 \qquad (4.1.22)$$

which lead to

$$W_5 = -\frac{p \cdot q}{q^2} W_2, \qquad (4.1.23)$$

$$W_4 = \left(\frac{p \cdot q}{q^2}\right)^2 W_2 + \frac{M^2}{q^2} W_1. \qquad (4.1.24)$$

Hence, only two of the four inelastic structure functions of (4.1.19) are independent, and we can write without loss of generality

$$W^{\mu\nu} = W_1 \left(-g^{\mu\nu} + \frac{q^\mu q^\nu}{q^2}\right) + W_2 \frac{1}{M^2} \left(p^\mu - \frac{p \cdot q}{q^2} q^\mu\right)\left(p^\nu - \frac{p \cdot q}{q^2} q^\nu\right),$$
$$(4.1.25)$$

111

where the W_i's are functions of the Lorentz scalar variables that can be constructed from the four-momenta at the hadronic vertex. Unlike elastic scattering there are two independent variables, and we choose

$$q^2 \quad \text{and} \quad \nu \equiv \frac{p \cdot q}{M} . \qquad (4.1.26)$$

The invariant mass W of the final hadronic system is related to ν and q^2 by

$$W^2 = (p + q)^2 = M^2 + 2M\nu + q^2 . \qquad (4.1.27)$$

Evaluation of the cross section for $ep \to eX$ is straightforward repetition of the calculation for $e^- \mu^- \to e^- \mu^-$ scattering with the substituttion of $W_{\mu\nu}$, given by (4.1.25), for $L^{(\mu)}_{\mu\nu}$. Using the expression (3.2.42) for $L^{\mu\nu}_{(e)}$ and noting $q^\mu L^{(e)}_{\mu\nu} = q^\nu L^{(e)}_{\mu\nu} = 0$, we find

$$L^{\mu\nu}_{(e)} W_{\mu\nu} = 4W_1(k \cdot k') + \frac{2W_2}{M^2}[2(p \cdot k)(p \cdot k') - M^2 k \cdot k'] . \qquad (4.1.28)$$

In the laboratory frame, this becomes

$$L^{\mu\nu}_{(e)} W_{\mu\nu} = 4EE' \left\{ W_2(\nu, q^2) \cos^2 \frac{\theta}{2} + 2 W_1(\nu, q^2) \sin^2 \frac{\theta}{2} \right\} , \qquad (4.1.29)$$

see (E.0.3). By including the flux factor and the phase space factor for the outgoing electron, we can obtain the inclusive differential cross section for inelastic electron-proton scattering, $ep \to eX$,

$$d\sigma = \frac{1}{4 \left[(k \cdot p)^2 - m^2 M^2 \right]^{1/2}} \left\{ \frac{e^4}{q^4} L^{\mu\nu}_{(e)} W_{\mu\nu} 4\pi M \right\} \frac{d^3 k'}{2E'(2\pi)^3} , \qquad (4.1.30)$$

where $\overline{|\mathfrak{M}|^2}$ is given by the expression in the braces [recall (3.2.37)]. The extra factor of $4\pi M$ arises because we have adopted the standard convention

112

for the normalization of $W^{\mu\nu}$. Inserting (4.1.29) in (4.1.30) yields

$$
\begin{aligned}
\frac{d\sigma}{dE'd\Omega}\bigg|_{\text{lab}} &= \frac{1}{16\pi^2}\frac{E'}{E}\frac{|\mathfrak{M}|^2}{4\pi M} \\
&= \frac{(4\pi\alpha)^2}{16\pi^2 q^4}\frac{E'}{E}L^{\mu\nu}W_{\mu\nu} \\
&= \frac{4\alpha^2 E'^2}{q^4}\left\{W_2(\nu,q^2)\cos^2\frac{\theta}{2}+2W_1(\nu,q^2)\sin^2\frac{\theta}{2}\right\} \\
&= \frac{\alpha^2}{4E^2\sin^4(\theta/2)}\left\{W_2(\nu,q^2)\cos^2\frac{\theta}{2}+2W_1(\nu,q^2)\sin^2\frac{\theta}{2}\right\},
\end{aligned}
$$
$$(4.1.31)$$

where we neglect the mass of the electron; to obtain the final result we used (E.0.3). It is often more convenient to express the differential cross section with respect to the invariants ν and Q^2

$$
\begin{aligned}
\frac{d\sigma}{dQ^2\,d\nu}\bigg|_{\text{lab}} &= \frac{\pi}{EE'}\frac{d\sigma}{dE'd\Omega}\bigg|_{\text{lab}} \\
&= \frac{4\pi\alpha^2}{Q^4}\frac{E'}{E}\left\{W_2(Q^2,\nu)\cos^2\frac{\theta}{2}+2W_1(Q^2,\nu)\sin^2\frac{\theta}{2}\right\}.
\end{aligned}
$$

In experimental settings one may mantain the same values of Q^2 and ν upon changing E, E', and θ, and then in principle could separate the two structure functions W_1 and W_2.

For future reference, it is useful to make a compendium of our results on form factors. We keep to the laboratory kinematics (see Appendix E) and neglect the mass of the electron. For all the interactions, the differential cross section in the energy (E') and angle (θ) of the scattered electron can be written in the form

$$
\frac{d\sigma}{dE'd\Omega}\bigg|_{\text{lab}} = \frac{4\alpha^2 E'^2}{q^4}\left\{\quad\right\}. \tag{4.1.32}
$$

First, for a muon target of mass m (or a quark target of mass m after substitutions $\alpha^2 \to \alpha^2 e_q^2$ where e_q is the quark's fractional charge),

$$
\left\{\quad\right\}_{e\mu\to e\mu} = \left(\cos^2\frac{\theta}{2}-\frac{q^2}{2m^2}\sin^2\frac{\theta}{2}\right)\delta\left(\nu+\frac{q^2}{2m}\right). \tag{4.1.33}
$$

113

For elastic scattering from a proton target

$$\left\{\ \right\}_{ep\to ep} = \left(\frac{G_E^2 + \tau G_M^2}{1+\tau} \cos^2 \frac{\theta}{2} + 2\tau G_M^2 \sin^2 \frac{\theta}{2} \right) \delta\left(\nu + \frac{q^2}{2M} \right) \quad (4.1.34)$$

where $\tau = -q^2/4M^2$ and M is the mass of the proton. Finally, for the case when the proton target is broken up by the bombarding electron

$$\left\{\ \right\}_{ep\to eX} = W_2(\nu, q^2) \cos^2 \frac{\theta}{2} + 2W_1(\nu, q^2) \sin^2 \frac{\theta}{2}. \quad (4.1.35)$$

Making use of the delta function, (4.1.33) and (4.1.34) can be integrated over E' with the result [see (E.0.12)]

$$\left. \frac{d\sigma}{d\Omega} \right|_{\text{lab}} = \frac{\alpha^2}{4E^2 \sin^4(\theta/2)} \frac{E'}{E} \left[\ \right]. \quad (4.1.36)$$

If simple, point-like, spin-$\frac{1}{2}$ quarks reside inside the proton, we should be able to illuminate them with a small wavelength (large $-q^2$) virtual photon beam. The fact that such photons break up the proton target can be handled by using the inelastic form factors described above. The sign that there are structureless particles inside a complex system like a proton is that for small wavelengths, the proton described by (4.1.35) suddenly starts behaving like a free Dirac particle (a quark) and (4.1.35) turns into (4.1.33). The proton structure functions thus become simply

$$2W_1^{\text{point}} = \frac{Q^2}{2m^2} \delta\left(\nu - \frac{Q^2}{2m} \right) \qquad W_2^{\text{point}} = \delta\left(\nu - \frac{Q^2}{2m} \right), \quad (4.1.37)$$

where $Q^2 \equiv -q^2$ and m is the quark mass. (The "point" notation reminds us that the quark is a structureless Dirac particle.)

Using the identity $\delta(x/a) = a\delta(x)$, (4.1.37) may be rearranged to introduce dimensionless structure functions

$$2mW_1^{\text{point}}(\nu, Q^2) = \frac{Q^2}{2m\nu} \delta\left(1 - \frac{Q^2}{2m\nu} \right),$$

$$\nu W_2^{\text{point}}(\nu, Q^2) = \delta\left(1 - \frac{Q^2}{2m\nu} \right). \quad (4.1.38)$$

114

These "point" functions now display the intriguing property that they are only functions of the ratio $Q^2/2m\nu$ and not Q^2 and ν independently. This behavior can be contrasted with that for ep elastic scattering. For simplicity, set $\kappa = 0$, so that $G_E = G_M \equiv G$; then comparing (4.1.34) and (4.1.35) we have

$$
\begin{aligned}
W_1^{\text{elastic}} &= \frac{Q^2}{4M^2} G^2(Q^2)\, \delta\left(\nu - \frac{Q^2}{2M}\right) \\
W_2^{\text{elastic}} &= G^2(Q^2)\, \delta\left(\nu - \frac{Q^2}{2M}\right).
\end{aligned}
\tag{4.1.39}
$$

In contrast to (4.1.37), the structure functions of (4.1.39) contain a form factor $G(Q^2)$, and so cannot be rearranged to be functions of a single dimensionless variable. A mass scale is explicitly present; it is set by the empirical value 0.71 GeV in the dipole formula for $G(Q^2)$ which reflects the inverse size of the proton. As Q^2 increases above $(0.71\ \text{GeV})^2$, the form factor depresses the chance of elastic scattering; the proton is more likely to break up. The point structure functions, on the other hand, depend only on a dimensionless variable $Q^2/2m\nu$, and no scale of mass is present.[4] The mass m merely serves as a scale for the momenta Q^2, ν.

The so-called "Bjorken scaling" can be summarized as follows: in the limit $Q \to \infty$ and $2M\nu \to \infty$ such that $\omega = 2(q \cdot p)/Q^2 = 2M\nu/Q^2$, the structure functions would have the following property

$$
\begin{aligned}
MW_1(\nu, Q^2) &\xrightarrow[\text{large } Q^2]{} F_1(\omega), \\
\nu W_2(\nu, Q^2) &\xrightarrow[\text{large } Q^2]{} F_2(\omega).
\end{aligned}
\tag{4.1.40}
$$

Note that in (4.1.40) we have changed the scale from what it was in (4.1.38). We have introduced the proton mass instead of the quark mass to define the dimensionless variable ω. The presence of free quarks is signaled by the fact that the inelastic structure functions are independent of Q^2 at given value of ω. In the late 60s, deep inelastic scattering experiments conducted by the SLAC-MIT Collaboration showed that at sufficiently large $Q^2 \gg \Lambda_{\text{QCD}}^2$, the structure functions were approximately independent of Q^2.[5]

---

[4]J. D. Bjorken, Phys. Rev. **179**, 1547 (1969).

[5]The data exhibited Bjorken scaling to about 10% accuracy for values of Q^2 above
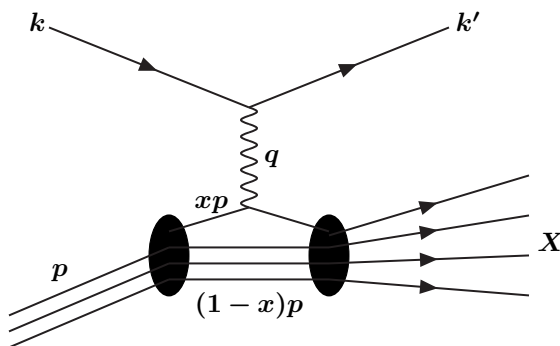
Figure 4.4: *Kinematics of lepton-proton scattering in the parton model.*

4.2 Parton Model

Now that scaling is an approximate experimental fact, we adopt the spirit of the parton model.[6] The basic idea in the model, shown in Fig. 4.4, is to represent the inelastic scattering as quasi-free scattering from point-like constituents within the proton, when viewed from a frame in which the proton has infinite momentum. Imagine a reference frame in which the target proton has a very large 3-momentum, i.e, $\vec{p} \gg M$ the so-called "infinite momentum frame." In this frame, the proton is Lorentz-contracted into a thin pancake, and the lepton scatters instantaneously. Furthermore, the proper motion of the constituents (i.e., of partons) within the proton is slowed down by time dilation. We envisage the proton momentum p as being made of partons carrying longitudinal momentum $p_i = x_i p$, where the momentum fractions x_i satisfy:

$$0 \leq x_i \leq 1 \quad \text{and} \quad \sum_{\text{partons}\,(i)} x_i = 1 \ . \tag{4.2.41}$$

Assigning a variable mass xM to the parton is of course out of the question. Clearly, if the parton's momentum is xp, its energy can only be xE if we put $m = M = 0$. Equivalently, a proton can only emit a parton moving parallel to it ($p_\perp = 0$ for both) if they both have zero mass. Moreover, because of the large momentum transfer ($-q^2 \gg M$) interactions between partons can be neglected and therefore the individual current-parton interactions may be

(1 GeV)^2. E. D. Bloom *et al.*, Phys. Rev. Lett. **23**, 930 (1969); M. Breidenbach *et al.*, Phys. Rev. Lett. **23**, 935 (1969); J. I. Friedman and H. W. Kendall, Ann. Rev. Nucl. Part. Sci. **22**, 203 (1972); J. S. Poucher *et al.*, Phys. Rev. Lett. **32**, 118 (1974).

[6]R. P. Feynman, Phys. Rev. Lett. **23**, 1415 (1969); J. D. Bjorken and E. A. Paschos, Phys. Rev. **185**, 1975 (1969).

treated incoherently

$$\frac{d\sigma}{dtdu}\bigg|_{ep\to eX} = \sum_{\text{partons}(i)} \int dx f_i(x) \left.\frac{d\sigma}{dtdu}\right|_{eq_i\to eq_i}, \qquad (4.2.42)$$

where $f_i(x)$ indicates the probability of finding constituent i inside the proton, and the sum is over all the contributing partons.

Assuming $s \gg M$, the invariant variables of (3.3.48) become

$$
\begin{aligned}
\hat{s} &= (k + xp)^2 \simeq x(2k \cdot p) \simeq xs, \\
\hat{t} &= (k - k')^2 = t = q^2, \\
\hat{u} &= (k' - xp)^2 \simeq x(-2k' \cdot p) \simeq xu;
\end{aligned}
\qquad (4.2.43)
$$

therefore

$$-\frac{t}{s+u} = -\frac{q^2}{2p \cdot q} = \frac{Q^2}{2M\nu} = x. \qquad (4.2.44)$$

Consequently, from (4.2.44) we have $x(s+u) + t = 0$, or $\hat{s} + \hat{u} + \hat{t} = 0$. With this in mind, the invariant amplitude follows directly from (3.3.48),

$$\overline{|\mathfrak{M}|^2} = 2\,(4\pi\alpha e_q)^2\,\frac{\hat{s}^2 + \hat{u}^2}{\hat{t}^2}. \qquad (4.2.45)$$

Inserting (4.2.45) into (3.1.27) we obtain an expression for the differential cross section

$$\frac{d\sigma}{d\hat{t}} = \frac{2\pi\alpha^2 e_q^2}{\hat{s}^2}\left(\frac{\hat{s}^2 + \hat{u}^2}{\hat{t}^2}\right). \qquad (4.2.46)$$

Using the invariant relations (4.2.44), Eq. (4.2.46) can be rewritten as

$$
\begin{aligned}
\left.\frac{d\sigma}{dtdu}\right|_{eq_i\to eq_i} &= x\frac{d\sigma}{d\hat{t}d\hat{u}} \\
&= x\frac{d}{d\hat{u}}\int \frac{2\pi\alpha^2 e_q^2}{\hat{s}^2}\left(\frac{\hat{s}^2 + \hat{u}^2}{\hat{t}^2}\right)\delta(\hat{s} + \hat{u} + \hat{t})d\hat{u} \\
&= x\frac{2\pi\alpha^2 e_q^2}{t^2}\left(\frac{s^2 + u^2}{s^2}\right)\delta(x(s+u) + t)). \qquad (4.2.47)
\end{aligned}
$$

Now, we can rewrite (4.1.28) in terms of the invariant variables

$$L_{(e)}^{\mu\nu}W_{\mu\nu} = -2W_1 t + \frac{W_2}{M^2}\left[-su + M^2 t\right], \qquad (4.2.48)$$

and because we assume $s \gg M^2$, we have

$$L_{(e)}^{\mu\nu} W_{\mu\nu} = \frac{2}{M(s+u)}[x(s+u)^2 F_1 - su F_2], \qquad (4.2.49)$$

where $t = -x(s+u)$, $F_1 \equiv MW_1$ and $F_2 \equiv \nu W_2$. Substituting (4.2.49) into (4.1.31) we have

$$\left.\frac{d\sigma}{dtdu}\right|_{ep \to eX} = \frac{4\pi\alpha^2}{t^2 s^2} \frac{1}{s+u} \left[(s+u)^2 x F_1 - us F_2\right], \qquad (4.2.50)$$

where we have used the kinematic relations in the lab frame (see Appendix E)

$$s = 2ME, \quad u = -2ME', \quad t = -Q^2 = -4EE' \sin^2(\theta/2) \qquad (4.2.51)$$

and

$$d\Omega dE' = 2\pi d(\cos\theta)dE' = \frac{4\pi M^2}{su} dt \left(-\frac{1}{2M} du\right). \qquad (4.2.52)$$

Substituting (4.2.47) and (4.2.50) into (4.2.42) and comparing coefficients of us and $s^2 + u^2$, we obtain the master formula of the parton model[7]

$$2x F_1(x) = F_2(x) = \sum_i e_{q_i}^2 \, x \, f_i(x). \qquad (4.2.53)$$

We see that F_1 and F_2 are functions only of the scaling variable x, here fixed by the delta function in (4.2.47).

Next, using the lab frame kinematic relation (E.0.3), we obtain

$$\sin^2 \frac{\theta}{2} = \frac{Q^2}{4EE'} = \frac{2M\nu x}{4E'\nu/y} = \frac{xyM}{2E'} \qquad (4.2.54)$$

and

$$\cos^2 \frac{\theta}{2} = \frac{E}{E'}\left(1 - y - \frac{Mxy}{2E}\right), \qquad (4.2.55)$$

where

$$y = \frac{p \cdot q}{p \cdot k} \underbrace{=}_{(\text{lab})} \frac{\nu}{E}. \qquad (4.2.56)$$

---

[7]Note that $F_2(\omega) = \sum_i \int dx e_{q_i}^2 \, f_i(x) \, x \, \delta(x - 1/\omega)$, and $F_1(\omega) = (\omega/2) F_2(\omega)$. Recalling the identification (4.1.40), we see that, at large Q^2, we can redefine $F_{1,2}(\omega)$ as $F_{1,2}(x)$; namely, $\nu W_2(\nu, Q^2) \mapsto F_2(x) = \sum_i e_{q_i}^2 x f_i(x)$ and $MW_1(\nu Q^2) \mapsto F_1(x) = F_2(x)/(2x)$.

Substituting (4.2.54) and (4.2.55) into (4.1.31) we get

$$\frac{d\sigma}{dxdy} = \frac{8ME\pi\alpha^2}{Q^4} \left[xy^2 F_1 + \left(1 - y - \frac{Mxy}{2E} \right) F_2 \right] \tag{4.2.57}$$

where we have used the identity

$$dE'd\Omega = \frac{\pi}{EE'}dQ^2\,d\nu = \frac{2ME}{E'}\pi\,y\,dx\,dy\,. \tag{4.2.58}$$

Substituting (4.2.53) into (4.2.57), we obtain the Callan-Gross relation

$$\frac{d\sigma}{dxdy} = \frac{2\pi\alpha^2}{Q^4}\,s\,[1 + (1-y)^2] \sum_i e_{q_i}^2\,x\,f_i(x)\,, \qquad (E \gg Mx). \tag{4.2.59}$$

The behavior $[1 + (1-y)^2]$ in (4.2.59) is specific to the scattering of electrons from massless fermions.[8] This relation gave evidence that the partons involved in deep inelastic scattering were fermions, at a time when the relation between partons and quarks was still unclear.

There are three independent variables which describe the kinematics: E', θ, and ϕ, though the dependence on the latter is trivial. It is convenient to plot the allowed kinematic region in the $(Q^2/2ME) - (\nu/E)$ plane, as shown in Fig. 4.5.[9] The boundary of the physical region is given by the requirements that $0 \leq \theta \leq \pi$, $\;0 \leq \nu \leq E$, $\;0 \leq x \leq 1$. Because $x = Q^2/2M\nu = (Q^2/2ME)/(\nu/E)$, the contours of constant x are straight lines through the origin with slope x. The relation between Q^2 and θ follows from (E.0.3) and is given by

$$\frac{Q^2}{2ME} = \frac{1}{M}(E - \nu)(1 - \cos\theta). \tag{4.2.60}$$

Therefore, lines of constant θ are straight lines passing through the point $\nu/E = 1$, and intersecting the $Q^2/2ME$ axis at $Q^2/2ME = (E/M)(1 - \cos\theta)$. Lines of fixed θ become steeper as the beam energy increases, whereas lines of fixed x remain constant. The Q^2 dependence of the kinematic variables is crucial to understand which terms are important in the deep inelastic

---

[8]C. G. . Callan and D. J. Gross, Phys. Rev. Lett. **22**, 156 (1969).

[9]A. V. Manohar, in Symmetry and Spin in the Standard Model, (eds. B. A. Campbell, L. G. Greeniaus, A. N. Kamal, F. C. Khanna, World Scientific, Singapore, 1992),p.1.

limit. A generic point in the kinematic plane is given by some value of x and y. As $E \to \infty$, for a fixed value of x and y, the variables ν/E and $Q^2/2ME$ are fixed. Therefore, in the deep inelastic regime $\nu \propto Q^2/M$ and $E \propto Q^2/M$. This implies that a generic point in the physical region has $(1 - \cos\theta) \propto M/E \propto M^2/Q^2$, and hence the scattering angle, $\theta \propto M/Q$, goes to zero as $Q^2 \to \infty$. We can also see in Fig. 4.5 that for fixed beam energy E, there is a limit to the $Q^2 - x$ region which can be explored experimentally. The small x region is also the small Q^2 region, because lines of constant x approach the horizontal axis for small x. For a fixed value of x, the maximum allowed value of Q^2 is at the intersection of the line $\theta = \pi$ with the line for fixed x. It is elementary to find the intersection point of the two lines,

$$Q^2_{\max} = 2MEx \left(\frac{2E}{2E + Mx} \right) \approx 2MEx, \qquad (E \gg Mx). \qquad (4.2.61)$$

To be in the deep inelastic region, one needs Q^2 to be larger than a few $(\text{GeV})^2$, so this places a limit on the smallest value of x accessible for a given beam energy. For example, with a 500 GeV lepton beam, and assuming $Q^2 \geq 10$ $(\text{GeV})^2$ is large enough to be considered deep inelastic scattering, the smallest measurable value of x is 10^{-2}.

The Hadron-Elektron-Ring-Anlage (HERA) at DESY was the first ever constructed storage ring to collide positrons or electrons with protons. It started operating at the end of 1991 and ceased running in June 2007. Two experiments, H1 and ZEUS, collected data from collisions of e^- or e^+ with an energy of 27.5 GeV and protons accelerated to an energy of 820 GeV until 1997 and 920 GeV starting from 1998 onwards. This corresponds to $s = 4 \times 28 \times 820 \, (920) \, (\text{GeV})^2$, allowing measurements of structure functions down to $x \approx 10^{-4}$. (A similar measurement in a fixed target experiment would require a 50 TeV lepton beam.) One of the first important results of the H1 and ZEUS measurements was the observation of a steep rise of the proton structure function F_2 towards low values of the Bjorken variable x.[10] This phenomenon has been successfully described by (perturbative) pQCD calculations. Furthermore, pQCD seems to give a very good description of the F_2 behaviour down to low values of momentum transfers squared: Q^2 of

---

[10]M. Derrick *et al.* [ZEUS Collaboration], Phys. Lett. B **316**, 412 (1993); I. Abt *et al.* [H1 Collaboration], Nucl. Phys. B **407**, 515 (1993); Phys. Lett. B **321**, 161 (1994).
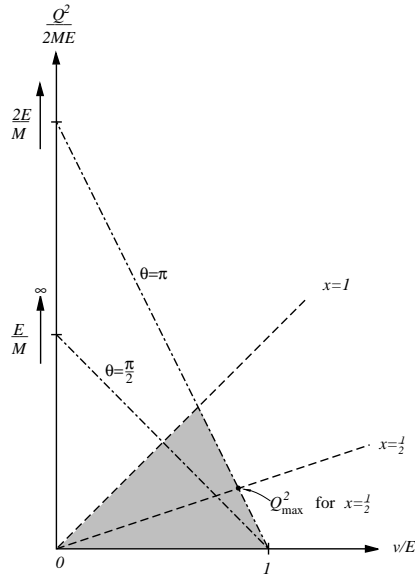
Figure 4.5: *The triangle is the allowed kinematic region for deep inelastic scattering. The dot-dashed lines are curves of constant scattering angle θ. The dashed lines are lines of constant x. In the deep inelastic limit, the intercept of the constant θ lines with the vertical axis becomes infinite.*

the order of a few GeV^2. We discuss this next.

4.3   QCD Improved Parton Model

The simple parton model described in the previous section is not true in QCD, because the properties we assumed for the hadronic blob are explicitly violated by certain classes of graphs in perturbation theory. Nevertheless, much of the structure of the parton model remains in perturbation theory, because of the property of factorization. Factorization permits scattering amplitudes with incoming high energy hadrons to be written as a product of a hard scattering piece and a remainder factor which contains the physics of low energy and momenta. The former contains only high energy and momentum components and, because of asymptotic freedom, is calculable in perturbation theory. The latter piece describes non-perturbative physics, but is described

by a single process independent function for each type of parton called the parton distribution function (PDF). Without this property of factorization we would be unable to make predictions for processes involving hadrons using perturbation theory.

The factorization has been proven within perturbation theory, but it is assumed to have a validity which transcends perturbation theory. The proofs require a detailed examination of all the dangerous regions of phase space in Feynman graphs.[11] The plausibility of the factorization property can be seen from the following argument. The presence of infrared singularities or singularities coming from regions of collinear emission reveals the sensitivity of a Feynman graph to very low momentum scales. Because of the Landau rules, such singularities are associated with real physical processes rather than virtual processes which occur only as short-live fluctuations. Because these real processes occur long before the hard interaction, it is appropriate that they are included in the wave function of the incoming hadron and not in the short distance cross section. The proofs of factorization establish that this simple picture is in fact valid in perturbation theory.

Assuming the property of factorization holds we can derive the QCD improved parton model. The result for any process with a single incoming hadron leg is

$$\sigma(|q|, p) = \sum_i \int_0^1 dx \, \hat{\sigma}(|q|, xp, \alpha_s(\mu^2)) \, f_i(x, \mu^2) \,, \qquad (4.3.62)$$

where μ^2 is the large momentum scale which characterizes the hardness of the interaction, the sum i runs over all partons in the incoming hadron, and $\hat{\sigma}$ is the short distance cross section calculable as a perturbation series in the QCD coupling α_s. It is referred to as the short distance cross section because the singularities corresponding to a long distance physics have been factored out and absorbed in the structure functions f_i. The structure functions themselves are not calculable in perturbation theory. In order to perform the factorization we have introduced a scale μ^2 which separates the high and low momentum physics.[12] No physical results can depend on the particular

---

[11]R. K. Ellis, H. Georgi, M. Machacek, H. D. Politzer and G. G. Ross, Nucl. Phys. B **152**, 285 (1979); J. C. Collins, D. E. Soper and G. Sterman, Phys. Lett. B **134**, 263 (1984).

[12]Indeed all quantities in (4.3.62) depend on the renormalization and factorization scales,

value chosen for this scale. This implies that any dependence on μ in σ has to vanish at least to order in α_s considered,

$$\frac{d}{d \ln \mu^2} \sigma^{(n)} = \mathcal{O}(\alpha_s^{n+1}) \,. \tag{4.3.63}$$

The evolution of the parton distributions with changes of the scale μ are predicted by the Dokshitzer-Gribov-Lipatov-Altarelli-Parisi (DGLAP) equation,[13]

$$\frac{d}{d \ln \mu^2} f_i(x, \mu^2) = \frac{\alpha_s(\mu^2)}{2\pi} \sum_j \int_x^1 dz \, d\zeta \, \delta(x - z\zeta) \, P_{ij}(z, \alpha_s(\mu^2)) \, f_j(\zeta, \mu^2) \,, \tag{4.3.64}$$

where the matrix $\boldsymbol{P}$ is calculable as a perturbation series

$$P_{ij}(z, \alpha_s) = P_{ij}^{(0)}(z) + \frac{\alpha_s}{2\pi} P_{ij}^{(1)}(z) + \dots \,. \tag{4.3.65}$$

Examples of Feynman diagrams contributing to $\boldsymbol{P}$ in leading order QCD are shown in Fig. 4.6. The first two terms of (4.3.65) are needed for next-to-leading order (NLO) predictions, which is the standard approximation, although often still with large uncertainties. Currently, the splitting functions P_{ij} are known to NNLO.

Performing the ζ integration we obtain

$$\frac{d}{d \ln \mu^2} \begin{pmatrix} q_i(x, \mu^2) \\ g(x, \mu^2) \end{pmatrix} = \frac{\alpha_s(\mu^2)}{2\pi} \sum_j \int_x^1 \frac{dz}{z} \begin{pmatrix} P_{q_i q_j}(z) & P_{q_i g}(z) \\ P_{g q_j}(z) & P_{gg}(z) \end{pmatrix}$$
$$\times \begin{pmatrix} q_j(x/z, \mu^2) \\ g(x/z, \mu^2) \end{pmatrix} \,, \tag{4.3.66}$$

which is a system of coupled integro-differential equations corresponding to the different possible parton splittings

$$\frac{dq_i(x, \mu^2)}{d \ln \mu^2} = \frac{\alpha_s(\mu^2)}{2\pi} \int_x^1 \frac{dz}{z} \left[q_i(x/z, \mu^2) P_{qq}(z) + g(x/z, \mu^2) P_{qg}(z) \right] \,, \tag{4.3.67}$$

which are usually taken to be the same ($\mu_r = \mu_f = \mu$).

[13]V. N. Gribov and L. N. Lipatov, Yad. Fiz. **15**, 1218 (1972) [Sov. J. Nucl. Phys. **15**, 675 (1972)]; Yad. Fiz. **15**, 781 (1972) [Sov. J. Nucl. Phys. **15**, 438 (1972)]; Y. L. Dokshitzer, Sov. Phys. JETP **46**, 641 (1977) [Zh. Eksp. Teor. Fiz. **73**, 1216 (1977)]; G. Altarelli and G. Parisi, Nucl. Phys. B **126**, 298 (1977).

123
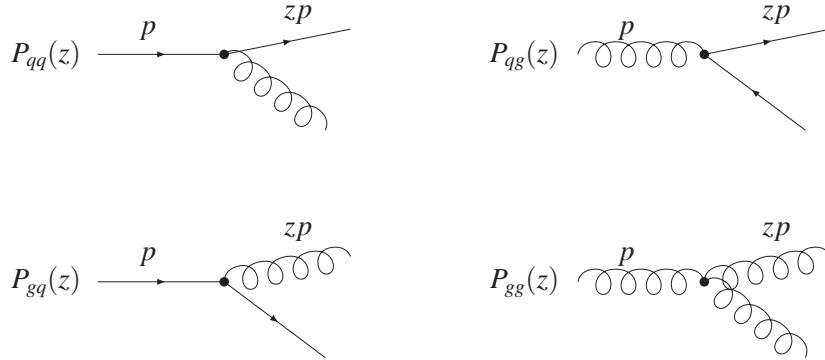
Figure 4.6: *Sample of Feynman diagrams for parton-parton splitting in leading order QCD. We indicate the collinear momentum flow (p incoming and zp outgoing) as it enters the calculation of the corresponding splitting function P_{ij}.*

$$\frac{dg(x,\mu^2)}{d\ln\mu^2} = \frac{\alpha_s(\mu^2)}{2\pi} \sum_j \int_x^1 \frac{dz}{z} \left[q_j(x/z,\mu^2)P_{gq}(z) + g(x/z,\mu^2)P_{gg}(z) \right] .$$

(4.3.68)

The physical interpretation of the PDFs $f_j(x,\mu^2)$ again relies on the infinite momentum frame. In this frame $f_j(x,\mu^2)$ is the number of partons of type j carrying a fraction x of the longitudinal momentum of the incoming hadron and having a transverse dimension $r < 1/\mu$. As we increase μ, the DGLAP equation predicts that the number of partons will increase. Viewed on a smaller scale of transverse dimension r', such that $r' \ll 1/\mu$, a single parton of transverse dimension $1/\mu$ is resolved into a greater number of partons.

The DGLAP kernels P_{ij} have an attractive physical interpretation as the probability of finding parton i in a parton of type j with a fraction z of the longitudinal momentum of the parent parton and transverse size less than $1/\mu$. The interpretation as probabilities implies that the DGLAP kernels are positive definite for $z < 1$. They satisfy the following relations: $\int_0^1 dz\, P_{qq}(z) = 0$, $\int_0^1 dz\, x[P_{qq}(z) + P_{gq}(z)] = 0$, and $\int_0^1 dz\, z[2\, n_f\, P_{qg} + P_{gg}] = 0$, where n_f is the number of flavors. These equations correspond to quark number conservation and momentum conservation in the splittings of quarks and gluons.

The DGLAP kernels at LO become

$$P_{qq}(z) = \frac{4}{3} \frac{1 + z^2}{1 - z} , \qquad (4.3.69)$$

$$P_{gq}(z) = \frac{4}{3} \frac{1 + (1 - z)^2}{z} , \qquad (4.3.70)$$

$$P_{qg}(z) = \frac{z^2 + (1 - z)^2}{2} , \qquad (4.3.71)$$

and

$$P_{gg}(z) = 6 \left(\frac{z}{1 - z} + \frac{1 - z}{z} + z(1 - z) \right) . \qquad (4.3.72)$$

In the double-leading-logarithmic approximation, that is $\lim_{x \to 0} \ln(1/x)$ and $\lim_{Q^2 \to \infty} \ln(Q^2/\Lambda_{\mathrm{QCD}})$, the DGLAP equation predicts a steeply rising gluon density at low x, in agreement with the experimental results from HERA, shown in Fig. 4.7.[14] The PDFs, however, cannot be calculated "from first principles" in pQCD. The DGLAP evolution equations (4.3.67) and (4.3.68) are solved by inserting certain analytical functions at some starting scale Q_0^2 and evolving them up to higher Q^2. The structure function F_2 found as a result of this procedure is adjusted to the experimentally measured one. For example, as displayed in Fig. 4.8, an input distribution at $Q_0^2 = 10$ GeV^2 can be determined in a global fit from comparison to HERA data.[15] The large difference in the hard squared momentum scale Q^2 between HERA and LHC requires the parton evolution based on Eqs. (4.3.67) and (4.3.68) to be sufficiently accurate in pQCD. Benchmark CTEQ and MSTW parametrizations from global fits of hard-scattering data account for the effects of experimental errors and come with the according uncertainties.[16] An example is given in Fig. 4.9, which shows the NLO PDFs at scales of $Q^2 = 10$ GeV^2 and $Q^2 = 10^4$ GeV^2, including the associated 68%CL uncertainty bands.

---

[14]S. Chekanov *et al.* [ZEUS Collaboration], Phys. Rev. D **67**, 012007 (2003); C. Adloff *et al.* [H1 Collaboration], Eur. Phys. J. C **30**, 1 (2003).

[15]In the framework of QCD a proton consists of three *valence* quarks interacting via gluon exchange. The gluons can produce virtual quark-antiquark pairs, so-called *sea* quarks, and, because of their selfcoupling (2.2.41) and (2.2.42), other gluons. The gluon radiation explains the F_2 scaling violation, i.e., the F_2 dependence on Q^2.

[16]J. Pumplin, D. R. Stump, J. Huston, H. L. Lai, P. M. Nadolsky and W. K. Tung, JHEP **0207**, 012 (2002); A. D. Martin, W. J. Stirling, R. S. Thorne and G. Watt, Eur. Phys. J. C **63**, 189 (2009).
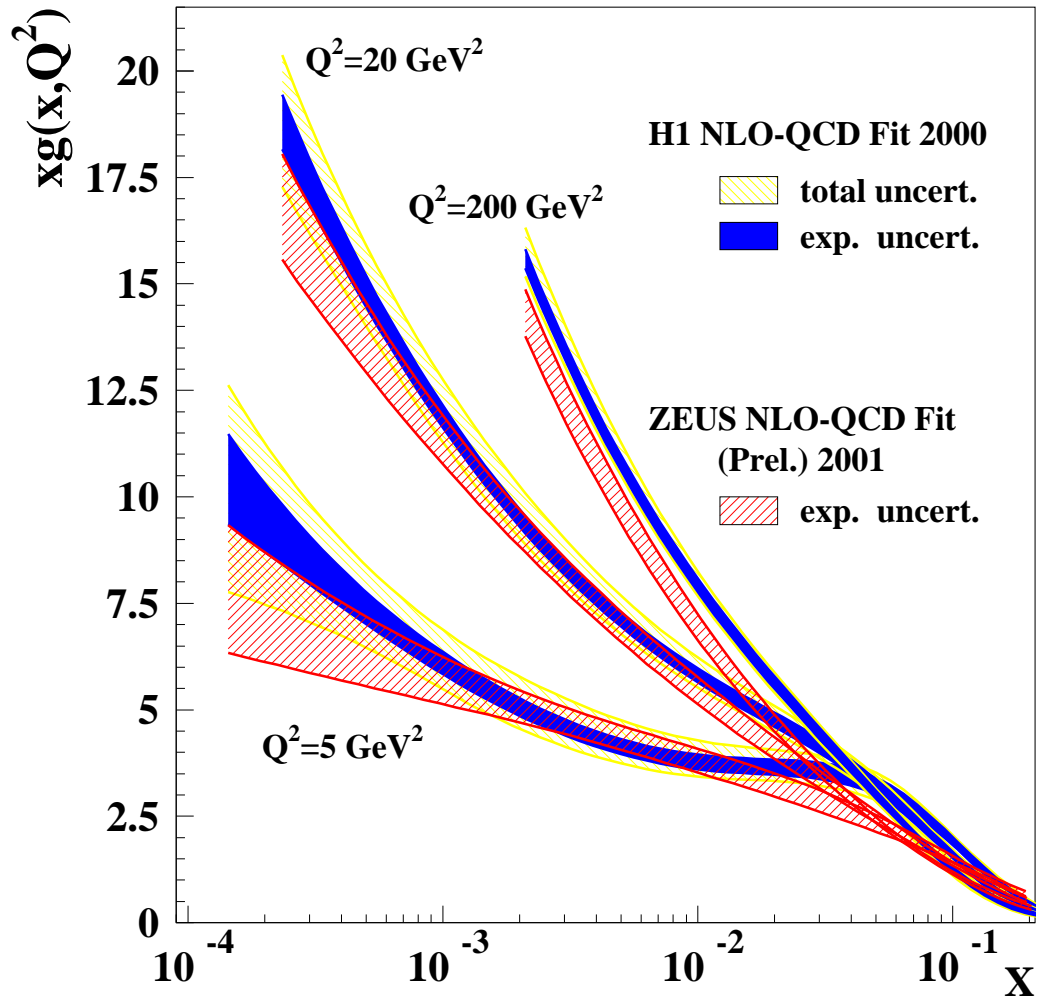
Figure 4.7: *Gluon momentum distributions $xf(x, Q^2)$ in the proton as measured by the ZEUS and H1 experiments at various Q^2.*
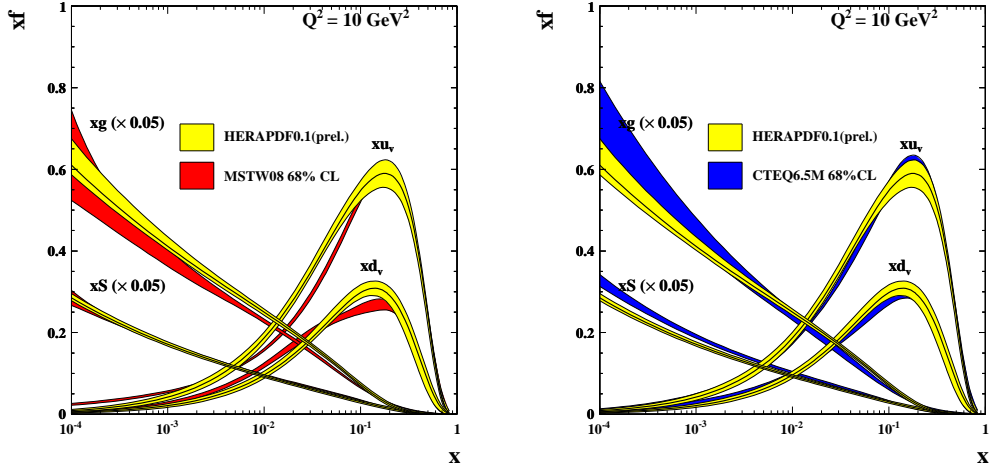
Figure 4.8: *The valence, sea and gluon momentum distributions $xf(x, Q^2)$ in the proton as measured by the ZEUS and H1 experiments at $Q^2 = 10$ GeV^2 are compared to the MSTW (left) and CTEQ (right) parametrizations.*
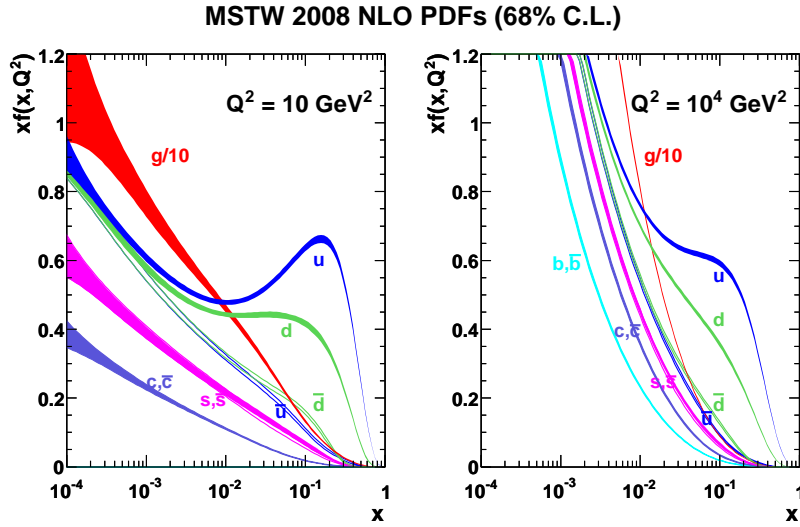
Figure 4.9: *Evolution of gluon and quarks momentum distributions $xf(x, Q^2)$ in the proton from a low scale at $Q^2 = 10$ GeV (left) to LHC energies at $Q^2 = 10^4$ GeV (right).*

In passing, we should note that because of gluon exchange corrections in pQCD the longitudinal structure function F_L could differ from zero: because quarks can have a non-negligible virtuality before scattering on the probing photon, helicity may not be conserved in this process, and hence the coupling of a quark on a longitudinally polarized photon becomes possible.

So far, we have not faced the problem of how the quarks turn into hadrons that hit the detector. It was sufficient to state that quarks must fragment into hadrons with unit probability. This gives (3.5.83). For more detailed calculations, this problem cannot be sidestepped.

For example, for $e^+\epsilon^- \to q\bar{q}$, the produced quark and antiquark separate with equal and opposite momentum in the center-of-mass frame and materialize into back-to-back jets of hadrons which have momenta roughly collinear with the original q and $\bar{q}$ directions. The hadrons may be misaligned by a momentum transverse to the q or $\bar{q}$ direction by an amount not exceeding about 300 MeV.

We can visualize jet formation as hadron bremsstrahlung once the q and $\bar{q}$ separate by a distance of around 1 fm. Namely, α_s becomes large, and strong color forces pull on the separating q and $\bar{q}$. The potential energy becomes so large that one or more $q\bar{q}$ pairs are created. Eventually, all the energy is degraded into two jets of hadrons moving more or less in the direction of the q and $\bar{q}$.

To describe the fragmentation of quarks into hadrons, we use an analogous formalism to that introduced to describe the quarks inside hadrons. Thus, for a cross section $\sigma_{pp \to X}$ of some hadronic final state X in, say, proton-proton scattering we can write

$$
\begin{aligned}
\sigma_{pp \to X} \;=\; & \sum_{ijk} \int dx_1 \, dx_2 \, dz \, f_i(x_1, \mu^2) \, f_j(x_2, \mu^2) \\
& \times \;\; \hat{\sigma}_{ij \to k}(x_1, x_2, z, Q^2, \alpha_s(\mu^2), \mu^2) D_{k \to X}(z, \mu^2) \,, \quad (4.3.73)
\end{aligned}
$$

where $D_{k \to z}(z, \mu^2)$ is the fragmentation function and all other functions have a clear interpretation. The fragmentation function $D(z)$, describes the transition (parton $\to$ hadron) in the same way that the structure function $f(x)$ describes the embedding (hadron $\to$ parton). Like f functions, the D functions are subject to constraints imposed by momentum and probability con-

servation:

$$\sum_h \int_0^1 z D_q^h(z) dz = 1 \,, \tag{4.3.74}$$

$$\sum_q \int_{z_{\min}}^1 [D_q^h(z) + D_{\bar{q}}^h(z)] dz = n_h \,, \tag{4.3.75}$$

where $z_{\min}$ is the threshold energy $2m_h/Q$ for producing a hadron of mas m_h, where n_h is the average multiplicity of hadrons of type h. Equation (4.3.74) simply states that the sum of the energies of all hadrons is the energy of the parent quark. Clearly the same relation holds for $D_{\bar{q}}^h(z)$. Equation (4.3.75) says that the number n_h of hadrons of type h is given by the sum of probabilities of obtaining h from all possible parents, namely, from q to $\bar{q}$ of any flavor.

A parametrization of the fragmentation spectrum, which is consistent with the so-called "leading-log QCD" behavior and seems to reproduce quite well the multiplicity growth as seen in colliders experiments, can be cast in the following form

$$\frac{dn_h}{dz} \approx 0.08 \ \exp\left[2.6\sqrt{\ln(1/z)}\right] \ (1-z)^2 \ \left[z\sqrt{\ln(1/z)}\right]^{-1} \,, \tag{4.3.76}$$

where $z \equiv E/E_{\mathrm{jet}}$, E is the energy of any hadron in the jet, and E_{jet} is the total energy in the jet.[17] With the infrared cutoff set to $z = 10^{-3}$, the average multiplicity per jet is approximately 54. The main features of the jet fragmentation process derived from $dn_h/dz \approx (15/16) z^{-3/2} (1-z)^2$ (which provides a reasonable parametrization of Eq. (4.3.76) for $10^{-3} < z < 1$) are summarized in Table 4.1.

4.4   Physics of Hadronic Jets

Jet studies in hadron-hadron collisions have traditionally been viewed as less incisive than those carried out in electron-positron annihilations or in lepton nucleon scattering because of the added complexity of events. However, in what follows we illustrate by two brief examples that hard scattering events

---

[17]C. T. Hill, Nucl. Phys. B **224**, 469 (1983).

Table 4.1: *Properties of jet hadronization.*

z_1	z_2	$\int_{z_1}^{z_2}(dn_h/dz)\,dz$	$\int_{z_1}^{z_2} z\,(dn_h/dz)\,dz$	$z_{\text{equivalent}}$
0.0750	1.0000	3	0.546	0.182
0.0350	0.0750	3	0.155	0.052
0.0100	0.0350	9	0.167	0.018
0.0047	0.0100	9	0.062	0.007
0.0010	0.0047	30	0.069	0.002

take on a much simpler aspect at high energies, and that there is no major impediment to detailed analyses.

4.4.1   Hadroproduction of Direct Photons

Hadronic reactions producing large-$k_\perp$ direct photons provide remarkable tests of perturbative QCD.[18] Because of the point-like coupling of the photons to the quarks, the trigger photon represents the full jet; therefore, no (non-perturbative) decay function enters into the prediction. Moreover, starting at leading order only two subprocesses are relevant: namely the QCD Compton process $qg \to q\gamma$, $\bar{q}g \to \bar{q}\gamma$ and the annihilation process $q\bar{q} \to g\gamma$, shown in Fig. 4.10. These two subprocesses may even be disentangled by taking cross section differences of the type $\sigma_{p\bar{p}\to\gamma+\text{jet}} - \sigma_{pp\to\gamma+\text{jet}}$; the valence-quark and gluon properties in the incident particles can then be studied separately.[19] In this section we show that, at the LHC, Compton scattering becomes the dominant process contributing to the prompt photon production over most of the kinematical region. Thus, the reaction $pp \to \gamma + \text{jet}$ provides a quite sensitive probe of the gluon distribution. (The quark distributions can be taken from deep-inelastic scattering.)

---

[18]G. R. Farrar, Phys. Lett. B **67**, 337 (1977); F. Halzen and D. M. Scott, Phys. Rev. Lett. **40**, 1117 (1978); Phys. Rev. D **18**, 3378 (1978).

[19]P. Aurenche, R. Baier, M. Fontannaz, J. F. Owens and M. Werlen, Phys. Rev. D **39**, 3275 (1989).
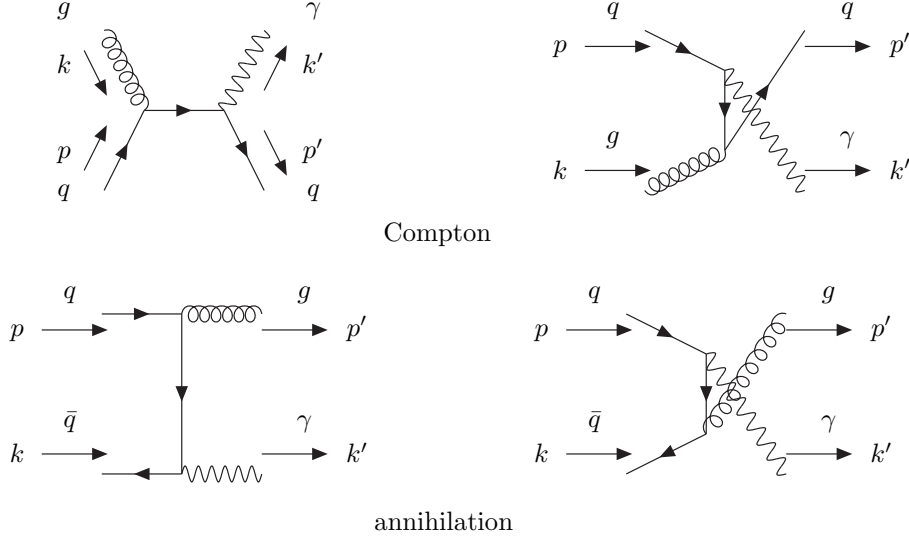
Figure 4.10: *Leading order processes contributing to direct photon production.*

The differential cross section for direct-photon production is

$$2E' \frac{d\sigma}{d^3k'}\bigg|_{pp\to\gamma X} = \sum_{ijk} \int dx_a\, dx_b\, f_i(x_a, Q)\, f_j(x_b, Q)\, 2E' \frac{d\hat\sigma}{d^3k'}\bigg|_{ij\to\gamma k} \quad (4.4.77)$$

where x_a and x_b are the fraction of momenta of the parent hadrons carried by the partons which collide, k' (E') is the photon momentum (energy), $d\hat\sigma/d^3k'|_{ij\to\gamma k}$ is the cross section for scattering of partons of type i and j according to elementary QCD diagrams, $f_i(x_a, Q)$ and $f_j(x_b, Q)$ are PDFs, Q is the momentum transfer, and the sum is over the parton species: $g, q = u,\ d,\ s,\ c,\ b$. In what follows we focus on $gq \to \gamma q$, which results in the dominant contribution to the total cross section at the LHC. Corrections from the other two processes can be computed in a similar fashion. The hard parton-level cross section reads,

$$
\begin{aligned}
2E' \frac{d\hat\sigma}{d^3k'}\bigg|_{gq\to\gamma q} &= \frac{(2\pi)^4}{(2\pi)^6} \frac{1}{2\hat s} \delta[(k+p-k')^2] \frac{1}{4} \sum_{\text{spins}} |\mathfrak{M}|^2 \\
&= \frac{1}{(2\pi)^2} \frac{1}{2\hat s} \delta(2p\cdot q + q^2) \frac{1}{4} \sum_{\text{spins}} |\mathfrak{M}|^2, \quad (4.4.78)
\end{aligned}
$$

where k and p are the momenta of the incoming partons, $q = k - k'$, the parton-parton center-of-mass energy $\hat s = x_a\, x_b\, s$, and $-q^2 = -\hat t = Q^2$. The

131

result

$$\frac{1}{4}\sum_{\text{spins}}|\mathfrak{M}|^2 = \frac{1}{3}g_s^2 e^2 e_q^2 \left(\frac{\hat{s}}{\hat{s}+\hat{t}} + \frac{\hat{s}+\hat{t}}{\hat{s}}\right), \qquad (4.4.79)$$

follows directly on substitution of $\alpha^2 \to e_q^2 \alpha \alpha_s$ in the corresponding QED amplitude given in Table 3.1 and insertion of the color factor $1/6$ (see Appendix F). Recall that g_s and e are the QCD and electromagnetic coupling constants, and e_q is the fractional electric charge of species q. Likewise, for $q\bar{q} \to g\gamma$,

$$\frac{1}{4}\sum_{\text{spins}}|\mathfrak{M}|^2 = \frac{8}{9}g_s^2 e^2 e_q^2 \left(-\frac{\hat{t}}{\hat{s}+\hat{t}} - \frac{\hat{s}+\hat{t}}{\hat{t}}\right). \qquad (4.4.80)$$

Equation (4.4.78) can be most conveniently integrated in terms of the rapidity y and transverse momentum $k_\perp$ of the final photon

$$\frac{d^3 k'}{2E'} = \frac{1}{2}d^2 k_\perp \, dy = \pi k_\perp \, dk_\perp \, dy. \qquad (4.4.81)$$

Considering that the incoming momentum of the gluon is $k = x_a p_1$ and that of the quark is $p = x_b p_2$, we can re-write the argument of the delta function as

$$2p \cdot q + q^2 = 2\,x_b\,p_2 \cdot (x_a p_1 - k') + \hat{t} = x_a\,x_b\,s - 2\,x_b\,p_2 \cdot k' + \hat{t}, \quad (4.4.82)$$

where p_1 and p_2 are the initial momenta of the parent protons. Introducing, $k_0' = k_\perp \cosh y$, $k_\parallel' = k_\perp \sinh y$, $p_1 = (\sqrt{s}/2,\, 0,\, 0,\, \sqrt{s}/2)$, and $p_2 = (\sqrt{s}/2,\, 0,\, 0,\, -\sqrt{s}/2)$ we obtain

$$p_2 \cdot k' = \frac{\sqrt{s}}{2}k_\perp(\cosh y + \sinh y) = \frac{\sqrt{s}}{2}k_\perp\,e^y \qquad (4.4.83)$$

and

$$\hat{t} = -2k \cdot k' = -2x_a\frac{\sqrt{s}}{2}k_\perp\,e^{-y} = -\sqrt{s}\,k_\perp\,e^{-y}\,x_a, \qquad (4.4.84)$$

so that

$$\begin{aligned}
\delta(x_a\,x_b\,s - \sqrt{s}\,x_b\,k_\perp\,e^y - \sqrt{s}\,x_a\,k_\perp\,e^{-y}) &= \frac{1}{s}\,\delta(x_a\,x_b - x_b\,x_\perp\,e^y - x_a\,x_\perp\,e^{-y}) \\
&= \frac{1}{s\,[x_a - x_\perp\,e^y]} \\
&\times\ \delta\left(x_b - \frac{x_a\,x_\perp\,e^{-y}}{x_a - x_\perp\,e^y}\right), \qquad (4.4.85)
\end{aligned}$$

where $x_\perp = k_\perp/\sqrt{s}$. The lower bound $x_b > 0$ implies $x_a > x_\perp e^y$. The upper bound $x_b < 1$ leads to a stronger constraint

$$x_a > \frac{x_\perp e^y}{1 - x_\perp e^{-y}}, \tag{4.4.86}$$

which requires $x_\perp e^y < 1 - x_\perp e^{-y}$, yielding $x_\perp < (2\cosh y)^{-1}$. Of course there is another completely symmetric term, in which g comes from p_2 and q comes from p_1. Putting all this together, the total contribution from $gq \to \gamma q$ reads

$$
\begin{aligned}
\sigma_{pp \to \gamma X}^{qg \to \gamma q} &= 2 \sum_q \int \frac{d^3 k'}{2E'} \int dx_a \int dx_b \, f_g(x_a, Q) \, f_q(x_b, Q) \frac{1}{(2\pi)^2} \\
&\times \frac{1}{s\,[x_a - x_\perp e^y]} \frac{1}{2\hat{s}} \, \delta\left(x_b - \frac{x_a x_\perp e^{-y}}{x_a - x_\perp e^y}\right) \\
&\times \frac{e^2 g_s^2 e_q^2}{3} \left(\frac{\hat{s}+\hat{t}}{\hat{s}} + \frac{\hat{s}}{\hat{s}+\hat{t}}\right) .
\end{aligned} \tag{4.4.87}
$$

With the change of variables $z = e^y$ Eq. (4.4.87) can be rewritten as

$$
\begin{aligned}
\sigma_{pp \to \gamma X}^{qg \to \gamma q} &= 2 \sum_q \int \frac{\pi \, k_\perp \, dk_\perp \, dz}{z} \int dx_a \int dx_b \, f_g(x_a, Q) \, f_q(x_b, Q) \\
&\times \frac{1}{(2\pi)^2 \, 2 x_a \, x_b \, s^2 (x_a - x_\perp z)} \, \delta\left(x_b - \frac{x_a x_\perp z^{-1}}{x_a - x_\perp z}\right) \\
&\times \frac{e^2 g_s^2 e_q^2}{3} \left(\frac{\hat{s}+\hat{t}}{\hat{s}} + \frac{\hat{s}}{\hat{s}+\hat{t}}\right) .
\end{aligned} \tag{4.4.88}
$$

Now, since

$$\frac{\hat{t}}{\hat{s}} = -\frac{\sqrt{s}\,k_\perp e^{-y}}{x_b s} = -\frac{x_\perp}{x_b z} = \frac{x_\perp z}{x_a} - 1, \tag{4.4.89}$$

Eq. (4.4.88) becomes

$$
\begin{aligned}
\sigma_{pp \to \gamma X}^{qg \to \gamma q} &= \frac{e^2 g_s^2}{12\pi s} \int_{x_{\perp\min}}^{1/2} dx_\perp \int_{z_{\min}}^{z_{\max}} dz \int_{x_{a,min}}^{1} dx_a \, f_g(x_a, Q) \\
&\times \left[\sum_q e_q^2 \, f_q\left(\frac{x_a x_\perp z^{-1}}{x_a - x_\perp z}, Q\right)\right] \frac{1}{x_a^2} \left(\frac{x_\perp z}{x_a} + \frac{x_a}{x_\perp z}\right) , \tag{4.4.90}
\end{aligned}
$$

133
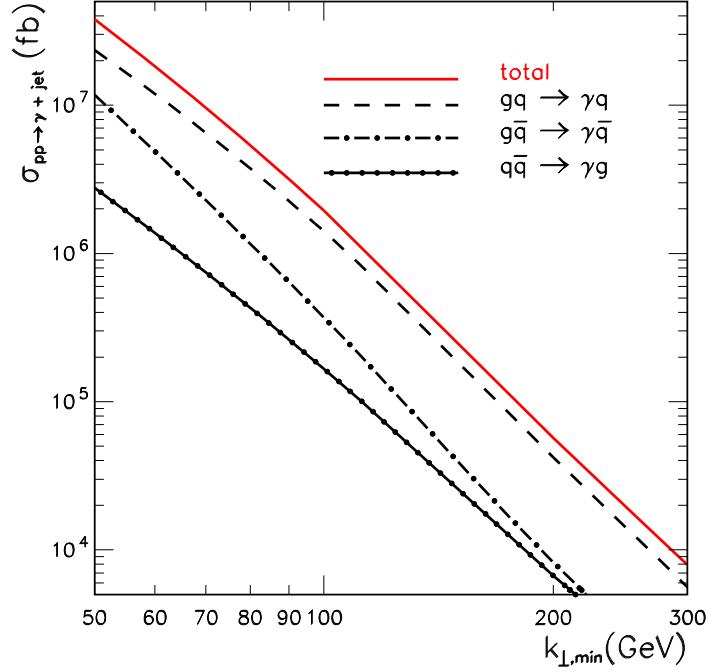
Figure 4.11: *Leading order QCD $\sigma_{pp\to\gamma+\text{jet}}$ vs. $k_{\perp,\min}$, for $\sqrt{s} = 14$ TeV. It is clearly seen that the $gq \to \gamma q$ process provides the dominant contribution.*

where the integration limits,

$$z_{\min}^{\max} = \frac{1}{2}\left[\frac{1}{x_\perp} \pm \sqrt{\frac{1}{x_\perp^2} - 4}\right] \qquad \text{and} \qquad x_{a,\min} = \frac{x_\perp z}{1 - x_\perp z^{-1}}\,, \quad (4.4.91)$$

are obtained from Eq. (4.4.86). Figure 4.11 shows the leading order QCD cross section $\sigma_{pp\to\gamma+\text{jet}}$ *vs* $k_{\perp,\min}$, as obtained through numerical integration of Eq. (4.4.90).[20] To accommodate the minimal acceptance cuts on final state photons from the LHC experiments, an additional kinematic cut, $|y| < 2.4$, has been included in the calculation.[21]

Unfortunately, the advantages of direct photons as a clean probe of parton distributions are offset by large QCD backgrounds which are about 10^2 to

---

[20]L. A. Anchordoqui, H. Goldberg, S. Nawata and T. R. Taylor, Phys. Rev. Lett. **100**, 171603 (2008); Phys. Rev. D **78**, 016005 (2008).

[21]G. L. Bayatian *et al.* [CMS Collaboration], J. Phys. G **34**, 995 (2007).

10^3 times larger than direct photon production. This background is mainly caused by events where high $k_\perp$ photons are produced in the decay of neutral mesons or else are radiated from the quark (such as bremsstrahlung photons in the NLO QCD subprocesses). Of course, the hadronic activity around the background photons tends to be much more than around the direct photons, and therefore isolation cuts can be imposed to separate the hard scattering $\gamma + $ jet topology. For example, in the so-called tracker isolation criteria one defines a cone (in $k_\perp$ and rapidity) around the direction of the photon, and demands an absence of other particle tracks within that cone. This effectively supresses the photon background by about two orders of magnitude while the signal efficiency remains between 70% - 80%.

The LO contribution to diphoton reactions is given by the tree level process $q\bar{q} \to \gamma\gamma$. The invariant amplitude for such a process can be simply obtained by multiplying Eq. (4.4.80) for a factor of e^2/g_s^2 and then dividing by a factor of 2 to account for identical particles in the final state. The LO contribution to the cross section for direct production of photon pairs can then be estimated by scaling the dot-solid line in Fig. 4.11 by a factor of about 0.036.

4.4.2   Two-Jet Final States

Hard scattering processes in high-energy hadron-hadron collisions are dominated by events with most of the central hadronic activity concentrated in two jets. These events provide a testing ground for perturbative QCD, which at LO describes two-body to two-body processes. The description of events with more than two jets requires higher-order calculations (which are beyond the scope of this course) that should account, at the parton level, for the radiation which can occur from the initial and final state partons.[22]

The physical processes underlying dijet production in pp and $p\bar{p}$ collisions are the scattering of two partons ij, producing two final partons kl that fragment into hadronic jets. Consider two-body processes leading to final states consisting of partons, with equal and opposite transverse momenta $k_\perp$

---

[22]For a comprehensive description of multijet phenomena see e.g., E. Eichten, I. Hinchliffe, K. D. Lane and C. Quigg, Rev. Mod. Phys. **56**, 579 (1984) [Addendum-ibid. **58**, 1065 (1986)].

and $p_\perp$, respectively. The distribution of invariant masses $W^2 = (k' + p')^2$ is given by

$$
\frac{d\sigma}{dW^2} = \frac{(2\pi)^4}{(2\pi)^6} \int \frac{d^3k'}{2E_1'} \int \frac{d^3p'}{2E_2'} \sum_{ijkl} \int dx_a \int dx_b \, f_i(x_a, W) \, f_j(x_b, W)
$$

$$
\times \quad \delta^4(p - k' - p') \, \delta(p^2 - W^2) \frac{1}{2\hat{s}} \, \overline{|\mathfrak{M}|^2} \, , \tag{4.4.92}
$$

where $p^2 = \hat{s} = (k' + p')^2 = 2k' . p' = 2E_1'E_2' - k_\parallel' p_\parallel' + p_\perp^2$, and

$$
\delta^4(p - k_\perp' - p_\perp') = \delta(E - E_1 - E_2) \, \delta(p_\parallel - k_\parallel' - p_\parallel') \, \delta(\vec{k}_\perp + \vec{p}_\perp) \, . \tag{4.4.93}
$$

Using Eqs. (3.1.27) and (3.2.35) we obtain

$$
\overline{|\mathfrak{M}|^2} = \frac{1}{4} \sum_{\text{spins}} |\mathfrak{M}|^2 = 64\pi^2 \hat{s} \frac{d\sigma}{d\Omega} = 16\pi\hat{s}^2 \left. \frac{d\sigma}{d\hat{t}} \right|_{ij \to kl} , \tag{4.4.94}
$$

where the differential cross sections $(d\sigma/d\hat{t}|_{ij \to kl})$ for partonic subprocesses yielding jet pair production (shown in Fig. 4.12) are summarized in Appendix F.

The invariants may be expressed in terms of

$$
\cos\theta = (1 - 4\,p_\perp^2/\hat{s})^{1/2} \, , \tag{4.4.95}
$$

the cosine of the scattering angle in the parton-parton center-of-mass, as

$$
\hat{t} = -\frac{\hat{s}}{2} \, (1 - \cos\theta) \tag{4.4.96}
$$

and

$$
\hat{u} = \frac{\hat{s}}{2} \, (1 + \cos\theta) \, . \tag{4.4.97}
$$

The integration over $d^3k' \, d^3p'$ can be conveniently rewritten in terms of jet rapidities y_1 and y_2, and their common transverse momentum:

$$
\frac{d^3p}{2E} = \frac{\pi}{2} \, dp_\perp^2 \, dy \, , \tag{4.4.98}
$$

where $y \equiv \frac{1}{2}(y_1 - y_2)$. Since $E_1' = p_\perp \cosh y_1$, $k_\parallel' = p_\perp \sinh y_1$, $E_2' = p_\perp \cosh y_2$, and $p_\parallel' = p_\perp \sinh y_2$, a straightforward calculation leads to

$$
E_1'E_2' - k_\parallel'p_\parallel' = p_\perp^2 \, \cosh(y_1 - y_2) \equiv p_\perp^2 \cosh 2y \, . \tag{4.4.99}
$$
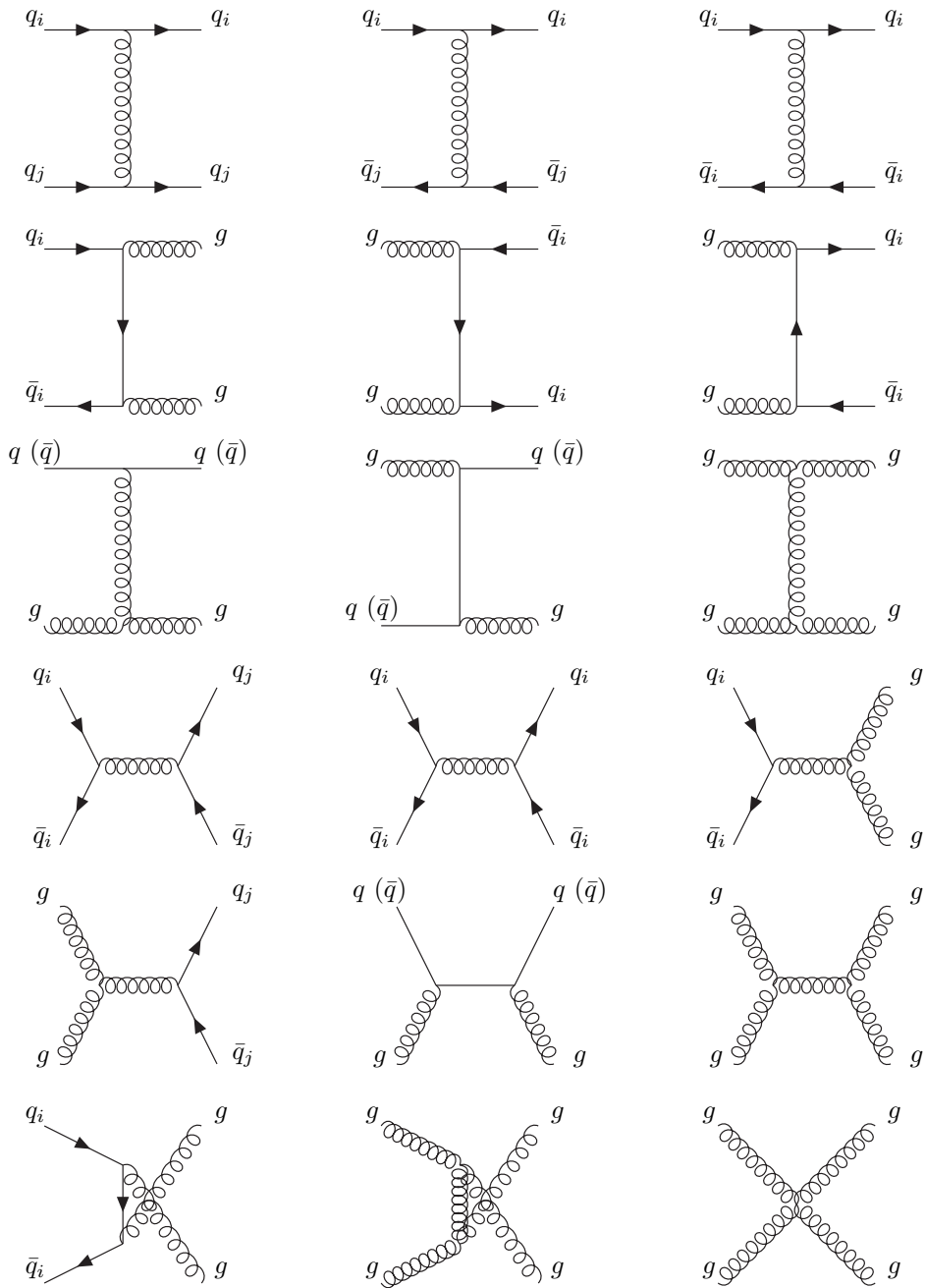
Figure 4.12: *Leading order Feynman diagrams for jet pair production.*

Now, using the identity of hyperbolic functions, $1 + \cosh 2y = 2\cosh^2 y$, we define

$$\tau = \frac{\hat{s}}{s} = \frac{W^2}{s} = \frac{4p_\perp^2}{s}\cosh^2 y \qquad (4.4.100)$$

so that

$$\delta(\hat{s} - W^2) = \delta(4p_\perp^2 \cosh^2 y - W^2) = \frac{1}{4\cosh^2 y}\ \delta\left(p_\perp^2 - \frac{W^2}{4\cosh^2 y}\right). \qquad (4.4.101)$$

Using

$$\int d^2\vec{k}_\perp\ d^2\vec{p}_\perp\ \delta(\vec{k}_\perp + \vec{p}_\perp)\ \delta(p_\perp^2 - W^2/4\cosh^2 y) = \pi \int dp_\perp^2$$
$$\times\ \delta(p_\perp^2 - W^2/4\cosh^2 y)$$
$$= \pi\,, \qquad (4.4.102)$$

Eq. (4.4.92) becomes

$$\frac{d\sigma}{dW^2} = \frac{\pi}{(2\pi)^2}\,(2\pi W^2)\int dy_1 \int dy_2 \sum_{ijkl} \int dx_a \int dx_b\, f_i(x_a, W)\, f_j(x_b, W)$$
$$\times\ \frac{1}{4\cosh^2 y}\ \delta(E - E_1' - E_2')\ \delta(p_\parallel - k_\parallel' - p_\parallel')\ \left.\frac{d\sigma}{d\hat{t}}\right|_{ij \to kl}. \qquad (4.4.103)$$

We now define $a = E - E_1 - E_2$ and $b = p_\parallel - k_\parallel' - p_\parallel'$ to perform the change of variables $A = a + b$ and $B = a - b$, such that $\delta(a)\delta(b) = N\delta(A)\,\delta(B)$, with normalization N given by

$$\int da\, db\, \delta(a)\, \delta(b) = \int dA\, dB\, \frac{\partial(a, b)}{\partial(A, B)}\, N\, \delta(A)\, \delta(B) = \frac{N}{2} = 1\,. \qquad (4.4.104)$$

The new variables can be rewritten as $\left\{{A \atop B}\right\} = E \pm p_\parallel - (E_1 \pm k_\parallel') - (E_2 \pm p_\parallel')$, where $E \pm p_\parallel = \left\{{\sqrt{s}x_a \atop \sqrt{s}x_b}\right\}$, $E_1 \pm k_\parallel' = p_\perp e^{\pm y_1} = p_\perp e^{\pm(Y+y)}$, $Y = \frac{1}{2}(y_1 + y_2)$, and $E_2 \pm p_\parallel' = p_\perp e^{\pm y_2} = p_\perp e^{\pm(Y-y)}$. Putting all this together, the product of delta functions in Eq. (4.4.103) becomes

$$\delta(E - E_1 - E_2)\ \delta(p_\parallel - k_\parallel' - p_\parallel') = 2\delta(\sqrt{s}x_a - 2p_\perp e^Y \cosh y)$$
$$\times\ \delta(\sqrt{s}x_b - 2p_\perp e^{-Y}\cosh y)$$
$$= 2\delta(\sqrt{s}x_a - We^Y)\,\delta(\sqrt{s}x_b - We^{-Y})\,, \qquad (4.4.105)$$

138
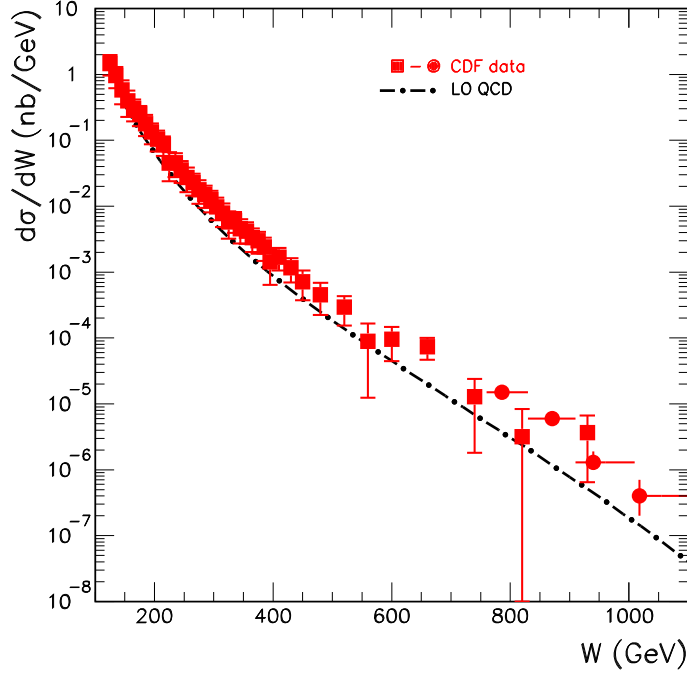
Figure 4.13: *Dijet invariant mass distribution in $p\bar{p}$ collisions, as measured by the CDF Collaboration, at $\sqrt{s} = 1.8$ TeV. The measurement is compared to a LO QCD calculation.*

and hence integration over the fraction of momenta is straightforward, yielding

$$\frac{d\sigma}{dW} = \frac{1}{2} W \tau \int dy_1 \, dy_2 \, \frac{1}{\cosh^2 y} \sum_{ijkl} f_i(\sqrt{\tau}e^Y, W) \, f_j(\sqrt{\tau}e^{-Y}, W) \, \left. \frac{d\sigma}{d\hat{t}} \right|_{ij \to kl} . \tag{4.4.106}$$

The Jacobian is found to be

$$dy_1 \, dy_2 = \frac{\partial(y_1, y_2)}{\partial(Y, y)} dY \, dy = 2 \, dY \, dy \,, \tag{4.4.107}$$

and the region of integration becomes $|y_1| = |y + Y|$ and $|y_2| = |y - Y|$. Note that $x_a, x_b < 1$, implying $-\ln(1/\sqrt{\tau}) < Y < \ln(1/\sqrt{\tau})$. The cross section

per interval of W for $pp \to$ dijet can be rewritten in the form

$$
\begin{aligned}
\frac{d\sigma}{dW} = {}& W\tau \sum_{ijkl} \left[\int_{-Y_{\max}}^{0} dY \; f_i(x_a, W) \; f_j(x_b, W) \right. \\
& \times \int_{-(y_{\max}+Y)}^{y_{\max}+Y} dy \; \left. \frac{d\sigma}{d\hat{t}} \right|_{ij \to kl} \frac{1}{\cosh^2 y} \\
& + \int_{0}^{Y_{\max}} dY \; f_i(x_a, W) \; f_j(x_b, W) \\
& \times \left. \int_{-(y_{\max}-Y)}^{y_{\max}-Y} dy \; \frac{d\sigma}{d\hat{t}} \right|_{ij \to kl} \frac{1}{\cosh^2 y} \right]
\end{aligned}
\tag{4.4.108}
$$

where $x_a = \sqrt{\tau}e^Y$, $x_b = \sqrt{\tau}e^{-Y}$ and the Mandelstam invariants occurring in the cross section are given by $\hat{t} = -\frac{1}{2}W^2\, e^{-y}/\cosh y$, $\hat{u} = -\frac{1}{2}W^2\, e^{+y}/\cosh y$, and $\hat{s} = W^2$.

The CDF Collaboration made a precise measurement of the inclusive dijet differential cross section in $p\bar{p}$ collisions at $\sqrt{s} = 1.8$ TeV. The measurement is based on data binned according to the dijet invariant mass, setting cuts on jet rapidities, $|y_1|, |y_2| < 2$, and on the scattering angle in the dijet center-of-mass frame, $\cos\theta < 2/3$. The data sample, collected with the Collider Detector at Fermilab, corresponds to an integrated luminosity of 106 pb^{-1}. Figure 4.13 shows the dijet invariant mass distribution as measured by the CDF Collaboration.[23] The measurement is compared to a LO QCD calculation obtained through numerical integration of Eq. (4.4.108). The stated cuts on jet rapidities are equivalent to $|y+Y|, |y-Y| < 2$. Using (4.4.95), the cut $\cos\theta < 2/3$ translates into a cut on the transverse momentum, $p_\perp > (\sqrt{5}/6)\,W = 0.37\,W$. The Y integration range in Eq. (4.4.108) is then $Y_{\max} = \min\{\ln(1/\sqrt{\tau}), \; y_{\max}\}$, with rapidity cuts $|y_1|, |y_2| < 2$. The kinematics of the scattering (4.4.100) provides the relation $W = 2p_\perp \cosh y$, which, when combined with the $p_\perp$ cut further constrains the rapidity space: $|y| < 0.81$. The cross section calculated at the partonic level using CTEQ6D PDFs and renormalization scale $\mu = p_\perp$ is normalized to the low energy data (180 GeV $< W < 321$ GeV) dividing the result of the calculation by 0.66. The data distributions are in good agreement with LO QCD predictions.

---

[23]Squares are from F. Abe *et al.* [CDF Collaboration], Phys. Rev. D **48**, 998 (1993); circles are from F. Abe *et al.* [CDF Collaboration], Phys. Rev. D **55**, 5263 (1997).
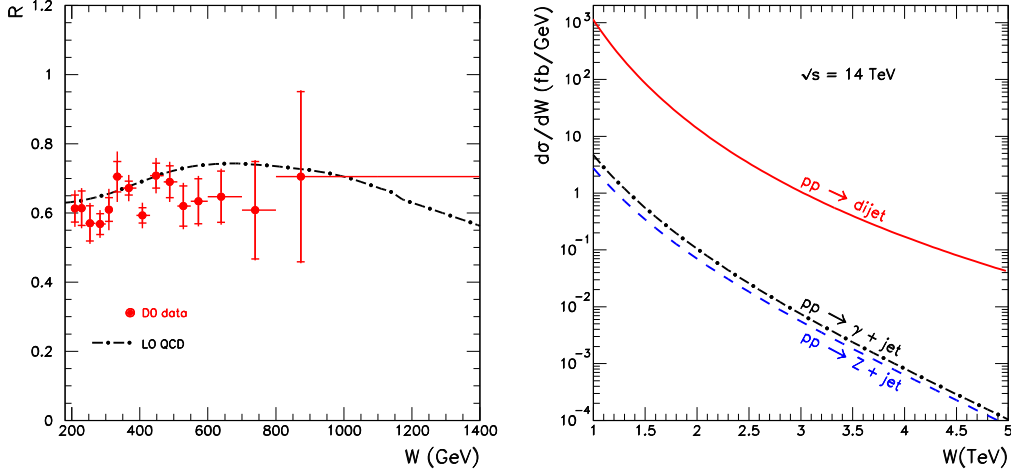
Figure 4.14: *Left Panel: Ratio of dijet invariant mass cross sections for rapidities in the interval $0 < |y_1|, |y_2| < 0.5$ and $0.5 < |y_1|, |y_2| < 1$. The experimental points (solid circles) reported by the DO Collaboration are compared to a LO QCD calculation indicated by a dot-dashed line. The error bars show the statistical and systematic uncertainties added in cuadrature, and the crossbar shows the size of the statistical error. Right Panel: LO QCD differential cross section as a function of dijet (γ + jet) invariant mass, for $y < 1$ ($y < 2.4$) and $\sqrt{s} = 14$ TeV. The Z + jet invariant mass spectrum is also shown. (For details of the $pp \to Z$ + jet calculation see Appendix G).*

As shown in Fig. 4.12 QCD parton-parton cross sections are dominated by t-channel exchanges that produce dijet angular distributions which peak at small center-of-mass scattering angles. In contrast, excitations of (hidden) recurrences result in a more isotropic distribution. In terms of rapidity variable for standard transverse momentum cuts, $\cosh y = (1 - \cos^2 \theta)^{-1/2}$, dijets resulting from QCD processes will preferentially populate the large rapidity region while the "new resonant" processes generate events more uniformly distributed in the entire rapidity region. To analyze the details of the rapidity space it is useful to introduced a new parameter,

$$R = \frac{d\sigma/dW|_{(|y_1|,|y_2|<0.5)}}{d\sigma/dW|_{(0.5<|y_1|,|y_2|<1.0)}} \,, \tag{4.4.109}$$

141

the ratio of the number of events, in a given dijet mass bin, for both rapidities $|y_1|, |y_2| < 0.5$ and both rapidities $0.5 < |y_1|, |y_2| < 1.0$. Figure 4.14 shows the ratio R. The experimental points reported by the DO Collaboration[24] (with integrated luminosities $L = 0.353 \pm 0.027$, 4.69 ± 0.37, 54.7 ± 3.4, and 91 ± 5.6 pb^{-1} for jet transverse energy thresholds of 30, 50, 85, and 115 GeV, respectively) are in good agreement with LO QCD calculation obtained through numerical integration of Eq. (4.4.109).[25]

In Fig. 4.14 we show the dijet invariant mass distribution at $\sqrt{s} = 14$ TeV, as obtained through numerical integration of (4.4.108). To accommodate the minimal acceptance from the LHC experiments an additional kinematic cut on the different jet rapidities, $|y_1|, |y_2| \leq 1$, has been included in the calculation. For comparison we also show the invariant mass distribution of the photon + jet final state, as obtained from numerical integration of

$$
\begin{aligned}
\frac{d\sigma}{dW} \;=\; & W\tau \sum_{ijk} \left[\int_{-Y_{\max}}^{0} dY\; f_i(x_a, W)\; f_j(x_b, W) \right. \\
& \times \int_{-(y_{\max}+Y)}^{y_{\max}+Y} dy\; \left.\frac{d\sigma}{d\hat{t}}\right|_{ij\to\gamma k} \frac{1}{\cosh^2 y} \\
& + \int_{0}^{Y_{\max}} dY\; f_i(x_a, W)\; f_j(x_b, W) \\
& \times \left. \int_{-(y_{\max}-Y)}^{y_{\max}-Y} dy\; \frac{d\sigma}{d\hat{t}}\right|_{ij\to\gamma k} \frac{1}{\cosh^2 y} \right] ,
\end{aligned}
\tag{4.4.110}
$$

with the corresponding cuts on photon and jet rapidities. As we anticipated in the previous section, the cross section for the inclusive process $pp \to$ dijet is about 2 to 3 orders of magnitude larger than $pp \to \gamma + $ jet.

The dijet invariant mass distribution from pp collisions of the early LHC run at $\sqrt{s} = 7$ TeV is consistent with standard model expectations. The data, recorded by the ATLAS and CMS detectors, correspond to an integrated luminosity of 1 fb^{-1}.[26]

[24]B. Abbott *et al.* [D0 Collaboration], Phys. Rev. Lett. **82**, 2457 (1999).

[25]L. A. Anchordoqui, H. Goldberg, D. Lust, S. Nawata, S. Stieberger and T. R. Taylor, Phys. Rev. Lett. **101**, 241803 (2008).

[26]S. Chatrchyan *et al.* [CMS Collaboration], Phys. Lett. B **704**, 123 (2011); G. Aad *et al.* [ATLAS Collaboration], arXiv:1108.6311.

Chapter 5

Precision Electroweak Physics

5.1 Charged and Neutral Currents

The oldest and best-known examples of weak processes are the β-decay of atomic nuclei and the more fundamental neutron decay, $n \to p\bar{\nu}e^-$. By analogy to the emission of photons in nuclear-γ decay, Fermi considered the neutrino-electron pair to be created and emitted in the nuclear transition of a neutron to a proton. Inspired by the current-current form of the electromagnetic interaction he proposed that the invariant amplitude for the β-decay process be given by

$$\mathfrak{M} = G_F \left(\overline{u}_n \gamma^\mu u_p \right) \left(\overline{\nu}_e \gamma_\mu u_e \right), \tag{5.1.1}$$

where the effective coupling G_F, known as the Fermi constant, needs to be determined by experiment.[1] The amplitude (5.1.1) explained the properties of some features of β-decay, but not others. Over the following 25 years or so, attempts to unravel the true form of the weak interaction lead to a whole series of ingenious β-decay experiments, reaching the climax with the discovery of parity violation in 1956.[2] Amazingly, the only essential

---

[1]E. Fermi, Nuovo Cim. **11**, 1 (1934); Z. Phys. **88**, 161 (1934).

[2]T. D. Lee and C. N. Yang, Phys. Rev. **104**, 254 (1956); C. S. Wu, E. Ambler, R. W. Hayward, D. D. Hoppes and R. P. Hudson, Phys. Rev. **105**, 1413 (1957); R. L. Garwin, L. M. Lederman and M. Weinrich, Phys. Rev. **105**, 1415 (1957); J. I. Friedman and V. L. Telegdi, Phys. Rev. **105**, 1681 (1957).

change required in Fermi's original proposal was the replacement of γ^μ by $\gamma^\mu(\mathbb{1} - \gamma^5)$.[3] Fermi had not forseen parity violation and had no reason to include a $\gamma^5\gamma^\mu$ contribution; a mixture of γ^μ and $\gamma^5\gamma^\mu$ automatically violates parity conservation; e.g., the *charge-raising* weak current

$$J^\mu = \overline{u}_\nu \gamma^\mu \tfrac{1}{2}(\mathbb{1} - \gamma^5)u_e \tag{5.1.2}$$

couples an ingoing negative helicity electron e_L to an outgoing negative helicity neutrino. Besides the configuration (e_L^-, ν_L), the *charge-raising* weak current also couples the following (ingoing, outgoing) lepton pair configurations: $(\overline{\nu}_R, e_R^+)$, $(0, \nu_L e_R^+)$, and $(e_L^- \overline{\nu}_R, 0)$.[4] Further, the *charge-lowering* weak current (1.5.137) is the hermitian conjugate of (5.1.2),

$$\begin{aligned}
J^{\mu\dagger} &= [\overline{u}_\nu \, \gamma^\mu \tfrac{1}{2}(\mathbb{1} - \gamma^5)u_e]^\dagger \\
&= [u_\nu^\dagger \, \gamma^0 \, \gamma^\mu \tfrac{1}{2}(\mathbb{1} - \gamma^5)u_e]^\dagger \\
&= u_e^\dagger \gamma^0 \gamma^0 \tfrac{1}{2}(\mathbb{1} - \gamma^5)\gamma^{\mu\dagger}\gamma^0 u_\nu \\
&= \overline{u}_e \gamma^0 \tfrac{1}{2}(\mathbb{1} - \gamma^5)\gamma^0 \gamma^\mu u_\nu \\
&= \overline{u}_e \, \gamma^\mu \tfrac{1}{2}(\mathbb{1} - \gamma^5)u_\nu \,.
\end{aligned} \tag{5.1.3}$$

Weak interaction amplitudes are of the form

$$\mathfrak{M} = \frac{4G_F}{\sqrt{2}} J^\mu J_\mu^\dagger \,. \tag{5.1.4}$$

Charge conservation requires that $\mathfrak{M}$ is the product of a charge-raising and a charge-lowering current. The factor of 4 arises because the currents are defined with the normalized projection operator $\tfrac{1}{2}(\mathbb{1} - \gamma^5)$ rather than the old-fashioned $(\mathbb{1} - \gamma^5)$. The $1/\sqrt{2}$ is pure convention (to keep the original definition of G_F which did not include γ^5).

---

[3]S. S. Gershtein and Y. B. Zel'dovich, Zh. Eksp. Teor. Fiz. **29**, 698 (1955); R. P. Feynman and M. Gell-Mann, Phys. Rev. **109**, 193 (1958); E. C. G. Sudarshan and R. E. Marshak, Phys. Rev. **109**, 1860 (1958); J. J. Sakurai, Nuovo Cim. **7**, 649 (1958).

[4]Recall that the spinor component of a right-handed antiparticle corresponds to the spinor component of a left-handed particle with negative energy. This implies that the projection operator of the right-handed antiparticle is $(\mathbb{1} - \gamma^5)/2$. Therefore, (5.1.2) represents a right-handed antineutrino $\overline{\nu}_R$ incoming and the right-handed positron e_R^+ outgoing, $(\overline{\nu}_R, e^+)$; *viz.*, outgoing ν_L is the same as incoming $\bar{\nu}_R$ and viceversa.

The cumulative evidence of many experiments is that indeed only $\overline{\nu}_R$ (and ν_L) are involved in weak interactions. The absence of the "mirror image" states, $\overline{\nu}_L$ and ν_R, is a clear violation of parity invariance. Also, charge conjugation, C, is violated, since C transforms a ν_L state into a $\bar{\nu}_L$ state.[5] However, the $(\mathbb{1} - \gamma^5)$ form leaves the weak interaction invariant under the combined CP operation. For example,

$$\Gamma(\pi^+ \to \mu^+ \nu_L) \neq \Gamma(\pi^+ \to \mu^+ \nu_R) = 0 \qquad P \text{ violation},$$
$$\Gamma(\pi^+ \to \mu^+ \nu_L) \neq \Gamma(\pi^- \to \mu^- \bar{\nu}_L) = 0 \qquad C \text{ violation},$$

but

$$\Gamma(\pi^+ \to \mu^+ \nu_L) = \Gamma(\pi^- \to \mu^- \bar{\nu}_R) \qquad CP \text{ invariance}.$$

In this example, ν denotes a muon neutrino. We discuss CP invariance in the next section.

The values of G_F obtained from the measurements of the neutron lifetime,

$$G_F = (1.136 \pm 0.003) \times 10^{-5} \text{ GeV}^{-2}, \tag{5.1.5}$$

and muon lifetime

$$G_F = 1.16637(1) \times 10^{-5} \text{ GeV}^{-2}, \tag{5.1.6}$$

are found to be within a few percent. Comparison of these results supports the assertion that the Fermi constant is the same for all leptons and nucleons, and hence universal. It means that nuclear β-decay and the decay of the muon (see Appendix H) have the same physical origin. The reason for the small difference is important and is discussed in the next section.

Although the experiments exposing the violation of parity in weak interactions (polarized ^{60}Co decay, K decay, π decay, etc) are some of the highlights in the development of particle physics, parity violation and its $V - A$ structure can now be demonstrated experimentally much more directly. In fact, these days, neutrinos, particularly muon neutrinos, can be prepared in intense beams which are scattered off hadronic targets to probe the structure of the weak interaction. This is analogous to the study of the

---

[5]T. D. Lee, R. Oehme and C. N. Yang, Phys. Rev. **106**, 340 (1957).

electromagnetic lepton-quark interaction by scattering high-energy electron beams off hadronic targets, which we described in Chapter 4.

To predict the neutrino-quark cross sections, we clearly need to know the form of the quark weak currents. Quarks interact electromagnetically just like leptons, apart from their fractional charge. Our inclination therefore is to construct the quark weak current just as we did for leptons. For example, we model the charge-raising quark current,

$$J_q^\mu = \overline{u}_u \gamma^\mu \tfrac{1}{2}(\mathbb{1} - \gamma^5)u_d, \tag{5.1.7}$$

on the weak current

$$J_e^\mu = \overline{u}_\nu \gamma^\mu \tfrac{1}{2}(\mathbb{1} - \gamma^5)u_e \, ; \tag{5.1.8}$$

the hermitian conjugates give the charge-lowering weak currents. The short range of the weak interaction results from the exchange of a heavy gauge boson of mass m_W:

$$= \left(\frac{g}{\sqrt{2}}J_\mu\right)\frac{1}{m_W^2}\left(\frac{g}{\sqrt{2}}J_\mu^\dagger\right) \tag{5.1.9}$$

$$= \frac{4G_F}{\sqrt{2}}J_\mu J^{\mu\dagger} \, . \tag{5.1.10}$$

Upon inserting the currents (5.1.7) and (5.1.8) into (5.1.10), we obtain the invariant amplitude for the *charged current* (CC) neutrino-quark scattering.

To confront pQCD predictions with experiment, it is simplest to consider isoscalar nucleon targets, in which the nuclei contain equal numbers of protons and neutrons, $N = (p + n)/2$. The procedure to embed the constituent cross sections in the overall νN inclusive cross section is familiar from Chapter 4:

$$\sigma = \int_0^1 dx \int_0^{xs} dQ^2 \frac{d^2\sigma_{\nu N}^{\mathrm{CC}}}{dx dQ^2} \, , \tag{5.1.11}$$

where

$$\frac{d^2\sigma_{\nu N}^{CC}}{dxdQ^2} = \frac{G_F^2}{4\pi x}\left(\frac{m_W^2}{Q^2+m_W^2}\right)^2\left[Y_+ F_2^\nu(x,Q^2) - y\,F_L^\nu(x,Q^2) + Y_-\,xF_3^\nu(x,Q^2)\right],$$
(5.1.12)

is the differential cross-section given in terms of the structure functions, with $Y_+ = 1 + (1-y)^2$, $Y_- = 1 - (1-y)^2$, $y = Q^2/sx$, and $s = 2E_\nu m_N$. At LO in pQCD, the structure functions are given in terms of parton distributions as $F_2^\nu = x(u+d+2s+2b+\bar{u}+\bar{d}+2\bar{c}+2\bar{t})$, $xF_3^\nu = x(u+d+2s+2b-\bar{u}-\bar{d}-2\bar{c}-2\bar{t})$, and $F_L^\nu = 0$, and hence (5.1.12) can be written in an "old hat" form

$$\frac{d^2\sigma_{\nu N}^{CC}}{dxdy} = \frac{G_F^2\,s}{\pi}\left(\frac{m_W^2}{Q^2+m_W^2}\right)^2\left[xq_\nu^{CC}(x,Q^2) + (1-y)^2 x\bar{q}_\nu^{CC}(x,Q^2)\right],$$
(5.1.13)

where

$$q_\nu^{CC}(x,Q^2) = \frac{u_v(x,Q^2)+d_v(x,Q^2)}{2} + \frac{u_s(x,Q^2)+d_s(x,Q^2)}{2}$$
$$+ \; s_s(x,Q^2) + b_s(x,Q^2),$$
(5.1.14)

$$\bar{q}_\nu^{CC}(x,Q^2) = \frac{\bar{u}_s(x,Q^2)+\bar{d}_s(x,Q^2)}{2} + \bar{c}_s(x,Q^2) + \bar{t}_s(x,Q^2),$$
(5.1.15)

the subscripts v and s label valence and sea contributions, and u, d, c, s, t, and b denote the distributions for various quark flavors in a proton.

The calculation of $\bar{\nu}N$ scattering proceeds along the lines of that for νN scattering, except for the replacement of F_2^ν, xF_3^ν and F_L^ν by $F_2^{\bar{\nu}}$, $xF_3^{\bar{\nu}}$ and $F_L^{\bar{\nu}}$, respectively. At leading order $F_2^{\bar{\nu}} = x(u + d + 2c + 2t + \bar{u} + \bar{d} + 2\bar{s} + 2\bar{b})$, $xF_3^{\bar{\nu}} = x(u + d + 2c + 2t - \bar{u} - \bar{d} - 2\bar{s} - 2\bar{b})$. Going through the same steps, we obtain

$$\frac{d^2\sigma_{\bar{\nu} N}^{CC}}{dxdy} = \frac{G_F^2\,s}{\pi}\left(\frac{m_W^2}{Q^2+m_W^2}\right)^2\left[x\bar{q}_{\bar{\nu}}^{CC}(x,Q^2) + (1-y)^2 xq_{\bar{\nu}}^{CC}(x,Q^2)\right].$$
(5.1.16)

If there were just three valence quarks in a nucleon, $\bar{q}^{CC}(x,Q^2) = 0$, the neutrino-nucleon and antineutrino-nucleon scattering data would exhibit the dramatic $V - A$ properties of the weak interaction. That is,

$$\frac{d\sigma_{\nu N}^{CC}}{dy} = c, \qquad \frac{d\sigma_{\bar{\nu} N}^{CC}}{dy} = c(1-y)^2,$$
(5.1.17)

147

where c can be found from (5.1.13); and for the integrated cross sections

$$\frac{\sigma_{\bar{\nu}N}^{\mathrm{CC}}}{\sigma_{\nu N}^{\mathrm{CC}}} = \frac{1}{3}.$$ (5.1.18)

At NLO, the relation between the structure functions and the quark momentum distributions involve further QCD calculable coefficient functions, and contributions from F_{L} can no longer be neglected. Therefore, QCD predictions for the structure functions are obtained by solving the DGLAP evolution equations at NLO in the $\overline{MS}$ scheme with the renormalization and factorization scales both chosen to be Q^2. Recall that these equations yield the PDFs at all values of Q^2 provided these distributions have been input as functions of x at some input scale Q_0^2. The resulting PDFs are then convoluted with coefficient functions, to obtain the structure functions. Predictions for high energy νN CC inclusive cross sections have been calculated within the conventional DGLAP formalism of NLO QCD using the ZEUS-S global fit PDF analysis (updated to include *all* the HERA-I data).[6] The calculation accounts in a systematic way for PDF uncertainties deriving from both model uncertainties and from experimental uncertainties of the input data set. In Fig. 5.1, the NLO predictions for νN and $\overline{\nu}N$ CC inclusive cross sections are compared to those from a LO calculation using (5.1.13) and CTEQ4 PDFs.[7] The NLO results show a less steep rise of σ at high energies, reflecting the fact that more recent HERA data display a less dramatic rise at low-x than early data which was used to calculate the CTEQ4 PDFs. At low energies, where the contribution of the valence quarks predominates, the $\bar{\nu}$ cross sections are about a factor of 3 smaller than the corresponding νN cross sections, because of the $(1-y)^2$ behavior of the $\bar{\nu}q$ cross section. Above $E_\nu \approx 10^6$ GeV, the valence contribution is negligible and the νN and $\bar{\nu}N$ cross sections become equal.[8]

---

[6]L. A. Anchordoqui, A. M. Cooper-Sarkar, D. Hooper and S. Sarkar, Phys. Rev. D **74**, 043008 (2006); A. Cooper-Sarkar and S. Sarkar, JHEP **0801**, 075 (2008).

[7]R. Gandhi, C. Quigg, M. H. Reno and I. Sarcevic, Phys. Rev. D **58**, 093009 (1998).

[8]Ultrahigh energy cosmic neutrinos are unique probes of new physics as their interactions are uncluttered by the strong and electromagnetic forces and upon arrival at the Earth may experience interactions with $\sqrt{s} \gtrsim 200$ TeV. Rates for new physics processes, however, are difficult to test since the flux of cosmic neutrinos is virtually unknown. It is
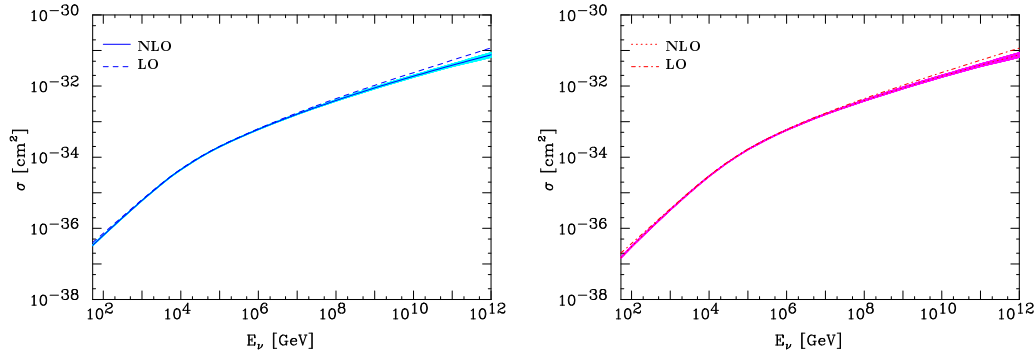
Figure 5.1: *The NLO inclusive νN (left) and $\bar{\nu} N$ (right) cross section along with the $\pm 1\sigma$ uncertainties (shaded band), compared with LO calculation.*

The discovery of neutrino-induced muonless events in 1973 heralded a new era in particle physics.[9] These events, most readily interpretable as $\nu_\mu(\overline{\nu})N \to \nu_\mu(\overline{\nu})+$ hadrons, are evidence of a weak neutral current,

$$J_\mu^{\mathrm{NC}}(\nu) = \tfrac{1}{2}\left(\overline{u}_\nu \gamma^\mu \tfrac{1}{2}(\mathbb{1} - \gamma^5)u_\nu\right) , \qquad (5.1.19)$$

$$J_\mu^{\mathrm{NC}}(q) = \left(\overline{u}_q \gamma^\mu \tfrac{1}{2}(c_V^q \mathbb{1} - c_A^q \gamma^5)u_q\right) . \qquad (5.1.20)$$

If we compare (5.1.20) with (2.4.96), we see that the vector and axial-vector couplings, c_V and c_A are determined in the standard model (given the value of $\sin^2\theta_w$). Their values are

$$c_V^f = T_f^3 - 2\sin^2\theta_w\, Q_f \qquad c_A^f = T_f^3 , \qquad (5.1.21)$$

where T_f^3 and Q_f are, respectively, the third component of the weak isospin and the charge of the fermion f (given in Table 2.1). In general, the J_μ^{NC}, unlike the charged current J_μ, are not pure $V - A$ currents ($c_V \neq c_A$); they have right-handed components. The neutral current interaction is described

---

possible to mitigate this by using multiple observables which allow one to decouple effects of the flux and cross section; see e.g., L. A. Anchordoqui, J. L. Feng, H. Goldberg and A. D. Shapere, Phys. Rev. D **65**, 124027 (2002).

[9]F. J. Hasert *et al.* [Gargamelle Neutrino Collaboration], Phys. Lett. B **46**, 138 (1973).

by a coupling $g/\cos\theta_w$,

$$
\begin{aligned}
&= \left(\frac{g}{\cos\theta_w}J^{\mathrm{NC}}_\mu\right)\left(\frac{1}{m_Z^2}\right)\left(\frac{g}{\cos\theta_w}J^{\mathrm{NC}\mu\dagger}\right) && (5.1.22)\\[2ex]
&= \frac{4G_F}{\sqrt{2}}2\rho J^{\mathrm{NC}}_\mu J^{\mathrm{NC}\mu\dagger}\,. && (5.1.23)
\end{aligned}
$$

where the diagram shows J^{NC}_μ at the top vertex with coupling $g/\cos\theta_w$, the Z propagator, and $J^{\mathrm{NC}\,\mu+}$ at the bottom vertex.

The relative strength of the neutral and charged currents is parametrized by the weak angle $\cos\theta_w$, or by the ρ-parameter as can be seen by comparing (5.1.9) with (5.1.22) and (5.1.10) with (5.1.23), respectively. Identification of (5.1.9) and (5.1.10) yields

$$
\frac{G_F}{\sqrt{2}} = \frac{g^2}{8m_W^2}\,, \qquad\qquad (5.1.24)
$$

while combining (5.1.22) with (5.1.23) gives

$$
\rho\frac{G_F}{\sqrt{2}} = \frac{g^2}{8m_Z^2\cos^2\theta_w}\,; \qquad\qquad (5.1.25)
$$

from the last two equations and (2.4.88)

$$
\rho = \frac{m_W^2}{m_Z^2\cos^2\theta_w} = 1\,. \qquad\qquad (5.1.26)
$$

In other words, if the model is successful, all neutral current phenomena will be described by a common parameter. For the moment we will leave c_V^i, c_A^i and ρ as free parameters to be determined by experiment. For further discussion it is useful to remember that neutral currents have a coupling ρG_F and that ρ represents the relative strength of neutral and charged weak

currents, e.g. for neutrino-quark scattering:

$$
\rho = \cfrac{
\begin{array}{c}
\nu \;\rule[0.5ex]{2cm}{0.4pt} \\[-0.3em]
\vdots\; Z \qquad + \qquad t\;\bigcirc\;\bar{t} \qquad + \cdots \\[-0.3em]
q \;\rule[0.5ex]{2cm}{0.4pt}
\end{array}
}{
\begin{array}{c}
\nu \;\rule[0.5ex]{2cm}{0.4pt}\; \mu \\[-0.3em]
\vdots\; W \qquad + \qquad t\;\bigcirc\;\bar{b} \qquad + \cdots \\[-0.3em]
q \;\rule[0.5ex]{2cm}{0.4pt}\; q'
\end{array}
}
\tag{5.1.27}
$$

$\Delta\rho$ measures the quantum corrections to the ratio of the neutral- and charged-current amplitudes at low energy.

The calculation of inclusive cross sections $\nu N \to \nu X$ proceeds exactly as that for the charged current processes. At LO in pQC we find

$$
\frac{d^2\sigma_{\nu N}^{\mathrm{NC}}}{dx\,dy} = \frac{\rho G_F^2\, M\, E_\nu}{2\pi} \left(\frac{m_Z^2}{Q^2 + m_Z^2} \right)^2 \left[x q_\nu^{\mathrm{NC}}(x, Q^2) + (1-y)^2 x \overline{q}_\nu^{\mathrm{NC}}(x, Q^2) \right] \;,
\tag{5.1.28}
$$

where the quark densities are given by

$$
\begin{aligned}
q_\nu^{\mathrm{NC}}(x, Q^2) \;=\; & \left[\frac{u_v(x, Q^2) + d_v(x, Q^2)}{2} \right] \left[(c_V^d + c_A^d)^2 + (c_V^u + c_A^u)^2 \right] \\
& + \; 2 \left[\frac{u_s(x, Q^2) + d_s(x, Q^2)}{2} \right] \left[(c_V^d)^2 + (c_A^d)^2 + (c_V^u)^2 + (c_A^u)^2 \right] \\
& + \; 2[s_s(x, Q^2) + b_s(x, Q^2)] \left[(c_V^d)^2 + (c_A^d)^2 \right] \\
& + \; 2[c_s(x, Q^2) + t_s(x, Q^2)] \left[(c_V^u)^2 + (c_A^u)^2 \right] \;,
\end{aligned}
\tag{5.1.29}
$$

and

$$
\begin{aligned}
\overline{q}_\nu^{NC}(x, Q^2) \;=\; & \left[\frac{u_v(x, Q^2) + d_v(x, Q^2)}{2} \right] \left[(c_V^d - c_A^d)^2 + (c_V^u - c_A^u)^2 \right] \\
& + \; 2 \left[\frac{u_s(x, Q^2) + d_s(x, Q^2)}{2} \right] \left[(c_V^d)^2 + (c_A^d)^2 + (c_V^u)^2 + (c_A^u)^2 \right] \\
& + \; 2[s_s(x, Q^2) + b_s(x, Q^2)] \left[(c_V^d)^2 + (c_A^d)^2 \right] \\
& + \; 2[c_s(x, Q^2) + t_s(x, Q^2)] \left[(c_V^u)^2 + (c_A^u)^2 \right] .
\end{aligned}
\tag{5.1.30}
$$

A quantitative comparison of the strength of NC to CC weak processes has been obtained by the NuTeV Collaboration, by scattering neutrinos off an iron target.[10] The experimental values are

$$R_\nu^{\text{exp}} \equiv \frac{\sigma_{\nu_\mu N \to \nu_\mu X}^{\text{NC}}}{\sigma_{\nu_\mu N \to \mu X}^{\text{CC}}} = 0.3916 \pm 0.0007 \,, \qquad (5.1.31)$$

$$R_{\bar\nu}^{\text{exp}} \equiv \frac{\sigma_{\bar\nu_\mu N \to \bar\nu_\mu X}^{\text{NC}}}{\sigma_{\bar\nu_\mu N \to \mu X}^{\text{CC}}} = 0.4050 \pm 0.0016 \,, \qquad (5.1.32)$$

whereas for $E_\nu > 10^7$ GeV, the prediction from (5.1.13), (5.1.16), and (5.1.28), using CTEQ4 PDFs, is $R_\nu = R_{\bar\nu} \simeq 0.4$.

5.2 Quark Flavor Mixing

So far, we have seen that leptons and quarks participate in weak interactions through charged $V - A$ currents constructed from the following pairs of (left-handed) fermion states:

$$\begin{pmatrix} \nu_e \\ e^- \end{pmatrix}, \quad \begin{pmatrix} \nu_\mu \\ \mu^- \end{pmatrix}, \quad \text{and} \quad \begin{pmatrix} u \\ d \end{pmatrix}. \qquad (5.2.33)$$

All these charged currents couple with universal coupling G_F. It is natural to attempt to extend this universality to embrace the doublet

$$\begin{pmatrix} c \\ s \end{pmatrix} \qquad (5.2.34)$$

formed from the heavier quark states. However, we already know that this cannot be quite correct. For example, the decay $K^+ \to \mu^+ \nu_\mu$ occurs. The K^+ is made of u and $\bar{s}$ quarks. There must thus be a weak current which couples a u to an $\bar{s}$ quark. This contradicts the above scheme, which only allows weak transitions between $u \leftrightarrow d$ and $c \leftrightarrow s$.

---

[10]G. P. Zeller *et al.* [NuTeV Collaboration], Phys. Rev. Lett. **88**, 091802 (2002) [Erratum-ibid. **90**, 239902 (2003)].

Instead of introducing new couplings to accommodate observations like $K^+ \to \mu^+\nu_\mu$, let's try to keep universality but modify the quark doublets. We assume that the charged current couples "rotated" quark states

$$\begin{pmatrix} u \\ d' \end{pmatrix}, \quad \begin{pmatrix} c \\ s' \end{pmatrix}, \dots, \tag{5.2.35}$$

where

$$d' = d\cos\theta_c + s\sin\theta_c$$
$$s' = -d\sin\theta_c + s\cos\theta_c. \tag{5.2.36}$$

This introduces an arbitrary parameter θ_c, the quark mixing angle, known as the Cabibbo angle.[11] In 1963, Cabibbo first introduced the doublet u, d' to account for the weak decays of strange particles. Indeed the mixing of the d and s quark can be determined by comparing $\Delta S = 1$ and $\Delta S = 0$ decays. For example

$$\frac{\Gamma(K^+ \to \mu^+\nu_\mu)}{\Gamma(\pi^+ \to \mu^+\nu_\mu)} \sim \sin^2\theta_c,$$

$$\frac{\Gamma(K^+ \to \pi^0 e^+\nu_e)}{\Gamma(\pi^+ \to \pi^0 e^+\nu_e)} \sim \sin^2\theta_c.$$

After allowing for the kinematic factors arising from the different particle masses, the data show that $\Delta S = 1$ transitions are suppressed by a factor of about 20 as compared to the $\Delta S = 0$ transitions. This corresponds to $\sin\theta_c = 0.2255 \pm 0.0019$.

What we have done is to change our mind about the CC (5.1.7). We now have Cabibbo favored transitions (proportional to $\cos\theta_c$)

and "Cabibbo suppressed" transitions

[11]N. Cabibbo, Phys. Rev. Lett. **10**, 531 (1963).
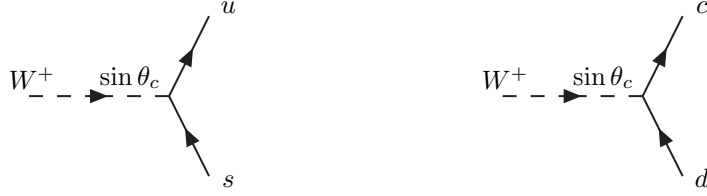
[see (5.2.36)], and similar diagrams for the charge lowering transitions. We can summarize this by writing down the explicit form of the matrix element describing the CC weak interactions of the quarks. From (5.1.4)

$$\mathfrak{M} = \frac{4G_F}{\sqrt{2}} J^\mu J_\mu^\dagger \tag{5.2.37}$$

with

$$J^\mu = (\bar{u} \quad \bar{c}) \frac{\gamma^\mu(\mathbb{1} - \gamma^5)}{2} \, U \begin{pmatrix} d \\ s \end{pmatrix}. \tag{5.2.38}$$

The unitary matrix U performs the rotation (5.2.36) of the d and s quarks states:

$$U = \begin{pmatrix} \cos\theta_c & \sin\theta_c \\ -\sin\theta_c & \cos\theta_c \end{pmatrix}. \tag{5.2.39}$$

Of course, there will be amplitudes describing semileptonic decays constructed from the product of a quark with a lepton current, J^μ (quark) $J_\mu^\dagger$ (lepton). All this has implications for our previous calculations. For example, we must replace G_F in (5.1.5) by $\widetilde{G}_F = G_F \cos\theta_c$, whereas the purely leptonic μ-decay rate, which involves no mixing, is unchanged. The detailed comparison of these rates, (5.1.5) and (5.1.6) supports Cabibbo's hypothesis.

The form (5.2.39) gives a zeroth-order approximation to the weak interactions of the u, d, s, and c quarks; their coupling to the third family, though non-zero, is very small. It is straightforward to extend the weak current, (5.2.38), to embrace the additional doublet of quarks

$$J^\mu = (\bar{u} \quad \bar{c} \quad \bar{t}) \frac{\gamma^\mu(\mathbb{1} - \gamma^5)}{2} \, U \begin{pmatrix} d \\ s \\ b \end{pmatrix}. \tag{5.2.40}$$

154

The 3×3 matrix U contains three real parameters (Cabibbo-like mixing angles) and a phase factor $e^{i\delta}$. The original parametrization was due to Kobayashi and Maskawa.[12] An easy-to-remember approximation to the observed magnitude of each element in the 3-family matrix is

$$U = \begin{pmatrix} |U_{ud}| & |U_{us}| & |U_{ub}| \\ |U_{cd}| & |U_{cs}| & |U_{cb}| \\ |U_{td}| & |U_{ts}| & |U_{tb}| \end{pmatrix} \sim \begin{pmatrix} 1 & \lambda & \lambda^3 \\ \lambda & 1 & \lambda^2 \\ \lambda^3 & \lambda^2 & 1 \end{pmatrix} . \tag{5.2.41}$$

where $\lambda = \sin\theta_c$.[13] These are order of magnitude only; each element may be multiplied by a phase and a coefficient of $\mathcal{O}(1)$. The approximation in (5.2.41) displays a suggestive but not well understood hierarchical structure. Unlike the 2×2 matrix of (5.2.39), because of the phase δ, the Cabibbo-Kobayashi-Maskawa (CKM) matrix is complex. This has fundamental implications concerning CP invariance, which we discuss next.

To investigate CP invariance, we first compare the amplitude for a weak process, say the quark scattering process $ab \to cd$, with that for an antiparticle reaction $\bar{a}\bar{b} \to \bar{c}\bar{d}$. We take $ab \to cd$ to be the charged current interaction of Fig. 5.2.a. The amplitude is

$$\begin{aligned} \mathfrak{M} &\sim J^\mu_{ca} J^\dagger_{\mu bd} \\ &\sim \left(\bar{u}_c \gamma^\mu (\mathbb{1} - \gamma^5) U_{ca} u_a \right) \left(\bar{u}_b \gamma_\mu (\mathbb{1} - \gamma^5) U_{bd} u_d \right)^\dagger \\ &\sim U_{ca} U^*_{db} \left(\bar{u}_c \gamma^\mu (\mathbb{1} - \gamma^5) u_a \right) \left(\bar{u}_d \gamma_\mu (\mathbb{1} - \gamma^5) u_b \right) , \end{aligned} \tag{5.2.42}$$

because $U^\dagger_{bd} = U^*_{db}$. $\mathfrak{M}$ describes either $ab \to cd$ or $\bar{c}\bar{d} \to \bar{a}\bar{b}$ (remembering the antiparticle prescription of Sec. 1.4).

On the other hand, the amplitude $\mathfrak{M}'$ for the antiparticle process $\bar{a}\bar{b} \to \bar{c}\bar{d}$ (or $cd \to ab$) is

$$\begin{aligned} \mathfrak{M}' &\sim \left(J^\mu_{ca} \right)^\dagger J_{\mu bd} \\ &\sim U^*_{ca} U_{db} \left(\bar{u}_a \gamma^\mu (\mathbb{1} - \gamma^5) u_c \right) \left(\bar{u}_b \gamma_\mu (\mathbb{1} - \gamma^5) u_d \right) ; \end{aligned} \tag{5.2.43}$$

that is, $\mathfrak{M}' = \mathfrak{M}^\dagger$. This should not be surprising. It is demanded by the hermiticity of the Hamiltonian. By glancing back at (3.1.3) and (3.1.11), we

[12]M. Kobayashi and T. Maskawa, Prog. Theor. Phys. **49**, 652 (1973).

[13]L. Wolfenstein, Phys. Rev. Lett. **51**, 1945 (1983).
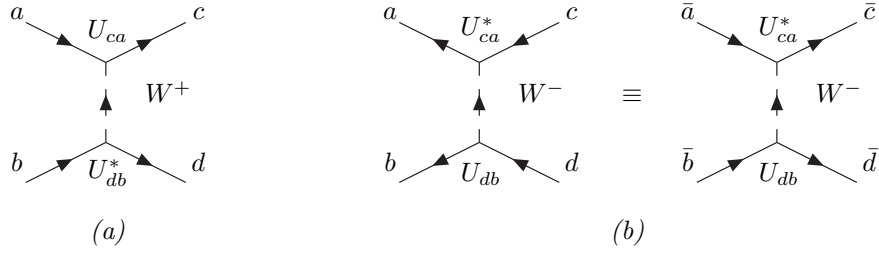
Figure 5.2: *The processes described by (a) the weak amplitude $\mathfrak{M}(ab \to cd)$ and (b) its hermitian conjugate.*

see that $\mathfrak{M}$ is essentially the interaction Hamiltonian V for the process. The total interaction Hamiltonian must contain $\mathfrak{M} + \mathfrak{M}^\dagger$, where $\mathfrak{M}$ describes the $i \to f$ transition and $\mathfrak{M}^\dagger$ describes the $f \to i$ transition in the notation of Chapter 3.

In Sec. 5.1, we have seen that weak interactions violate both P invariance and C invariance, but have indicated that invariance under the combined CP operation may hold. How do we verify that the theory is CP invariant? We calculate from $\mathfrak{M}(ab \to cd)$ of (5.2.42) the amplitude $\mathfrak{M}_{CP}$, describing the CP-transformed process, and see whether or not the Hamiltonian remains hermitian. If it does, that is, if $\mathfrak{M}_{CP} = \mathfrak{M}^\dagger$, then the theory is CP invariant. If it does not, then is CP violated.

$\mathfrak{M}_{CP}$ is obtained by substituting the CP-transformed Dirac spinors in (5.2.42)

$$u_i \to P(u_i)^c, \qquad i = a, \dots d, \tag{5.2.44}$$

where u^c are charged conjugate spinors defined by

$$u^c = C\bar{u}^T, \tag{5.2.45}$$

see Sec. 1.4. Clearly to form $\mathfrak{M}_{CP}$, we need $\bar{u}^c$ and also, to know how $\gamma^\mu(\mathbb{1} - \gamma^5)$ transforms under C. In the standard representation of gamma matrices we have

$$\bar{u}^c = u^{c\dagger}\gamma^0 = (C\gamma^0 u^*)^\dagger\gamma^0 = u^T\gamma^0 C^\dagger\gamma^0 = -u^T C^\dagger\gamma^0\gamma^0 = -u^T C^{-1}, \tag{5.2.46}$$

$$\gamma^\mu = -(C\gamma^0)\gamma^{\mu*}(C\gamma^0)^{-1} = -C\gamma^0\gamma^{\mu*}\gamma^0 C^{-1} = -C\gamma^{\mu T}C^{-1} \tag{5.2.47}$$

156

$$\begin{aligned}
C^{-1}\gamma^\mu\gamma^5 C &= -\gamma^{\mu T}C^{-1}i\gamma^0\gamma^1\gamma^2\gamma^3 C \\
&= -i\gamma^{\mu T}(C^{-1}\gamma^0 C)(C^{-1}\gamma^1 C)(C^{-1}\gamma^2 C)(C^{-1}\gamma^3 C) \\
&= -i\gamma^{\mu T}\gamma^{0T}\gamma^{1T}\gamma^{2T}\gamma^{3T} \\
&= -\gamma^{\mu T}(i\gamma^3\gamma^2\gamma^1\gamma^0)^T \\
&= -\gamma^{\mu T}(i\gamma^0\gamma^1\gamma^2\gamma^3)^T \\
&= -\gamma^{\mu T}\gamma^{5T} \\
&= -(\gamma^5\gamma^\mu)^T \\
&= (\gamma^\mu\gamma^5)^T .
\end{aligned} \tag{5.2.48}$$

With the replacements (5.2.44), the first charged current of (5.2.42) becomes

$$\begin{aligned}
(J^\mu_{ca})^c &= U_{ca}(\bar{u}_c)^c\gamma^\mu(\mathbb{1}-\gamma^5)(u_a)^c \\
&= -U_{ca}u_c^T C^{-1}\gamma^\mu(\mathbb{1}-\gamma^5)C\bar{u}_a^T \\
&= U_{ca}u_c^T[\gamma^\mu(\mathbb{1}+\gamma^5)]^T\bar{u}_a^T \\
&= (-)U_{ca}\bar{u}_a\gamma^\mu(\mathbb{1}+\gamma^5)u_c .
\end{aligned} \tag{5.2.49}$$

The origin of the extra minus sign introduced in the last line is subtle but important. The minus sign is related to the connection between spin and statistics; in field theory it occurs because of the antisymmetric nature of the fermion fields. In field theory, the charge conjugation operator C changes a positive-energy particle into a positive-energy antiparticle, and the formalism is completely $f \Leftrightarrow \bar{f}$ symmetric. However, in a single-particle theory, antiparticles states are not allowed; rather C changes a positive-energy particle state into a negative-energy particle state. As a result, we must add to our Feynmann rules the requirement that we insert by hand an extra minus sign for every negative-energy particle in the final state of the process. The parity operation $P = \gamma^0$, and so $P^{-1}\gamma^\mu(\mathbb{1}+\gamma^5)P = \gamma^{\mu\dagger}(\mathbb{1}-\gamma^5)$. Thus

$$(J^\mu_{ca})_{CP} = (-)U_{ca}\bar{u}_a\gamma^{\mu\dagger}(\mathbb{1}-\gamma^5)u_c , \tag{5.2.50}$$

and hence

$$\mathfrak{M}_{CP} \sim U_{ca}U^*_{db}\left[\bar{u}_a\gamma^\mu(\mathbb{1}-\gamma^5)u_c\right]\left[\bar{u}_b\gamma_\mu(\mathbb{1}-\gamma^5)u_d\right] . \tag{5.2.51}$$

We can now compare $\mathfrak{M}_{CP}$ with $\mathfrak{M}^\dagger$ of (5.2.43). Provided the elements of the matrix U are real, we find $\mathfrak{M}_{CP} = \mathfrak{M}^\dagger$, and the theory is CP invariant.

At the four-quark (u, d, c, s) level, this is the case as the 2×2 matrix U, (5.2.39), is indeed real. However, with the advent of the b and t quarks, the matrix U becomes the 3×3 CKM matrix. It now contains a complex phase factor $e^{i\delta}$. Therefore, in general, we have $\mathfrak{M}_{CP} \neq \mathfrak{M}^\dagger$ and the theory neccesarily violates CP invariance.

In fact, a tiny CP violation had been established many years before the introduction of the CKM matrix. The evidence for the indirect violation of CP-invariance was first revealed in 1964 in the mixing of neutral kaons.[14] These particles offer a unique "window" through which to look for small CP violating effects. In particular, direct CP-violation, not mixing-assisted, has been established in the decay $B_d \to K\pi$ with a significance in excess of 5σ. Today, precision data on neutral kaons have been accumulated over 40 years; thus far, the measurements can, without exception, be accommodated by the standard model with three families. Whenever the experimental precision in CP-violation measurements has increased, the results have fit snugly within the standard model. Given the rapid progress and the better theoretical understanding of the standard model expectations relative to the K system, the hope is that at this point, the glass is half full and that improved data will pierce the standard model's resistant armor.[15]

5.3 Scalars were already part of the Theory!

One can illustrate this statement simply by calculating the cross section for top quark annihilation into Z's, $t\bar{t} \to ZZ$, in a standard model without scalars. In the energy limit, $\sqrt{s} \gg m_t$, straightforward Feynmanology yields

$$\frac{d\sigma}{d\Omega}\left[\begin{array}{c} t \\ \\ \bar{t} \end{array} + \begin{array}{c} \text{crossed} \\ \text{diagram} \end{array}\right] = \frac{\alpha^2 m_t^2}{m_Z^4} + \mathcal{O}\left(\frac{1}{s}\right) . \qquad (5.3.52)$$

[14]J. H. Christenson, J. W. Cronin, V. L. Fitch and R. Turlay, Phys. Rev. Lett. **13**, 138 (1964).

[15]F. Halzen, M. C. Gonzalez-Garcia, T. Stelzer and R. A. Vazquez, Phys. Rev. D **51**, 4861 (1995); A. Masiero and O. Vives, Ann. Rev. Nucl. Part. Sci. **51**, 161 (2001).

We first notice there is no angular dependence; $d\sigma/d\Omega$ is independent of Ω. The process is purely S-wave. We therefore have to conclude that the process violates S-wave unitarity, which requires that

$$\sigma_{J=0} \sim \frac{1}{s}, \tag{5.3.53}$$

where s is the square of the $t\bar{t}$ annihilation energy.

We remind the reader that the unitarity constraint (5.3.53) simply follows from the partial wave expansion of the cross section in ordinary quantum mechanics:

$$\sigma = \frac{16\pi}{s} \sum_J (2J+1) |f_J|^2 , \tag{5.3.54}$$

with

$$f_J = \exp(i\delta_J) \sin\delta_J . \tag{5.3.55}$$

Here δ_J are the phase shifts. Obviously $|f_J|^2 < 1$ from (5.3.55) which, when combined with (5.3.54), yields

$$\sigma_J < 16\pi (2J+1)\frac{1}{s} \tag{5.3.56}$$

and (5.3.53) represents the special case $J = 0$.

The Higgs particle comes to the rescue, introducing the additional diagram:

$$\propto \frac{Y_t^2}{m_Z^4} , \tag{5.3.57}$$

which cancels the ill-behaved $J = 0$ term (5.3.52).[16] The cancellation requires that the top-Higgs coupling Y_t (endowing the top quark with mass) satisfies

$$Y_t^2 \sim m_t^2 , \tag{5.3.58}$$

a result indeed intrinsic to the Higgs origin of fermion masses. So, if scalars were not invented to solve the problem of mass, they would have to be introduced to salvage unitarity.

---

[16]C. H. Llewellyn Smith, Phys. Lett. B **46**, 233 (1973).

We have not found the Higgs particle, but we know that

$$114.4 \text{ GeV} < m_H \lesssim 1 \text{ TeV} \,. \tag{5.3.59}$$

The lower limit can be deduced from unsuccessful searches.[17] The vacuum expectation value

$$v^2 = \frac{1}{g^2} 4 m_W^2 = \frac{1}{\sqrt{2} G_F} = (246 \text{ GeV})^2 \tag{5.3.60}$$

yields the upper limit

$$m_H = \left(2\lambda v^2\right)^{1/2} < \sqrt{2}\, v \simeq 350 \text{ GeV} \,. \tag{5.3.61}$$

The inequality follows from $\lambda < 1$, a requirement which follows from the recognition that the standard model's perturbative predictions are correct. This requires couplings to be small, an argument which cannot be taken too literally as it cannot distinguish $\lambda < 1$ from $\lambda < 4\pi$, for instance. Hence our 1 TeV value quoted in (5.3.59).

5.4 Electroweak Model @ Born Level

Some 150 years ago Maxwell unified the electric and magnetic forces by postulating the identity of the electric and magnetic charges:

$$\vec{F} = e\vec{E} + e_M\, \vec{v} \times \vec{B} \,, \tag{5.4.62}$$

with

$$e = e_M \,. \tag{5.4.63}$$

Note that the velocity v is the variable which mixes electric and magnetic interactions; when $v \to 0$ magnetic interactions are simply absent but, for charges moving with significant velocity v, the two interactions become similar in importance. Unification of the two forces introduces a scale in the mixing variable v: the speed of light.

---

[17]The combination of LEP data yields a 95% CL lower mass of 114.4 GeV. Very recently, Tevatron data excluded the mass range (160 GeV, 170 GeV) at 95% CL.

Unification of the electromagnetic and weak interaction follows this pattern with

$$e = g \sin \theta_w \,, \tag{5.4.64}$$

expressing the equality of electric and weak charge g in terms of the parameter θ_w introduced in (5.1.22). In the electroweak theory (5.4.64) generalizes (5.4.63) to include the weak force. What is the variable mixing electromagnetic and weak forces? At low energy the effects of weak forces between charged particles are swamped by their electromagnetic interaction. At a modern accelerator the weak and electromagnetic forces are equally obvious in the collisions of high energy particles, just like the electric and magnetic forces are in the interaction of high velocity charges. Energy is the mixing variable of electromagnetic and weak forces. The energy scale introduced by their unification is the weak boson mass m_W.

The sad reality is that electroweak unification (5.4.64) contains a parameter θ_w which is left to be determined by experiment. The parameter represents the relative strength of charged and neutral currents (cf. (5.1.9) and (5.1.22) and recall (5.1.27)) as well as the ratio of the weak boson masses m_W and m_Z; see (2.4.88). The first and only tangible confirmation of electroweak unified theory has been provided by verification that the ratio of the weak boson masses determined at proton-antiproton colliders yields a value of the weak angle which is in agreement with the value determined in the pioneering neutral current neutrino experiments. On a more mundane level, this common value verifies the doublet nature of the scalar field introduced in Sec. 2.4 via (2.4.88).

Not until the mid-ninties did true verification of the electroweak theory become possible with the first confrontation of its calculated radiative corrections with high statistics measurements performed at the LEP and SLC e^+e^- colliders and at the $p\bar{p}$ Fermilab Tevatron.[18] We have barely started down the road of high precision tests familiar from quantum electrodynamics. We describe the first successful steps next.

---

[18]The first phase of the LEP/SLC program involved running at the Z pole, $e^+e^- \to Z \to \ell^+\ell^-,\ q\bar{q}$, and $\nu\bar{\nu}$. During the period 1989-1995 the four LEP experiments ALEPH, DELPHI, L3, and OPAL at CERN observed $\sim 2 \times 10^7$ Z bosons. The SLD experiment at the SLC at SLAC observed some 5×10^5 events. LEP2 ran from 1995-2000, with center-of-mass energy gradually increasing from about 140 GeV to 209 GeV.

Figure 5.3: *Electromagnetic and weak contributions to $e^+e^- \to \mu^+\mu^-$.*

5.4.1 Interference in e^+e^- annihilation

When contemplating the vast amount of evidence for the standard model, covering strong and electroweak interactions, collider and fixed-target experiments with lepton, photon, and hadron beams, it is easy to overlook the fact that verification of the theory at the quantum level is in its infancy, at least by QED standards. In the electroweak sector familiar tests of the standard model probe the Lagrangian at Born level. Perhaps, the oldest of these tests has been the measurement of electroweak interference in e^+e^- collisions.

e^+e^- annihilations can occur through electromagnetic (γ) or weak neutral current (Z) interactions. Therefore, high-energy e^+e^- colliding beam machines are an ideal testing ground for the interference effect of the electromagnetic and the neutral weak amplitude. As we discussed in Sec. 3.3, the measurement of the reaction $e^+e^- \to \mu^+\mu^-$ at PETRA energies provides tests of the validity of QED at small distances. In what follows, we show that such a measurement also provides a unique test of the asymmetry arising (in the angular distribution of muon pairs) from the interference of the electromagnetic amplitude $\mathfrak{M}^{EM} \sim e^2/k^2$, with a small weak contribution. The size of this effect is found to be

$$\frac{|\mathfrak{M}^{\mathrm{EM}}\,\mathfrak{M}^{\mathrm{NC}}|}{|\mathfrak{M}^{\mathrm{EM}}|^2} \approx \frac{G_F}{e^2/k^2} \approx \frac{10^{-4}k^2}{m_N^2}, \qquad (5.4.65)$$

using $G_F \approx 10^{-5}/m_N^2$ [see Appendix H] and $e^2/4\pi = 1/137$. For PETRA e^+e^- beam energies ~ 20 GeV we have $k^2 \approx s \approx (40 \text{ GeV})^2$ and so predicts about a 15% effect, which is readily observable.

To make a detailed prediction, we assume that the neutral current process is mediated by a Z boson with couplings given by (5.1.20). Using Feynman

rules, the amplitudes $\mathfrak{M}_\gamma$ and $\mathfrak{M}_Z$ corresponding to the diagrams of Fig. 5.3 are

$$\mathfrak{M}_\gamma = -\frac{e^2}{k^2}(\bar{\mu}\gamma^\nu\mu)(\bar{e}\gamma_\nu e)\,, \tag{5.4.66}$$

$$\begin{aligned}
\mathfrak{M}_Z &= -\frac{g^2}{4\cos^2\theta_w}\left[\bar{\mu}\gamma^\nu(c_V^\mu\mathbb{1} - c_A^\mu\gamma^5)\mu\right]\left(\frac{g_{\nu\sigma} - k_\nu k_\sigma/m_Z^2}{k^2 - m_Z^2}\right) \\
&\times \left[\bar{e}\gamma^\sigma(c_V^e\mathbb{1} - c_A^e\gamma^5)e\right]\,,
\end{aligned} \tag{5.4.67}$$

where k is the four-momentum of the virtual γ (or Z), $s \simeq k^2$. With electron-muon universality, the superscripts on $c_{V,A}$ are superfluous here, but we keep them so as one is able to translate the results directly to $e^+e^- \to q\bar{q}$. We ignore the lepton masses, so the Dirac equation for the incident positron reads $(\frac{1}{2}k_\sigma)\bar{e}\gamma^\sigma = 0$ and the numerator of the propagator simplifies to $g_{\mu\sigma}$. Thus, (5.4.67) becomes

$$\mathfrak{M}_Z = -\frac{\sqrt{2}G_F m_Z^2}{s - m_Z^2}\left[c_R^\mu(\bar{\mu}_R\gamma^\nu\mu_R) + c_L^\mu(\bar{\mu}_L\gamma^\nu\mu_L)\right]\left[c_R^e(\bar{e}_R\gamma_\nu e_R) + c_L^e(\bar{e}_L\gamma_\nu e_L)\right]\,, \tag{5.4.68}$$

using (5.1.24) and (5.1.26) with $\rho = 1$, and where

$$c_R \equiv c_V - c_A, \qquad c_L \equiv c_V + c_A\,. \tag{5.4.69}$$

That is we have chosen to write

$$c_V\mathbb{1} - c_A\gamma^5 = (c_V - c_A)\tfrac{1}{2}(\mathbb{1} + \gamma^5) + (c_V + c_A)\tfrac{1}{2}(\mathbb{1} - \gamma^5)\,. \tag{5.4.70}$$

The $(\mathbb{1} \pm \gamma^5)$ are projection operators, which enable $\mathfrak{M}_Z$ to be expressed explicitly in terms of right- and left-handed spinors. It is easier to calculate $|\mathfrak{M}_\gamma + \mathfrak{M}_Z|^2$ in this form. With definite electron and muon helicities, we can apply the results of the QED calculation of $e^+e^- \to \mu^+\mu^-$ given in Sec. 3.3. For example,

$$\left.\frac{d\sigma}{d\Omega}\right|_{e_L^- e_R^+ \to \mu_L^- \mu_R^+} = \frac{\alpha^2}{4s}(1 + \cos\theta)^2\left[1 + rc_L^\mu c_L^e\right]^2\,, \tag{5.4.71}$$

$$\left.\frac{d\sigma}{d\Omega}\right|_{e_L^- e_R^+ \to \mu_R^- \mu_L^+} = \frac{\alpha^2}{4s}(1 + \cos\theta)^2\left[1 + rc_R^\mu c_L^e\right]^2\,, \tag{5.4.72}$$

163

[see (3.3.51)]. Here, r is the ratio of the coefficients in front of the brackets in (5.4.68) and (5.4.66), that is,

$$r = \frac{\sqrt{2}G_F m_Z^2}{s - m_Z^2 + i m_Z \Gamma_Z} \left(\frac{s}{e^2}\right) , \qquad (5.4.73)$$

where we have included the finite resonance width Γ_Z, which is important for $s \sim m_Z^2$ [see Appendix A].

Expressions similar to (5.4.71) and (5.4.72) hold for the other two non-vanishing helicity configurations. To calculate the unpolarized $e^+ e^- \to \mu^+ \mu^-$ cross section, we average over the four allowed L, R helicity combinations. We find,

$$\frac{d\sigma}{d\Omega} = \frac{\alpha^2}{4s} \left[A_0 (1 + \cos^2 \theta) + A_1 \cos \theta \right] , \qquad (5.4.74)$$

where, (assuming electron-muon universality $c_i^\mu = c_i^e \equiv c_i$)

$$
\begin{aligned}
A_0 &\equiv 1 + \tfrac{1}{2} \Re e(r)(c_L + c_R)^2 + \tfrac{1}{4}|r|^2 (c_L^2 + c_R^2)^2 \\
&= 1 + 2\Re e(r) c_V^2 + |r|^2 (c_V^2 + c_A^2)^2 , \qquad (5.4.75)
\end{aligned}
$$

$$
\begin{aligned}
A_1 &\equiv \Re e(r)(c_L - c_R)^2 + \tfrac{1}{2}|r|^2 (c_L^2 - c_R^2)^2 \\
&= 4\Re e(r) c_A^2 + 8|r|^2 c_V^2 c_A^2 . \qquad (5.4.76)
\end{aligned}
$$

The lowest-order QED result ($A_0 = 1$, $A_1 = 0$) gives a symmetric regular distribution. We now see that the weak interaction introduces a forward-backward asymmetry ($A_1 \neq 0$). Let us calculate the size of the integrated asymmetry defined by

$$A_{FB} \equiv \frac{F - B}{F + B} \qquad \text{with } F = \int_0^1 \frac{d\sigma}{d\Omega} d\Omega , \qquad B = \int_{-1}^0 \frac{d\sigma}{d\Omega} d\Omega . \qquad (5.4.77)$$

Integrating (5.4.74), we obtain for $s \ll m_Z^2$ (i.e., $|r| \ll 1$)

$$A_{FB} = \frac{A_1}{(8A_0/3)} \simeq \frac{2}{3} \Re e(r) c_A^2 \simeq -\frac{3c_A^2}{\sqrt{2}} \left(\frac{G_F s}{e^2}\right) . \qquad (5.4.78)$$

This is in agreement with the expectations of the order of magnitude estimate, $G_F s/e^2$, of (5.4.65); an asymmetry which grows quadratically with the
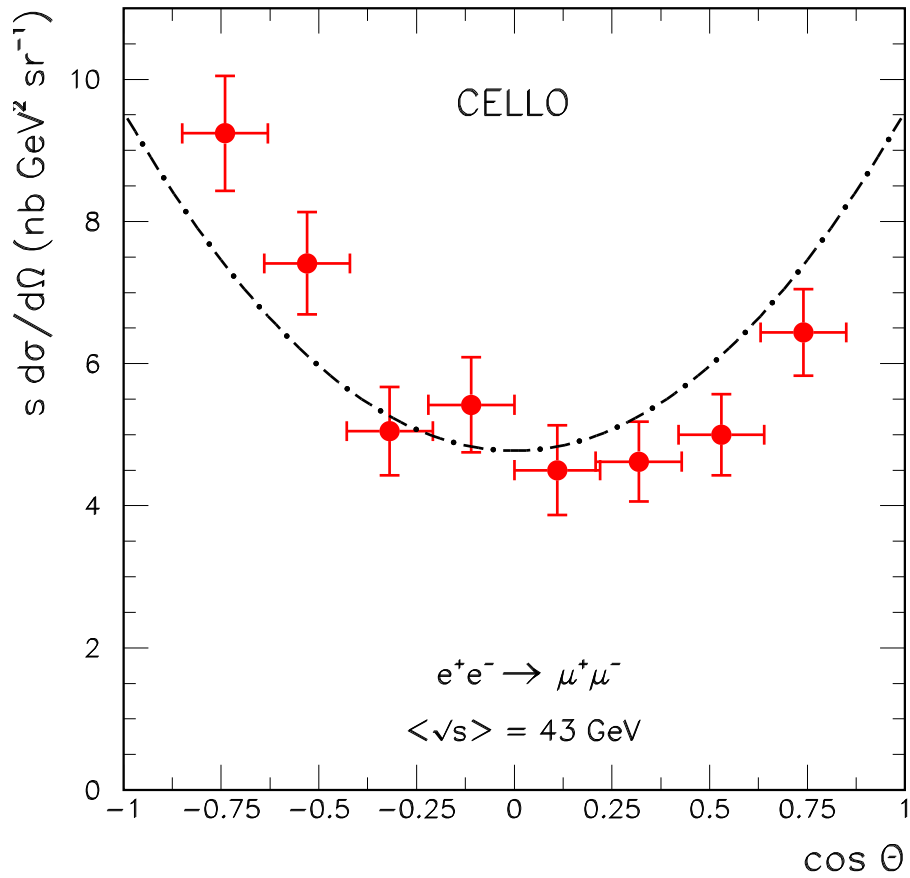
Figure 5.4: *The $e^+e^- \rightarrow \mu^+\mu^-$ angular distribution for all CELLO data $\langle\sqrt{s}\rangle = 43$ GeV. The $\cos\theta$ distribution does not follow the $1 + \cos^2\theta$ QED prediction.*

energy of the colliding e^+e^- beams (for $s \ll m_Z^2$). We may use the standard model couplings ($c_A = -\frac{1}{2}$, $c_V = -\frac{1}{2} + 2\sin^2\theta_w \simeq 0$) to compare (5.4.74) with the experimental measurements of the high-energy $e^+e^- \to \mu^+\mu^-$ angular distribution, see Fig. 5.4. Compared to the results shown in Fig. 3.8, we see in this case the larger statistics clearly reveal the data are inconsistent with QED predictions. Since $c_V \simeq 0$, these data do not, however, offer an accurate determination of $\sin^2\theta_w$.

5.4.2 The NuTeV anomaly

Neutral current processes in deep inelastic neutrino-nucleon scattering provide a direct measurement of the electroweak mixing angle. LO analytic expressions for the strength of NC to CC weak processes can be easily obtained from (5.1.13) and (5.1.28). Including only first generation quarks, for an isoscalar target ($q = \frac{u+d}{2}$), these are given by

$$
\begin{aligned}
R_\nu &= \frac{(3g_L^2 + g_R^2)xq(x,Q^2) + (3g_R^2 + g_L^2)x\bar{q}(x,Q^2)}{3xq(x,Q^2) + x\bar{q}(x,Q^2)} \\
&= g_L^2 + rg_R^2
\end{aligned}
\tag{5.4.79}
$$

and

$$
\begin{aligned}
R_{\bar{\nu}} &= \frac{(3g_R^2 + g_L^2)xq(x,Q^2) + (3g_L^2 + g_R^2)x\bar{q}(x,Q^2)}{xq(x,Q^2) + 3x\bar{q}(x,Q^2)} \\
&= g_L^2 + \frac{1}{r}g_R^2,
\end{aligned}
\tag{5.4.80}
$$

where

$$
r \equiv \frac{\sigma_{\bar{\nu}_\ell N \to \bar{\ell}X}}{\sigma_{\nu_\ell N \to \ell X}} = \frac{3x\bar{q}(x,Q^2) + xq(x,Q^2)}{3xq(x,Q^2) + x\bar{q}(x,Q^2)},
\tag{5.4.81}
$$

$$
g_L^2 \equiv (g_L^u)^2 + (g_L^d)^2 = \frac{1}{2} - \sin^2\theta_w + \frac{5}{9}\sin^4\theta_w,
\tag{5.4.82}
$$

$$
g_R^2 \equiv (g_R^u)^2 + (g_R^d)^2 = \frac{5}{9}\sin^4\theta_w,
\tag{5.4.83}
$$

and

$$
g_L^q \equiv \tfrac{1}{2}(c_V^q + c_A^q), \qquad g_R^q \equiv \tfrac{1}{2}(c_V^q - c_A^q).
\tag{5.4.84}
$$

The difference of the effective couplings $g_L^2 - g_R^2$ is subject to smaller theoretical and systematic uncertainties than the individual couplings. Indeed, under the assumptions of equal momentum carried by the u and d valence quarks in the target and of equal momentum carried by the heavy quark and antiquark seas, we obtain

$$
\begin{aligned}
R_{\mathrm{PW}} &\equiv \frac{R_\nu - r R_{\bar\nu}}{1 - r} \\
&= \frac{\sigma_{\nu N \to \nu X} - \sigma_{\bar\nu N \to \bar\nu X}}{\sigma_{\nu N \to \ell X} - \sigma_{\bar\nu N \to \bar\ell X}} \\
&= g_L^2 - g_R^2 \\
&= \tfrac{1}{2} - \sin^2 \theta_w,
\end{aligned}
\tag{5.4.85}
$$

which is seen to be independent of q and $\bar q$, and therefore of the information on the partonic structure of the nucleon.[19]

Actually, the observables R_ν^{exp}, $R_{\bar\nu}^{\mathrm{exp}}$, $R_{\mathrm{PW}}^{\mathrm{exp}}$ measured at NuTeV differ from the expressions given in (5.4.79), (5.4.80), and (5.4.85). On the theoretical side, this is because of contributions from second–generation quarks, as well as QCD and electroweak corrections. On the experimental side, this is because total cross sections can only be determined up to experimental cuts and uncertainties, such as those related to the spectrum of the neutrino beam, the contamination of the muon neutrino beam by electron neutrinos, and the efficiency of NC/CC discrimination.[20] Once all these effects are taken into account, the NuTeV data can be viewed as a measurement of the ratios between the CC and the NC squared neutrino effective couplings.

The electroweak parameter $\sin^2 \theta_w$ extracted from a single parameter fit to the NuTeV data is about 3σ at variance with the overall fit of the standard model to precision observables, a fact that is known as "the NuTeV anomaly." A 3σ effect is not neccesarily cause for excitement; of every 100 experiments you expect about one 3σ effect. Furthermore, the NuTeV measurement is

---

[19] E. A. Paschos and L. Wolfenstein, Phys. Rev. D **7**, 91 (1973).

[20] As a matter of fact, R_{PW} is more difficult to measure than the ratio of the neutral current to charged current cross sections, primarily because the neutral current scattering of ν and $\bar\nu$ yield identical observed final states which can only be distinguished through *a priori* knowledge of the initial state neutrino. Therefore, the measurement of R_{PW} requires separated neutrino antineutrino beams.

fraught with hadronic uncertainties, e.g., the $\sim 3\sigma$ result is reduced to $\sim 2\sigma$ if one incorporates the effects of the difference between the strange and anti-strange quark momentum distributions.[21] Other possible systematic effects that could contribute to bridge the gap are large isospin violation in the nucleon sea, NLO QCD effects, electroweak radiative corrections, and nuclear shadowing. A full re-analysis of the data, taking into account all these considerations and their uncertainties, is yet to see the light of day.

5.5   Radiative Corrections

As a rule, the size of radiative corrections to a given process is determined by the discrepancy between the various mass and energy scales involved. In Z-boson physics, the dominant effects arise from light charged fermions, which induced large logarithms of the form $\alpha^n \ln^m[m_Z^2/m_f^2]$ (with $m \leq n$) in the fine structure constant, and from the top quark, which generates power corrections of the orders $G_F m_t^2$, $G_F m_t^4$, $\alpha_s G_F m_t^2$, etc.

For a wide class of low-energy and Z-boson observables, the dominant effects originate entirely in the gauge boson propagators (oblique corrections) and may be parametrized conveniently in terms of four electroweak parameters: $\Delta\alpha$, $\Delta\rho$, Δr, and $\Delta\kappa$.[22] These parameters bear the following physical meanings: (i) $\Delta\alpha$ determines the running fine structure constant at the Z boson scale $\alpha(m_Z)/\alpha = (1 - \Delta\alpha)^{-1}$; (ii) $\Delta\rho$ measures the quantum corrections to the ratio of the neutral- and charged-current amplitudes at low energy; (iii) Δr embodies the non-photonic corrections to the muon lifetime; (iv) $\Delta\kappa$ controls the effective weak mixing angle, $\sin^2\bar\theta_w = \sin^2\theta_w(1 + \Delta\kappa)$, that occurs in the ratio of the $Zf\bar f$ vector and axial-vector couplings, i.e., $c_V^f/c_A^f = 1 - 4|Q_f|\sin^2\bar\theta_w$.

The ensuing discussion contains an aperçu of the theory of electroweak

[21]D. Mason *et al.*, Phys. Rev. Lett. **99**, 192001 (2007).

[22]D. A. Ross and M. J. G. Veltman, Nucl. Phys. B **95**, 135 (1975); M. J. G. Veltman, Nucl. Phys. B **123**, 89 (1977); A. Sirlin, Rev. Mod. Phys. **50**, 573 (1978) [Erratum-ibid. **50**, 905 (1978)]; Phys. Rev. D **22**, 971 (1980); S. Sarantakos, A. Sirlin and W. J. Marciano, Nucl. Phys. B **217**, 84 (1983); A. Sirlin, Phys. Lett. B **232**, 123 (1989); W. F. L. Hollik, Fortsch. Phys. **38**, 165 (1990); S. Fanchiotti and A. Sirlin, Phys. Rev. D **41**, 319 (1990); G. Degrassi, S. Fanchiotti and A. Sirlin, Nucl. Phys. B **351**, 49 (1991).

radiative corrections and its role in testing the standard model, predicting the top quark mass, constraining the Higgs boson mass, and searching for deviations that may signal the presence of new physics. Implementing such a program can be first formulated from the point of view of the experimentalist. Introducing the notation

$$\sin^2 \theta_w = s^2 = 1 - c^2 \ , \qquad m_W^2 \equiv w \ , \qquad m_Z^2 \equiv z \ , \qquad (5.5.86)$$

electroweak theory predicts at the Born level that:

$$\frac{\sigma(\nu_\mu e)}{\sigma(\bar{\nu}_\mu e)} = \frac{3 - 12s^2 + 16s^4}{1 - 4s^2 + 16s^4} \ , \qquad (5.5.87)$$

$$\frac{w}{z} = 1 - s^2 \ , \qquad (5.5.88)$$

$$\frac{\pi \alpha}{\sqrt{2}\, G_F} \frac{1}{w} = s^2 \ , \qquad (5.5.89)$$

$$\frac{\Gamma(Z \to f\bar{f})}{m_Z} = \frac{\alpha}{3} C_F \left((c_V^f)^2 + (c_A^f)^2 \right) \ , \qquad (5.5.90)$$

$$A_{\mathrm{LR}} \simeq A_\tau \simeq \left[\frac{4}{3} A_{\mathrm{FB}} \right]^{1/2} \simeq 2(1 - 4s^2) \ . \qquad (5.5.91)$$

Equations (5.5.87)–(5.5.91) represent an incomplete list of experiments capable of measuring $\sin^2 \theta_w$. Validity of the standard model requires that each measurement yields the same value of s^2: (i) the ratio (5.5.87) of ν_μ scattering on left- and right-handed electrons, which is a function of $\sin^2 \theta_w$ only; (ii) the measurement of the weak boson masses (5.5.88); (iii) the combination of m_W, α, and G_F as determined by the muon lifetime (5.5.89); (iv) the partial widths (5.5.90) of the Z into a fermion pair with vector and axial coupling c_V^f and c_A^f, and color factor $C_F = 3$ (1) for quarks (leptons); and (v) the various asymmetries (5.5.91) measured at Z-factories (see Appendix I).

The study of the quantum corrections to the measurements (5.5.87)–(5.5.91) is not straightforward. After inclusion of the $\mathcal{O}(\alpha)$ corrections, the $\sin^2 \theta_w$ values obtained from the different methods will no longer be the same because radiative corrections modify (5.5.87)–(5.5.91) in different ways. For

169

example, the diagram

$$(5.5.92)$$

modifies the t-channel Z propagator measured by (5.5.87); see also (5.1.27). It does not, however, contribute to $\mathcal{O}(\alpha)$ shifts in the W, Z masses

$$(5.5.93)$$

$$(5.5.94)$$

which yield an improved $\sin^2 \theta_w$ value via (5.5.88). There is no real mystery here. After inclusion of $\mathcal{O}(\alpha)$ contributions in Eqs. (5.5.87)–(5.5.91), they represent different definitions of $\sin^2 \theta_w$. The experimentalist has to make a choice and define the Weinberg angle to $\mathcal{O}(\alpha)$ by one of the observables (5.5.87)–(5.5.91). Subsequently, all other experiments should be reformulated in terms of the preferred "$\sin^2 \theta$." What this choice should be is no longer a matter of debate and we will define $\sin^2 \theta_w$ in terms of the physical masses of the weak bosons, *i.e.*

$$\sin^2 \theta_w \equiv 1 - \frac{m_W^2}{m_Z^2} = 0.23122(15) \, . \tag{5.5.95}$$

A most straightforward test of the theory is now obtained by fixing (5.5.95) in terms of the measured weak boson masses and verifying that its value coincides with the value of $\sin^2 \theta_w$ obtained from an analysis of ν deep-inelastic scattering data using the $\mathcal{O}(\alpha)$ prediction for (5.5.87) written in terms of (5.5.88). The same procedure can be repeated for the other measurements of θ_w, e.g., (5.5.89), (5.5.90) and (5.5.91).

The choice (5.5.95) is particularly useful in that one can estimate the radiative corrections in terms of the renormalization group, which has been previously introduced. The $\mathcal{O}(\alpha)$ corrections can be qualitatively understood in terms of the loop corrections to the vector-boson propagators (5.5.93) and (5.5.94). In a more technical sense the choice (5.5.95) is closely related to the use of the on-mass-shell (OMS) renormalization scheme, which generalizes the renormalization techniques, introduced for electrodynamics, in a straightforward way to the electroweak model.

Renormalization techniques take care of UV divergences appearing in gauge theories at the quantum level. In Sec. 3.5 we illustrated how the divergence in the photon vacuum polarization is absorbed into the Thomson charge. We pay a price: the Thomson charge is no longer predicted and the charge is renormalized to its measured value at $q^2 = 0$. Not all predictive power is lost. The screening of the charge $\alpha(q^2)$ can still be predicted and confronted with experiment. All UV divergences in QED can be absorbed in two parameters, α and m_e. It is eminently reasonable to copy this scheme for calculations in electroweak theory. The list of parameters, to be fixed by experiment, now includes

$$\alpha, \; m_W, \; m_Z, \; m_H, \; m_f, \qquad (5.5.96)$$

where m_f represents the lepton and quark masses $m_e, \ldots, m_t$. The weak mixing angle $\sin^2 \theta_w$ does not appear in the list of parameters; its value is automatically determined by m_W, m_Z via (5.5.95). For some this procedure may seem unfamiliar. Traditionally the standard model Lagrangian is determined in terms of

$$g, \; g', \; \lambda, \; \mu, \; Y_f, \qquad (5.5.97)$$

which represent the bare electroweak couplings, the parameters of the minimal Higgs potential, and the "Yukawa" couplings of the Higgs particle to

fermions. There is no mystery here. In principle any choice will do. There is, in fact, a direct translation between sets (5.5.96) and (5.5.97)

$$g^2 = e^2 \frac{z}{z-w} \ , \tag{5.5.98}$$

$$g'^2 = e^2 \frac{z}{w} \ , \tag{5.5.99}$$

$$\lambda = e^2 \frac{zm_H^2}{8w(z-w)} \ , \tag{5.5.100}$$

and

$$Y_f = e^2 \frac{zm_f^2}{2w(z-w)} \ . \tag{5.5.101}$$

As an example we will show how the relation (5.5.89) is calculated to $\mathcal{O}(\alpha)$ in terms of the weak angle θ_w defined by (5.5.88). The origin of the relation (5.5.89) is the muon's lifetime which, to leading order, is given by the diagram

$$\Gamma_\mu^{(0)} = \qquad\qquad\qquad\qquad \tag{5.5.102}$$

In Fermi theory, electromagnetic radiative corrections must be included to obtain the result to $\mathcal{O}(\alpha)$. Symbolically,

$$\Gamma_\mu^{(1)} = \frac{G_F}{\sqrt{2}} \left[1 + \text{photonic corrections} \right] , \tag{5.5.103}$$

where

$$\text{photonic corrections} = \qquad\qquad + \cdots \tag{5.5.104}$$

172

In electroweak theory, on the other hand,

$$\Gamma_\mu^{(1)} = \frac{e^2}{8s^2c^2z} \left[1 \quad + \quad \text{photonic corrections} \right.$$
$$+ \quad \text{propagator}$$
$$+ \quad \text{vertex}$$
$$\left. + \quad \text{box} \right]$$

(5.5.105)

where

propagator $=$

$+$ $\cdots$ (5.5.106)

vertex $=$ Z_0

$+ \cdots$ (5.5.107)

and

box $=$

$+ \cdots$ (5.5.108)

Equating (5.5.103) and (5.5.105) we obtain

$$G_F = \frac{\pi\alpha}{\sqrt{2}}\frac{1}{ws^2}\left(1 + \Delta r\right),$$

(5.5.109)

173

with

$$\Delta r = \Delta\alpha - \frac{c^2}{s^2}\Delta\rho + \Delta_{\rm rem}\,. \qquad (5.5.110)$$

We note that the purely photonic corrections drop out. As mentioned above, the electroweak radiative corrections are gathered in Δr. Notation (5.5.110) recognizes the fact that in the OMS scheme, vacuum polarization loops dominate this quantity. We specifically isolated the fermions which are responsible for the running of α from the muon to the Z mass,

$$\Delta\alpha = \sum_f \quad\text{(diagram)}\qquad\qquad\qquad\qquad (5.5.111)$$

as well as the third generation, heavy quark diagram

$$\Delta\rho = \quad\text{(diagram)}\qquad\qquad\qquad\qquad (5.5.112)$$

Other contributions are small in the OMS scheme and are grouped in the "remainder" $\Delta_{\rm rem}$.

Before discussing the status of measurements of Δr, we make several comments. To leading order $\Delta r = 0$ and, using (3.5.87) and (2.4.88), (5.5.109) reduces to the Born relation (5.5.89). The full order α calculation of Δr will not be presented here. We have attempted to describe the full formalism in a relatively accessible way elsewhere.[23] To the extent that $\Delta_{\rm rem}$ is small, one

---

[23]F. Halzen and D. A. Morris, Phys. Lett. B **237**, 107 (1990); Part. World **2**, 10 (1991); F. Halzen and B. A. Kniehl, Nucl. Phys. B **353**, 567 (1991); F. Halzen, P. Roy and M. L. Stong, Phys. Lett. B **277**, 503 (1992); F. Halzen, B. A. Kniehl and M. L. Stong, Z. Phys. C **58**, 119 (1993); M. C. Gonzalez-Garcia, F. Halzen and R. A. Vazquez, Phys. Lett. B **322**, 233 (1994).

can imagine summing the series

$$(5.5.113)$$

by the replacement $(1 + \Delta r) \to (1 - \Delta r)^{-1}$ in (5.5.109).

We already discussed the running of α from the small lepton masses to m_Z; see (3.5.111). The other large contribution $\Delta \rho$, which represents the loop (5.5.112), is our primary focus here. Its value is given by

$$\Delta\rho = \frac{\alpha}{4\pi}\frac{z}{\omega(z-\omega)}N_C|U_{tb}|^2\left[m_t^2 F(m_t^2, m_b^2) + m_b^2 F(m_b^2, m_t^2)\right], \quad (5.5.114)$$

with

$$F(m_1^2, m_2^2) = \int_0^1 dx\, x \ln\left[m_1^2(1-x) + m_2^2 x\right], \quad (5.5.115)$$

where $N_C = 3$ is the number of colors and U_{tb} is the CKM matrix element; $|U_{tb}|^2 \simeq 1$. The diagram has the important property that, defining $m_t = m_b + \epsilon$,

$$\Delta\rho \simeq \frac{G_F}{3\pi^2}\,\epsilon\,. \quad (5.5.116)$$

So in QED, where only equal mass fermions and antifermions appear in neutral photon loops, $\epsilon = 0$ and diagrams of this type are not possible. They are, in fact, prohibited in QED by general arguments. This can be seen by rewriting (5.5.114) and (5.5.115) in the form

$$\begin{aligned}\Delta\rho &= \frac{G_F}{4\pi}\left[m_t^2 + m_b^2 - \frac{2m_b^2 m_t^2}{m_t^2 - m_b^2}\ln\frac{m_t^2}{m_b^2}\right] \\ &\simeq \frac{G_F}{4\pi}m_t^2 \simeq \frac{3\alpha}{16\pi}\frac{1}{c^2 s^2}\frac{m_t^2}{z}\,. \end{aligned} \quad (5.5.117)$$

The appearance of a m_t^2/z contribution to an observable is far from routine. It is indeed forbidden in QED and QCD where virtual particle effects are suppressed by "inverse" powers of their masses; (5.5.116) embodies this requirement because $\epsilon = 0$ for photon loops. Conversely, the appearance of an m_t^2/z term is a characteristic feature of the electroweak theory. $\Delta\rho$ provides us with a most fundamental probe of electroweak theory short of discovering the Higgs boson.

We are now ready to illustrate that $\Delta\rho \neq 0$ and is, in fact, consistent with the standard model value (5.5.117) calculated using the experimental value of the mass of the top quark. We first determine the experimental value of Δr from (5.5.109). Using (5.1.24) and (5.4.64):

$$\Delta r_{\text{exp}} \simeq 1 - (37.281 \text{ GeV})^2 \frac{z}{\omega(z-\omega)} \simeq 0.035 . \qquad (5.5.118)$$

We next recall (3.5.111):

$$\Delta\alpha \simeq 1 - \frac{\alpha(0)}{\alpha(m_Z^2)} \simeq 1 - \frac{128}{137} \simeq 0.066 . \qquad (5.5.119)$$

The crucial point is that $\Delta r_{\text{exp}} \neq \Delta\alpha$; cf. (5.5.118) and (5.5.119). The $\mathcal{O}(\alpha)$ standard model relation (5.5.110) requires a non-vanishing value of $\Delta\rho$. Using (5.5.117), we obtain that $\Delta\rho = 0.0086$ and (5.5.110) yields

$$(\Delta r)_{\text{calculated}} = \Delta\alpha - \frac{c^2}{s^2}\Delta\rho = 0.037 , \qquad (5.5.120)$$

in agreement with the experimental value (5.5.118). We leave it as an exercise to insert errors into the calculation and show that our argument survives a straightforward statistical analysis.

The Higgs particle makes a contribution to Δr:

$$\Delta h = \quad \text{[diagram: } W \text{ boson loop with } H \text{ propagator]} \quad = \frac{11\alpha}{48\pi}\frac{1}{c^2}\ln\frac{m_H^2}{z} . \qquad (5.5.121)$$

From (5.3.59) we obtain that $\Delta h < 0.0006$, a contribution too small to be sensed by the simple analysis presented above. The quantity Δr is in principle sensitive to the Higgs mass. More sophisticated analyses which include the dominant $\mathcal{O}(\alpha^2)$ corrections are now yielding weak, but definite, constraints on the value of m_H.

Other measurements support the electroweak model's radiative correction associated with the $t\bar{b}$ loop $\Delta\rho$. Recall that charged weak currents couple with strength G_F, while neutral currents couple as ρG_F; see (5.1.10) and (5.1.23).

The neutral current decay of Z into neutrinos is therefore proportional to ρG_F:

$$\Gamma(Z \to \nu\bar{\nu}) = (\rho G_F)\frac{3\sqrt{2}}{24\pi}m_Z^3 \,. \qquad (5.5.122)$$

The measured value of 499.0 ± 1.5 MeV is larger than the value calculated from the above equation which is 497.9, although the statistics are not overwhelming. Nevertheless, the loop contribution (5.5.117) increases ρ to a value $1 + \Delta\rho = 1.0086$, bridging the gap. In the end a professional approach follows the technique we previously mentioned: generalize the theoretical expressions for the observables (5.5.87)–(5.5.91) to 1-loop and show that all measurements yield a common value of $\sin^2\theta_w$.

The radiative corrections predicted by the standard model have successfully confronted experiment. The program is however far from complete. It will not have escaped the reader's attention that the precision of the confrontation between theory and experiment is limited by the relatively large errors on the measurements of m_W and m_t. The problem can be quantified by rewriting (5.5.118) and (5.5.110) as

$$\Delta r_{\text{exp}} = F(m_W, m_t, m_H)\,, \qquad (5.5.123)$$

using (5.5.117), (5.5.119) and (5.5.121). Using the Z-pole measurements of SLD and LEP1, electroweak radiative corrections are evaluated to predict the masses of the top quark and the W-boson. The resulting 68% CL contour curve in the (m_t, m_W) plane is shown in Fig. 5.5. Also shown is the contour curve corresponding to the direct measurements of both quantities at the Tevatron and LEP2. The two contours overlap, successfully testing the standard model at the level of electroweak radiative corrections. The diagonal band in the figure shows the constraint between the two masses within the standard model, which depends on the unknown mass of the Higgs boson, and to a small extent also on the hadronic vacuum polarization (small arrow labeled $\Delta\alpha$). Both the direct and the indirect contour curves prefer a low value for the Higgs mass. The combined LEP2 and Tevatron data (solid line) prefers a region outside the diagonal band. Confirmation of the standard model will, of course, require the detection of the Higgs particle within this band.

Failure to do so will undoubtedly raise the question of the precision of the
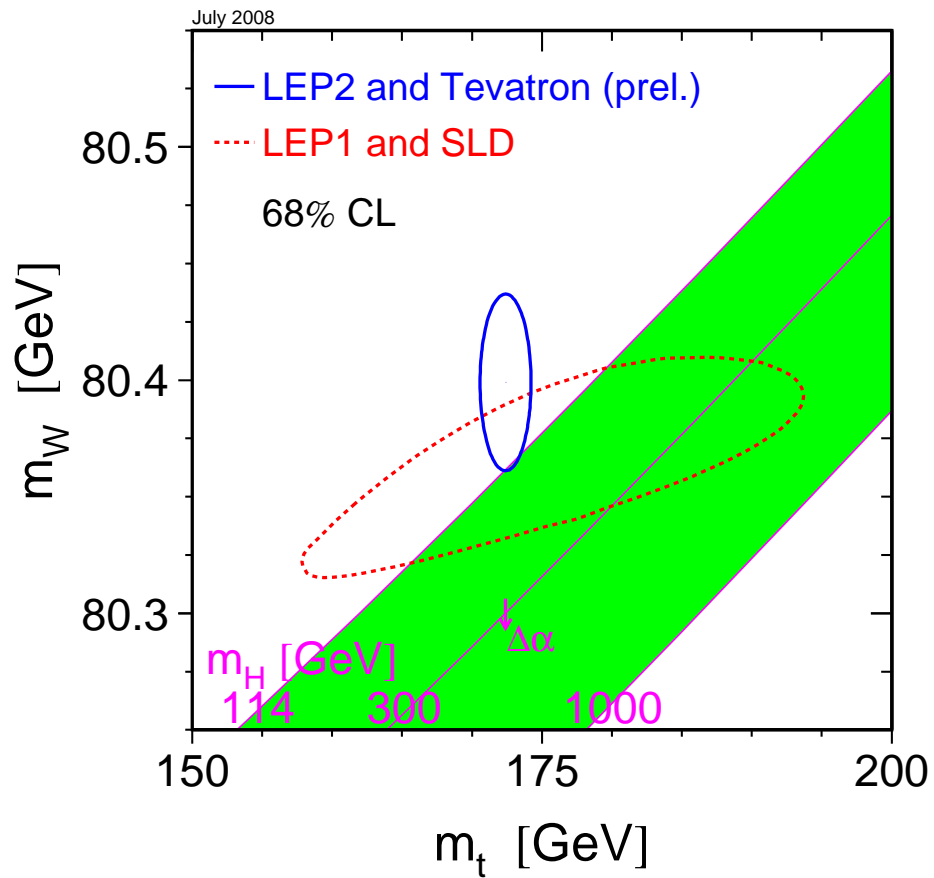
Figure 5.5: *Contour curves of 68% CL in the (m_t, m_W) plane for direct measurements and the indirect determinations. The band shows the correlation between m_W and m_t expected in the standard model.*

computations. State of the art calculations include all dominant 2-loop effects. This should be sufficient to confront Higgs vacuum polarization effects such as (5.5.121) with experiment. Some doubts remain about the accuracy of the e^+e^- data in the vicinity of charm thresholds which are used to evaluate the charm quark contribution to the running of α; see (5.5.111). The evaluation of the threshold contribution of the $t\bar{t}$ loops to the same integral is not totally understood. These most likely represent the true limitation of the calculation but neither problem is likely to preclude the indirect measurement of m_H.

5.6   Lepton Flavor Mixing

5.6.1   Neutrino Oscillations

At present, convincing experimental evidence exists for (time dependent) oscillatory transitions $\nu_\alpha \rightleftharpoons \nu_\beta$ between the different neutrino flavors. The simplest and most direct interpretation of the atmospheric data is that of muon neutrino oscillations.[24] The evidence of atmospheric ν_μ disappearing is now at $> 15\sigma$, most likely converting to ν_τ. The angular distribution of contained events shows that for $E_\nu \sim 1$ GeV, the deficit comes mainly from $L_{\mathrm{atm}} \sim 10^2 - 10^4$ km. These results have been confirmed by the KEK-to-Kamioka (K2K) experiment which observes the disappearance of accelerator ν_μ's at a distance of 250 km and finds a distortion of their energy spectrum with a CL of $2.5 - 4\sigma$.[25] Data collected by the Sudbury Neutrino Observatory (SNO) in conjuction with data from Super-Kamiokande (SK) show that solar $\nu_e's$ convert to ν_μ or ν_τ with CL of more than 7σ.[26] The KamLAND

[24]Y. Fukuda *et al.* [Super-Kamiokande Collaboration], Phys. Lett. B **433**, 9 (1998); Phys. Rev. Lett. **81**, 1562 (1998); S. Fukuda *et al.* [Super-Kamiokande Collaboration], Phys. Rev. Lett. **85**, 3999 (2000); Y. Ashie *et al.* [Super-Kamiokande Collaboration], Phys. Rev. D **71**, 112005 (2005).

[25]S. H. Ahn *et al.* [K2K Collaboration], Phys. Lett. B **511**, 178 (2001); Phys. Rev. Lett. **90**, 041801 (2003);Phys. Rev. Lett. **93**, 051801 (2004).

[26]Y. Fukuda *et al.* [Super-Kamiokande Collaboration], Phys. Rev. Lett. **81**, 1158 (1998) [Erratum-ibid. **81**, 4279 (1998)]; Phys. Rev. Lett. **82**, 1810 (1999); S. Fukuda *et al.* [Super-Kamiokande Collaboration], Phys. Rev. Lett. **86**, 5656 (2001); Phys. Lett. B **539**, 179

Collaboration has measured the flux of $\overline{\nu}_e$ from distant reactors and find that $\overline{\nu}_e$'s disappear over distances of about 180 km.[27] All these data suggest that the neutrino eigenstates that travel through space are not the flavor states that we measured through the weak force, but rather mass eigenstates.[28]

The flavor eigenstates $|\nu_\alpha\rangle$ and the mass eigenstates $|\nu_i\rangle$ are related by a unitary transformation U (i.e., mixing matrix)

$$|\nu_\alpha\rangle = \sum_i U_{\alpha i}|\nu_i\rangle \Leftrightarrow |\nu_i\rangle = \sum_\alpha (U^\dagger)_{i\alpha}|\nu_\alpha\rangle = \sum_\alpha U^*_{\alpha i}|\nu_\alpha\rangle\,, \qquad (5.6.124)$$

with

$$U^\dagger U = \mathbb{1}, \text{ i.e., } \sum_i U_{\alpha i}U^*_{\beta i} = \delta_{\alpha\beta} \quad \text{and} \quad \sum_i U_{\alpha i}U^*_{\alpha j} = \delta_{ij}\,. \qquad (5.6.125)$$

For antineutrinos one has to replace $U_{\alpha i}$ by $U^*_{\alpha i}$, i.e.,

$$|\bar{\nu}_\alpha\rangle = \sum_i U^*_{\alpha i}|\bar{\nu}_i\rangle\,. \qquad (5.6.126)$$

The number of parameters of an $n \times n$ unitary matrix is n^2. It is easy to see that $2n - 1$ relative phases of the $2n$ neutrino states can be redefined such that $(n-1)^2$ independent parameters are left. For these it is convenient to take the $\frac{1}{2}n(n-1)$ "weak mixing angles" of an n-dimensional rotation and $\frac{1}{2}(n-1)(n-2)$ "CP-violating phases."

Being eigenstates of the mass matrix, the states $|\nu_i\rangle$ are stationary states, i.e., they have the time dependence

$$|\nu_i(t)\rangle = e^{-iE_i t}|\nu_i\rangle \qquad (5.6.127)$$

with

$$E_i = \sqrt{p^2 + m_i^2} \approx p + \frac{m_i^2}{2p} \approx E + \frac{m_i^2}{2E}\,, \qquad (5.6.128)$$

(2002); S. N. Ahmed *et al.* [SNO Collaboration], Phys. Rev. Lett. **92**, 181301 (2004).

[27]T. Araki *et al.* [KamLAND Collaboration], Phys. Rev. Lett. **94**, 081801 (2005).

[28]Contrariwise, charged leptons are states of definite mass and hence cannot undergo oscillations. S. Pakvasa, Lett. Nuovo Cim. **31**, 497 (1981); E. K. Akhmedov, JHEP **0709**, 116 (2007).

where $E \approx p$ is the total neutrino energy. (Here it is assumed that neutrinos are stable.) Thus a pure flavor state $|\nu_\alpha\rangle = \sum_i U_{\alpha i}|\nu_i\rangle$, present at $t = 0$, develops with time into the state

$$|\nu(t)\rangle = \sum_i U_{\alpha i}e^{-iE_i t}|\nu_i\rangle = \sum_{i,\beta} U_{\alpha i}U^*_{\beta i}e^{-iE_i t}|\nu_\beta\rangle \,. \qquad (5.6.129)$$

The time dependent transition amplitude for the transition from flavor ν_α to flavor ν_β therefore is

$$\begin{aligned}
\mathfrak{A}(\nu_\alpha \to \nu_\beta) \equiv \langle \nu_\beta|\nu(t)\rangle &= \sum_i U_{\alpha i}U^*_{\beta i}e^{-iE_i t} \\
&= \sum_{i,j} U_{\alpha i}\delta_{ij}e^{-iE_i t}(U^\dagger)_{j\beta} \\
&= (UDU^\dagger)_{\alpha\beta} \,, \qquad (5.6.130)
\end{aligned}$$

with $D_{ij} = \delta_{ij}e^{-iE_i t}$ (diagonal matrix). An equivalent expression for the transition amplitude is obtained by inserting (5.6.128) into (5.6.130) and extracting an overall phase factor e^{-iEt}

$$\begin{aligned}
\mathfrak{A}(\nu_\alpha \to \nu_\beta, t) &= \sum_i U_{\alpha i}U^*_{\beta i}\, e^{-\frac{im_i^2 t}{2E}} \\
&= \sum_i U_{\alpha i}U^*_{\beta i}\, e^{-\frac{im_i^2 L}{2E}} \,, \qquad (5.6.131)
\end{aligned}$$

where $L = ct$ (recall c=1) is the distance of the detector, in which ν_β is observed, from the ν_α source. For an arbitrary chosen fixed j the transition amplitude becomes

$$\begin{aligned}
\widetilde{\mathfrak{A}}(\nu_\alpha \to \nu_\beta, t) &= e^{iE_j t}\mathfrak{A}(\nu_\alpha \to \nu_\beta, t) \\
&= \sum_i U_{\alpha i}U^*_{\beta i}\, e^{-i(E_i - E_j)t} \\
&= \delta_{\alpha\beta} + \sum_i U_{\alpha i}U^*_{\beta i}\left[e^{-i(E_i - E_j)t} - 1\right] \\
&= \delta_{\alpha\beta} + \sum_{i \neq j} U_{\alpha i}U^*_{\beta i}\left[e^{-i\Delta_{ij}} - 1\right] \,, \qquad (5.6.132)
\end{aligned}$$

with

$$\Delta_{ij} = (E_i - E_j) = 1.27\,\frac{\delta m_{ij}^2 L}{E} \qquad (5.6.133)$$

181

when L is measured in km, E in GeV and $\delta m_{ij}^2 = m_i^2 - m_j^2$ in eV^2. In (5.6.132) the unitarity relation (5.6.125) has been used. The transition amplitudes are thus given by the $(n-1)^2$ independent parameters of the unitary matrix (which determines the sizes of the oscillations) and the $n-1$ mass square differences (which determine the frequencies of the oscillations), i.e., by $n(n-1)$ real parameters. If CP is conserved in neutrino oscillations, all CP-violating phases vanish and the $U_{\alpha i}$ are real, i.e., U is an orthogonal matrix ($U^{-1} = U^T$) with $\frac{1}{2}n(n-1)$ parameters. The number of parameters for the transition amplitude is then $\frac{1}{2}(n-1)(n+2)$.

Using (5.6.126) we obtain the amplitudes for the transitions between antineutrinos

$$\mathfrak{A}(\bar\nu_\alpha \to \bar\nu_\beta; t) = \sum_i U_{\alpha i}^* U_{\beta i} e^{-iE_i t}. \qquad (5.6.134)$$

Therefore, comparing (5.6.130) and (5.6.134), the following relation holds for transformations between neutrinos and antineutrinos, which also follows directly from the CPT theorem: C changes particle into antiparticle, P provides the necessary flip from left-handed neutrino to right-handed antineutrino and vice versa, and T reverses the arrow indicating the transition

$$\mathfrak{A}(\bar\nu_\alpha \to \bar\nu_\beta) = \mathfrak{A}(\nu_\beta \to \nu_\alpha) \neq \mathfrak{A}(\nu_\alpha \to \nu_\beta). \qquad (5.6.135)$$

If CP is conserved, $U_{\alpha i}$ and $U_{\beta i}$ are real in (5.6.130) and (5.6.134). That is, if time reversal invariance holds, one has

$$\mathfrak{A}(\bar\nu_\alpha \to \bar\nu_\beta) = \mathfrak{A}(\nu_\alpha \to \nu_\beta) = \mathfrak{A}(\bar\nu_\beta \to \bar\nu_\alpha) = \mathfrak{A}(\nu_\beta \to \nu_\alpha). \qquad (5.6.136)$$

Therefore, CP violation can be searched for by e.g., comparing the oscillations $\nu_\alpha \to \nu_\beta$ and $\nu_\beta \to \nu_\alpha$.[29]

The transition probabilities are obtained by squaring the moduli of the amplitudes (5.6.130)

$$\begin{aligned}
P_{\nu_\alpha \to \nu_\beta} &= \left| \sum_i U_{\alpha i} U_{\beta i}^* e^{-iE_i t} \right|^2 \\
&= \delta_{\alpha\beta} - 4 \sum_{i>j} \mathfrak{Re}\,(U_{\alpha i}^* U_{\beta i} U_{\alpha j} U_{\beta j}^*) \sin^2 \Delta_{ij} \\
&\quad + 2 \sum_{i>j} \mathfrak{Im}\,(U_{\alpha i}^* U_{\beta i} U_{\alpha j} U_{\beta j}^*) \sin 2\Delta_{ij}. \qquad (5.6.137)
\end{aligned}$$

[29]V. D. Barger, K. Whisnant and R. J. N. Phillips, Phys. Rev. Lett. **45**, 2084 (1980).

In the standard treatment of neutrino oscillations, the flavor eigenstates $|\nu_\alpha\rangle$ ($\alpha = e, \mu, \tau$) are expanded in terms of 3 mass eigenstates $|\nu_i\rangle$ ($i = 1, 2, 3$). In such a case, atmospheric neutrino data suggest that the corresponding oscillation phase must be maximal, $\Delta_{\text{atm}} \sim 1$, which requires $\delta m^2_{\text{atm}} \sim 10^{-4} - 10^{-2}$ eV^2. Moreover, assuming that all upgoing ν_μ's which would yield multi-GeV events oscillate into a different flavor while none of the downgoing ones do, the observed up-down asymmetry leads to a mixing angle very close to maximal, $\sin^2 2\theta_{\text{atm}} > 0.85$. The combined analysis of atmospheric neutrinos with K2K leads to a best fit-point and 1σ ranges, $\delta m^2_{\text{atm}} = 2.2^{+0.6}_{-0.4} \times 10^{-3}$ eV^2 and $\tan^2 \theta_{\text{atm}} = 1^{+0.35}_{-0.26}$. On the other hand, reactor data suggest $|U_{e3}|^2 \ll 1$.[30] This twin happenstance, $\theta_{\text{atm}} \simeq 45°$ and $\Re(U_{e3}) \simeq 0$, is sufficient to generate "ν_μ-ν_τ interchange symmetry."

To simplify the discussion hereafter we use the fact that $|U_{e3}|^2$ is nearly zero to ignore possible CP violation and assume that the elements of U are real. With this in mind, we can define a mass basis as follows,

$$|\nu_1\rangle = \sin\theta_\odot |\nu^\star\rangle + \cos\theta_\odot |\nu_e\rangle \ , \qquad (5.6.138)$$

$$|\nu_2\rangle = \cos\theta_\odot |\nu^\star\rangle - \sin\theta_\odot |\nu_e\rangle \ , \qquad (5.6.139)$$

and

$$|\nu_3\rangle = \frac{1}{\sqrt{2}}(|\nu_\mu\rangle + |\nu_\tau\rangle) \ , \qquad (5.6.140)$$

where $\theta_\odot$ is the solar mixing angle and

$$|\nu^\star\rangle = \frac{1}{\sqrt{2}}(|\nu_\mu\rangle - |\nu_\tau\rangle) \qquad (5.6.141)$$

is the eigenstate orthogonal to $|\nu_3\rangle$. Inversion of the neutrino mass-to-flavor mixing matrix leads to

$$|\nu_e\rangle = \cos\theta_\odot |\nu_1\rangle - \sin\theta_\odot |\nu_2\rangle \qquad (5.6.142)$$

and

$$|\nu^\star\rangle = \sin\theta_\odot |\nu_1\rangle + \cos\theta_\odot |\nu_2\rangle \ . \qquad (5.6.143)$$

---

[30]M. Apollonio *et al.* [CHOOZ Collaboration], Phys. Lett. B **466**, 415 (1999); S. M. Bilenky, D. Nicolo and S. T. Petcov, Phys. Lett. B **538**, 77 (2002).

Finally, by adding Eqs. (5.6.140) and (5.6.141) one obtains the ν_μ flavor eigenstate,

$$|\nu_\mu\rangle = \frac{1}{\sqrt{2}} \left[|\nu_3\rangle + \sin\theta_\odot|\nu_1\rangle + \cos\theta_\odot|\nu_2\rangle\right] \ , \qquad (5.6.144)$$

and by substracting these same equations the ν_τ eigenstate. The combined analysis of Solar neutrino data and KamLAND data are consistent at the 3σ CL, with best-fit point and 1σ ranges: $\delta m_\odot^2 = 8.2^{+0.3}_{-0.3} \times 10^{-5}$ eV^2 and $\tan^2\theta_\odot = 0.39^{+0.05}_{-0.04}$. [31]

For $\Delta_{ij} \gg 1$ (as would be the case for far-out neutrinos propagating over cosmic distances), the phases will be erased by uncertainties in L and E. Consequently, averaging over $\sin^2\Delta_{ij}$ in (5.6.137) we obtain

$$P(\nu_\alpha \to \nu_\beta) = \delta_{\alpha\beta} - 2\sum_{i>j} U_{\alpha i}\, U_{\beta i}\, U_{\alpha j}\, U_{\beta j}\,. \qquad (5.6.145)$$

Now, using $2\sum_{1>j} = \sum_{i,j} - \sum_{i=j}$, Eq. (5.6.145) can be re-written as

$$
\begin{aligned}
P(\nu_\alpha \to \nu_\beta) &= \delta_{\alpha\beta} - \sum_{i,j} U_{\alpha i}\, U_{\beta i}\, U_{\alpha j}\, U_{\beta j} + \sum_i U_{\alpha i}\, U_{\beta i}\, U_{\alpha i}\, U_{\beta i} \\
&= \delta_{\alpha\beta} - \left(\sum_i U_{\alpha i} U_{\beta i}\right)^2 + \sum_i U_{\alpha i}^2 U_{\beta i}^2\,. \qquad (5.6.146)
\end{aligned}
$$

Since $\delta_{\alpha\beta} = \delta_{\alpha\beta}^2$, the first and second terms in Eq. (5.6.146) cancel each other, yielding

$$P(\nu_\alpha \to \nu_\beta) = \sum_i U_{\alpha i}^2\, U_{\beta i}^2 \ . \qquad (5.6.147)$$

The probabilities for flavor oscillation are then

$$P(\nu_\mu \to \nu_\mu) = P(\nu_\mu \to \nu_\tau) = \frac{1}{4}\left(\cos^4\theta_\odot + \sin^4\theta_\odot + 1\right)\,, \qquad (5.6.148)$$

$$P(\nu_\mu \to \nu_e) = P(\nu_e \to \nu_\mu) = P(\nu_e \to \nu_\tau) = \sin^2\theta_\odot\,\cos^2\theta_\odot\,, \qquad (5.6.149)$$

and

$$P(\nu_e \to \nu_e) = \cos^4\theta_\odot + \sin^4\theta_\odot \ . \qquad (5.6.150)$$

---

[31] For a general discussion of the mixing parameters see e.g., M. C. Gonzalez-Garcia and M. Maltoni, Phys. Rept. **460**, 1 (2008).

Now, let the ratios of neutrino flavors at production in the cosmic sources be written as $w_e : w_\mu : w_\tau$ with $\sum_\alpha w_\alpha = 1$, so that the relative fluxes of each mass eigenstate are given by $w_j = \sum_\alpha \omega_\alpha \, U_{\alpha j}^2$. From our previous discussion, we conclude that the probability of measuring on Earth a flavor α is given by

$$P_{\nu_\alpha \text{ detected}} = \sum_j U_{\alpha j}^2 \sum_\beta w_\beta \, U_{\beta j}^2 \; . \qquad (5.6.151)$$

Straightforward calculation shows that any initial flavor ratio that contains $w_e = 1/3$ will arrive at Earth with equipartition on the three flavors. Since neutrinos from astrophysical sources are expected to arise dominantly from the decay of charged pions (and kaons) and their muon daughters, their initial flavor ratios of nearly $1 : 2 : 0$ should arrive at Earth democratically distributed. So there is a fairly robust prediction of 1:1:1 flavor ratios for measurements of cosmic neutrinos. In contrast, the prediction for a pure $\bar\nu_e$ source, originating via neutron β-decay, has different implications for the flavor ratios: $w_e = 1$ yields Earthly ratios $\sim 5 : 2 : 2$.[32] Such a unique ratio would appear above the 1:1:1 background in the direction of the neutron source. Such a beam from the heavens could be used to study the neutrino oscillation parameters by comparing flavor ratios in the direction of the beam and the rest of the sky. With the growth of neutrino observatories, flavor identification of cosmic neutrinos on a statistical basis becomes possible, opening up a window for discoveries in particle physics not otherwise accessible to experiment.[33]

Altogether, neutrinos are massive and therefore the standard model needs to be extended as we discuss next.

5.6.2   How to kill a vampire

In the standard model masses arise from Yukawa interactions, which couple a right-handed fermion with its left-handed doublet and the Higgs field, after spontaneous symmetry breaking [see Sec. 2.4]. However, because no right-handed neutrinos exist in the standard model, Yukawa interactions (2.4.106)

[32]L. A. Anchordoqui, H. Goldberg, F. Halzen and T. J. Weiler, Phys. Lett. B **593**, 42 (2004).

[33]F. Halzen, Science **315**, 66 (2007).

leave the neutrinos massless. One may wonder if neutrino masses could arise from loop corrections or even by non-perturbative effects, but this cannot happen because any neutrino mass term that can be constructed with standard model fields would violate the total lepton symmetry. Therefore, in order to introduce a neutrino mass term we must either extend the particle content, or else abandon gauge invariance and/or renormalizability. In this section we illustrate different types of neutrino mass terms, assuming we keep the gauge symmetry and we introduce an arbitrary number m of additional right-handed neutrino states (singlets under hypercharge) $\nu_R(1, 1)_0$.

With the particle contents of the standard model and the addition of an arbitrary m number of right-handed neutrinos one can construct two types of mass terms that arise from gauge invariant renormalizable operators

$$-\mathscr{L}_{M_\nu} = \sum_{\alpha=e,\mu,\tau} \sum_{i=1}^{m} M_D{}^{i\alpha} \, \bar{\nu}_{Ri} \, \nu_{L\alpha} + \frac{1}{2} M_N{}^{ij} \, \bar{\nu}_{Ri} \, \nu_{Rj}^c + \text{h.c.} \,, \qquad (5.6.152)$$

where ν^c indicates a charge conjugated field ($\nu^c = C\bar{\nu}^T$), M_D is a complex $m \times 3$ matrix, and M_N is a symmetric matrix of dimension $m \times m$.

Forcing $M_N = 0$ leads to a Dirac mass term, which is generated after spontaneous electroweak symmetry breaking from Yukawa interactions

$$Y_\nu{}^{i\alpha} \, \bar{\nu}_{Ri} \, \bar{\phi}^\dagger \, L_{L\alpha} \Rightarrow M_D{}^{i\alpha} = Y_\nu{}^{i\alpha} \frac{v}{\sqrt{2}} \,, \qquad (5.6.153)$$

similarly to the charged fermion masses. Such a mass term conserves total lepton number, but it breaks the lepton flavor number symmetries. For $m = 3$ we can identify the hypercharge singlets with the right-handed component of four-spinor neutrino fields. Since the matrix Y is, in general, a complex 3×3 matrix, the flavor neutrino fields ν_e, ν_μ, and ν_τ do not have a definite mass. The massive neutrino fields are obtained via diagonalization of $\mathscr{L}_{M_\nu}$. This is achieved through the transformations

$$\nu_{L\alpha} = \sum_{k=1}^{3} V_\nu{}^{\alpha k} \nu_{Lk}, \qquad \nu_{Rj} = \sum_{k=1}^{3} V_{\nu R}{}^{jk} \nu_{Rk} \qquad (5.6.154)$$

with two 3×3 unitary matrices, V_ν and $V_{\nu R}$ which perform the biunitary diagonalization

$$V_{\nu R}^\dagger M_D V_\nu = \frac{v}{\sqrt{2}} \left(V_{\nu R}^\dagger Y_\nu V_\nu \right)^{jk} = m_k \delta_{jk} \,, \qquad (5.6.155)$$
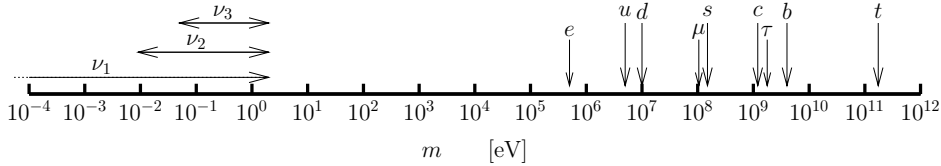
Figure 5.6: *Order of magnitude of the masses of quarks and leptons.*

with real positive masses m_k. The resulting diagonal mass term can be written as

$$-\mathscr{L}_{M_\nu} = \sum_{k=1}^{3} m_k \bar{\nu}_{Rk} \nu_{Lk} + \text{h.c.} = \sum_{k=1}^{3} m_k \overline{\nu}_k \nu_k \qquad (5.6.156)$$

where $\nu_k = \nu_{Lk} + \nu_{Rk}$ are the Dirac fields of massive neutrinos.

As shown in Fig. 5.6, neutrino masses are much lighter than the corresponding charged fermion masses. Therefore, to get reasonable neutrino masses (below the eV range) the Yukawa couplings would have to be exceedingly small: $Y_\nu{}^{i\alpha} < 10^{-11}$. (For charged fermions, the Yukawa couplings range from $Y_t \simeq 1$ for the top quark down to $Y_e \simeq 10^{-5}$ for the electron). Dirac neutrino masses in the experimentally preferred range can be generated if right-handed neutrinos are not complete singlets of the low energy gauge group, but they are charged under additional $U(1)$ gauge symmetries broken at the TeV-scale.[34] Such additional $U(1)$ symmetries are theoretically well motivated, as they represent the simplest augmentation of the standard model, and carry a large amount of interesting phenomenology. For example, the gauge-extended $U(1)_C \times SU(2)_L \times U(1)_R \times U(1)_L$ model has the attractive property of elevating the two major global symmetries of the standard model, B and L, to local gauge symmetries; but of course neutrinos are able to oscillate in the standard way since it is only the diagonal lepton number, $L = L_e + L_\mu + L_\tau$, which is an exact symmetry.[35]

If $M_N \neq 0$, neutrino masses receive an important contribution from the Majorana mass term. Such a term is different from the Dirac mass term in many important aspects. It is a singlet of the standard model gauge group.

[34] D. A. Demir, L. L. Everett and P. Langacker, Phys. Rev. Lett. **100**, 091804 (2008).

[35] L. A. Anchordoqui, I. Antoniadis, H. Goldberg, X. Huang, D. Lust and T. R. Taylor, arXiv:1107.4309.

Therefore, it can appear as a bare mass term. Furthermore, since it involves two neutrino fields, it breaks lepton number by two units. More generally, such a term is allowed only if the neutrinos carry no additive conserved charge. This is the reason that such terms are not allowed for any charged fermions which, by definition, carry $U(1)_{\text{EM}}$ charges.

In general (5.6.152) can be rewritten as

$$-\mathscr{L}_{M_\nu} = \frac{1}{2}\,\overline{\vec{\nu}^c}\,M_\nu\,\vec{\nu} + \text{h.c.},\qquad(5.6.157)$$

where

$$M_\nu = \begin{pmatrix} 0 & M_D^T \\ M_D & M_N \end{pmatrix},\qquad(5.6.158)$$

and $\vec{\nu} = (\vec{\nu}_L,\,\vec{\nu}_R^c)^T$ is a $(3+m)$-dimensional vector. The matrix M_ν is complex and symmetric. It can be diagonalized by a unitary matrix of dimension $(3+m)$, V_ν, so that

$$V_\nu{}^T M_\nu V_\nu = \text{diag}(m_1, m_2, \ldots, m_{3+m})\,.\qquad(5.6.159)$$

In terms of the resulting $3+m$ mass eigenstates, $\vec{\nu}_{\text{mass}} = (V_\nu)^\dagger\,\vec{\nu}$, (5.6.157) can be rewritten as

$$-\mathscr{L}_{M_\nu} = \frac{1}{2}\sum_{k=1}^{3+m} m_k \left(\bar{\nu}_{\text{mass},k}^c \nu_{\text{mass},k} + \bar{\nu}_{\text{mass},k}\nu_{\text{mass},k}^c\right) = \frac{1}{2}\sum_{k=1}^{3+m} m_k \bar{\nu}_{Mk}\nu_{Mk}\,,$$
$$(5.6.160)$$

where
$$\nu_{Mk} = \nu_{\text{mass},k} + \nu_{\text{mass},k}^c = (V_\nu^\dagger\,\vec{\nu})_k + (V_\nu^\dagger\,\vec{\nu})_k^c\,,\qquad(5.6.161)$$

which obey the Majorana condition, $\nu_M = \nu_M^c$, and are referred to as Majorana neutrinos.[36] Notice that this condition implies that there is only one field which describes both neutrino and antineutrino states. Thus a Majorana neutrino can be described by a two-component spinor unlike the charged fermions, which are Dirac particles, and are represented by four-component spinors.

We have seen that the order of magnitude of the elements of the Dirac mass matrix M_D is expected to be smaller than v, because Yukawa couplings

---

[36] E. Majorana, Nuovo Cim. **14**, 171 (1937).

are expected to be unnaturally small. In general, since a Dirac mass term is forbidden by the symmetries of the standard model, it can arise only as a consequence of symmetry breaking and hence Dirac mass terms are proportional to the symmetry-breaking scale. This fact is often summarized by saying that Dirac masses are *protected* by the symmetries of the standard model. On the other hand, since a Majorana mass term is a standard model singlet, the elements of the Majorana mass matrix M_N are not protected by the standard model symmetries. It is plausible that the Majorana mass term is generated by new physics beyond the standard model and the right-handed chiral neutrino fields ν_R belong to nontrivial multiplets of the symmetries of the high energy theory. In this case, the elements of the mass matrix M_N are protected by the symmetries of the high energy theory and their order of magnitude corresponds to the breaking scale of these symmetries, which could be much higher than the scale of electroweak symmetry breaking $\langle \phi \rangle$. The mass matrix can be diagonalized by blocks, up to corrections of order $(M_N^{-1} M_D)$

$$V_\nu{}^T M_\nu V_\nu \simeq \begin{pmatrix} M_l & 0 \\ 0 & M_h \end{pmatrix} \qquad (5.6.162)$$

with

$$V_\nu \simeq \begin{bmatrix} \left(1 - \tfrac{1}{2} M_D^\dagger M_N^{*\,-1} M_N^{-1} M_D\right) V_l & M_D^\dagger M_N^{*\,-1} V_h \\ -M_N^{-1} M_D V_l & \left(1 - \tfrac{1}{2} M_N^{-1} M_D M_D^\dagger M_N^{*\,-1}\right) V_h \end{bmatrix}$$
$$(5.6.163)$$

where V_l and V_h are 3×3 and $m \times m$ unitary matrices respectively. The light 3×3 mass matrix M_l and the heavy $m \times m$ matrix M_h are given by

$$M_l \simeq -V_l^T M_D^T M_N^{-1} M_D V_l, \qquad M_h \simeq V_h^T M_N V_h. \qquad (5.6.164)$$

The heavy masses are given by the eigenvalues of M_N, whereas the light masses are given by the eigenvalues of M_l, whose elements are suppressed with respect to the elements of the Dirac mass matrix M_D by the very small matrix factor $(M_D^T M_N^{-1})$. This is the *see-saw mechanism* which explains naturally the smallness of light neutrino masses.[37] Note, however, that the

[37]P. Minkowski, Phys. Lett. B **67**, 421 (1977); R. N. Mohapatra and G. Senjanovic, Phys. Rev. Lett. **44**, 912 (1980).

values of the light neutrino masses and their relative sizes can vary over wide ranges, depending on the specific values of the elements of M_D and M_N. Because the off-diagonal block elements of V_ν are very small, the three flavor neutrinos are mainly composed by the three light neutrinos. Thus, the see-saw mechanism implies the effective low-energy mixing of three Majorana neutrinos with an approximately unitary 3×3 mixing matrix U composed by the first three rows and the first three columns of V_ν.

5.7   The Good, the Bad, and the Ugly

The saga of the standard model is still exhilarating because it leaves all questions of consequence unanswered. The most evident of unanswered questions is why the weak interactions are weak — in gauge theory the only natural values for m_W are zero or the Planck mass, and the model does not contain the physics that dictates why its actual value is of order 100 GeV.

Already in 1934 Fermi provided an answer with a theory that prescribed a quantitative relation between the fine structure constant and the weak coupling, $G_F \sim \alpha/m_W^2$. Although Fermi adjusted m_W to accommodate the strength and range of nuclear radioactive decays, one can readily obtain a value of m_W of 40 GeV from the observed decay rate of the muon for which the proportionality factor is $\pi/\sqrt{2}$. The answer is off by a factor of 2 because the discovery of parity violation and neutral currents was in the future and introduces an additional factor $1 - m_W^2/m_Z^2$,

$$G_F = \left[\frac{\pi\alpha}{\sqrt{2}m_W^2}\right]\left[\frac{1}{1 - m_W^2/m_Z^2}\right](1 + \Delta r). \qquad (5.7.165)$$

Fermi could certainly not have anticipated that we now have a renormalizable gauge theory that allows us to calculate the radiative correction Δr to his formula. Besides regular higher order diagrams, loops associated with the top quark and the Higgs boson contribute; they have been observed. There is no feeling though that we are now dotting the i's and crossing the t's of a mature theory. As a matter of fact, the present victories are bittersweet. If one calculates the radiative corrections to the mass μ appearing in the Higgs potential, the same theory that withstood the onslaught of precision experiments at LEP/SLC and the Tevatron yields a result that grows quadratically;

the difference between the bare and renormalized masses is

$$\Delta\mu^2 \;=\; \frac{1}{64\pi^2}\left(9g^2 + 3g'^2 + 24\,\lambda - 8\sum_f N_f\,Y_f^2\right)\Lambda^2$$

$$\simeq\; \frac{3}{16\pi^2 v^2}\left(2m_W^2 + m_Z^2 + m_H^2 - 4m_t^2\right)\Lambda^2\;, \qquad (5.7.166)$$

where g and g' are the $SU(2)_L \times U(1)_Y$ gauge couplings, λ is the quartic Higgs coupling, Y_f are the Yukawa couplings, $N_f = 1\,(3)$ for leptons (quarks), $m_W^2 = \frac{1}{4}g^2 v^2$, $v = 246$ GeV, $m_Z^2 = \frac{1}{4}(g^2 + g'^2)v^2$, $m_t^2 = \frac{1}{2}Y_t^2 v^2$, $m_H^2 = 2\lambda v^2$, and Λ is a cutoff.[38] Upon minimization of the potential, this translates into a dangerous contribution to the Higgs vacuum expectation value which destabilizes the electroweak scale. The standard model works amazingly well by fixing Λ at the electroweak scale. It is generally assumed that this indicates the existence of new physics beyond the standard model. Following Weinberg,

$$\mathscr{L}(m_{\rm W}) = |\mu^2|\,H^\dagger H + \frac{1}{4}\,\lambda(H^\dagger H)^2 + \mathscr{L}_{\rm SM}^{\rm gauge} + \mathscr{L}_{\rm SM}^{\rm Yukawa} + \frac{1}{\Lambda}\,\mathscr{L}^5 + \frac{1}{\Lambda^2}\mathscr{L}^6 + \dots\;,$$
$$(5.7.167)$$

where the operators of higher dimension parametrize physics beyond the standard model. The optimistic interpretation of all this is that, just like Fermi anticipated particle physics at 100 GeV in 1934, the electroweak gauge theory requires new physics to tame the divergences associated with the Higgs potential. By the most conservative estimates this new physics is within our reach. Avoiding fine tuning requires $\Lambda \lesssim 2 - 3$ TeV to be revealed by the CERN LHC. For example, for $m_H = 115 - 200$ GeV,

$$\left|\frac{\Delta\mu^2}{\mu^2}\right| = \frac{\delta v^2}{v^2} \le 10 \Rightarrow \Lambda = 2 - 3 \text{ TeV}\;, \qquad (5.7.168)$$

where we have implicity used $v^2 = -\mu^2/\lambda$ [valid in the approximation of disregarding terms beyond $\mathcal{O}(H^4)$ in the Higgs potential].

Dark clouds have built up around this sunny horizon because some electroweak precision measurements match the standard model predictions with too high precision, pushing Λ to 10 TeV. The data push some of the higher order dimensional operators in Weinberg's effective Lagrangian to scales beyond

---

[38]M. J. G. Veltman, Acta Phys. Polon. B **12**, 437 (1981).

10 TeV. Some have resorted to rather extreme lengths by proposing that the factor multiplying the unruly quadratic correction $(2m_W^2 + m_Z^2 + m_H^2 - 4m_t^2)$ must vanish; exactly! This has been dubbed the Veltman condition. The problem is now "solved" because scales as large as 10 TeV, possibly even higher, can be accommodated by the observations once one eliminates the dominant contribution. One can even make this stick to all orders and for $\Lambda \leq 10$ TeV, this requires that $m_H \sim 210 - 225$ GeV.

Figure 5.7: *Supersymmetry offers a neat solution of the bad behavior of radiative corrections in the standard model. As for every boson there is a companion fermion, the bad divergence associated with the Higgs loop is cancelled by a fermion loop with opposite sign.*

Let's contemplate the possibilities. The Veltman condition happens to be satisfied and this would leave particle physics with an ugly fine tuning problem. This is very unlikely; LHC must reveal the Higgs physics already observed via radiative correction, or at least discover the physics that implements the Veltman condition. It must appear at $2 - 3$ TeV, even though higher scales can be rationalized when accommodating selected experiments. Supersymmetry (SUSY) is a textbook example (see Appendix J). Even though it elegantly controls the quadratic divergence by the cancellation of boson and fermion contributions (see Fig. 5.7), it is already fine-tuned at a scale of $\sim 2 - 3$ TeV. There has been an explosion of creativity to resolve the challange in other ways; the good news is that all involve new physics in the form of scalars, new gauge bosons, non-standard interactions... Alternatively, it is possible that we may be guessing the future while holding too small a deck of cards and LHC will open a new world that we did not anticipate. Particle physics would return to its early traditions where experiment leads theory, as it should be, and where innovative techniques introduce new accelerators and detection methods that allow us to observe with an open mind and without a plan, leading us to unexpected discoveries.

192

Chapter 6

Big Bang Cosmology

6.1　Lookback Time

At first sight, elementary particles and cosmology seem to be completely different branches of physics, one concerned with the universe's elementary constituents and the other concerned with the universe as a whole. In recent years, however, the most powerful particle accelerators have recreated conditions that existed in the universe just a fraction of a second after the big-bang, opening a window to the very early history of the universe. At the same time, a flood of high-quality data from the Supernova Cosmology Project, the Supernova Search Team, the Wilkinson Microwave Anisotropy Probe (WMAP), and the Sloan Digital Sky Survey (SDSS) pin down cosmological parameters to percent-level precision, establishing a new paradigm of cosmology.[1] The standard big-bang model assumes homogeneity and isotropy. A surprisingly good fit to the data is provided by a simple geometrically flat (expanding) universe, in which 30% of the energy density is in the form of non-relativistic matter and 70% is in the form of a new, unknown dark energy component

---

[1] A. G. Riess *et al.* [Supernova Search Team Collaboration], Astron. J. **116**, 1009 (1998); S. Perlmutter *et al.* [Supernova Cosmology Project Collaboration], Astrophys. J. **517**, 565 (1999); D. N. Spergel *et al.* [WMAP Collaboration], Astrophys. J. Suppl. **148**, 175 (2003); R. A. Knop *et al.* [Supernova Cosmology Project Collaboration], Astrophys. J. **598**, 102 (2003); M. Tegmark *et al.* [SDSS Collaboration], Phys. Rev. D **69**, 103501 (2004).

with strongly negative pressure. Adding to the puzzle, baryons represent only a minor percentage (about 4%) of the matter-energy budget of the universe.

The most general form for the metric tensor (consistent with WMAP and SDSS data) is that of the flat Robertson–Walker spacetime, which in co-moving coordinates is given by

$$ds^2 = dt^2 - a^2(t) \left[dr^2 + r^2 \left(d\theta^2 + \sin^2 \theta d\phi^2 \right) \right], \qquad (6.1.1)$$

where $a(t)$ is the cosmological scale factor that distinguishes the metric from flat Minkowski space.[2] (A co-moving volume is a volume where expansion effects are removed.) It is common to assume that the matter content of the universe is a perfect fluid. The Friedmann equations,

$$H^2 \equiv \left(\frac{\dot{a}}{a} \right)^2 = \frac{8\pi G_N \rho}{3} + \frac{\Lambda}{3} \qquad (6.1.2)$$

and

$$\frac{\ddot{a}}{a} = \frac{\Lambda}{3} - \frac{4\pi G_N}{3}(\rho + 3p), \qquad (6.1.3)$$

are the result of applying general relativity (with a pefect fluid source) to a (3+1)-dimensional spacetime that is homogeneous and isotropic, where $H(t)$ is the Hubble parameter, $G_N = M_{\mathrm{Pl}}^{-2}$ is Newton's constant, Λ is the cosmological constant, and p and ρ are the pressure and energy density of the matter and radiation driving the expansion of the universe.[3] Energy conservation leads to a third useful equation [which can also be derived from (6.1.2) and (6.1.3)]

$$\dot{\rho} = -3H(\rho + p). \qquad (6.1.4)$$

These equations form the basis of the standard big-bang model. The expansion rate of the universe as a function of time can be determined by specifying the matter or energy content through an equation of state, which relates energy density to pressure. For a perfect fluid, the equation of state is characterized by a dimensionless number $\omega = p/\rho$.

[2]H. P. Robertson, Astrophys. J. **82**, 284 (1935); **83**, 187, 257 (1936); A. G. Walker, Proc. Lond. Math. Soc. (2), **42** 90 (1936).

[3]A. Friedmann, Z. Phys. **10**, 377 (1922); **21**, 326 (1924).

Aside from the well-known Hubble parameter, it is useful to define several other measurable cosmological parameters. The Friedmann equation can be used to define a critical density such that when $\Lambda = 0$,

$$\rho_c \equiv \frac{3H^2}{8\pi G_N} = 1.05 \times 10^{-5} h^2 \ \text{GeVcm}^{-3} \tag{6.1.5}$$

where the scaled Hubble parameter, h, is defined by

$$H = 100\, h \ \text{km s}^{-1} \text{Mpc}^{-1}. \tag{6.1.6}$$

The cosmological density parameter is defined as the energy density relative to the critical density

$$\Omega_{\text{tot}} = \rho/\rho_c. \tag{6.1.7}$$

Since the universe is expanding, the galaxies should be moving away from each other. Hence, we should observe galaxies receding from us. Recall that the wavelength of light emitted from a receding object is stretched out so that the observed wavelength is larger than the emitted one. It is convenient to define this stretching factor as the redshift z,

$$1 + z \equiv \frac{\lambda_{\text{observed}}}{\lambda_{\text{emitted}}} = \frac{1}{a}. \tag{6.1.8}$$

Perhaps the most conclusive piece of evidence for the big-bang is the cosmic microwave background (CMB), discovered by chance in 1965.[4] One fascinating feature of the CMB is its Planck spectrum: it follows the black-body curve at a temperature $T_\gamma^{\text{CMB}} = 2.725 \pm 0.001 \ \text{K} \, (1\sigma)$ to extremely high precision over more than three decades in frequency.[5] This implies that the universe was in thermal equilibrium when these photons were last scattered. An even more fascinating feature is that, to better than a part in 10^5, the CMB temperature is the same over the entire sky. This strongly suggests that everything in the observable universe was in thermal equilibrium at one time in its evolution.

Because the early universe was to a good approximation in thermal equilibrium, particle reactions can be modeled using the tools of thermodynamics

---

[4]A. A. Penzias and R. W. Wilson, Astrophys. J. **142**, 419 (1965).

[5]J. C. Mather, D. J. Fixsen, R. A. Shafer, C. Mosier and D. T. Wilkinson, Astrophys. J. **512**, 511 (1999).

and statistical mechanics. The number density n, energy density ρ and pressure p of a dilute weakly-interacting gas of particles with g internal degrees of freedom is given in terms of its phase space distribution (or occupancy) function $f(\vec{p})$

$$
\begin{aligned}
n &= \frac{g}{(2\pi)^3} \int f(\vec{p})d^3p \,, \\
\rho &= \frac{g}{(2\pi)^3} \int E(\vec{p})\, f(\vec{p})d^3p \,, \\
p &= \frac{g}{(2\pi)^3} \int \frac{|\vec{p}|^2}{3E}\, f(\vec{p})\, d^3p \,,
\end{aligned}
\tag{6.1.9}
$$

with E and $\vec{p}$ satisfying the relativistic relation (1.4.42). For a particle species of type i in kinetic equilibrium, the phase space occupancy f is given by the familiar Fermi-Dirac or Bose-Einstein distrubutions,

$$
f(\vec{p_i}) = \frac{1}{e^{(E_i - \mu_i)/T_i} \pm 1},
\tag{6.1.10}
$$

where T_i is the temperature, μ_i is the chemical potential (if present), and $\pm$ corresponds to either Fermi or Bose statistics. Moreover, if the species of type i is in chemical equilibrium, then its chemical potential is related to the chemical potentials of other species j, k, l with which it interacts; e.g., if

$$
i + j \leftrightarrow k + l \,,
\tag{6.1.11}
$$

then $\mu_i + \mu_j = \mu_k + \mu_l$, whenever chemical equilibrium holds.

From the equilibrium distributions, it follows that for a particle species of mass m_i

$$
\begin{aligned}
\rho_i &= \frac{g_i}{2\pi^2} \int_{m_i}^{\infty} \frac{(E_i^2 - m_i^2)^{1/2}}{e^{(E_i - \mu_i)/T_i} \pm 1}\, E_i^2 \, dE_i \,, \\
n_i &= \frac{g_i}{2\pi^2} \int_{m_i}^{\infty} \frac{(E_i^2 - m_i^2)^{1/2}}{e^{(E_i - \mu_i)/T_i} \pm 1}\, E_i \, dE_i \,, \\
p_i &= \frac{g_i}{6\pi^2} \int_{m_i}^{\infty} \frac{(E_i^2 - m_i^2)^{3/2}}{e^{(E_i - \mu_i)/T_i} \pm 1}\, dE_i \,,
\end{aligned}
\tag{6.1.12}
$$

where g_i counts the total degrees of freedom for type i. The entropy density is

$$
s_i = \frac{\rho_i + p_i - \mu_i n_i}{T_i} \,.
\tag{6.1.13}
$$

196

In the standard model, a chemical potential is often associated with baryon number, and since the net baryon density relative to the photon density is known to be very small, $\mathcal{O}(10^{-10})$, we can neglect any such chemical potential when computing total thermodynamic quantities.

For a nondegenerate $(T_i \gg \mu_i)$, relativistic species $(T_i \gg m_i)$, we have

$$
n_i = \begin{cases} \frac{1}{\pi^2}\, \zeta(3)\, g_i T_i^3 & \text{for bosons} \\ \frac{3}{4}\frac{1}{\pi^2}\, \zeta(3)\, g_i T_i^3 & \text{for fermions} \end{cases},
$$

$$
\rho_i = \begin{cases} \frac{\pi^2}{30}\, g_i\, T_i^4 & \text{for bosons} \\ \frac{7}{8}\frac{\pi^2}{30}\, g_i\, T_i^4 & \text{for fermions} \end{cases}, \qquad (6.1.14)
$$

$$
p_i = \rho_i/3,
$$

where $\zeta(3) = 1.20206...$ is the Riemann Zeta function of 3. On the other hand, for a nonrelativistic particle species $(T_i \ll m_i)$, the relevant statistical quantities follow a Maxwell-Boltzmann distribution and thus there is no difference between fermions and bosons

$$
n_i = g_i \left(\frac{m_i T_i}{2\pi} \right)^{3/2} e^{-m_i/T_i},
$$

$$
\rho_i = m_i\, n_i, \qquad (6.1.15)
$$

$$
p_i = n_i T_i \ll \rho_i.
$$

For a nongenerate, relativistic species, the average energy per particle is

$$
\langle E_i \rangle = \rho_i/n_i \begin{cases} \frac{\pi^4}{30\zeta(3)}\, T_i & \simeq 2.701\, T_i \ \text{for bosons} \\ \frac{7\pi^4}{180\zeta(3)}\, T_i & \simeq 3.151\, T_i \ \text{for fermions} \end{cases}, \qquad (6.1.16)
$$

whereas for a non-relativistic species

$$
\langle E_i \rangle = m_i + \frac{3}{2} T_i. \qquad (6.1.17)
$$

For photons, we can compute all of the thermodynamic quantities rather easily

$$
\rho_\gamma = \frac{\pi}{15} T_\gamma^4; \quad p_\gamma = \frac{1}{3}\rho_\gamma; \quad s_\gamma = \frac{4\rho_\gamma}{3 T_\gamma}; \quad n_\gamma = \frac{2\zeta(3)}{\pi^2} T_\gamma^3. \qquad (6.1.18)
$$

Table 6.1: *Effective numbers of degrees of freedom in the standard model*

Temperature	New particles	$4N(T)$
$T < m_e$	γ's $+ \nu$'s	29
$m_e < T < m_\mu$	$e^\pm$	43
$m_\mu < T < m_\pi$	$\mu^\pm$	57
$m_\pi < T < T_c^*$	π's	69
$T_c < T < m_{\text{charm}}$	- π's $+ u, \bar{u}, d, \bar{d}, s, \bar{s} +$ gluons	247
$m_c < T < m_\tau$	$c, \bar{c}$	289
$m_\tau < T < m_{\text{bottom}}$	$\tau^\pm$	303
$m_b < T < m_{W,Z}$	$b, \bar{b}$	345
$m_{W,Z} < T < m_{\text{Higgs}}$	$W^\pm, Z$	381
$m_H < T < m_{\text{top}}$	H^0	385
$m_t < T$	$t, \bar{t}$	427

*T_c corresponds to the confinement–deconfinement transition between quarks and hadrons.

In the limit $T \gg m_i$, the total energy density can be conveniently expressed by

$$\rho_R = \left(\sum_B g_B + \frac{7}{8} \sum_F g_F \right) \frac{\pi^2}{30} T^4 \equiv \frac{\pi^2}{30} N(T) T^4, \qquad (6.1.19)$$

where $g_{B(F)}$ is the total number of boson (fermion) degrees of freedom and the sum runs over all boson (fermion) states with $m_i \ll T$. The factor of 7/8 is due to the difference between the Fermi and Bose integrals. Equation (6.1.19) defines the effective number of degrees of freedom, $N(T)$, by taking into account new particle degrees of freedom as the temperature is raised. The change in $N(T)$ (ignoring mass effects) is given in Table 6.1. At higher temperatures, $N(T)$ will be model dependent.[6]

At early times, $t < 10^5$ yr, the universe is thought to have been dominated by radiation. The equation of state can be given by $\omega = 1/3$. If we neglect

---

[6]See e.g., E. W. Kolb and M. S. Turner, *The Early universe,* Front. Phys. **69**, 1 (1990).

the contributions to H from Λ (this is always a good approximation for small enough a) then we find that $a \sim t^{1/2}$ and $\rho_R \sim a^{-4}$. Substituting (6.1.19) into (6.1.2) we can rewrite the expansion rate as a function of the temperature in the plasma

$$
\begin{aligned}
H = \left(\frac{8\pi G_N \rho_R}{3}\right)^{1/2} &= \left(\frac{8\pi^3}{90}N(T)\right)^{1/2} T^2/M_{\mathrm{Pl}} \\
&\sim 1.66\sqrt{N(T)}T^2/M_{\mathrm{Pl}} \, .
\end{aligned}
\tag{6.1.20}
$$

Neglecting the T-dependence of N (i.e. away from mass thresholds and phase transitions), integration of (6.1.20) yields the useful commonly used approximation

$$
t \simeq \left(\frac{3M_{\mathrm{Pl}}^2}{32\pi\rho_R}\right)^{1/2} \simeq 2.42\frac{1}{\sqrt{N(T)}}\left(\frac{T}{\mathrm{MeV}}\right)^{-2} \mathrm{s} \, .
\tag{6.1.21}
$$

The universe made the transition between radiation and matter domination when $\rho_R = \rho_m$, or when $T \simeq \text{few} \times 10^3$ K at $z_{\mathrm{eq}} \sim 3300$. For a matter or dust dominated universe, $\omega = 0$, and therefore $a(t) \sim t^{2/3}$ and $\rho_m \sim a^{-3}$. In a vacuum or Λ dominated universe (which we are approaching today) $\omega = -1$, yielding $a \sim e^{\sqrt{\Lambda/3}\,t}$. The current best measurement of the equation of state (assumed constant) is $\omega_{z=0} = -1.006^{+0.067}_{-0.068}$.

For a system in thermodynamic equilibrium, (6.1.4) can be converted into an equation for conservation of entropy per co-moving volume. Recognizing that $\dot{p} = s\dot{T}$, (6.1.4) becomes

$$
\frac{d}{dt}(sa^3) = 0 \, ,
\tag{6.1.22}
$$

viz., a non-evolving system would stay at constant number or entropy density in co-moving coordinates even though the number or entropy density is in fact decreasing due to the expansion of the universe. For radiation, this corresponds to the relationship between expansion and cooling, $T \propto a^{-1}$ in an adiabatically expanding universe. Note that both s and n scale as T^3.

The nucleosynthesis taking place in the primordial plasma is undoubtedly one of the observational pillars of the standard cosmological model, indeed known simply as big-bang nucleosynthesis (BBN).[7] BBN probes the

---

[7]K. A. Olive, G. Steigman and T. P. Walker, Phys. Rept. **333**, 389 (2000).

t-channel
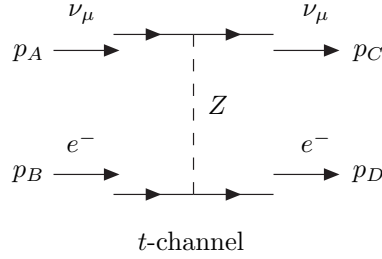
Figure 6.1: *The neutral current $\nu_\mu e^- \to \nu_\mu e^-$ interaction.*

evolution of the universe during its first few minutes, providing a glimpse into its earliest epochs ($z \sim 10^8$). The physical processes involved, which have been well-understood for some time, interrelate the four fundamental interactions: gravity sets the dynamics of the "expanding cauldron," weak interactions determine the neutrino decoupling and the neutron-proton equilibrium freeze-out, and electromagnetic and nuclear processes regulate the nuclear reaction network. The final abundance of the synthesized elements is sensitive to a variety of parameters and physical constants, allowing many interesting probes on physics beyond the standard model. In the following we provide a simple illustrative example.

Extrapolating the present state of the cosmos backwards in time, we infer that at a temperature of say a few tens of MeV the universe was filled with a plasma of protons, neutrons, electrons, positrons, photons, neutrinos, and antineutrinos (p, n, γ, e^-, e^+, ν, and $\bar{\nu}$). The baryons are of course nonrelativistic while all the other particles are relativistic. Introducing the ratio of the baryon number density to the photon number density, $\eta = n_{\rm b}/n_\gamma \sim 5 \times 10^{-10}$, we see that $\eta m_N/T \sim 10^{-8}$ and thus nucleons contribute a negligible fraction to ρ_R. These particles are kept in thermal equilibrium by various electromagnetic and weak processes of the sort $\bar{\nu}\nu \rightleftharpoons e^+ e^-$, $\nu e^- \rightleftharpoons \nu e^-$, $n\nu_e \rightleftharpoons pe^-$, $\gamma\gamma \rightleftharpoons e^+ e^-$, $\gamma p \rightleftharpoons \gamma p$, etc.

The $\nu_\mu e^-$ and $\bar{\nu}_\mu e^-$ scattering processes can only proceed via a neutral current interaction (see Fig. 6.1). The current-current form of the invariant amplitude for the process $\nu_\mu e^- \to \nu_\mu e^-$ is analogous to that of $\nu q \to \nu q$ scattering,

$$\mathfrak{M}^{\rm NC}(\nu e \to \nu e) = \frac{\rho G_F}{\sqrt{2}} \left[\bar{\nu}\gamma^\mu(1 - \gamma^5)\nu \right] \left[\bar{e}\gamma_\mu(c_V^e - c_A^e \gamma^5)e \right] . \qquad (6.1.23)$$

200

In what follows, we take $\rho = 1$ and define the momenta according to

$$\nu_\mu(\omega, \vec{k}) + e^-(E, \vec{p}) \rightarrow \nu_\mu(\omega', \vec{k}') + e^-(E', \vec{p}') , \qquad (6.1.24)$$

Since mean energies of interacting particles are of the order of the temperature $T \simeq$ MeV $\ll m_Z$, we can express the averaged square amplitude (for massless electrons) as

$$|\mathfrak{M}^{\mathrm{NC}}|^2 = 16 G_F^2 [(c_V^e + c_A^e)^2 (p^\alpha k_\alpha)(p'^\alpha k'_\alpha) + (c_V^e - c_A^e)^2 (p'^\alpha k_\alpha)(p^\alpha k'_\alpha)] . \quad (6.1.25)$$

Now, using (3.3.48) we rewrite (6.1.25) as

$$\begin{aligned}
|\mathfrak{M}^{\mathrm{NC}}|^2 &= 4 G_F^2 [(c_V^e + c_A^e)^2 s^2 + (c_V^e - c_A^e)^2 u^2] \\
&= G_F^2 s^2 \left[4(c_V^e + c_A^e)^2 + (c_V^e - c_A^e)^2 (1 + \cos\theta)^2 \right] . \quad (6.1.26)
\end{aligned}$$

The integration over the phase space (3.1.27) is straightforward, yielding

$$\sigma(\nu_\mu e^- \rightarrow \nu_\mu e^-) = \frac{G_F^2}{3\pi} s \left(c_A^{e\,2} + c_A^e c_V^e + c_V^{e\,2} \right) . \qquad (6.1.27)$$

Comparing (5.1.29) and (5.1.30) it is easily seen that for $\bar{\nu}_\mu e^-$ elastic scattering, $c_A \rightarrow -c_A$ in (6.1.26) and so

$$\sigma(\bar{\nu} e^- \rightarrow \bar{\nu} e^-) = \frac{G_F^2}{3\pi} s \left(c_A^{e\,2} - c_A^e c_V^e + c_V^{e\,2} \right) . \qquad (6.1.28)$$

The process $\nu_e e^- \rightarrow \nu_e e^-$ offers the intriguing possibility of studying charged current and neutral current interference. The scattering amplitude comes from two diagrams, with Z in the t–channel and W in the u–channel (see Fig. 6.2). The amplitude for t-channel process is $\mathfrak{M}^{\mathrm{NC}}$ of (6.1.23) with $\nu = \nu_e$. For the u-channel we have

$$\mathfrak{M}^{\mathrm{CC}} = -\frac{G_F}{\sqrt{2}} \left[\bar{e}\gamma^\mu(1 - \gamma^5)\nu_e \right] \left[\bar{\nu}_e \gamma_\mu (1 - \gamma^5)e \right] , \qquad (6.1.29)$$

where the minus sign relative to (6.1.23) arises from interchange of the outgoing leptons. We may use Fierz reordering theorem to rewrite (6.1.29) as

$$\mathfrak{M}^{\mathrm{CC}} = -\frac{G_F}{\sqrt{2}} \left[\bar{\nu}_e \gamma^\mu(1 - \gamma^5)\nu_e \right] \left[\bar{e}\gamma_\mu (1 - \gamma^5)e \right] . \qquad (6.1.30)$$
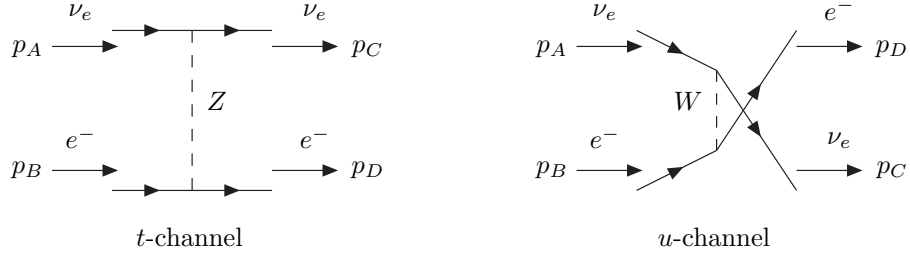
Figure 6.2: *The neutral and charged current $\nu_e e^- \to \nu_e e^-$ interaction.*

To obtain the amplitude $\mathfrak{M}(\nu_e e^- \to \nu_e e^-)$, we add the amplitudes ($\mathfrak{M}^{\mathrm{NC}}$ and $\mathfrak{M}^{\mathrm{CC}}$) for the two diagrams of Fig. 6.2. We find $\mathfrak{M} = \mathfrak{M}^{\mathrm{NC}} + \mathfrak{M}^{\mathrm{CC}}$ is given by (6.1.23) with

$$c_V \to c_V + 1, \qquad c_A \to c_A + 1. \tag{6.1.31}$$

Thus, with these replacements, the $\nu_e e^-$ and $\bar{\nu}_e e^-$ elastic scattering cross sections are in turn given by (6.1.27) and (6.1.28).

Now, from (6.1.15) we first obtain the number density of massless particles $n_{e^-}(T) = 0.182\, T^3$ and then compute the weak interaction rate (per neutrino species)

$$\Gamma_{\nu_\alpha} \sim n_{e^-}\, \sigma(\nu e^- \to \nu e^-)\, v, \tag{6.1.32}$$

where $v = p^\alpha k_\alpha/(E\omega) = (1 - \cos\theta)$ is the Moller velocity. Ocurring in the rate is the product of σv. We adopt a thermal average followed by the angular average on this factor; namely

$$\langle v\sigma \rangle_\alpha = \frac{1}{2} \int_1^1 \frac{G_F^2}{3\pi} s \mathcal{Z}_{\nu_\alpha} (1 - \cos\theta)\, d(\cos\theta) = \frac{8}{9\pi} G_F^2\, \mathcal{Z}_{\nu_\alpha} \langle E \rangle \langle \omega \rangle, \tag{6.1.33}$$

where $s = 2E\,\omega(1 - \cos\theta)$, $\langle E \rangle$ and $\langle \omega \rangle$ are given by (6.1.16), $\mathcal{Z}_{\nu_\mu} = \mathcal{Z}_{\nu_\tau} = c_V^{e\,2} + c_V^e c_A^e + c_A^{e\,2}$, and $\mathcal{Z}_{\nu_e} = (1 + c_V^e)^2 + (1 + c_A^e)(1 + c_V^e) + (1 + c_A^e)^2$. The electron neutrino interaction rate is then

$$\Gamma_{\nu_e} = 1.16 \times 10^{-22} \left(\frac{T_{\nu_e}}{\mathrm{MeV}} \right)^5. \tag{6.1.34}$$

Comparing (6.1.34), with the expansion rate (6.1.20) calculated for $N(T) = 10.75$

$$H \simeq 4.46 \times 10^{-22} \left(\frac{T}{\mathrm{MeV}} \right)^3, \tag{6.1.35}$$

202

we see that at high T, weak interaction processes are fast enough. But as the temperature drops below some characteristic decoupling temperature, $T_{\nu_\alpha}^{\text{dec}}$, neutrinos "decouple" - they lose thermal contact with electrons.[8] The condition $\Gamma_{\nu_\alpha}(T_{\nu_\alpha}^{\text{dec}}) = H(T_{\nu_\alpha}^{\text{dec}})$ sets the decoupling temperature for neutrinos: $T_{\nu_e}^{\text{dec}} \approx 1.56$ MeV and $T_{\nu_\mu}^{\text{dec}} \simeq T_{\nu_\tau}^{\text{dec}} \approx 2.88$ MeV. In complying with the precision demanded of our phenomenological approach it would be sufficient to consider that all neutrino species decouple at $T_\nu^{\text{dec}} \approx 2$ MeV.

The much stronger electromagnetic interaction continues to keep the protons, neutrons, electrons, positrons, and photons in equilibrium. The reaction rate per nucleon, $\Gamma_N \sim T^3 \alpha^2 / m_N^2$, is larger than the expansion rate as long as

$$T > \frac{m_N^2}{\alpha^2 M_{\text{Pl}}} \sim \text{a very low temperature}, \qquad (6.1.36)$$

where the non-relativistic form of the electromagnetic cross section, $\sigma \sim \alpha^2/m_N^2$, has been obtained by dimensional analysis. The nucleons are thus mantianed in kinetic equilibrium. The average kinetic energy per nucleon is $\frac{3}{2}T$. One must be careful to distinguish between kinetic equilibrium and chemical equilibrium. Reactions like $\gamma\gamma \to p\bar{p}$ have long been suppressed, as there are essentially no anti-nucleons around.

For $T > m_e \sim 0.5$ MeV $\sim 5 \times 10^9$ K, the number of electrons, positrons, and photons are comparable, $n_{e^-} \sim n_{e^+} \sim n_\gamma$. The exact ratios are of course easily supplied by inserting the appropriate "g-factors." Because the universe is electrically neutral, $n_{e^-} - n_{e^+} = n_p$ and so there is a slight excess of electrons over positrons. When T drops below m_e, the process $\gamma\gamma \to e^+e^-$ is severely suppressed by the Boltzmann factor $e^{-m_e/T}$, as only very energetic photons in the "tail-end" of the Bose distribution can participate. Thus positrons and electrons annihilate rapidly via $e^+e^- \to \gamma\gamma$ and are not replenished (leaving a small number of electrons $n_{e^-} \sim n_p \sim 5 \times 10^{-10} n_\gamma$). As long as thermal equilibrium was preserved, the total entropy remained fixed. We have seen that if a is the separation between any pair of typical particles, then $sa^3 \propto N(T)T^3 a^3 = $ constant. For $T \gtrsim m_e$, the particles in thermal equilibrium with the photons include the photon ($g_\gamma = 2$) and $e^\pm$ pairs

---

[8]R. A. Alpher, J. W. Follin and R. C. Herman, Phys. Rev. **92**, 1347 (1953); Ya. B. Zel'dovich, Adv. Astron. Astrophys. **3**, 241 (1965); Sov. Phys. Usp. **9**, 602 (1967).

($g_{e^\pm} = 4$). The effective total number of particle species before annihilation is $N_{\text{before}} = 11/2$. On the other hand, after the annihilation of electrons and positrons, the only remaining abundant particles in equilibrium are photons. Hence the effective number of particle species is $N_{\text{after}} = 2$. It follows from the conservation of entropy that

$$\frac{11}{2} \left(T_\gamma a \right)^3 \bigg|_{\text{before}} = 2 \left(T_\gamma a \right)^3 \bigg|_{\text{after}} . \tag{6.1.37}$$

That is, the heat produced by the annihilation of electrons and positrons increases the quantity $T_\gamma a$ by a factor of

$$\frac{(T_\gamma a)|_{\text{after}}}{(T_\gamma a)|_{\text{before}}} = \left(\frac{11}{4} \right)^{1/3} \simeq 1.4 . \tag{6.1.38}$$

Before the annihilation of electrons and positrons, the neutrino temperature T_ν is the same as the photon temperature T_γ. But from then on, T_ν simply dropped like a^{-1}, so for all subsequent times, $T_\nu a$ equals the value before annihilation,

$$(T_\nu a)|_{\text{after}} = (T_\nu a)|_{\text{before}} = (T_\gamma a)|_{\text{before}} . \tag{6.1.39}$$

We conclude therefore that after the annihilation process is over, the photon temperature is higher than the neutrino temperature by a factor of

$$\left(\frac{T_\gamma}{T_\nu} \right) \bigg|_{\text{after}} = \frac{(T_\gamma a)|_{\text{after}}}{(T_\nu a)|_{\text{after}}} \simeq 1.4 . \tag{6.1.40}$$

The energy density stored in relativistic species is customarily given in terms of the so-called "effective number of neutrino species," N_ν^{eff}, through the relation

$$\rho_R = \left[1 + \frac{7}{8} \left(\frac{4}{11} \right)^{4/3} N_\nu^{\text{eff}} \right] \rho_\gamma . \tag{6.1.41}$$

Without a doubt,

$$\begin{aligned}
N_\nu^{\text{eff}} &\equiv \left(\frac{\rho_R - \rho_\gamma}{\rho_\nu} \right) \\
&\simeq \frac{8}{7} {\sum_B}' \frac{g_B}{2} \left(\frac{T_B}{T_\nu} \right)^4 + {\sum_F}' \frac{g_F}{2} \left(\frac{T_F}{T_\nu} \right)^4 ,
\end{aligned} \tag{6.1.42}$$

where ρ_ν denotes the energy density of a single species of massless neutrinos, $T_{B(F)}$ is the effective temperature of boson (fermion) species, and the primes indicate that electrons and photons are excluded from the sums.[9] The normalization of N_ν^{eff} is such that it gives $N_\nu^{\text{eff}} = 3$ for three families of massless left-handed standard model neutrinos. For most practical purposes, it is accurate enough to consider that neutrinos freeze-out completely at about 1 MeV. However, as the temperature dropped below this value, neutrinos were still interacting with the electromagnetic plasma and hence received a tiny portion of the entropy from pair annihilations. The non-instantaneous neutrino decoupling gives a correction to the normalization $\Delta N_\nu^{\text{eff}} = 0.046$.[10]

Near 1 MeV, the CC weak interactions,

$$n\nu_e \rightleftharpoons pe^-, \quad ne^+ \rightleftharpoons p + \bar\nu_e, \quad n \rightleftharpoons p + e^- + \nu_e \tag{6.1.43}$$

guarantee neutron-proton chemical equilibrium. Defining λ_{np} as the summed rate of the reactions which convert neutrons to protons,

$$\lambda_{np} = \lambda(n\nu_e \to pe^-) + \lambda(ne^+ \to p\bar\nu_e) + \lambda(n \to pe^-\bar\nu_e) , \tag{6.1.44}$$

the rate λ_{pn} for the reverse reactions which convert protons to neutrons is given by detailed balance:

$$\lambda_{pn} = \lambda_{np} \, e^{-\Delta m/T(t)}, \tag{6.1.45}$$

where $\Delta m \equiv m_n - m_p = 1.293$ MeV. For simplicity, in (6.1.45) we ignored the possibility of a large chemical potential in electron neutrinos. The chemical potential of electrons is negligible since any excess of electrons that survive the annihilation epoch at $T \sim m_e$ must equal the small observed excess of protons, given that the universe appears to be electrically neutral to high

[9]G. Steigman, D. N. Schramm and J. E. Gunn, Phys. Lett. B **66**, 202 (1977); G. Steigman, K. A. Olive, D. N. Schramm and M. S. Turner, Phys. Lett. B **176**, 33 (1986).

[10]D. A. Dicus, E. W. Kolb, A. M. Gleeson, E. C. G. Sudarshan, V. L. Teplitz and M. S. Turner, Phys. Rev. D **26**, 2694 (1982); S. Dodelson and M. S. Turner, Phys. Rev. D **46**, 3372 (1992); G. Mangano, G. Miele, S. Pastor and M. Peloso, Phys. Lett. B **534**, 8 (2002); G. Mangano, G. Miele, S. Pastor, T. Pinto, O. Pisanti and P. D. Serpico, Nucl. Phys. B **729**, 221 (2005).

accuracy. The evolution of the fractional neutron abundance $X_{n/N} \equiv n_n/n_N$ is described by the balance equation

$$\frac{dX_{n/N}(t)}{dt} = \lambda_{pn}(t)[1 - X_{n/N}(t)] - \lambda_{np}(t)X_{n/N}(t) \,, \qquad (6.1.46)$$

where n_N is the total nucleon density at this time, $n_N = n_n + n_p$. The equilibrium solution is obtained by setting $dX_{n/N}(t)/dt = 0$:

$$X_{n/N}^{\mathrm{eq}}(t) = \frac{\lambda_{pn}(t)}{\lambda_{pn}(t) + \lambda_{np}(t)} = \left[1 + e^{\Delta m/T(t)}\right]^{-1} \,. \qquad (6.1.47)$$

The neutron abundance tracks its value in equilibrium until the inelastic neutron-proton scattering rate decreases sufficiently so as to become comparable to the Hubble expansion rate. At this point the neutrons freeze-out, i.e. go out of *chemical* equilibrium. The neutron abundance at the freeze-out temperature $T_{n/N}^{\mathrm{FO}} = 0.75$ can be approximated by its equilibrium value (6.1.47),

$$X_{n/N}(T_{n/N}^{\mathrm{FO}}) \simeq X_{n/N}^{\mathrm{eq}}(T_{n/N}^{\mathrm{FO}}) = \left[1 + e^{\Delta m/T_{n/N}^{\mathrm{FO}}}\right]^{-1} \,. \qquad (6.1.48)$$

Since the ratio $\Delta m/T_{n/N}^{\mathrm{FO}}$ is of $\mathcal{O}(1)$, a substantial fraction of neutrons survive when chemical equilibrium between neutrons and protons is broken.

At this time, the photon temperature is already below the deuterium binding energy $\Delta_{\mathrm{D}} \simeq 2.2$ MeV, thus one would expect sizable amounts of D to be formed via $n\,p \to \mathrm{D}\,\gamma$ process. However, the large photon-nucleon density ratio η^{-1} delays deuterium synthesis until the photo–dissociation process become ineffective (deuterium *bottleneck*). Defining the onset of nucleosynthesis by the criterion

$$e^{\Delta_D/T_{\mathrm{BBN}}}\eta \sim 1 \,, \qquad (6.1.49)$$

we obtain $T_{\mathrm{BBN}} \approx 89$ keV. Note that (6.1.49) ensures that below T_{BBN} the high energy tail in the photon distribution, with energy larger than Δ_D, has been sufficiently diluted by the expansion. At this epoch, $N(T) = 3.36$, hence the time-temperature relationship (6.1.21) dictates that nucleosynthesis begins at

$$t_{\mathrm{BBN}} \simeq 167 \text{ s} \approx 180 \text{ s} \,, \qquad (6.1.50)$$

as widely popularized by Weinberg.[11]

Once D starts forming, a whole nuclear process network sets in. When the temperature dropped below ~ 80 keV, the universe has cooled sufficiently that the cosmic nuclear reactor can begin in earnest, building the lightest nuclides through the following sequence of two-body reactions

$$
\begin{aligned}
&p\,n \to \gamma\,\mathrm{D}, \\
&p\,\mathrm{D} \to {}^3\mathrm{He}\,\gamma, &&\mathrm{D\,D} \to {}^3\mathrm{He}\,n, &&\mathrm{D\,D} \to p\,\mathrm{T}, \\
&\mathrm{T\,D} \to {}^4\mathrm{He}\,n, &&{}^4\mathrm{He\,T} \to {}^7\mathrm{Li}\,\gamma, \\
&{}^3\mathrm{He}\,n \to p\,\mathrm{T}, &&{}^3\mathrm{He\,D} \to {}^4\mathrm{He}\,p, &&{}^3\mathrm{He}\,{}^4\mathrm{He} \to {}^7\mathrm{Be}\,\gamma, \\
&{}^7\mathrm{Li}\,p \to {}^4\mathrm{He}\,{}^4\mathrm{He}, &&{}^7\mathrm{Be}\,n \to {}^7\mathrm{Li}\,p, \\
&\;\;\vdots
\end{aligned}
\tag{6.1.51}
$$
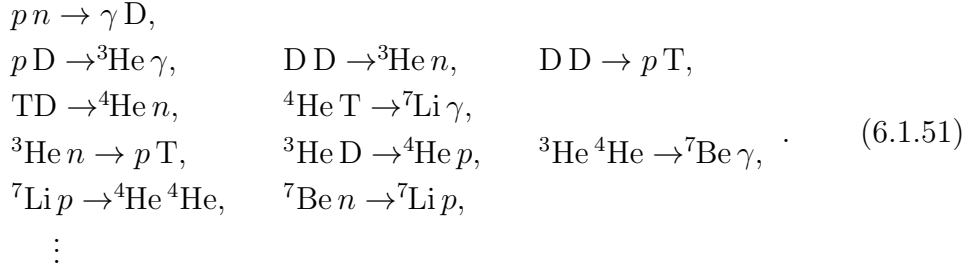
By this time the neutron abundance surviving at freeze-out has been depleted by β-decay to

$$
X_{n/N}(T_{\mathrm{BBN}}) \simeq X_{n/N}(T_{n/N}^{\mathrm{FO}})\, e^{-t_{\mathrm{BBN}}/\tau_n}\,,
\tag{6.1.52}
$$

where $\tau_n \simeq 887$ s is the neutron lifetime. Nearly *all* of these surviving neutrons are captured in ^{4}He because of its large binding energy ($\Delta_{{}^4\mathrm{He}} = 28.3$ MeV) via the reactions listed in (6.1.51). Heavier nuclei do not form in any significant quantity both because of the absence of stable nuclei with $A{=}5$ or 8, which impedes nucleosynthesis via $n\,{}^4$He, $p\,{}^4$He or ^{4}He ^{4}He reactions, and because of the large Coulomb barrier for reactions such as ^{4}He T $\to$ ^{7}Li γ and ^{3}He ^{4}He $\to$ ^{7}Be γ. By the time the temperature has dropped below ~ 30 keV, a time comparable to the neutron lifetime, the average thermal energy of the nuclides and nucleons is too small to overcome the Coulomb barriers; any remaining free neutrons decay, and BBN ceases. The resulting *mass* fraction of helium, conventionally referred to Y_{p}, is simply given by

$$
Y_{\mathrm{p}} \simeq 2X_{n/N}(t_{\mathrm{BBN}}) = 0.251\,,
\tag{6.1.53}
$$

where the subscript p denotes primordial. The above calculation demonstrates how the synthesized helium abundance depends on the physical parameters. After a bit of algebra, (6.1.53) can be rweritten as[12]

$$
Y_{\mathrm{p}} \simeq 0.251 + 0.014\,\Delta N_\nu^{\mathrm{eff}} + 0.0002\Delta\tau_n + 0.009\ln\left(\frac{\eta}{5 \times 10^{-10}}\right)\,.
\tag{6.1.54}
$$

---

[11]S. Weinberg, *The First Three Minutes* (Basic Books, New York, 1977).
[12]S. Sarkar, Rept. Prog. Phys. **59**, 1493 (1996).

In summary, primordial nucleosynthesis has a single adjustable parameter: the baryon density. Observations that led to the determination of primordial abundance of D, ^{3}He and ^{7}Li can determine η. The internal consistency of BBN can then be checked by comparing the abundances of the other nuclides, predicted using this same value of η, with observed abundances. Interestingly, in contrast to the other light nuclides, the BBN-predicted primordial abundance of ^{4}He is very insensitive to the baryon density parameter. Rather, the ^{4}He mass fraction depends on the neutron-to-proton ratio at BBN because virtually all neutrons available at that time are incorporated into ^{4}He. Therefore, while D, ^{3}He, and ^{7}Li are potential baryometers, ^{4}He provides a potential chronometer.

The observationally-inferred primordial fractions of baryonic mass in ^{4}He ($Y_{\rm p} = 0.2472 \pm 0.0012$, $Y_{\rm p} = 0.2516 \pm 0.0011$, $Y_{\rm p} = 0.2477 \pm 0.0029$, and $Y_{\rm p} = 0.240 \pm 0.006$)[13] have been constantly favoring $N_\nu^{\rm eff} \lesssim 3$.[14] Out of the blue, two recent independent studies yield $Y_{\rm p}$ values somewhat higher than previous estimates: $Y_{\rm p} = 0.2565 \pm 0.001({\rm stat}) \pm 0.005({\rm syst})$ and $Y_{\rm p} = 0.2561 \pm 0.011$.[15] For $\tau_n = 885.4 \pm 0.9$ s and $\tau_n = 878.5 \pm 0.8$ s, the updated effective number of light neutrino species is reported as $N_\nu^{\rm eff} = 3.68^{+0.80}_{-0.70}$ (2σ) and $N_\nu^{\rm eff} = 3.80^{+0.80}_{-0.70}$ (2σ), respectively.

The photons in the presently observed CMB were last scattered at $T \sim 3\times10^3$ K, when ions and electrons combined to make hydrogen atoms and the primordial plasma became predominantly neutral.[16] In practice, this takes place at $z \simeq 1100$, some $400,000$ yr after BBN. A key observable quantity inherent of the relic photons is the variation in temperature (or intensity) from one part of the microwave sky to another. Observations show that the CMB contains anisotropies, $\Delta T_\gamma^{\rm CMB}(\theta, \phi)/T_\gamma^{\rm CMB} \lesssim 10^{-5}$, over a wide range

---

[13]Y. I. Izotov, T. X. Thuan and G. Stasinska, Astrophys. J. **662**, 15 (2007); M. Peimbert, V. Luridiana and A. Peimbert, Astrophys. J. **666**, 636 (2007); G. Steigman, Ann. Rev. Nucl. Part. Sci. **57**, 463 (2007).

[14]V. Simha and G. Steigman, JCAP **0806**, 016 (2008).

[15]Y. I. Izotov and T. X. Thuan, Astrophys. J. **710**, L67 (2010); E. Aver, K. A. Olive and E. D. Skillman, JCAP **1103**, 043 (2011); E. Aver, K. A. Olive and E. D. Skillman, JCAP **1005**, 003 (2010).

[16]This is often referred to as the "recombination era" a singularly inappropriate term, for at the time we were considering, the nuclei and electrons had never in the previous history of the universe been combined into atoms!

of angular scales. These anisotropies are usually expressed using a spherical harmonic expansion of the CMB sky

$$T_\gamma^{\text{CMB}}(\theta, \phi) = \sum_{\ell m} a_{\ell m} Y_{\ell m}(\theta, \phi) \,. \tag{6.1.55}$$

The vast majority of the cosmological information is contained in the temperature 2-point function, i.e., the variance as a function of only angular separation, since we notice no preferred direction.

The CMB has a mean temperature of T_γ^{CMB}, which can be considered as the monopole component of CMB maps, a_{00}. Monopole measurements can only be made with absolute temperature devices, such as the FIRAS instrument on the COBE satellite. A blackbody of the measured temperature from (6.1.18) corresponds to

$$\rho_\gamma = \frac{8\pi (k T_\gamma^{\text{CMB}})^4}{15(hc)^3} = 7.56464 \times 10^{-15} (T_\gamma^{\text{CMB}}/\text{K})^4 \text{ erg/cm}^3 \,, \tag{6.1.56}$$

and

$$n_\gamma = \frac{2\zeta(3)}{\pi^2} T_\gamma^{\text{CMB3}} \simeq 411 \text{ cm}^{-3} \,. \tag{6.1.57}$$

(Recall that $1 \text{ J} \equiv 10^7 \text{ erg} = 6.24 \times 10^{18} \text{ eV}$.)

The largest anisotropy is in the $\ell = 1$ (dipole) first spherical harmonic, with amplitude 3.355 ± 0.008 mK. The dipole is interpreted to be the result of the Doppler shift caused by the solar system motion relative to the nearly isotropic blackbody field, as confirmed by measurements of the radial velocities of local galaxies. The motion of an observer with velocity $\beta = v/c$ relative to an isotropic Planckian radiation field of temperature T_0 produces a Doppler-shifted temperature pattern

$$\begin{aligned} T(\theta) &= T_0 \frac{(1 - \beta^2)^{1/2}}{1 - \beta \cos\theta} \\ &\simeq T_0 \left[1 + \beta \cos\theta + (\beta^2/2) \cos(2\theta) + \mathcal{O}(\beta^3) \right] \,. \end{aligned} \tag{6.1.58}$$

At every point in the sky, one observes a blackbody spectrum with temperature $T(\theta)$. The implied velocity for the solar system barycenter is $v = 369.0 \pm 0.9$ km/s, assuming a value $T_0 = T_\gamma^{\text{CMB}}$, towards $(l, b) = (263.99° \pm 0.14°, 48.26°0.03°)$, in galactic coordinates. Such a solar system motion implies a velocity for the Galaxy and the Local Group of galaxies relative

to the CMB. The derived value is $v_{\text{LG}} = 627 \pm 22$ km/s towards $(l, b) = (276° \pm 3°, 30° \pm 3°)$, where most of the error comes from uncertainty in the velocity of the solar system relative to the Local Group. The dipole is a frame-dependent quantity, and one can thus determine the "absolute rest frame" as that in which the CMB dipole would be zero. Our velocity relative to the Local Group, as well as the velocity of the Earth around the Sun and any velocity of the receiver relative to the Earth, is normally removed for the purposes of further CMB anisotropy study.

The variations in the CMB temperature maps at higher multipoles ($\ell \geq 2$) are interpreted as being mostly the result of perturbations in the density of the early universe, manifesting themselves at the epoch of the last scattering of the CMB photons. On sub-degree scales, $100 \lesssim \ell \lesssim 1000$, the rich structure in the anisotropy spectrum is the consequence of gravity-driven acoustic oscillations occurring before the primordial plasma in the universe became neutral. Perturbations inside the horizon at last scattering have been able to evolve causally and produce anisotropy at the last scattering epoch, which reflects this evolution. The frozen-in phases of these sound waves imprint a dependence on the cosmological parameters, which gives CMB anisotropies their great constraining power.

The underlying physics can be understood as follows. Before the universe became neutral, the proton-electron plasma was tightly coupled to the photons, and these components behaved as a single photon-baryon fluid. Perturbations in the gravitational potential dominated by the dark matter component (see Sec. 6.2) were steadily evolving. They drove oscillations in the photon-baryon fluid, with photon pressure providing most of the restoring force and baryons giving some additional inertia. The perturbations were quite small in amplitude, $\mathcal{O}(10^{-5})$, and so evolved linearly. That means each Fourier mode developed independently, and hence can be described by a driven harmonic oscillator with frequency determined by the sound speed in the fluid. Thus the fluid density underwent oscillations, giving time variations in temperature. After the universe (re)combined, the radiation decoupled from the baryons and freely streamed towards us. At that point, the phases of the oscillations were frozen-in and became projected on the sky as a harmonic series of peaks. The physical length scale associated with the peaks is the sound horizon at last scattering. This length is projected onto

the sky, leading to an angular scale that depends on the geometry of space, as well as the distance to last scattering. Hence the angular position and relative heights of the peaks can be used to pull out information about the cosmological parameters (such as the spatial curvature of the universe, the cosmological baryon and dark matter densities, etc.).[17]

The way that we use CMB measurements to determine N_ν^{eff} is relatively simple. The relativistic particles that stream freely influence the CMB in two ways: *(i)* their energy density changing the matter-radiation equality epoch, and *(ii)* their anisotropic stress acting as an additional source for the gravitational potential via Einstein's equations. Incidentally, the relativistic particles that *do not* stream freely, but interact with matter frequently, do not have a significant anisotropic stress because they isotropize themselves via interactions with matter; thus, anisotropic stress of photons before the decoupling epoch was very small. Neutrinos, on the other hand, decoupled from matter much earlier (~ 2 MeV), and thus their anisotropic stress was significant at the decoupling epoch.

The number of light relativistic species becomes a function of the matter density $(\Omega_m h^2)$ and the redshift of matter-radiation equality (z_{eq}),

$$1 + z_{\text{eq}} = \frac{\Omega_m h^2}{\Omega_R h^2} = \frac{\Omega_m h^2}{\Omega_\gamma h^2} \left[1 + \frac{7}{8} \left(\frac{4}{11} \right)^{4/3} N_\nu^{\text{eff}} \right]^{-1}, \qquad (6.1.59)$$

where $\Omega_\gamma h^2 = 2.469 \times 10^{-5}$ is the present-day photon energy density. The variation in N_ν^{eff} reads

$$\frac{\Delta N_\nu^{\text{eff}}}{N_\nu^{\text{eff}}} \simeq 2.45 \, \frac{\Delta(\Omega_m h^2)}{\Omega_m h^2} - 2.45 \, \frac{\Delta z_{\text{eq}}}{1 + z_{\text{eq}}} . \qquad (6.1.60)$$

The equality redshift is one of the fundamental observables that one can extract from the CMB power spectrum. More specifically, WMAP data constrain z_{eq} mainly from the height of the third acoustic peak relative to the first peak.[18] The fractional error in $\Omega_m h^2$ is determined using external data: the latest distance measurements from the Baryon Acoustic Oscillations (BAO) in the distribution of galaxies and precise measurements of the

---

[17] For a thorough introduction to CMB anisotropies, see for example, S. Dodelson, *Modern Cosmology,* (Academic Press, Amsterdam, Netherlands, 2003).

[18] E. Komatsu *et al.* [WMAP Collaboration], Astrophys. J. Suppl. **192**, 18 (2011).

Hubble constant H_0.[19] The parameter constraints from the combination of WMAP 7-year data, BAO, and H_0 lead to $N_\nu^{\text{eff}} = 4.34^{+0.86}_{-0.88}$ (68%CL).

All in all, though significant uncertainties remain, the most recent cosmological observations show a consistent preference for additional relativistic degrees of freedom during BBN and the CMB epochs,

$$\Delta N_\nu^{\text{eff}} = \begin{cases} 0.68^{+0.40}_{-0.35} & (1\sigma) \quad \text{BBN} \\ 1.34^{+0.86}_{-0.88} & (1\sigma) \quad \text{WMAP} + \text{BAO} + H_0 \end{cases} . \qquad (6.1.61)$$

We have seen that in models involving new TeV-scale gauge bosons, the new $U(1)$ symmetry often prevents the generation of Majorana masses, leading to three superweakly interacting right-handed neutrinos. Interestingly, the superweak interactions of these Dirac states (through their coupling to the TeV-scale gauge bosons) tolerate right-handed neutrino decoupling just above the QCD phase transition (180 MeV $\lesssim T_{\nu_R}^{\text{dec}} \lesssim$ 220 MeV). In this intermediate temperature range, the residual temperature ratio between ν_L and ν_R at BBN and at the CMB epochs is such as to generate extra relativistic degrees of freedom consistent (within 1σ) with WMAP observation and the most recent estimate of the primordial ^{4}He mass fraction.[20]

6.2 Dark Matter

6.2.1 Observational Evidence

The earliest, and perhaps still most convincing, evidence for dark matter comes from the observation that various luminous objects (stars, gas, clouds, globular clusters, or entire galaxies) move faster than one would expect if they only felt the gravitational atraction of other visible objects.[21] The classic example is the measurement of galactic rotation curves. The rotational

---

[19]W. J. Percival *et al.* [SDSS Collaboration], Mon. Not. Roy. Astron. Soc. **401**, 2148 (2010); A. G. Riess *et al.*, Astrophys. J. **699**, 539 (2009).

[20]L. A. Anchordoqui and H. Goldberg, arXiv:1111.7264.

[21]F. Zwicky, Helv. Phys. Acta **6**, 110 (1933); V. C. Rubin, N. Thonnard and W. K. . Ford, Astrophys. J. **238**, 471 (1980); K. G. Begeman, A. H. Broeils and R. H. Sanders, Mon. Not. Roy. Astron. Soc. **249**, 523 (1991).

velocity v of an object on a stable Keplerian orbit with radius r around a galaxy scales like $v(r) \propto \sqrt{M(r)/r}$, where $M(r)$ is the mass inside the orbit. If r lies outside the visible part of the galaxy and mass tracks light, one would expect $v(r) \propto 1/\sqrt{r}$. Instead, in most galaxies one finds that v becomes approximately constant out to the largest values of r where the rotation curve can be measured; in our own galaxy, $v \simeq 220$ km/s at the location of our solar system, with little change out to the largest observable radius. This implies the existence of a dark halo, with mass density $\rho(r) \propto 1/r^2$, i.e., $M(r) \propto r$. Of course, at some point ρ will have to fall off faster (in order to keep the total mass of the galaxy finite), but we do not know at what radius this will happen. This leads to a lower bound on the cold dark matter mass density, $\Omega_{\mathrm{CDM}} \gtrsim 0.1$.

The observation of clusters of galaxies tends to give somewhat larger values, $\Omega_{\mathrm{CDM}} \gtrsim 0.2$. A particularly compelling example involves the bullet cluster (1E0657-558), which recently (on cosmological time scales) passed through another cluster. As a result, the hot gas forming most of the clusters baryonic mass was shocked and decelerated, whereas the galaxies in the clusters proceeded on ballistic trajectories. Gravitational lensing shows that most of the total mass also moved ballistically, indicating that dark matter self-interactions are indeed weak.[22]

The most accurate, if somewhat indirect, determination of Ω_{CDM} currently comes from global fits of cosmological parameters. In this regard, the WMAP mission has recently produced sky maps from 7 years of observations. These data rigorously test the standard cosmological model and place constraints on the matter and vacuum energy densities: $\Omega_m = 0.266 \pm 0.26$ and $\Omega_\Lambda = 0.734 \pm 0.029$, respectively.[23] The matter budget has only 3 free parameters: the present day Hubble expansion rate $h_0 = 0.710 \pm 0.025$, the matter density $\Omega_m h_0^2 = 0.1334^{+0.0056}_{-0.0055}$, and the density in baryons, $\Omega_{\mathrm{b}} h_0^2 = 0.02258^{+0.00057}_{-0.00056}$.[24] This confirms that the structure of the

---

[22]D. Clowe, M. Bradac, A. H. Gonzalez, M. Markevitch, S. W. Randall, C. Jones and D. Zaritsky, Astrophys. J. **648**, L109 (2006).

[23]D. Larson *et al.* [WMAP Collaboration], Astrophys. J. Suppl. **192**, 16 (2011).

[24]The latter is consistent with the estimate from BBN, based on measurements of deuterium in high redshift absorption systems, $\Omega_{\mathrm{b}} h^2 = 0.020 \pm 0.002$. S. Burles, K. M. Nollett and M. S. Turner, Astrophys. J. **552**, L1 (2001); R. H. Cyburt, B. D. Fields and

universe is dictated by the physics of as-yet-undiscovered cold dark matter $(\Omega_{\mathrm{CDM}} h^2 = 0.1109 \pm 0.0056)$ and the galaxies we see today are the remnants of relatively small overdensities in the nearly uniform distribution of matter in the very early universe.

The particle (or particles) that make up most of the dark matter must be stable, at least on cosmological time scales, and non-baryonic, so that they do not disturb the subprocesses of BBN. They must also be cold or warm to properly seed structure formation, and their interactions must be weak enough to avoid violating current bounds from dark matter searches.[25] Among the plethora of dark matter candidates, weakly interacting massive particles (WIMPs) represent a particularly attractive and well-motivated class of possibilities. This is because they combine the virtues of weak scale masses and couplings and their stability often follows as a result of discrete symmetries that are mandatory to make electroweak theory viable, independent of cosmology (see Appendix J). Moreover, WIMPs are naturally produced with the cosmological densities required of dark matter.[26] It is this that we now turn to study.

6.2.2 WIMP Relic Density

Generic WIMPs were once in thermal equilibrium, but decoupled while strongly non-relativistic. Consider a particle χ (of mass m_χ) in thermal equilibrium in the early universe. The evolution of the number density as the universe expands is driven by Boltzmann's equation,

$$\frac{dn_\chi}{dt} + 3H(T)\, n_\chi = -\langle \sigma v \rangle (n_\chi^2 - n_\chi^{\mathrm{eq}2})\,, \qquad (6.2.62)$$

where n_χ is the number density of WIMPs, n_χ^{eq} is the equilibrium number density, and $\langle \sigma v \rangle$ is the thermally averaged annihilation cross section of the χ particles multiplied by their relative velocity. The product σv is usually

K. A. Olive, Phys. Lett. B **567**, 227 (2003).

[25]G. Bertone, D. Hooper and J. Silk, Phys. Rept. **405**, 279 (2005); J. L. Feng, Annals Phys. **315**, 2 (2005).

[26]R. J. Scherrer and M. S. Turner, Phys. Rev. D **33**, 1585 (1986) [Erratum-ibid. D **34**, 3263 (1986)]; K. Griest, M. Kamionkowski and M. S. Turner, Phys. Rev. D **41**, 3565 (1990).

referred to as the *annihilation cross section*, with the velocity implied. At equilibrium, (6.1.15) gives the number density of a non-relativistic species

$$n_\chi^{\rm eq} = g_\chi \left(\frac{m_\chi T_\chi}{2\pi} \right)^{3/2} e^{-m_\chi/T_\chi} \tag{6.2.63}$$

where g_χ is the number of internal degrees of freedom of the WIMP particle. Note that in the very early universe, when $n_\chi \simeq n_\chi^{\rm eq}$, the right hand side of Eq. (6.2.62) is small and the evolution of the density is dominated by Hubble expansion. As the temperature falls below m_χ, however, the equilibrium number density becomes suppressed and the annihilation rate increases, rapidly reducing the number density. Finally, when the number density falls enough, the rate of depletion due to expansion becomes greater than the annihilation rate and the χ particles freeze-out of thermal equilibrium. Defining freeze-out temperature to be the time when $n_\chi \langle \sigma v \rangle = H$, we have

$$\frac{T_\chi^{\rm FO}}{m_\chi} \equiv \frac{1}{x_{\rm FO}} \simeq \left[\ln \left(\sqrt{\frac{45}{8}} \frac{g_\chi}{2\pi^3} \frac{m_\chi M_{\rm Pl} \langle \sigma v \rangle}{\sqrt{x_{\rm FO} \, N(T_\chi^{\rm FO})}} \right) \right]^{-1}. \tag{6.2.64}$$

When solved by integration, for weak scale cross sections and masses, one obtains $x_{\rm FO} \simeq 20 - 30$. Recall that $m_\chi v^2/2 = 3T/2$, and so WIMPs freeze-out with velocity $v \sim 0.3$. In (6.2.64) we have taken a typical weak cross section derived from dimensional analysis

$$\sigma \sim \left(\frac{g^2}{4\pi} \right) \frac{1}{M_{\rm W}^2} \sim 10^{-8} \ {\rm GeV}^{-2} \,, \tag{6.2.65}$$

with $g \simeq 0.65$ and $M_{\rm W} = (G_F)^{-1/2} \simeq 300$ GeV. Freeze-out temperatures 5 GeV $< T_\chi^{\rm FO} <$ 80 GeV correspond to WIMPs with 100 GeV $< m_\chi <$ 1500 GeV. Adding up the standard model degrees of freedom lighter than 80 GeV leads to $N(T_\chi^{\rm FO}) = 92$. (For a very heavy or very light WIMP, this number may change somewhat, but is not expected to significantly modify the result.) Altogether,

$$\langle \sigma v \rangle \sim 3 \times 10^{-9} \ {\rm GeV}^{-2} \simeq 3 \times 10^{-26} \ {\rm cm}^3/{\rm s} \,. \tag{6.2.66}$$

After freeze-out, the density of χ particles that remain is given by

$$\Omega_\chi h^2 = \frac{\rho_\chi}{\rho_c} = \frac{m_\chi n_\chi}{\rho_c} \simeq \frac{10^9 \ {\rm GeV}^{-1}}{M_{\rm Pl}} \frac{x_{\rm FO}}{\sqrt{N(T_{\rm FO})}} \frac{1}{\langle \sigma v \rangle} \,. \tag{6.2.67}$$

215

Numerically, this expression yields

$$\Omega_\chi h^2 \sim 0.1 \times \frac{3 \times 10^{-26} \, \text{cm}^3/\text{s}}{\langle \sigma v \rangle}. \qquad (6.2.68)$$

Thus we see that the observed cold dark matter density ($\Omega_{\text{CDM}} h^2 \simeq 0.1$) can be obtained for a thermal relic with weak scale interactions.

Using direct and indirect detection methods, the hypothesis that relic WIMPs are the constituents of dark matter halos can be experimentally verified for the local dark matter halo of our Galaxy.

6.2.3   WIMP Detection Schemes

When our galaxy was formed the cold dark matter inevitably clustered with the luminous matter to form a sizeable fraction of the

$$\rho_\chi = 0.4 \, \text{GeV}/\text{cm}^3 \qquad (6.2.69)$$

galactic matter density implied by observed rotation curves. Unlike the baryons, the dissipationless WIMPs fill the galactic halo which is believed to be an isothermal sphere of WIMPs with average velocity

$$v_\chi = 300 \, \text{km}/\text{s} \,. \qquad (6.2.70)$$

In summary, we know everything about these particles (except whether they really exist!). We know that their mass is of order of the weak boson mass; we know that they interact weakly. We also know their density and average velocity in our Galaxy given the assumption that they constitute the dominant component of the density of our galactic halo as measured by rotation curves.

For a first look at the experimental problem of how to detect these particles it is sufficient to recall that they are weakly interacting with masses in the range

$$\text{tens of GeV} < m_\chi < \text{several TeV} \,. \qquad (6.2.71)$$

WIMPs have a mass of order the weak boson mass, in the tens of GeV to several TeV range. Lower masses are excluded by accelerator and (in)direct

searches with existing detectors while masses beyond several TeV are excluded by cosmological considerations. Two general techniques, referred to as direct (D) and indirect (ID), are pursued to demonstrate the existence of WIMPs. In direct detectors one observes the energy deposited when WIMPs elastically scatter off nuclei. The indirect method infers the existence of WIMPs from observation of their annihilation products. WIMPs will annihilate into neutrinos which can be detected in a generic Cherenkov detector which measures the direction and, to some extent, the energy of a secondary muon produced by a neutrino of WIMP origin in or near the instrument.

A series of first-generation experiments have demostrated that high energy neutrinos with $\sim$ 100 GeV energy and above can be detected by observing the Cherenkov radiation from secondary particles produced in neutrino interactions inside large volumes of highly transparent ice or water instrumented with a lattice of photomultiplier tubes. The IceCube neutrino telescope, deployed near the Amundsen-Scott station, is the first second-generation detector. This facility comprises a cubic-kilometer of ultra-clear ice instrumented with long strings of sensitive photon detectors which record light produced when neutrinos interact in the Antarctic ice-cap. The In-ice array is complemented by IceTop, a surface air shower detector consisting of frozen water tanks, which serve as a veto for atmospheric muon background. The IceCube DeepCore sub-array is being built to expand the neutrino energy threshold by an order of magnitude, to energies as low as about 10 GeV. With its lower neutrino energy threshold, DeepCore will have sensitivity to WIMP masses 2-3 times lighter than the standard IceCube array.

The indirect detection is greatly facilitated by the fact that the sun represents a dense and nearby source of accumulated cold dark matter particles. Galactic WIMPs, scattering off nuclei in the sun, lose energy. They may fall below escape velocity and be gravitationally trapped. Trapped WIMPs eventually come to equilibrium temperature and accumulate near the center of the sun. While the WIMP density builds up, their annihilation rate into lighter particles increases until equilibrium is achieved where the annihilation rate equals half of the capture rate. The sun has thus become a reservoir of WIMPs which we expect to annihilate mostly into heavy quarks and, for the heavier WIMPs, into weak bosons. The leptonic decays of the heavy quark and weak boson annihilation products turn the sun into a source of

217

high-energy neutrinos with energies in the GeV to TeV range, rather than in the keV to MeV range typical for neutrinos from thermonuclear burning.

The performance of future detectors is determined by the rate of elastic scattering of WIMPs in a low-background, germanium detector and, for the indirect method, by the flux of solar neutrinos of WIMP origin. Both are a function of WIMP mass and of their elastic cross section on nucleons. In standard cosmology WIMP capture and annihilation interactions are weak, and we will suggest that, given this constraint, dimensional analysis is sufficient to compute the scattering rates in germanium detectors as well as the neutrino flux from the measured WIMP density in our galactic halo. We derive and compare rates for direct and indirect detection of weakly interacting particles with mass $m_\chi \simeq m_W$ assuming:

- that WIMPs represent the major fraction of the measured halo density, i.e.

$$\phi_\chi = n_\chi v_\chi = \frac{0.4 \text{ GeV}}{m_\chi \text{ cm}^3} \, 3 \times 10^6 \frac{\text{cm}}{\text{s}} = \frac{1.2 \times 10^7}{m_{\chi\,\text{GeV}}} \text{ cm}^{-2}\text{s}^{-1} \,, \quad (6.2.72)$$

where $m_{\chi\,\text{GeV}} \equiv (m_\chi/1 \text{ GeV})$ is in GeV units;

- a WIMP-nucleon interaction cross section based on dimensional analysis

$$\sigma(\chi N) = \left(G_F m_N^2\right)^2 \frac{1}{m_W^2} \equiv \sigma_{\text{DA}} = 6 \times 10^{-42} \text{ cm}^2 \,; \quad (6.2.73)$$

- that WIMPs annihilate 10% of the time in neutrinos (this is just the leptonic branching ratio of the final state particles in the dominant annihilation channels $\chi\bar{\chi} \to W^+W^-$ or $Q\bar{Q}$, where Q is a heavy quark).

Clearly the cross section for the interaction of WIMPs with matter is uncertain. Arguments can be invoked to raise or decrease it. Important points are that *(1)* our choice represents a typical intermediate value, *(2)* all our results for event rates scale linearly in the cross section and can be easily reinterpreted, and *(3)* the comparison of direct and indirect event rates is independent of the choice.

Our conclusions will not be surprising. We find that the direct method is superior if the WIMP interacts coherently and, if its mass is lower or comparable to the weak boson mass m_W. In all other cases, i.e. for relatively heavy WIMPs and for all WIMPs interacting incoherently, the indirect method is competitive or superior. Especially for heavier WIMPs the indirect technique is powerful because underground high energy neutrino detectors have been optimized to be sensitive in the energy region where the neutrino interaction cross section and the range of the muon are large. The IceCube + DeepCore facility (with effective area $\sim 10^6$ m^2 and with appropriately low threshold) can probe WIMP masses up to the TeV-range, beyond which they are excluded by cosmological considerations.

For high energy neutrinos the muon and neutrino are aligned, with good angular resolution, along a direction pointing back to the sun. The number of background events of atmospheric neutrino origin in the pixel containing the signal will be small. The angular spread of secondary muons from neutrinos coming from the direction of the sun is well described by the relation $\sim 1.2°\left/\sqrt{E_\mu(\text{TeV})}\right.$.[27] Measurement of muon energy, which may be only up to order of magnitude accuracy in some experiments, can be used to infer the WIMP mass from the angular spread of the signal. The spread contains information on the neutrino energy and, therefore, the WIMP mass. More realistically, measurement of the muon energy can be used to reduce the search window around the sun, resulting in a reduced background.

Our analysis will quantify all statements above in a simple and totally transparent framework. It finesses all detailed dynamics and gives answers that are sufficiently accurate considering that the mass of the particle has not been pinned down.

The number of solar neutrinos of WIMP origin can be calculated in 5 easy steps by determining

- the capture cross section in the sun, which is given by the product of the number of target nucleons in the sun and the elastic scattering cross section

$$\sigma_\odot = f\left[1.2 \times 10^{57}\right]\sigma_{\text{DA}} \ . \tag{6.2.74}$$

[27] T. K. Gaisser, F. Halzen and T. Stanev, Phys. Rept. **258**, 173 (1995) [Erratum-ibid. **271**, 355 (1996)].

This includes a focussing factor f given, as usual, by the ratio of kinetic and potential energy of the WIMP near the sun. It enhances the capture rate by a factor 10;

- the WIMP flux from the sun which is given by

$$\phi_\odot = \phi_\chi \sigma_\odot / 4\pi d^2 \ , \tag{6.2.75}$$

where $d = 1$ a.u. $= 1.5 \times 10^{13}$ cm;

- the actual neutrino flux, which is obtained after inclusion of the branching ratio. From (6.2.72),(6.2.73) and (6.2.74),(6.2.75)

$$\phi_\nu = 10^{-1} \times \phi_\odot = \frac{3 \times 10^{-5}}{m_{\chi\,\mathrm{GeV}}} \ \mathrm{cm}^{-2}\,\mathrm{s}^{-1} \ ; \tag{6.2.76}$$

- the probability to detect the neutrino, which is proportional to

$P = \rho \sigma_\nu R_\mu$, with

$\rho = $ Avagadro $\# = 6 \times 10^{23}$

$\sigma_\nu = $ neutrino interaction cross section $= 0.5 \times 10^{-38} E_{\nu,\mathrm{GeV}}$ cm^2

$R_\mu = $ muon range $= 500$ cm $E_{\mu,\mathrm{GeV}}$,

yielding
$$P = 2 \times 10^{-13}\, m_{\chi\,\mathrm{GeV}}^2 \tag{6.2.77}$$

Here we assumed the kinematics of the decay chain

$$\chi\bar{\chi} \ \rightarrow \ W^+ W^- \\ \phantom{\chi\bar{\chi} \ \rightarrow \ W^+} {\llcorner\!\rightarrow} \mu\nu_\mu$$

with $E_\nu = m_\chi/2$ (this would be $m_\chi/3$ for Q decay) and $E_\mu = E_\nu/2 = m_\chi/4$;

- finally,

$$dN_{\mathrm{ID}}/dA = \phi_\nu P = 1.8 \times 10^{-6}\, m_{\chi\,\mathrm{GeV}} \ (\mathrm{year})^{-1}\, (\mathrm{m}^2)^{-1} \tag{6.2.78}$$

where dN_{ID}/dA represents the number of events from the sun per unit area (m^2) detected by a neutrino telescope.

The linear rise of σ_ν, R_μ with energy, which are the origin of the good detection capability of neutrino telescopes for large WIMP masses, are valid approximations up to

$$E_\nu \simeq \frac{m_\chi}{2} \gtrsim \frac{m_W^2}{m_N} \quad \text{and} \quad E_\mu \simeq \frac{m_\chi}{4} \gtrsim 500 \text{ GeV}, \qquad (6.2.79)$$

so the approximations are valid for m_χ well into the TeV mass range. This is sufficient as $m_\chi \gg 1$ TeV is cosmologically unacceptable.

The event rate in a direct detector is proportional to the WIMP cross section, flux and the density of targets m_N^{-1}, i.e.

$$\frac{dN_D}{dM} = \frac{1}{m_N}\phi_\chi \sigma_{DA}, \qquad (6.2.80)$$

where dN_D/dM represents the number of direct events per unit of target mass.

We can now summarize our results so far by comparing a 10^4 m^2 first generation neutrino detector (e.g., AMANDA) with a kilogram of hydrogen:

$$
\begin{aligned}
dN_{ID}/dA &= 1.8 \times 10^{-2} m_{\chi\,\text{GeV}} \, (10^4\,\text{m}^2)^{-1}(\text{year})^{-1} \\
dN_D/dM &= \frac{1.4}{m_{\chi\,\text{GeV}}} \, (\text{kg})^{-1}\,(\text{year})^{-1} \\
\frac{dN_D/dM}{dN_{ID}/dA}\left(\frac{10^4\,\text{m}^2}{\text{kg}}\right) &= \frac{7.8 \times 10^1}{m_{\chi\,\text{GeV}}^2}.
\end{aligned}
\qquad (6.2.81)
$$

Direct detection is superior only in the mass range $m_\chi < 10$ GeV, but this region is, arguably, ruled out by previous searches. Indirect detection is the preferred technique. This straightforward conclusion may, however, be invalidated when WIMPs interact coherently and targets other than hydrogen are considered.

The coherent enhancement factor for a nucleus A, including a factor A^{-1} for the target density, is given by

$$
\begin{aligned}
N(A) &= \frac{1}{A}\frac{A^2(Am_N)^2 m_\chi^2}{(Am_N + m_\chi)^2}\frac{(m_N + m_\chi)^2}{m_N^2 m_\chi^2} \\
&= A^3 \frac{(m_N + m_\chi)^2}{(Am_N + m_\chi)^2} \\
&= A^3 \left[\frac{1 + \frac{m_\chi}{m_N}}{A + \frac{m_\chi}{m_N}}\right]^2.
\end{aligned}
\qquad (6.2.82)
$$

After inclusion of above coherence factors in Eq. (6.2.81), the ratio of direct to indirect events (which is independent of the WIMP-nucleon cross section) can be summarised by the following equation:

$$\frac{dN_{\mathrm{D}}/dM}{dN_{\mathrm{ID}}/dA} \simeq \frac{7.8 \times 10^1}{m_{\chi\,\mathrm{GeV}}^2} \frac{N(A_{\mathrm{D}})}{N(A_{\mathrm{ID}})\,[\rho(A_{\mathrm{ID}})/\rho(H)]}. \tag{6.2.83}$$

As in Eq. (6.2.81) the units are $10^4\,\mathrm{m}^2/\mathrm{kg}$. A_{D} and A_{ID} are the atomic numbers appropriate for the nuclei involved in the direct detection and capture in the sun, respectively. The latter is weighted by its relative mass abundance $[\rho(A_{\mathrm{ID}})/\rho(H)]$ in the sun and a summation over elements is understood. Because of additional nuclear form factor effects, which are neglected in (6.2.83), it is adequate to consider oxygen, with a solar abundance of $\rho(A_{\mathrm{ID}})/\rho(H) = 0.011$ and $A_{\mathrm{ID}} = 16$, as a "typical" element.

Our simple evaluations, made so far, overestimate the indirect rates for very heavy WIMPS because high energy neutrinos, created by annihilation near the core, may be absorbed in the sun. Absorption is stronger for neutrinos and, therfore, mostly antineutrinos form the signature for very heavy WIMPS. The probability that an antineutrino escapes without absorption is well parametrized by $(1 + 3.8 \times 10^{-4} E_\nu)^{-7}$, where $E_\nu \simeq m_\chi/2$. The final rates for indirect detection are

$$
\begin{aligned}
dN_{\mathrm{ID}}/dA \quad \simeq \quad & \left\{1.8 \times 10^{-2} m_{\chi\,\mathrm{GeV}}\right\} \left\{0.011 A^3 \left[\frac{1 + \frac{m_\chi}{m_N}}{A + \frac{m_\chi}{m_N}}\right]^2\right\} \\
\times \quad & \left\{1 + 1.9 \times 10^{-4} m_{\chi\,\mathrm{GeV}}\right\}^{-7}.
\end{aligned}
\tag{6.2.84}
$$

Next, we estimate backgrounds. For the indirect detection the background event rate is determined by the flux of atmospheric neutrinos in the detector coming from a pixel around the sun. The number of events in a $10^4\,\mathrm{m}^2$ detector is $\sim 10^2/E_\mu(\mathrm{TeV})$ and the pixel size is determined by the angle between muon and neutrino $\sim 1.2^\circ \big/ \sqrt{E_\mu(\mathrm{TeV})}$. Using the kinematics $E_\mu \simeq m_\chi/4$ we obtain

$$B_{\mathrm{ID}} = \frac{10^2/E_\mu(\mathrm{TeV})}{2\pi \Big/ \left[\frac{1.2^\circ \frac{\pi}{180^\circ}}{\sqrt{E_\mu(\mathrm{TeV})}}\right]^2} = \frac{1.1 \times 10^5}{m_{\chi\,\mathrm{GeV}}^2} \text{ per } 10^4\,\mathrm{m}^2 \text{ per year}$$

This is only valid for large m_χ, i.e. for $E_\mu \cong m_\chi/4 > 100$ GeV. Estimates of background event rates without this approximation are given in Table 6.2. For large m_χ the signal to background ratio is

Table 6.2: *Indirect background.*

E_μ(GeV)	# bkgd. events in 10^4 m^2 in 2π	# pixels of solar size in 2π	bkgd. events per 10^4 m^2 per pixel, per year
10	3200	140	23
100	1060	1.4×10^3	0.8
1000	110	1.4×10^4	8×10^{-3}

$$\left(\frac{N}{B}\right)_{\text{ID}} \equiv \frac{dN_{\text{ID}}/dA}{dB_{\text{ID}}/dA} \simeq 7.2 \times 10^{-6} m_{\chi\,\text{GeV}}^3 \qquad (6.2.85)$$

Clearly, the extremely optimistic predictions for signal-to-noise are unlikely to survive the realities of experimental physics. One expects, typically, to measure muon energy only to order-of-magnitude accuracy in the initial experiments. The energy of showers initiated by electron neutrinos should be determined to a factor 2. It is not excluded that future, dedicated experiments may do better. The conclusion that high energy muons pointing at the sun represents a superb signature, is unlikely to be invalidated.

For direct detection experiments the background is estimated to be about 300 events per year per kg.[28] Signal-to-noise therefore exceeds unity up to 2 TeV WIMP mass.

The relative merits of the two methods are summarised in Table 6.3, which establishes that a kilogram of germanium and a 10^4 m^2 are competitive.

We conclude that the direct method yields more events for the lower masses, even when compared to a 10^6 m^2 detector like IceCube. As expected, the indirect method is competitive for heavier WIMPs with a detection rate growing like E_ν^2 or m_χ^2. A 10^5 m^2 covers the full WIMP mass range, even if the WIMPs do not coherently interact with nuclei in the sun. These conclusions are reinforced after considering the signal-to-noise for both techniques. Our final results are encapsulated in Fig. 6.3.

---

[28]G. Jungman, M. Kamionkowski and K. Griest, Phys. Rept. **267**, 195 (1996).
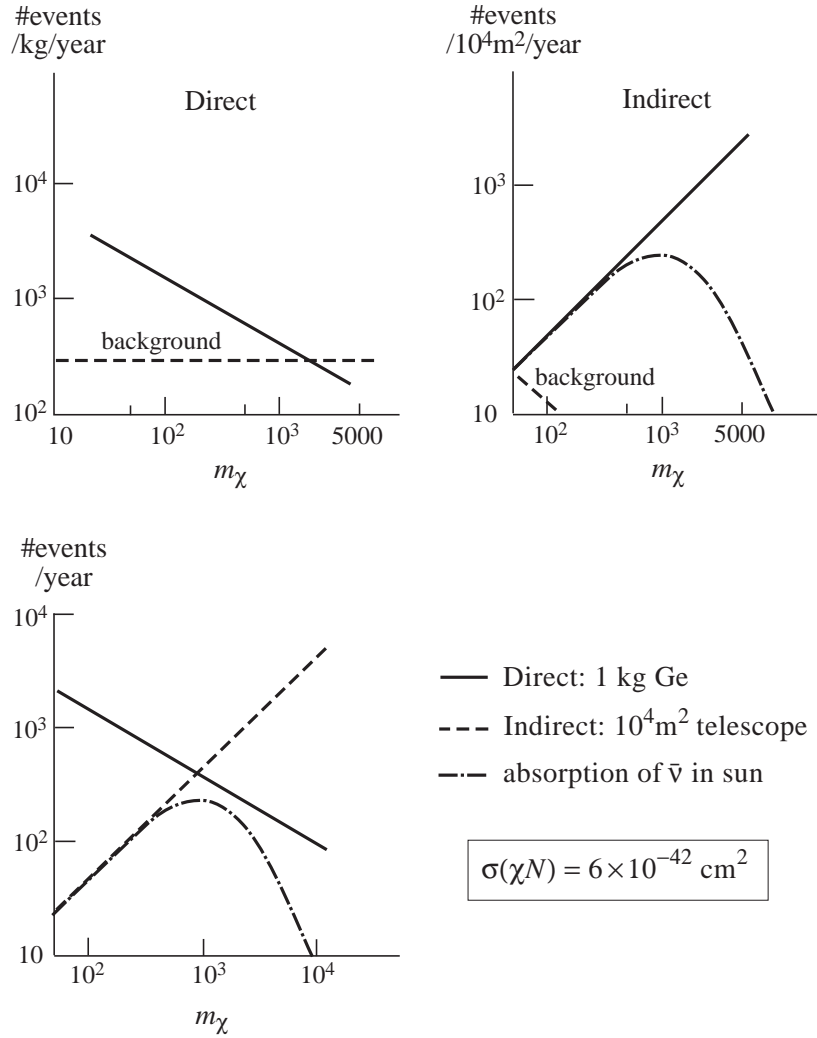
Figure 6.3: *The results shown are for $\sigma(\chi N) = 6 \times 10^{-42}$ cm^2. All event rates scale linearly in $\sigma(\chi N)$. The relative direct and indirect rates are independent of $\sigma(\chi N)$.*

Table 6.3: *Event rates and signal to background* (N/B).

m_χ (GeV)	Direct (/kg/year)		Indirect (/$10^4\,\mathrm{m}^2$/year)	
	events	N/B	events	N/B
50	2.2×10^3	7	2.3×10^1	$\simeq 1$
500	1.1×10^3	7	2×10^2	$\simeq 10^2$
2000	2.9×10^2	1	1.7×10^2	$\simeq 10^4$

We emphasize that above considerations are valid for the specific and much studied example where the lightest supersymmetric particle is Nature's WIMP. Clearly dynamics, which is now defined, can alter our conclusions, but only in "conspiratorial" ways. Dynamics can, on the other hand, increase rates as well, sometimes by well over an order of magnitude, over and above the rates obtained from dimensional analysis in this paper. Our qualitative conclusions are valid, at least in some average sense, in SUSY.

We feel that the development of detectors should be guided by an analysis like ours rather than by dynamics of theories beyond the standard model for which there is, at present, no experimental guidance.

The sensitivity of direct detection experiments has been improving at a steady rate. The data collected by the Cryogenic Dark Matter Search (CDMS-II) experiment and the XENON100 detector currently have produced the strongest limits on the coherent elastic scattering cross section.[29] These data exclude coherent elastic scattering cross sections larger than approximately 8×10^{-45} cm^2 for a 50 GeV WIMP and 5×10^{-44} cm^{-2} $(m_\chi/500 \text{ GeV})$ for a heavier WIMP. It is noteworthy that the allowed region of the parameter space is well below the weak-scale cross section σ_{DA}. The state of affairs is different for incoherent scattering. Even with data analyzed from only 22 of the 86 strings deployed, the IceCube Collaboration established the most stringent limit on WIMP incoherent interactions. For WIMP masses of about 500 GeV, cross sections larger than 2×10^{-40} cm^2 and 2×10^{-38} cm^2 are excluded at the 90%CL on the assumption of hard (W^+W^-) and soft $(Q\bar{Q})$ annihilation channels, respectively.[30]

[29]Z. Ahmed *et al.* [CDMS-II Collaboration], Science **327**, 1619 (2010); E. Aprile *et al.* [XENON100 Collaboration], Phys. Rev. Lett. **105**, 131302 (2010).

[30]R. Abbasi *et al.* [IceCube Collaboration], Phys. Rev. Lett. **102**, 201302 (2009).

6.3 Lookahead

Shielded at the nexus of particle physics, astrophysics, and cosmology grows one of the most compelling mysteries that faces physics today: that of unravelling the identity and properties of dark matter. From measurements of galactic rotation curves and velocity dispersions to observations of the gravitational lensing of galaxy clusters and the detection of specific acoustic peaks of the CMB, ample circumstantial evidence suggests that most of the matter in the universe does not interact strongly or electromagnetically. Such matter is therefore electrically neutral (dark) and presumed non-relativistic (cold). Beyond these properties, however, very little is known about the nature of dark matter.

To expose the identity of dark matter, it is necessary to measure its non-gravitational couplings. Many approaches have been developed to attempt to detect dark matter. Such endeavors include direct detection experiments that hope to observe the scattering of dark matter particles with the target material of the detector and indirect detection experiments, which are designed to search for the products of WIMP annihilation into gamma-rays, anti-matter, and neutrinos. In addition, particle accelerators of the next generation, such as the LHC, may have enough energy to directly produce WIMPs. Once produced, WIMPs would escape the detector without interactions, leading to an apparent energy imbalance, or "missing energy" signature. Monojets and final states with multiple jets plus $\displaystyle{\not}E_T$ could become the smoking gun for dark matter hunters. Should we be so lucky, the coming years of exploration will not only provide our first incisive probe of the Fermi scale, but they will no doubt open a wondrous new view of the cosmos, its contents, and its evolution.

Appendix A

Decay Rate in Terms of $\mathfrak{M}$

In nonrelativistic quantum mechanics, an unstable atomic state shows up in scattering experiments as a resonance. Such an unstable particle decays according to the exponential law,

$$|\psi(t)|^2 = |\psi(0)|^2 e^{-\Gamma t}, \tag{A.0.1}$$

where $\tau \equiv 1/\Gamma$ is called the lifetime of the state. (The particle half-life is $\tau \ln 2$.) Thus, the time dependence of $\psi(t)$ for an unstable state must include the decay factor $\Gamma/2$; that is

$$\psi(t) \sim e^{-iMt} e^{-\Gamma t/2}, \tag{A.0.2}$$

where M is the rest mass energy of the state. As a function of the center-of-mass energy E of the system, the state is described by the Fourier transform

$$\chi(E) = \int \psi(t) e^{iEt} dt \tag{A.0.3}$$

$$\sim \frac{1}{E - M + (i\Gamma/2)}; \tag{A.0.4}$$

the experimenter thus sees a reaction rate of the form

$$|\chi(E)|^2 \propto \frac{1}{(E - M)^2 + (\Gamma/2)^2}. \tag{A.0.5}$$

This function has a sharp peak centered at M with a width determined by Γ. In the narrow-width-approximation (A.0.5) becomes

$$|\chi(E)|^2 \propto \frac{(\Gamma/2\pi)}{(E-M)^2 + (\Gamma/2)^2} \frac{2\pi}{\Gamma} = \frac{2\pi}{\Gamma} \, \delta(E-M) \, . \qquad \text{(A.0.6)}$$

The Breit-Wigner formula (A.0.4) also applies in relativistic quantum mechanics.[1] In particular, it gives the scattering amplitude for processes in which initial particles combine to form an unstable particle, which then decays. The unstable particle viewed as an excited state of the vacuum, is a direct analogue of the unstable non-relativistic atomic state. Particles that decay by strong interactions do not live long enough to leave tracks in an experimentalist's detector. Rather, they are identified by tracking their decay products. The mass of the decaying particle is the total energy of these products as measured in its rest frame. Due to its short lifetime, the uncertainty in its mass ($\sim \hbar/\Delta t$) is sufficiently large to be directly observable. For example, in πp scattering, the Δ^{++} is formed and rapidly ($\tau \sim 10^{-23}$ s) decays, $\pi p \to \Delta^{++} \to \pi^+ p^+$. The *decay rate* of the Δ^{++} (assumed to be at rest) is

$$\Gamma \equiv \frac{\text{Number of decays per unit time}}{\text{Number of } \Delta^{++} \text{ particles present}} \, . \qquad \text{(A.0.7)}$$

Hence, the differential rate for the decay $\Delta^{++} \to \pi^+ p$ into momentum elements $d^3 p_{\pi^+}$, $d^3 p_p$ of the final state particles is

$$d\Gamma = \frac{1}{2E_\Delta^{++}} \, |\mathfrak{M}|^2 \, \frac{d^3 p_{\pi^+}}{(2\pi)^3 2E_{\pi^+}} \frac{d^3 p_p}{(2\pi)^3 2E_p} \, (2\pi)^4 \, \delta^{(4)}(p_\Delta^{++} - p_{\pi^+} - p_p) \, , \quad \text{(A.0.8)}$$

where $2E_\Delta^{++}$ is the number of decaying particles per unit volume and $\mathfrak{M}$ is the invariant amplitude which has been computed from the relevant Feynman diagram. The formula has the form of (3.1.20). In 1952, using a beam of π^+ with varying amounts of energy directed through a hydrogen target (protons), Fermi found that the number of interactions (π^+ scattered) when plotted versus the pion kinetic energy has a prominent peak around 200 MeV, with $\Gamma \sim 100$ MeV.[2]

---

[1] G. Breit and E. Wigner, Phys. Rev. **49**, 519 (1936).

[2] H. L. Anderson, E. Fermi, E. A. Long and D. E. Nagle, Phys. Rev. **85**, 936 (1952).

Appendix B

Trace Theorems and Properties of γ-Matrices

Using (1.5.58) the trace of a product of γ-matrices can be evaluated without ever explicitly calculating a matrix product. The trace of one γ matrix is easy,

$$
\begin{aligned}
\mathrm{Tr}(\gamma^\mu) &= \mathrm{Tr}(\gamma^5 \gamma^5 \gamma^\mu) && \text{because } (\gamma^5)^2 = \mathbb{1} \\
&= -\mathrm{Tr}(\gamma^5 \gamma^\mu \gamma^5 && \text{because} \\
&= -\mathrm{Tr}(\gamma^5 \gamma^5 \gamma^\mu) && \text{using cyclic property of trace} \\
&= -\mathrm{Tr}(\gamma^\mu) \,.
\end{aligned}
$$

The trace theorems are (using again the notation $\not{a} = \gamma_\mu a^\mu$):

- Tr $\mathbb{1} = 4$

- Trace of an odd number of γ_μ's vanishes.

  $\mathrm{Tr}(\not{a}_1 \ldots \not{a}_n) = \mathrm{Tr}(\not{a}_1 \ldots \not{a}_n \gamma^5 \gamma^5)$; now, the anticonmmutation relation $\{\gamma^\mu, \gamma^5\} = 0$ leads to: $(-1)^n \, \mathrm{Tr}(\gamma^5 \not{a}_1 \ldots \not{a}_n \gamma^5) = (-1)^n \, \mathrm{Tr}(\not{a}_1 \ldots \not{a}_n)$. Therefore, if n is odd, $\mathrm{Tr}(\not{a}_1 \ldots \not{a}_n) = 0$.

- $\mathrm{Tr}(\not{a} \not{b}) = 4\, a \cdot b$

  $\mathrm{Tr}(\not{a} \not{b}) = \frac{1}{2}\mathrm{Tr}(\not{a} \not{b} + \not{b} \not{a}) = \frac{1}{2}2g^{\mu\nu}a_\mu b_\nu \mathrm{Tr}(\mathbb{1}) = 4\, a \cdot b.$

- $\mathrm{Tr}(\not{a}\,\not{b}\,\not{c}\,\not{d}) = 4[(a \cdot b)(c \cdot d) - (a \cdot c)(b \cdot d) + (a \cdot d)(b \cdot c)]$

$$
\begin{aligned}
\mathrm{Tr}(\not{a}\,\not{b}\,\not{c}\,\not{d}) &= \mathrm{Tr}[(-\not{b}\,\not{a} + 2a \cdot b)\,\not{c}\,\not{d}] \\
&= 2a \cdot b\,\mathrm{Tr}(\not{c}\,\not{d}) - \mathrm{Tr}(\not{b}\,\not{a}\,\not{c}\,\not{d}) \\
&= 8(a \cdot b)(c \cdot d) - 2a \cdot c\,\mathrm{Tr}(\not{a}\,\not{b}) + \mathrm{Tr}(\not{b}\,\not{c}\,\not{a}\,\not{d}) \\
&= 8(a \cdot b)(c \cdot d) - 8(a \cdot c)(b \cdot d) + 8(a \cdot d)(b \cdot c) \\
&\quad - \mathrm{Tr}(\not{b}\,\not{c}\,\not{d}\,\not{a}) \,.
\end{aligned}
$$

Hence, $\mathrm{Tr}(\not{a}\,\not{b}\,\not{c}\,\not{d}) = 4[(a \cdot b)(c \cdot d) - (a \cdot c)(b \cdot d) + (a \cdot d)(b \cdot c)]$.

- $\mathrm{Tr}(\gamma_5) = 0$

$\mathrm{Tr}(\gamma_5) = \mathrm{Tr}(\gamma^0 \gamma^0 \gamma^5) = -\mathrm{Tr}(\gamma^0 \gamma^5 \gamma^0) = -\mathrm{Tr}(\gamma^0 \gamma^0 \gamma^5) = -\mathrm{Tr}(\gamma^5)$.

- $\mathrm{Tr}(\gamma_5\,\not{a}\,\not{b}) = 0$ \hfill (B.0.1)

$$
\begin{aligned}
\mathrm{Tr}(\gamma_5\,\not{a}\,\not{b}) &= \mathrm{Tr}(i\gamma^0 \gamma^1 \gamma^2 \gamma^3 \gamma^\mu \gamma^\nu)\,a_\mu b_\nu \\
&= [-2ig^{0\mu}\mathrm{Tr}(\gamma^1 \gamma^2 \gamma^3 \gamma^\nu) + 2ig^{0\nu}\mathrm{Tr}(\gamma^1 \gamma^2 \gamma^3 \gamma^\mu) \\
&\quad - \mathrm{Tr}(i\gamma_5 \gamma^1 \gamma^2 \gamma^3 \gamma^\mu \gamma^\nu)]\,a_\mu b_\mu
\end{aligned}
$$

Hence, $\mathrm{Tr}(\gamma_5\,\not{a}\,\not{b}) = 2i[-g^{0\mu}\mathrm{Tr}(\gamma^1 \gamma^2 \gamma^3 \gamma^\nu) + g^{0\nu}\mathrm{Tr}(\gamma^1 \gamma^2 \gamma^3 \gamma^\mu)]a_\mu b_\mu = 0$.

- $\mathrm{Tr}(\gamma_5\,\not{a}\,\not{b}\,\not{c}\,\not{d}) = 4i\,\epsilon_{\mu\nu\lambda\sigma}\,a^\mu\,b^\nu\,c^\lambda\,d^\sigma \,,$ \hfill (B.0.2)

where $\epsilon_{\mu\nu\lambda\sigma} = +1\,(-1)$ for $\mu, \nu, \lambda, \sigma$ and even (odd) permutation of $0, 1, 2, 3$; and 0 if two indices are the same. Interchanging any two of the indices simply changes the sign of the trace, and so it must be proportional to $\epsilon_{\mu\nu\lambda\sigma}$. The overall constant can be easily obtained by plugging in $(\mu\nu\lambda\sigma) = (0123)$. Expressions resulting from the use of the last formula can be simplified by means of the identities: $\epsilon^{\alpha\beta\gamma\delta}\,\epsilon_{\alpha\beta\gamma\delta} = -24$; $\epsilon^{\alpha\beta\gamma\mu}\epsilon_{\alpha\beta\gamma\nu} = -6\delta^\mu{}_\nu$;

$$
\epsilon^{\alpha\mu\beta\nu}\epsilon_{\rho\mu\sigma\nu} = \epsilon^{\mu\nu\alpha\beta}\epsilon_{\mu\nu\rho\sigma} = -2(\delta^\alpha{}_\rho\,\delta^\beta{}_\sigma - \delta^\beta{}_\rho\,\delta^\alpha{}_\sigma)\,. \tag{B.0.3}
$$

Other useful results for simplifying trace calculations (that follow directly from the trace theorems) are:

- $\gamma_\mu \gamma^\mu = 4 \times \mathbb{1} = 4$

- $\gamma_\mu \not{a} \gamma^\mu = \gamma_\mu(2a_\mu - \gamma^\mu \not{a}) = 2 \not{a} - 4 \not{a} = -2 \not{a}$

- $\gamma_\mu \not{a} \not{b} \gamma^\mu = (2a_\mu - \not{a}\gamma_\mu)(2b^\mu - \gamma^\mu \not{b}) = 4a \cdot b - 4 \not{a} \not{b} + 4 \not{a} \not{b} = 4a \cdot b$

- $\gamma_\mu \not{a} \not{b} \not{c} \gamma^\mu = (2a_\mu - \not{a}\gamma_\mu) \not{b} \not{c} \gamma^\mu = 2 \not{b} \not{c} \not{a} - 4(a \cdot c) \not{b}$
  $= 2[2(b \cdot c) - \not{c} \not{b}] \not{a} - 4(b \cdot c) \not{a} = -2 \not{c} \not{b} \not{a}.$

The following relations are useful for the computation of the invariant amplitude of weak interaction processes:

$$
\begin{aligned}
\bullet \operatorname{Tr}(\gamma^\mu \not{p}_1 \gamma^\nu \not{p}_2) &= 2p_1^\mu \operatorname{Tr}(\gamma^\nu \not{p}_2) - \operatorname{Tr}(\not{p}_1 \gamma^\mu \gamma^\nu \not{p}_2) \\
&= 2p_1^\mu \operatorname{Tr}(\gamma^\nu \not{p}_2) - 2g^{\mu\nu}\operatorname{Tr}(\not{p}_1 \not{p}_2) + \operatorname{Tr}(\not{p}_1 \gamma^\nu \gamma^\mu \not{p}_2) \\
&= 2p_1^\mu \operatorname{Tr}(\gamma^\nu \not{p}_2) - 2g^{\mu\nu}\operatorname{Tr}(\not{p}_1 \not{p}_2) + 2p_2^\mu \operatorname{Tr}(\not{p}_1 \gamma^\nu) - \operatorname{Tr}(\not{p}_1 \gamma^\nu \not{p}_2 \gamma^\mu) \\
&= 2\left[p_1^\mu \operatorname{Tr}(\gamma^\nu \not{p}_2 + p_2^\mu \operatorname{Tr}(\gamma^\nu \not{p}_1) - g^{\mu\nu}\operatorname{Tr}(\not{p}_1 \not{p}_2) \right] - \operatorname{Tr}(\gamma^\mu \not{p}_1 \gamma^\nu \not{p}_2) \\
&= 4\left[p_1^\mu p_2^\nu + p_2^\mu p_1^\nu - g^{\mu\nu}(p_1 \cdot p_2) \right] . \qquad (B.0.4)
\end{aligned}
$$

$$
\begin{aligned}
\bullet \operatorname{Tr}[\gamma^\mu(\mathbb{1} - \gamma^5)\not{p}_1 \gamma^\nu(\mathbb{1} - \gamma^5)\not{p}_2] &= \operatorname{Tr}[\gamma^\mu \not{p}_1 \gamma^\nu \not{p}_2 + \gamma^\mu \gamma^5 \not{p}_1 \gamma^\nu \gamma^5 \not{p}_2] \\
&- \operatorname{Tr}[\gamma^\mu \not{p}_1 \gamma^\nu \gamma^5 \not{p}_2 + \gamma^\mu \gamma^5 \not{p}_1 \gamma^\nu \not{p}_2] , \quad (B.0.5)
\end{aligned}
$$

and because $\{\gamma^\mu, \gamma^5\} = 0$ we have

$$
\operatorname{Tr}[\gamma^\mu(\mathbb{1} - \gamma^5)\not{p}_1 \gamma^\nu(\mathbb{1} - \gamma^5)\not{p}_2] = 2\operatorname{Tr}[\gamma^\mu \not{p}_1 \gamma^\nu \not{p}_2] + 2\operatorname{Tr}[\gamma^5 \gamma^\mu \not{p}_1 \gamma^\nu \not{p}_2] . \quad (B.0.6)
$$

Using (B.0.1) and (B.0.2) in the second term, we obtain

$$
\operatorname{Tr}[\gamma^\mu(\mathbb{1} - \gamma^5)\not{p}_1 \gamma^\nu(\mathbb{1} - \gamma^5)\not{p}_2] = 2\operatorname{Tr}(\gamma^\mu \not{p}_1 \gamma^\nu \not{p}_2) + 8i\epsilon^{\mu\alpha\nu\beta} p_{1\alpha} p_{2\beta} . \quad (B.0.7)
$$

$$
\begin{aligned}
\bullet \operatorname{Tr}(\gamma^\mu \not{p}_1 \gamma^\nu \not{p}_2)\operatorname{Tr}(\gamma_\mu \not{p}_3 \gamma_\nu \not{p}_4) &= 16[p_1^\mu p_2^\nu + p_2^\mu p_1^\nu - g^{\mu\nu}(p_1 \cdot p_2)] \\
&\times [p_{3\mu}p_{4\nu} + p_{4\mu}p_{3\nu} - g_{\mu\nu}(p_3 \cdot p_4)] \\
&= 16[(p_1 \cdot p_3)(p_2 \cdot p_4) + (p_1 \cdot p_4)(p_2 \cdot p_3) \\
&- (p_1 \cdot p_2)(p_3 \cdot p_4) + (p_2 \cdot p_3)(p_1 \cdot p_4) \\
&+ (p_2 \cdot p_4)(p_1 \cdot p_3) - (p_1 \cdot p_2)(p_3 \cdot p_4) \\
&- (p_1 \cdot p_2)(p_3 \cdot p_4) - (p_1 \cdot p_2)(p_3 \cdot p_4) \\
&+ 4(p_1 \cdot p_2)(p_3 \cdot p_4)] \\
&= 32[(p_1 \cdot p_3)(p_2 \cdot p_4) + (p_1 \cdot p_4)(p_2 \cdot p_3)] . \\
& \qquad\qquad\qquad\qquad\qquad\qquad (B.0.8)
\end{aligned}
$$

$$\begin{aligned}
\bullet \mathrm{Tr}(\gamma^\mu \not{p}_1 \gamma^\nu \gamma^5 \not{p}_2)\mathrm{Tr}(\gamma_\mu \not{p}_3 \gamma_\nu \gamma^5 \not{p}_4) &= \mathrm{Tr}(\gamma^5 \not{p}_2 \gamma^\mu \not{p}_1 \gamma^\nu)\mathrm{Tr}(\gamma^5 \not{p}_4 \gamma^\mu \not{p}_3 \gamma_\nu) \\
&= (4i)^2 \epsilon^{\alpha\mu\beta\nu} p_{2\alpha} p_{1\beta} \epsilon_{\rho\mu\sigma\nu} p_4^\rho p_3^\sigma \\
&= 32[(p_1\, p_3)(p_2 \,.\, p_4) - (p_1 \,.\, p_4)(p_2 \,.\, p_3)\,,
\end{aligned}$$
$$(\mathrm{B.0.9})$$

where to obtain the second line we have used (B.0.1) and (B.0.2), and to obtain the third line (B.0.3).

$$\begin{aligned}
\bullet \mathrm{II} &= \mathrm{Tr}[\gamma^\mu(\mathbb{1}-\gamma^5)\not{p}_1 \gamma^\nu(\mathbb{1}-\gamma^5)\not{p}_2]\mathrm{Tr}[\gamma_\mu(\mathbb{1}-\gamma^5)\not{p}_3 \gamma_\nu(\mathbb{1}-\gamma^5)\not{p}_4] \\
&= 64[p_1^\mu p_2^\nu + p_2^\mu p_1^\nu - g^{\mu\nu}(p_1\,.\,p_2) + i\epsilon^{\mu\alpha\nu\beta} p_{1\alpha} p_{2\beta}] \\
&\times\ [p_{3\mu} p_{4\nu} + p_{4\mu} p_{3\nu} - g_{\mu\nu}(p_3\,.\,p_4) + i\epsilon_{\mu\rho\nu\sigma} p_3^\rho p_4^\sigma] \\
&= 64[(p_1\,.\,p_3)(p_2\,.\,p_4) + (p_1\,.\,p_4)(p_2\,.\,p_3) - (p_1\,.\,p_2)(p_3\,.\,p_4) \\
&+\ (p_2\,.\,p_3)(p_1\,.\,p_4) + (p_2\,.\,p_4)(p_1\,.\,p_3) - (p_1\,.\,p_2)(p_3\,.\,p_4) - (p_3\,.\,p_4)(p_1\,.\,p_2) \\
&-\ (p_1\,.\,p_2)(p_3\,.\,p_4) + 4(p_1\,.\,p_2)(p_3\,.\,p_4) - \epsilon^{\mu\nu\alpha\beta}\epsilon_{\mu\nu\rho\sigma} p_{1\alpha} p_{2\beta} p_3^\rho p_4^\sigma] \\
&= 64[2(p_1\,.\,p_3)(p_2\,.\,p_4) + 2(p_1\,.\,p_4)(p_2\,.\,p_3) + 2(\delta_\rho^\alpha \delta_\sigma^\beta - \delta_\rho^\beta \delta_\sigma^\alpha) p_{1\alpha} p_{2\beta} p_3^\rho p_4^\sigma] \\
&= 64[2(p_1\,.\,p_3)(p_2\,.\,p_4) + 2(p_1\,.\,p_4)(p_2\,.\,p_3) + 2(p_1\,.\,p_3)(p_2\,.\,p_4) \\
&-\ 2(p_2\,.\,p_3)(p_1\,.\,p_4)] \\
&= 256(p_1\,.\,p_3)(p_2\,.\,p_4)\,. \qquad\qquad\qquad\qquad\qquad\qquad (\mathrm{B.0.10})
\end{aligned}$$

Appendix C

Dimensional Regularization

In QFT a charge is surrounded by virtual e^+e^- pairs (vacuum polarization) which are the origin of the s-dependence of α. This can be visualized in terms of Feynman diagrams
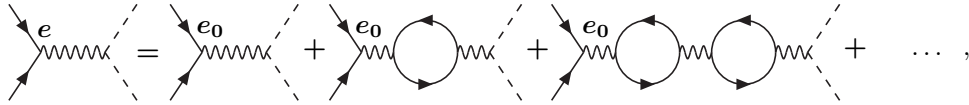
where the dashed lines represent a test charge "measuring" the electron charge on the left. The measured charged is obtained through a perturbative calculation including all vacuum polarization loops,

$$e^2(q^2) = e_0^2 - e_0^2 \Pi(q^2) + e_0^2 \Pi^2(q^2) - \dots . \qquad \text{(C.0.1)}$$

The geometric series can be summed to give

$$\alpha(q^2) = \frac{\alpha_0}{1 + \Pi(q^2)} . \qquad \text{(C.0.2)}$$

How to compute b, formally introduced in (3.5.110), or $\Pi(q^2)$ is clear. The answer is given by (3.5.100), (3.5.107) and (3.5.108). The UV cutoff Λ removes the infinite part of the loop which can, in a renormalizable gauge theory, be absorbed in a redefinition of the bare charge.[1] The latter becomes a parameter to be fixed by experiment. This is standard old-fashioned QED. Nowadays we avoid the explicit introduction of a cutoff such as Λ in (3.5.101)

---

[1]Here, bare refers to the fact that the vertex is stripped of all loops.

which spoils the gauge invariance of the calculation. One instead uses dimensional regularization to compute $\Pi(q^2)$.[2] The basic idea is to carry out loop integrations in a space with dimensions $n < 4$, where they are finite. The result is then analytically continued to $n = 4$ where the UV divergent part of the loop appears as a $1/(n-4)$ pole. Propagators and interaction vertices remain unchanged, e.g., for the loop (3.5.100)

$$
\begin{aligned}
i\Pi_{\mu\nu}(q) &= -i(q^2 g_{\mu\nu} - q_\mu q_\nu)\Pi(q^2) \\
&= \left(e_0\,\mu^{\frac{4-n}{2}}\right)^2 (-1) \int \frac{d^n k}{(2\pi)^n} \mathrm{Tr}\left\{ \frac{\gamma_\mu\,(\slashed{k} + m_e)\,\gamma_\nu\,(\slashed{q} + \slashed{k} + m_e)}{[k^2 - m_e^2]\,[(q+k)^2 - m_e^2]} \right\} \\
&= -4e_0^2\mu^{n-4} \int_0^1 dx \int \frac{d^n Q}{(2\pi)^n} \\
&\times \frac{g_{\mu\nu}\left[\frac{2-n}{n}Q^2 + m_e^2 + q^2 x(1-x)\right] - 2q_\mu q_\nu x(1-x)}{\left\{Q^2 - \left[m_e^2 + q^2 x(x-1)\right]\right\}^2}
\end{aligned}
$$

(C.0.3)

where m_e is the electron mass and k the 4-momentum circulating in the loop. The only modification is the introduction of the 't Hooft mass μ introduced as a factor $\mu^{(4-n)}$ in order to keep the coupling constant dimensionless. In the last line we have omitted terms linear in Q in the numerator which do not contribute to the integral; this last relation follows by executing the following steps:

i) use the Feynman trick for combining denominators

$$
\frac{1}{ab} = \int_0^1 dx\, \frac{1}{\left[ax + b(1-x)\right]^2}\ ,
$$

(C.0.4)

this equation can be verified by direct calculation

$$
\begin{aligned}
\int_0^1 \frac{dx}{[x(a-b)+b]^2} &= -\frac{1}{a-b}\left[\frac{1}{x(a-b)+b}\right]_0^1 \\
&= -\frac{1}{a-b}\left[\frac{1}{a} - \frac{1}{b}\right]\ ;
\end{aligned}
$$

---

[2]G. 't Hooft and M. J. G. Veltman, Nucl. Phys. B **44**, 189 (1972); C. G. Bollini and J. J. Giambiagi, Nuovo Cim. B **12**, 20 (1972); G. 't Hooft, Nucl. Phys. B **61**, 455 (1973).

ii) change the integration variable k by the variable

$$Q = k + qx \tag{C.0.5}$$

(this is chosen such that the term in the denominator linear in the integration variable disappears);

iii) do the traces as usual, but notice that

$$\gamma_\mu \gamma^\mu = n\, \mathbb{1}\,, \tag{C.0.6}$$
$$\gamma_\mu \gamma_\alpha \gamma^\mu = (2 - n)\gamma_\alpha\,. \tag{C.0.7}$$

From (C.0.3) we then find that

$$\Pi(q^2) = \frac{8e_0^2 \mu^{(4-n)}}{(16\pi^2)^{\frac{n}{4}}} \int_0^1 dx\, x(1-x)\left[m_e^2 + q^2 x(x-1)\right]^{\frac{n}{2}-2} \Gamma\!\left(2 - \frac{n}{2}\right) \tag{C.0.8}$$

by using the relation

$$\int \frac{d^n Q}{(2\pi)^n} \frac{1}{(Q^2 - C)^2} = \frac{i}{(16\pi^2)^{\frac{n}{4}}} \Gamma\!\left(2 - \frac{n}{2}\right) C^{\left(\frac{n}{2}-2\right)}\,. \tag{C.0.9}$$

We now make a Taylor expansion of (C.0.8) around $n = 4$ using the following relations:

$$\mu^{(4-n)} = 1 + \frac{4 - n}{2} \ln \mu^2 + \cdots\,,$$

$$(16\pi^2)^{\frac{n}{4}} = 16\pi^2 \left(1 + \frac{n - 4}{2} \ln 4\pi + \cdots\right)\,,$$

$$\Gamma\!\left(2 - \frac{n}{2}\right) = -\frac{2}{n - 4} - \gamma_E \left(= 0.5772\ldots\right)\,,$$

and

$$C^{\left(\frac{n}{2}-2\right)} = 1 + \frac{n - 4}{2} \ln C + \cdots\,.$$

We thus obtain the desired separation of the $n = 4$ infinite and finite parts of $\Pi(q^2)$ with

$$\begin{aligned}
\Pi(q^2) &= \frac{\alpha}{3\pi} \left[-\frac{2}{n - 4} - \gamma_E + \ln 4\pi - 6 \int_0^1 dx\, x(1-x)\right. \\
&\quad \times \left. \ln\left(\frac{m_e^2 + q^2 x(1-x)}{\mu^2}\right) + \mathcal{O}(n - 4)\right]\,, \tag{C.0.10}
\end{aligned}$$

which yields (3.5.101) in the limit of large $(-q^2)$.

In old-fashioned QED the renormalized charge (i.e., the Thomson charge at $q^2 = 0$) would be defined as

$$e^2 \equiv \frac{e_0^2 \mu^{n-4}}{1 + \Pi(0)} , \qquad \alpha \equiv \frac{e^2}{4\pi} \tag{C.0.11}$$

with $\Pi(0)$ given by (C.0.10). In the modern approach, previously introduced, vacuum polarization effects are completely absorbed in the "running" renormalized coupling by allowing μ to vary; $\alpha(\mu) \equiv e^2(\mu)/(4\pi)$ is related to α by

$$\frac{1}{\alpha(\mu^2)} - \frac{1}{\alpha} = -\frac{1}{3\pi} \ln\left(\frac{\mu^2}{m_e^2}\right) . \tag{C.0.12}$$

Equation (C.0.12) implements the so-called modified minimal subtraction ($\overline{\text{MS}}$) renormalization scheme where the terms $\frac{\gamma_E}{2} - \frac{1}{2}\ln 4\pi$ are subtracted out along with the $(n-4)^{-1}$ pole into the renormalized charge.[3] We have now succeeded in computing b appearing in the formal relation (3.5.110). Eq. (C.0.12) just evolves the $\overline{\text{MS}}$ charge from $Q^2 = 0$ to $Q^2 = \mu^2$ and one sees that

$$b = \frac{1}{3\pi} . \tag{C.0.13}$$

If μ^2 is such that other loops of leptons and quarks contribute then

$$\frac{1}{\alpha(\mu^2)} = \frac{1}{\alpha} - \frac{1}{3\pi} \sum_f Q_f^2 \ln\left(\frac{\mu^2}{m_f^2}\right) , \tag{C.0.14}$$

where the sum is over all fermions with charge Q_f.

---

[3]W. A. Bardeen, A. J. Buras, D. W. Duke and T. Muta, Phys. Rev. D **18**, 3998 (1978).

Appendix D

Mott Scattering

The scattering of electrons from nuclei has given us the most precise information about nuclear size and charge distribution. The electron is a better nuclear probe than the alpha particles of Rutherford scattering because it is a point particle and can penetrate the nucleus. For low energies and under conditions where the electron does not penetrate the nucleus, the electron scattering can be described by the Rutherford formula. As the energy of the electrons is raised enough to make them an effective nuclear probe, a number of other effects become significant, and the scattering behavior diverges from the Rutherford formula. The probing electrons are relativistic, they produce significant nuclear recoil, and they interact via their magnetic moment as well as by their charge. In the so-called "Mott scattering," the magnetic moment and recoil are taken into account.[1]

The electromagnetic field due to $-Ze\rho(x)$ may be described as an external field

$$A^\mu = (\phi, \vec{0}), \tag{D.0.1}$$

where using (3.4.65)

$$\nabla^2 \phi = Ze\,\rho(\vec{x})\,. \tag{D.0.2}$$

The Feynamn diagram for scattering of an electron by an external field is shown in Fig. 4.1. The general expression for the transition amplitude

---

[1]Mott scattering is also referred to as spin-coupling in elastic Coulomb scattering, because it is mostly used to measure the spin polarization of an electron beam scattering off the Coulomb field of heavy atoms.

follows from (3.2.30) and (3.2.31)

$$
\begin{aligned}
T_{fi} &= (-i) \int d^4x \, e \, j_\mu^{fi}(x) \, A^\mu(x) \\
&= (-i) \int d^4x \, e \overline{u}_f \gamma_\mu u_i e^{i(p_f - p_i) \cdot x} A^\mu(x), \quad\quad \text{(D.0.3)}
\end{aligned}
$$

or using (D.0.1)

$$
\begin{aligned}
T_{fi} &= (-i) \int dx^0 e^{i(E_f - E_i) \cdot x^0} e\overline{u}_f \gamma_0 u_i \int d^3x \, e^{i\vec{q} \cdot \vec{x}} \phi(\vec{x}) \\
&= (-2\pi i) \delta(E_f - E_i) \, e\overline{u}_f \gamma_0 u_i \int d^3x \, e^{i\vec{q} \cdot \vec{x}} \phi(\vec{x}), \quad\quad \text{(D.0.4)}
\end{aligned}
$$

where $\vec{q} = \vec{p}_f - \vec{p}_i$. Considering the boundary condition, $\phi(\vec{x}) \to 0$ when $|\vec{x}| \to \infty$, we first integrate by parts

$$
\int e^{i\vec{q} \cdot \vec{x}} \nabla^2 \phi(\vec{x}) \, d^3x = -|q|^2 \int e^{i\vec{q} \cdot \vec{x}} \phi(\vec{x}) \, d^3x, \quad\quad \text{(D.0.5)}
$$

then we substitute (D.0.2) into (D.0.5)

$$
\begin{aligned}
\int e^{i\vec{q} \cdot \vec{x}} \phi(\vec{x}) \, d^3x &= -\frac{Ze}{|q|^2} \int e^{i\vec{q} \cdot \vec{x}} \rho(\vec{x}) \, d^3x \\
&= -\frac{Ze}{|q|^2} F(\vec{q}), \quad\quad \text{(D.0.6)}
\end{aligned}
$$

and after that we substitute (D.0.6) into the scattering amplitude (D.0.4)

$$
T_{fi} = 2\pi i \delta(E_f - E_i) \frac{Ze^2}{|q|^2} F(\vec{q}) \, (\overline{u}_f \gamma_0 u_i). \quad\quad \text{(D.0.7)}
$$

Now, from (3.1.16) the differential cross section can be written as

$$
d\sigma = \frac{|T_{fi}|^2 / TV}{(\text{initial flux})} \, (\text{number of final states}), \quad\quad \text{(D.0.8)}
$$

where T and V are the time of the interaction and the normalized volume. We write the momentum and energy of the incoming (outgoing) electron as $\vec{k}_i$ ($\vec{k}_f$), E_i (E_f); then for $k = |\vec{k}_i| = |\vec{k}_f|$,

$$
(\text{initial flux}) = v \frac{2E_1}{V} \quad\quad \text{(D.0.9)}
$$

238

and

$$\text{(number of final states)} = \frac{d^3\vec{k}_f}{(2\pi)^3 2E_F} \,, \tag{D.0.10}$$

where $v = k_i/E_i$ is the velocity of the incoming electron. Using the above formulae we take over (D.0.8) to arrive at

$$d\sigma = \frac{|T_{fi}|^2}{T} \left(\frac{1}{v 2E_i}\right) \frac{d^3 k_f}{(2\pi)^3 2E_f} \,. \tag{D.0.11}$$

On squaring (D.0.7) one delta function remains and

$$2\pi\delta(E_f - E_i) = \int_{-T/2}^{T/2} e^{i(E_f - E_i)t} dt = T. \tag{D.0.12}$$

The remaining delta function can be integrated as follows

$$
\begin{aligned}
d^3 k_f \delta(E_f - E_i) &= k_f^2 \, dk_f \, d\Omega \delta(E_f - E_i) \\
&= k_f E_f dE_f d\Omega \delta(E_f - E_i) \\
&= kE d\Omega \,, \tag{D.0.13}
\end{aligned}
$$

where $E_i = E_f = E$ and $k_i = k_f = k$.

To obtain the unpolarized cross section, we rewrite (D.0.11) summing final, and averaging initial, electron spins

$$d\sigma = \frac{1}{2} \sum_{s_i, s_f} |\bar{u}_f \gamma_0 u_i|^2 (2\pi) \left[\frac{Ze^2 F(\vec{q})}{|\vec{q}|^2}\right]^2 \frac{kE d\Omega}{(2\pi)^3 2E} \left(\frac{1}{v 2E}\right) \,, \tag{D.0.14}$$

where

$$
\begin{aligned}
\frac{1}{2} \sum_{s_i, s_f} |\bar{u}_f \gamma_0 u_i|^2 \equiv L^{00}_{(e)} &= 2\left[k^0 k'^0 + k'^0 k^0 - (k \cdot k' - m^2)g^{00}\right] \\
&= 2[2E^2 - E^2 + k^2 \cos\theta + E^2 - k^2] \\
&= 4\left[E^2 - k^2 \frac{1 - \cos\theta}{2}\right] \\
&= 4E^2 \left[1 - \frac{k^2}{E^2} \sin^2\frac{\theta}{2}\right] \\
&= 4E^2 \left[1 - v^2 \sin^2\frac{\theta}{2}\right] \tag{D.0.15}
\end{aligned}
$$

and θ is the angle through which the electron is scattered. We can now rewrite (D.0.14) using $|\vec{q}|^2 = |\vec{k}_i - \vec{k}_f| = 4k^2 \sin^2(\theta/2)$

$$\frac{d\sigma}{d\Omega} = \frac{E^2}{4k^4 \sin^4(\theta/2)} \left(1 - v^2 \sin^2 \frac{\theta}{2}\right) \left(\frac{e^2 Z}{4\pi}\right)^2 |F(\vec{q})|^2 \qquad \text{(D.0.16)}$$

or equivalently

$$\left.\frac{d\sigma}{d\Omega}\right|_{\text{point}} \equiv \left.\frac{d\sigma}{d\Omega}\right|_{\text{Mott}} = \frac{(Z\alpha)^2 E^2}{4k^4 \sin^4(\theta/2)} \left(1 - v^2 \sin^2 \frac{\theta}{2}\right) , \qquad \text{(D.0.17)}$$

where $\alpha = e^2/4\pi$. Putting all this together yields the advertised result

$$\frac{d\sigma}{d\Omega} = \left.\frac{d\sigma}{d\Omega}\right|_{\text{Mott}} |F(\vec{q})|^2 \qquad \text{(D.0.18)}$$

with the form factor given by (4.1.3).

Appendix E

Laboratory Kinematics

In this appendix we determine the $e^- \mu^- \to e^- \mu^-$ cross section in the laboratory frame. To this end, we return to the exact formula (3.2.44) for $e^-(k)\ \mu^-(p) \to e^-(k')\ \mu^-(p')$ and neglect only the terms involving the electron mass m_e

$$
\begin{aligned}
\overline{|\mathfrak{M}|^2} &= \frac{8e^4}{q^4}[(k'.p')(k.p) + (k'.p)(k.p') - M^2\,k'.k] \\
&= \frac{8e^4}{q^4}\left[-\tfrac{1}{2}q^2(k.p - k'.p) + 2(k'.p)(k.p) + \tfrac{1}{2}M^2 q^2\right], \quad \text{(E.0.1)}
\end{aligned}
$$

where $m_\mu \equiv M$, and $q = k - k'$. To obtain the last line, we have used $p' = k - k' + p$, $k^2 = k'^2 \simeq 0$ and $q^2 \simeq -2k.k'$. We want to evaluate the cross section in the lab frame, i.e., the frame where the initial muon is at rest, $p = (M, \vec{0})$. Evaluating (E.0.1) in the lab frame we find

$$
\begin{aligned}
\overline{|\mathfrak{M}|^2} &= \frac{8e^4}{q^4}\left[-\frac{1}{2}q^2 M(E - E') + 2EE'M^2 + \frac{1}{2}M^2 q^2\right] \\
&= \frac{8e^4}{q^4}2M^2 E'E\left[1 + \frac{q^2}{4EE'} - \frac{q^2}{2M^2}\frac{M(E - E')}{2EE'}\right] \\
&= \frac{8e^4}{q^4}2M^2 E'E\left[\cos^2\frac{\theta}{2} - \frac{q^2}{2M^2}\sin^2\frac{\theta}{2}\right], \quad\quad\quad \text{(E.0.2)}
\end{aligned}
$$

where to reach the last line we have used the following kinemtic relations

$$
q^2 \simeq -2k.k' \simeq -2EE'(1 - \cos\theta) = -4EE'\sin^2(\theta/2). \quad\quad \text{(E.0.3)}
$$

In addition, squaring $q + p = p'$ we obtain

$$q^2 = -2p \cdot q = -2\nu M \qquad \text{so} \qquad \nu \equiv E - E' = -\frac{q^2}{2M}. \qquad \text{(E.0.4)}$$

To calculate the cross section, we make use of (3.1.20)

$$
\begin{aligned}
d\sigma &= \frac{1}{(2E)(2M)} \frac{|\mathfrak{M}|^2}{4\pi^2} \frac{d^3k'}{2E'} \frac{d^3p'}{2p'_0} \delta^{(4)}(p + k - p' - k') \\
&= \frac{1}{4ME} \frac{|\mathfrak{M}|^2}{4\pi^2} \frac{1}{2} E' dE' \ d\Omega \frac{d^3p'}{2p'_0} \delta^{(4)}(p + q - p'). \qquad \text{(E.0.5)}
\end{aligned}
$$

The flux is the product of beam and target densities $(2E)(2M)$ multiplied by the relative velocity which is 1 (i.e., the speed of light) in the limit where m_e has been neglected.

Now, from

$$
\begin{aligned}
\delta(p'^2 - M^2) &= \delta(p_0'^2 - \vec{p}'^2 - M^2) \\
&= \frac{1}{2\sqrt{\vec{p}'^2 + M^2}} [\delta(p'_0 - \sqrt{\vec{p}'^2 + M^2}) + \delta(p'_0 + \sqrt{\vec{p}'^2 + M^2})] \\
& \hspace{8cm} \text{(E.0.6)}
\end{aligned}
$$

we obtain the relation

$$\int dp'_0 \ 2p'_0 \ \Theta(p'_0) \ \delta(p'^2 - M^2) = 1 \qquad \text{(E.0.7)}$$

and so

$$
\begin{aligned}
\int \frac{d^3p'}{2p'_0} \delta^{(4)}(p + q - p') &= \int \frac{d^3p'}{2p'_0} dp'_0 \ \Theta(p'_0) \ 2p'_0 \ \delta(p'^2 - M^2) \ \delta^{(4)}(p + q - p') \\
&= \int d^3p' \ dp'_0 \ \Theta(p'_0) \ \delta(p'^2 - M^2) \ \delta^{(4)}(p + q - p') \\
&= \delta\left((p + q)^2 - M^2\right) \\
&= \delta(p^2 - M^2 + 2p \cdot q + q^2) \\
&= \frac{1}{2M} \delta\left(\nu + \frac{q^2}{2M}\right), \qquad \text{(E.0.8)}
\end{aligned}
$$

where the step function $\Theta(x)$ is 1 if $x > 0$ and 0 otherwise. To obtain the last line we have used $p^2 = M^2$ and the (E.0.4). Substitution of the kinematic

242

relation (E.0.3) into (E.0.8) leads to

$$\int \frac{d^3p'}{2p'_0} \delta^{(4)}(p+q-p') = \frac{1}{2M}\delta\left(E - E' - \frac{2EE'\sin^2(\theta/2)}{M}\right)$$

$$= \frac{1}{2M}\delta\left(E'\left(1 + \frac{2E\sin^2(\theta/2)}{M}\right) - E\right)$$

$$= \frac{1}{2MA}\delta\left(E' - \frac{E}{A}\right) \tag{E.0.9}$$

where

$$A = 1 + \frac{2E}{M}\sin^2\frac{\theta}{2}. \tag{E.0.10}$$

Inserting (E.0.2) into (E.0.5) and using (E.0.8), we obtain

$$\frac{d\sigma}{dE'd\Omega} = \frac{(2\alpha E')^2}{q^4}\left[\cos^2\frac{\theta}{2} - \frac{q^2}{2M^2}\sin^2\frac{\theta}{2}\right]\delta\left(\nu + \frac{q^2}{2M}\right). \tag{E.0.11}$$

Using (E.0.9) we can perform the dE' integration and, replacing q^2 by (E.0.3), we finally arrive at the following formula for the differential cross section for $e^-\mu^-$ scattering in the lab frame

$$\frac{d\sigma}{d\Omega}\bigg|_{\text{lab}} = \left(\frac{\alpha^2}{4E^2\sin^4(\theta/2)}\right)\frac{E'}{E}\left[\cos^2\frac{\theta}{2} - \frac{q^2}{2M^2}\sin^2\frac{\theta}{2}\right]. \tag{E.0.12}$$

Next, using (3.2.37) with $L_{\mu\nu}^{(\mu)}$ replaced by $(p+p')_\mu(p+p')_\nu$ we obtain the amplitude for elastic scattering of unpolarized electrons from spinless point-like particles

$$\overline{|\mathfrak{M}|^2} = \frac{e^4}{2\,q^4}\sum_{\text{spins}}[\overline{u}(k')\gamma^\mu u(k)]\,[\overline{u}(k')\gamma^\nu u(k)]^*\,(p+p')_\mu(p+p')_\nu$$

$$= \frac{e^2}{2q^4}\text{Tr}(\slashed{k}'\gamma^\mu\,\slashed{k}\gamma^\nu)(p+p')_\mu\,(p+p')_\nu. \tag{E.0.13}$$

In what follows, we neglect once more the mass of the electron and M again

243

denotes the target mass; using $p + k = p' + k'$ we obtain

$$
\begin{aligned}
\overline{|\mathfrak{M}|^2} &= \frac{4\,e^4}{q^4}\left\{ 4(k\,.\,p)(k'\,.\,p) + 2[(k\,.\,p) - (k'\,.\,p)](k\,.\,k') - (k\,.\,k')^2 \right. \\
&\quad \left. -\frac{(k\,.\,k')}{2}\,[4M^2 - q^2] \right\} \\
&= \frac{4\,e^4}{q^4}\left[4EE'M^2 + 2M(E - E')\left(\frac{-q^2}{2}\right) - \frac{q^4}{4} + \frac{q^2}{4}(4M^2 - q^2) \right] \\
&= \frac{4\,e^4}{q^4}\left[4EE'M^2 - q^2\left(\frac{-q^2}{2}\right) - \frac{q^4}{2} + M^2 q^2 \right] \\
&= \frac{4\,e^4}{q^4}[4EE'M^2 - 4EE'M^2 \sin^2(\theta/2)] \\
&= \frac{4\,e^4}{q^4}(4M^2 EE')\left[1 - \sin^2(\theta/2) \right] \\
&= \frac{4\,e^4}{q^4}(4M^2 EE')\cos^2(\theta/2) \ . \tag{E.0.14}
\end{aligned}
$$

After substituting (E.0.14) into (E.0.5), straightforward integration leads to

$$
\left.\frac{d\sigma}{d\Omega}\right|_{\text{lab}} = \left[\frac{\alpha^2}{4E^2 \sin^4(\theta/2)}\right]\frac{E'}{E}\,\cos^2\frac{\theta}{2} \ . \tag{E.0.15}
$$

Comparing (E.0.15) with the cross section for $e^- \mu^- \to e^- \mu^-$, we see that the $\sin^2(\theta/2)$ in (E.0.12) is due to the scattering from the magnetic moment of the muon.

244

Appendix F

Spin- and Color-Averaged Cross Sections

In QED, the strength of the electromagnetic coupling between two quarks is given by: $e_{q_1} \times e_{q_2} \times \alpha$, where e_{q_i} is the electric charge in units of e (that is $e_{q_i} = +\frac{2}{3}$, or $-\frac{1}{3}$) and α is the fine structure constant. Similarly, in QCD, the strength of the (strong) coupling for single-gluon exchange between two color charges is $\frac{1}{2} \times c_1 \times c_2 \times \alpha_s$, where c_1 and c_2 are the color coefficients associated with the vertices. It has become conventional to call $C_F \equiv \frac{1}{2}|c_1 c_2|$ the color factor (although, in fact, it would have been more natural to absorb the factor $\frac{1}{2}$ in a redefinition of the strong coupling α_s and just let the product $|c_1 c_2|$ be known as the color factor).

The simplest example to analyze is the Drell-Yan process, in which a high-mass lepton pair $\ell^+\ell^-$ emerges from $q\bar{q}$ annihilation in a pp collision.[1] The differential cross section follows from the relevant expression of conventional QED in Table 3.1, supplemented by the appropiate color factor

$$\frac{d\sigma}{d\hat{t}}\bigg|_{q\bar{q}\to\ell^+\ell^-} = C_F \frac{4\pi e_q^2 \alpha^2}{\hat{s}^2} \frac{\hat{t}^2 + \hat{s}^2}{\hat{s}^2} , \qquad (\text{F.0.1})$$

where $C_F = \frac{1}{2} \times \frac{1}{3} \times \frac{1}{3} \times 3 = \frac{1}{6}$. The factors of $\frac{1}{3}$ average over the initial q and $\bar{q}$ colors, and the factor of 3 sum over $q\bar{q}$ color combinations which

---

[1] S. D. Drell and T. M. Yan, Phys. Rev. Lett. **25**, 316 (1970) [Erratum-ibid. **25**, 902 (1970)].

can annihilate to form a colorless virtual photon. To LO QCD, the cross section for $q\bar{q} \to \ell^+\ell^-$, is simply related to the cross section for $e^+e^- \to q\bar{q}$ given in (3.5.82). The only difference between the two calculations is that we must average rather than sum over the color orientations of the quark and antiquark. Duplicating this reasoning we obtain for the annihilation process $q\bar{q} \to g\gamma$, $C_F = \frac{1}{2} \times \frac{1}{3} \times \frac{1}{3} \times 8$, and for the Compton process $qg \to q\gamma$, $C_F = \frac{1}{2} \times \frac{1}{3} \times \frac{1}{8} \times 8$.

In a similar fashion, the differential cross section for (massless) partonic subprocesses leading to jet pair production can be written, to lowest order in QCD, as

$$\left.\frac{d\sigma}{dt}\right|_{ij \to kl} = \frac{\pi\alpha_s^2}{s^2} \Sigma^{ij \to kl} , \tag{F.0.2}$$

where

$$\Sigma^{gg \to gg} = \frac{9}{2}\left(3 - \frac{tu}{s^2} - \frac{su}{t^2} - \frac{st}{u^2}\right) ,$$

$$\Sigma^{gg \to q\bar{q}} = \frac{1}{6}\left(\frac{t}{u} + \frac{u}{t}\right) - \frac{3}{8}\frac{t^2 + u^2}{s^2} ,$$

$$\Sigma^{q\bar{q} \to gg} = \frac{32}{27}\left(\frac{t}{u} + \frac{u}{t}\right) - \frac{8}{3}\frac{t^2 + u^2}{s^2} ,$$

$$\Sigma^{gq \to gq} = -\frac{4}{9}\left(\frac{s}{u} + \frac{u}{s}\right) + \frac{s^2 + u^2}{t^2} ,$$

$$\Sigma^{q_i q_j \to q_i q_j} = \frac{4}{9}\frac{s^2 + u^2}{t^2} ,$$

$$\Sigma^{q_i q_i \to q_i q_i} = \frac{4}{9}\left(\frac{s^2 + u^2}{t^2} + \frac{s^2 + t^2}{u^2}\right) - \frac{8}{27}\frac{s^2}{tu} ,$$

$$\Sigma^{q_i \bar{q}_i \to q_i \bar{q}_i} = \frac{4}{9}\left(\frac{s^2 + u^2}{t^2} + \frac{u^2 + t^2}{s^2}\right) - \frac{8}{27}\frac{u^2}{ts} ,$$

$$\Sigma^{q_i \bar{q}_i \to q_j \bar{q}_j} = \frac{4}{9}\frac{u^2 + t^2}{s^2} ,$$

and for simplicity, we drop carets for the parton subprocesses.[2]

---

[2] J. F. Owens, E. Reya and M. Gluck, Phys. Rev. D **18**, 1501 (1978).

Appendix G

Monojets

Events with a single jet plus missing energy ($\displaystyle{\not}E_T$) with balancing transverse momenta (so-called "monojets") are incisive probes of new physics. In the standard model the dominant source of this topology is $ij \to kZ^0$ followed by $Z^0 \to \nu\bar{\nu}$. Ignoring the Z mass (i.e., keeping only transverse Z's), the differential cross section follows from the relevant expression of conventional QED in Table 3.1, supplemented by the appropiate color factor, couplings, and mixings. For example, using (2.4.96) and

$$\left.\frac{d\sigma}{d\hat{t}}\right|_{\gamma e_L^- \to \gamma e_L^-} = \left.\frac{d\sigma}{d\hat{t}}\right|_{\gamma e_R^- \to \gamma e_R^-} = \frac{\pi\alpha^2}{\hat{s}^2}\left[-\frac{\hat{u}}{\hat{s}} - \frac{\hat{s}}{\hat{u}}\right], \qquad \text{(G.0.1)}$$

we obtain

$$
\begin{aligned}
\left.\frac{d\sigma}{d\hat{t}}\right|_{gu_L \to Zu_L} &= C_F \frac{g_s^2 g^2}{16\pi}\left[\frac{\frac{1}{2} - \frac{2}{3}\sin^2\theta_w}{\cos\theta_w}\right]^2 \frac{1}{\hat{s}^2}\left[-\frac{\hat{u}}{\hat{s}} - \frac{\hat{s}}{\hat{u}}\right] \\
&= \frac{1}{6}\frac{g_s^2 g^2}{16\pi}\left[\frac{\frac{1}{2} - \frac{2}{3}\sin^2\theta_w}{\cos\theta_w}\right]^2 \frac{1}{\hat{s}^2}\left[-\frac{\hat{u}}{\hat{s}} - \frac{\hat{s}}{\hat{u}}\right], \quad \text{(G.0.2)}
\end{aligned}
$$

$$\left.\frac{d\sigma}{d\hat{t}}\right|_{gd_L \to Zd_L} = \frac{1}{6}\frac{g_s^2 g^2}{16\pi}\left[\frac{-\frac{1}{2} + \frac{1}{3}\sin^2\theta_w}{\cos\theta_w}\right]^2 \frac{1}{\hat{s}^2}\left[-\frac{\hat{u}}{\hat{s}} - \frac{\hat{s}}{\hat{u}}\right], \qquad \text{(G.0.3)}$$

$$\left.\frac{d\sigma}{d\hat{t}}\right|_{gu_R \to Zu_R} = \frac{1}{6}\frac{g_s^2 g^2}{16\pi}\left[\frac{-\frac{2}{3}\sin^2\theta_w}{\cos\theta_w}\right]^2 \frac{1}{\hat{s}^2}\left[-\frac{\hat{u}}{\hat{s}} - \frac{\hat{s}}{\hat{u}}\right], \qquad \text{(G.0.4)}$$

and

$$\left.\frac{d\sigma}{d\hat{t}}\right|_{gd_R \to Zd_R} = \frac{1}{6}\frac{g_s^2 g^2}{16\pi}\left[\frac{\frac{1}{3}\sin^2\theta_w}{\cos\theta_w}\right]^2\frac{1}{\hat{s}^2}\left[-\frac{\hat{u}}{\hat{s}}-\frac{\hat{s}}{\hat{u}}\right]. \tag{G.0.5}$$

Now, combining (G.0.2), (G.0.3), (G.0.4), and (G.0.5) the contributions to $gq \to Zq$ become

$$\left.\frac{d\sigma}{d\hat{t}}\right|_{gu \to Zu} = \frac{\pi\,\alpha_s\,\alpha}{6}\frac{\frac{1}{4}-\frac{2}{3}\sin^2\theta_w+\frac{8}{9}\sin^4\theta_w}{\sin^2\theta_w\,\cos^2\theta_w}\frac{1}{\hat{s}^2}\left[-\frac{\hat{u}}{\hat{s}}-\frac{\hat{s}}{\hat{u}}\right], \tag{G.0.6}$$

$$\left.\frac{d\sigma}{d\hat{t}}\right|_{gd \to Zd} = \frac{\pi\,\alpha_s\,\alpha}{6}\frac{\frac{1}{4}-\frac{1}{3}\sin^2\theta_w+\frac{2}{9}\sin^4\theta_w}{\sin^2\theta_w\,\cos^2\theta_w}\frac{1}{\hat{s}^2}\left[-\frac{\hat{u}}{\hat{s}}-\frac{\hat{s}}{\hat{u}}\right]. \tag{G.0.7}$$

Finally, for $q\bar{q} \to Zg$ we obtain

$$\left.\frac{d\sigma}{d\hat{t}}\right|_{u\bar{u} \to Zg} = \frac{4\pi\,\alpha_s\,\alpha}{9}\frac{\frac{1}{4}-\frac{2}{3}\sin^2\theta_w+\frac{8}{9}\sin^4\theta_w}{\sin^2\theta_w\,\cos^2\theta_w}\frac{1}{\hat{s}^2}\left[\frac{\hat{u}}{\hat{t}}+\frac{\hat{t}}{\hat{u}}\right] \tag{G.0.8}$$

and

$$\left.\frac{d\sigma}{d\hat{t}}\right|_{d\bar{d} \to Zg} = \frac{4\pi\,\alpha_s\,\alpha}{9}\frac{\frac{1}{4}-\frac{1}{3}\sin^2\theta_w+\frac{2}{9}\sin^4\theta_w}{\sin^2\theta_w\,\cos^2\theta_w}\frac{1}{\hat{s}^2}\left[\frac{\hat{u}}{\hat{t}}+\frac{\hat{t}}{\hat{u}}\right]. \tag{G.0.9}$$

In Fig. 4.14 we show the invariant mass distribution of the Z + jet final state, as obtained from numerical integration of

$$\begin{aligned}
\frac{d\sigma}{dW} &= W\tau\sum_{ijk}\left[\int_{-Y_{\max}}^{0}dY\,f_i(x_a,W)\,f_j(x_b,W)\right.\\
&\quad\times\int_{-(y_{\max}+Y)}^{y_{\max}+Y}dy\,\left.\frac{d\sigma}{d\hat{t}}\right|_{ij \to Zk}\frac{1}{\cosh^2 y}\\
&\quad+\int_{0}^{Y_{\max}}dY\,f_i(x_a,W)\,f_j(x_b,W)\\
&\quad\times\left.\int_{-(y_{\max}-Y)}^{y_{\max}-Y}dy\,\frac{d\sigma}{d\hat{t}}\right|_{ij \to Zk}\frac{1}{\cosh^2 y}\right],
\end{aligned} \tag{G.0.10}$$

for $y_1, y_2 < 1$.[1] The branching fraction of Z into $\not{E}_T$ is $20.00 \pm 0.06\%$.

---

[1] L. A. Anchordoqui, H. Goldberg, D. Lust, S. Nawata, S. Stieberger and T. R. Taylor, Nucl. Phys. B **821**, 181 (2009).

Appendix H

Muon Decay

Muon decay

$$\mu^-(p) \to e^-(p') \, \overline{\nu}_e(k') \, \nu_\mu(k), \tag{H.0.1}$$

is the model reaction for weak decays. The particle four momenta are defined in (H.0.1), and the Feynman diagram is shown in Fig. H.1. According to the Feynman rules, it must be drawn using only particle lines; and so the outgoing $\bar{\nu}_e$ is shown as an incoming ν_e. The invariant amplitude for muon decay is

$$\mathfrak{M} = \tfrac{G_F}{\sqrt{2}} \left[\overline{u}(k)\gamma^\mu(\mathbb{1} - \gamma^5)u(p)\right] \left[\overline{u}(p')\gamma_\mu(\mathbb{1} - \gamma^5)v(k')\right], \tag{H.0.2}$$

where the spinors are labeled by the particle momenta. Recall that the outgoing $\bar{\nu}_e$ is described by $v(k')$. The muon decay rate can now be obtained using (A.0.8),

$$d\Gamma = \frac{1}{2E}\overline{|\mathfrak{M}|^2}\,dQ\,, \tag{H.0.3}$$

where the invariant phase space is

$$\begin{aligned}
dQ &= \frac{d^3p'}{(2\pi)^3 2E'}\frac{d^3k}{(2\pi)^3 2\omega}\frac{d^3k'}{(2\pi)^3 2\omega'}(2\pi)^4\,\delta^{(4)}(p - p' - k - k') \\
&= \frac{1}{(2\pi)^5}\frac{d^3p'}{2E'}\frac{d^3k'}{2\omega'}\Theta(E - E' - \omega')\delta\left((p - p' - k')^2\right),
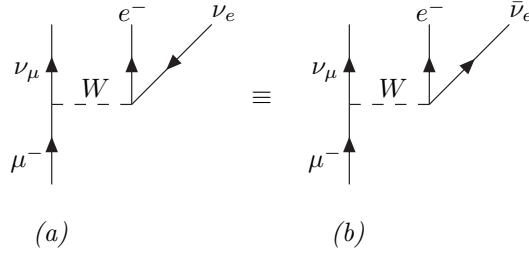\end{aligned} \tag{H.0.4}$$

249

Figure H.1: *Tree level diagram of muon decay. According to the Feynman rules introduced in Chapter 3, the diagram must be drawn using only particle lines; and so in (a) the outgoing $\bar\nu_e$ is shown as incoming ν_e. In (b) we show the time direction of the antiparticle's four-momentum.*

with $p^0 \equiv E$, $k^0 \equiv \omega$, and so on, and where in reaching the last line we have performed the d^3k integration using

$$\int d^4k\ \Theta(\omega)\delta(k^2) = \int d\omega \int d^3k\ \Theta(\omega)\,\delta(\omega^2 - |\vec{k}|^2)$$

$$= \int d^3k \int d\omega \frac{1}{2|\vec{k}|}\delta(\omega - |\vec{k}|) = \int \frac{d^3k}{2\omega}. \quad \text{(H.0.5)}$$

Using (H.0.2) and neglecting m_e we find the spin-averaged probability,

$$\overline{|\mathfrak{M}|^2} \equiv \frac{1}{2}\sum_{\text{spin}}|\mathfrak{M}|^2$$

$$= \frac{1}{2}\left(\frac{G_F}{\sqrt{2}}\right)^2 \sum_{\text{spin}}[\overline{u}(k)\gamma^\mu(\mathbb{1}-\gamma^5)u(p)\,\overline{u}(p)\gamma^\nu(\mathbb{1}-\gamma^5)u(k)$$

$$\times \sum_{\text{spin}}[\overline{u}(p')\gamma_\mu(\mathbb{1}-\gamma^5)v(k')\overline{v}(k')\gamma_\nu(\mathbb{1}-\gamma^5)u(p')$$

$$= \frac{1}{2}\left(\frac{G_F}{\sqrt{2}}\right)^2 \text{Tr}[\not{k}\gamma^\mu(\mathbb{1}-\gamma^5)(\not{p}-m_\mu)\gamma^\nu(\mathbb{1}-\gamma^5)]$$

$$\times \text{Tr}[\not{p}'\gamma_\mu(\mathbb{1}-\gamma^5)\ \not{k}'\gamma_\nu(\mathbb{1}-\gamma^5)]$$

$$= \frac{1}{2}\left(\frac{G_F}{\sqrt{2}}\right)^2 \{\text{Tr}[\not{k}\gamma^\mu(\mathbb{1}-\gamma^5)\not{p}\gamma^\nu(\mathbb{1}-\gamma^5)]$$

$$\times \text{Tr}[\not{p}'\gamma_\mu(\mathbb{1}-\gamma^5)\ \not{k}'\gamma_\nu(\mathbb{1}-\gamma^5)]$$

$$- m_\mu\text{Tr}[\not{k}\gamma^\mu(\mathbb{1}-\gamma^5)\gamma^\nu(\mathbb{1}-\gamma^5)]\text{Tr}[\not{p}'\gamma_\mu(\mathbb{1}-\gamma^5)\ \not{k}'\gamma_\nu(\mathbb{1}-\gamma^5)]\}\,.$$

$$\text{(H.0.6)}$$

Substituting (B.0.10) in the first term we obtain

$$\overline{|\mathfrak{M}|^2} = \left(\frac{G_F^2}{4}\right) 256\,(k\,.\,p')(k'\,.\,p) = 64 G_F^2(k\,.\,p')(k'\,.\,p)\,, \tag{H.0.7}$$

because the trace of the second term vanishes, i.e., $\text{Tr}[\not{k}\gamma^\mu(\mathbb{1} - \gamma^5)\gamma^\nu(\mathbb{1} - \gamma^5)] = \text{Tr}[\not{k}\gamma^\mu\gamma^\nu(\mathbb{1} + \gamma^5)(\mathbb{1} - \gamma^5)] = 0$. Because we neglected the mass of the electron $p - k' = p' + k$ and $k^2 = p'^2 = 0$, so

$$\begin{aligned} 2(k\,.\,p')(k'\,.\,p) &= (p' + k)^2(k'\,.\,p) \\ &= (p - k')^2(k'\,.\,p) \\ &= [p^2 - 2(p\,.\,k')](k'\,.\,p)\,. \end{aligned} \tag{H.0.8}$$

In the muon rest frame, where $p = (m_\mu, 0, 0, 0)$, we have $p\,.\,k' = m_\mu\omega'$; therefore $2(k\,.\,p')(k'\,.\,p) = (m_\mu^2 - 2m_\mu\omega')m_\mu\omega'$. Gathering these results together, the decay rate in the muon rest frame is

$$\begin{aligned} d\Gamma &= \frac{G_F^2}{2m_\mu\pi^5}\frac{d^3p'}{2E'}\frac{d^3k'}{2\omega'}m_\mu\omega'(m_\mu^2 - 2m_\mu\omega') \\ &\times \delta\left(m_\mu^2 - 2m_\mu E' - 2m_\mu\omega' + 2E'\omega'(1 - \cos\theta)\right)\,. \end{aligned} \tag{H.0.9}$$

Now, we can replace $d^3p'd^3k'$ by $4\pi E'^2 dE' 2\pi\omega'^2 d\omega' d\cos\theta$, and use the fact that

$$\delta(\cdots + 2E'\omega'\cos\theta) = \frac{1}{2E'\omega'}\delta(\cdots - \cos\theta) \tag{H.0.10}$$

to perform the integration over the opening angle θ between the emitted e^- and $\bar{\nu}_e$ and obtain

$$d\Gamma = \frac{G_F^2}{2\pi^3}dE'\,d\omega'\,m_\mu\,\omega'\,(m_\mu - 2\omega')\,. \tag{H.0.11}$$

The delta function integration introduces the following restrictions on the energies E', ω', stemming from the fact that $-1 \leq \cos\theta \leq 1$:

$$\tfrac{1}{2}m_\mu - E' \leq \omega' \leq \tfrac{1}{2}m_\mu\,, \tag{H.0.12}$$

$$0 \leq E' \leq \tfrac{1}{2}m_\mu\,. \tag{H.0.13}$$

These limits are easily understood in terms of the various limits in which three-body decay $\mu \to e\bar{\nu}_e\nu_\mu$ becomes effectively a two-body decay. For

example when the electron energy E' vanishes, (H.0.12) yields $\omega' = m_\mu/2$, which is expected because then the two neutrinos share equally the muon's rest energy.

To obtain the energy spectrum of the emitted electron, we perform the ω' integration of (H.0.11)

$$
\begin{aligned}
\frac{d\Gamma}{dE'} &= \frac{m_\mu G_F^2}{2\pi^3} \int_{\frac{1}{2}m_\mu - E'}^{\frac{1}{2}m_\mu} d\omega'\,\omega'(m_\mu - 2\omega') \\
&= \frac{G_F^2}{12\pi^3} m_\mu^2 E'^2 \left(3 - \frac{4E'}{m_\mu}\right) .
\end{aligned}
\tag{H.0.14}
$$

This prediction is in excellent agreement with the observed electron spectrum. Finally, we calculate the muon decay rate

$$
\Gamma \equiv \frac{1}{\tau} = \int_0^{m_\mu/2} dE' \frac{d\Gamma}{dE'} = \frac{G_F^2 m_\mu^5}{192\pi^3} .
\tag{H.0.15}
$$

Inserting the measured muon lifetime $\tau = (2.197019 \pm 0.000021) \times 10^{-6}$ s, we can calculate the Fermi coupling. We find

$$
G_F \simeq 10^{-5}/m_N^2 ,
\tag{H.0.16}
$$

where we have chosen to quote the value with respect to the nucleon mass.

Appendix I

Asymmetries at the Z-pole

Equation (5.5.91) is valid near $q^2 \simeq z$ with

$$
\begin{aligned}
A_{\mathrm{FB}} &= \left[\int_0^1 d\cos\theta \frac{d\sigma(e^+e^- \to f\bar{f})}{d\cos\theta} - \int_{-1}^0 d\cos\theta \frac{d\sigma(e^+e^- \to f\bar{f})}{d\cos\theta} \right] \\
&\times \left[\sigma(e^+e^- \to f\bar{f}) \right]^{-1},
\end{aligned}
\tag{I.0.1}
$$

$$
A_{\mathrm{LR}} = \left[\sigma\left(e^+ e_{\mathrm{R}}^- \to f\bar{f}\right) - \sigma\left(e^+ e_L^- \to f\bar{f}\right) \right] \Big/ \sigma\left(e^+ e^- \to f\bar{f}\right),
\tag{I.0.2}
$$

and

$$
A_\tau = \left[\sigma\left(e^+ e^- \to \tau_{\mathrm{L}}^- \tau^+\right) - \sigma\left(e^+ e^- \to \tau_{\mathrm{R}}^- \tau^+\right) \right] \Big/ \sigma(e^+ e^- \to \tau\bar{\tau}).
\tag{I.0.3}
$$

In the above asymmetries θ is the angle between the produced fermion f and the incoming e^- $e_{\mathrm{L,R}}^-$ represent left- and right-handed longitudinally polarized electrons and $\tau_{\mathrm{L,R}}^-$ left- and right-handed τ's whose polarization can be experimentally analyzed by observing the decay $\tau \to \pi \nu_\tau$.

The principal Z-pole observables and their standard model predictions are summarized in Table I.1[1] These include the Z mass m_Z, the total width Γ_Z, and partial widths $\Gamma(f\bar{f})$ for $Z \to f\bar{f}$, where fermion $f = e$, μ, τ, hadrons, b,

---

[1] H. Flacher, M. Goebel, J. Haller, A. Hocker, K. Monig and J. Stelzer, Eur. Phys. J. C **60**, 543 (2009) [Erratum-ibid. C **71**, 1718 (2011)].

Table I.1: *Z-pole physics.*

Quantity	Experimental Values	Standard Model
m_Z [GeV]	91.1875 ± 0.0021	91.1874 ± 0.0021
Γ_Z [GeV]	2.4952 ± 0.0023	2.4959 ± 0.0015
$\Gamma(\mathrm{had})$ [GeV]	1.7444 ± 0.0020	$--$
$\Gamma(\mathrm{inv})$ [MeV]	499.0 ± 1.5	$--$
$\Gamma(\ell^+\ell^-)$ [MeV]	83.984 ± 0.086	$--$
σ_{had} [nb]	41.540 ± 0.037	41.477 ± 0.014
R_ℓ	20.767 ± 0.025	20.743 ± 0.018
R_c	0.1721 ± 0.0030	0.17224 ± 0.00006
R_b	0.21629 ± 0.00066	$0.21581^{+0.00005}_{-0.00007}$
A^ℓ_{LR}	0.1499 ± 0.0018	$0.1478^{+0.0011}_{-0.0010}$
A^e_{LR}	0.15138 ± 0.00216	$--$
A^μ_{LR}	0.142 ± 0.015	$--$
A^τ_{LR}	0.136 ± 0.015	$--$
A^ℓ_{FB}	0.0171 ± 0.0010	0.01638 ± 0.0002
A^μ_{FB}	0.0169 ± 0.0013	$--$
A^τ_{FB}	0.0188 ± 0.0017	$--$
A_τ	$0.150 \pm 0.013 \pm 0.009$	$--$

or c. For the global electroweak fit, it is convenient to use the variables m_Z, Γ_Z, $R_\ell \equiv \Gamma(\mathrm{had})/\Gamma(\ell^+\ell^-)$, $R_b \equiv \Gamma(b\bar{b})/\Gamma(\mathrm{had})$, $R_c \equiv \Gamma(b\bar{b})/\Gamma(\mathrm{had})$, $\sigma_{\mathrm{had}} \equiv 12\pi\Gamma(e^+e^-)\Gamma(\mathrm{had})/m_Z^2\Gamma_Z^2$, most of which are weakly correlated experimentally. ($\Gamma(\mathrm{had})$ is the partial width into hadrons, and $\ell = e, \mu, \tau$). There are also measurements of various Z-pole asymmetries. The value for A^ℓ_{LR} is the average of LEP ($A^\ell_{\mathrm{LR}} = 0.1465 \pm 0.0033$) and SLD ($A^\ell_{\mathrm{LR}} = 0.1513 \pm 0.0021$) measurements.[2]

---

[2]K. Abe *et al.* [SLD Collaboration], Phys. Rev. Lett. **84**, 5945 (2000); **86**, 1162 (2001); S. Schael *et al.*, [ALEPH, DELPHI, L3, OPAL, and LSD collaborations], Phys. Rept. **427**, 257 (2006); T. C. Paul, CERN-THESIS-98-008.

Appendix J

Supersymmetry Essentials

SUSY is an extension of the known spacetime symmetries.[1] The spacetime symmetries of rotations, boosts, and translations are generated by angular momentum operators J, boost operators K, and momentum operators P, respectively. The J and K generators form Lorentz symmetry (1.3.22), and all 10 generators together form Lorentz-Poincaré symmetry: (1.3.21), (1.3.34) and (1.3.35). SUSY is the symmetry that results when these 10 generators are further supplemented by fermionic operators Q_α.[2]

If a symmetry exists in nature, acting on a physical state with any generator of the symmetry gives another physical state; e.g, acting on an electron with a momentum operator produces another physical state, namely, an electron translated in space or time. Spacetime symmetries leave the quantum numbers of the state invariant — in this example, the initial and final states have the same mass, electric charge, etc. In an exactly supersymmetric world, then, acting on any physical state with the SUSY generator Q_α produces another physical state. As with the other spacetime generators, Q_α does not change the mass, electric charge, and other quantum numbers of the physical state. In contrast to the Lorentz-Poincaré generators, however, a supersymmetric transformation changes bosons to fermions and vice versa:

$$Q_\alpha|\text{Boson}\rangle = |\text{Fermion}\rangle, \qquad Q_\alpha|\text{Fermion}\rangle = |\text{Boson}\rangle. \qquad \text{(J.0.1)}$$

---

[1] J. Wess and B. Zumino, Nucl. Phys. B **70**, 39 (1974); Phys. Lett. B **49**, 52 (1974).

[2] J. Wess and J. Bagger, *Supersymmetry and supergravity,* (Princeton University Press, Princeton, NJ, 1992).

It is straightforward to see that no particle of the standard model (SM) is the superpartner of another. SUSY therefore predicts a plethora of superpartners, none of which has (yet) been discovered. More specifically, to construct the minimal supersymmetric standard model (MSSM) we start enlarging the SM particle spectrum by adding a second complex $SU(2)$-doublet Higgs field, with hypercharge $Y = -1/2$. We denote the $Y = -1/2$ $[Y = +1/2]$ Higgs doublet fields by H_1^i $[H_2^i]$, where i is a weak $SU(2)$ index. Armed with this slightly augmented version of the SM, we construct the particle spectrum of the MSSM by adding supersymmetric partners to each SM particle, such that the supersymmetric theory has an equal number of bosonic and fermionic degrees of freedom. The end result is displayed in Table J.1. Note that some 'normal' particles have more than one superpartner, e.g., each quark has two squarks, $\tilde{q}_L$ and $\tilde{q}_R$, as superpartners, but the number of degrees of freedom (2 for the quark (spin $\frac{1}{2}$) and 1 for each squark (spin 0)) sums up to be the same for the normal particle and its superpartner(s). The general notation is to have a tilde on the symbol for the superpartners, but for the charginos and neutralinos we will usually drop the tilde since there is no risk for misinterpretations.

The novel feature of SUSY, its boson-fermion symmetry, also posses one *important* drawback: Bose-Fermi symmetry has not been observed in nature. Thus, if SUSY can serve as a theory of low energy interactions, it must be a broken symmetry. If SUSY were unbroken, a SM particle and its superpartner would have the same mass and quantum numbers (except for spin). From the phenomenological perspective, the most interesting mechanisms responsible for SUSY breaking are those with "low-energy" (or weak-scale") SUSY, in which the effective scale of SUSY breaking is tied to the scale of electroweak symmetry breaking.[3]

Although there are many reasons for considering SUSY as a candidate extension to the SM, one of the most compelling is its role in understanding the gauge hierarchy problem; namely, why/how is

$$M_{\mathrm{W}} \approx G_F^{-1/2} \ll M_{\mathrm{Pl}} \approx G_N^{-1/2} \,. \tag{J.0.2}$$

One might naively think that it would be sufficient to set $M_{\mathrm{W}} \ll M_{\mathrm{Pl}}$ by hand. However, we have seen in Sec. 5.7 that radiative corrections tend to

---

[3]S. Dimopoulos and H. Georgi, Nucl. Phys. B **193**, 150 (1981).

destroy this hierarchy. For example, one-loop diagrams generate

$$\delta M_{\text{W}}^2 = \mathcal{O}\left(\frac{\alpha}{\pi}\right) \Lambda^2 \gg M_{\text{W}}^2 \,, \tag{J.0.3}$$

where Λ is a cut-off representing the appearance of new physics. If the radiative corrections to a physical quantity are much larger than its measured values, obtaining the latter requires strong cancellations, which in general require fine-tuning of the bare input parameters. However, the necessary cancellations are natural in SUSY, where one has equal numbers of bosons $\mathfrak{b}$ and fermions $\mathfrak{f}$ with equal couplings, so that (J.0.3) is replaced by

$$\delta M_{\text{W}}^2 = \mathcal{O}\left(\frac{\alpha}{\pi}\right) |m_{\mathfrak{b}}^2 - m_{\mathfrak{f}}^2| \,. \tag{J.0.4}$$

The residual radiative correction is naturally small if $|m_{\mathfrak{b}}^2 - m_{\mathfrak{f}}^2| \lesssim 1$ TeV^2.

Weak-scale superpartners solve the gauge hierarchy problem through their virtual effects. However, without additional structure, they also mediate baryon and lepton number violation at unacceptable levels. For example, proton decay $p \to \pi^0 e^+$ may be mediated by a squark.

An elegant way to prevent this decay is to impose the conservation of R-parity $R_p \equiv (-1)^{3(B-L)+2S}$, where B, L, and S are baryon number, lepton number, and spin, respectively. All standard model particles have $R_p = 1$, and all superpartners have $R_p = -1$. R-parity conservation implies $\Pi R_p = 1$ at each vertex, and so both B and L violating processes are forbidden.

An immediate consequence of R-parity conservation is that the lightest supersymmetric particle cannot decay to SM particles and is therefore stable. Particle physics constraints therefore naturally suggest a symmetry that provides a new stable particle that may contribute significantly to the present energy density of the universe.[4]

Electroweak symmetry breaking is caused by the fields H_1 and H_2 acquiring vacuum expectation values

$$\langle H_1 \rangle = \begin{pmatrix} v_1 \\ 0 \end{pmatrix}, \qquad \langle H_2 \rangle = \begin{pmatrix} 0 \\ v_2 \end{pmatrix}, \tag{J.0.5}$$

---

[4]H. Goldberg, Phys. Rev. Lett. **50**, 1419 (1983); J. R. Ellis, J. S. Hagelin, D. V. Nanopoulos, K. A. Olive and M. Srednicki, Nucl. Phys. B **238**, 453 (1984).

where v_1 and v_2 can be chosen real and non-negative by using appropriate phases for the Higgs fields. They are related to the W boson mass by

$$m_W^2 = \frac{1}{2}g^2(v_1^2 + v_2^2) \qquad \text{(J.0.6)}$$

and we also have the convenient expression for the Z boson mass

$$m_Z^2 = \frac{1}{2}\left(g^2 + g'^2\right)\left(v_1^2 + v_2^2\right), \qquad \text{(J.0.7)}$$

where g and g' are the usual $SU(2)$ and $U(1)$ gauge coupling constants. We define the ratio of the vacuum expectation values,

$$\tan\beta = \frac{v_2}{v_1}. \qquad \text{(J.0.8)}$$

There are five physical Higgs bosons in the MSSM, H_1^0, H_2^0, A^0 and $H^\pm$. Of the neutral ones, A^0 is CP-odd and H_1^0 and H_2^0 are CP-even.

There are four neutralinos $(\tilde{\chi}_1^0, \tilde{\chi}_2^0, \tilde{\chi}_3^0, \tilde{\chi}_4^0)$, which are linear combinations of the superpartners of the neutral $SU(2)$ and $U(1)$ gauge bosons and of the neutral component of the two Higgs doublets: $(\tilde{W}_3, \tilde{B}, \tilde{H}_1^0, \tilde{H}_2^0)$, respectively. The the lightest one, to be called *the* neutralino χ, is an attractive dark matter candidate.

The first 1 fb^{-1} of data from the LHC has shown no evidence for SUSY.[5]

---

[5]S. Chatrchyan *et al.* [CMS Collaboration], arXiv:1109.2352; G. Aad *et al.* [ATLAS Collaboration], arXiv:1110.6189.

Table J.1: *The MSSM particle spectrum.*

Boson Fields	Fermionic Partners	$SU(3)_C$	$SU(2)_L$	$U(1)_Y$
g	$\widetilde{g}$	8	0	0
W^a	$\widetilde{W}^a$	1	3	0
B	$\widetilde{B}$	1	1	0
leptons $\begin{cases} \widetilde{L}^j = (\tilde{\nu}, \tilde{e}^-)_L \\ \widetilde{E} = \tilde{e}_R^+ \end{cases}$	$(\nu, e^-)_L$ e_L^c	1 1	2 1	$-1/2$ 1
quarks $\begin{cases} \widetilde{Q}^j = (\tilde{u}_L, \tilde{d}_L) \\ \widetilde{U} = \tilde{u}_R^* \\ \widetilde{D} = \tilde{d}_R^* \end{cases}$	$(u, d)_L$ u_L^c d_L^c	3 3* 3*	2 1 1	1/6 $-2/3$ 1/3
Higgs $\begin{cases} H_1^i \\ H_2^i \end{cases}$	$(\widetilde{H}_1^0, \widetilde{H}_1^-)_L$ $(\widetilde{H}_2^+, \widetilde{H}_2^0)_L$	1 1	2 2	$-1/2$ 1/2

Normal particles/fields		Supersymmetric partners			
		Interaction eigenstates		Mass eigenstates	
Symbol	Name	Symbol	Name	Symbol	Name
$q = d, c, b, u, s, t$	quark	$\tilde{q}_L, \tilde{q}_R$	squark	$\tilde{q}_1, \tilde{q}_2$	squark
$l = e, \mu, \tau$	lepton	$\tilde{l}_L, \tilde{l}_R$	slepton	$\tilde{l}_1, \tilde{l}_2$	slepton
$\nu = \nu_e, \nu_\mu, \nu_\tau$	neutrino	$\tilde{\nu}$	sneutrino	$\tilde{\nu}$	sneutrino
g	gluon	$\tilde{g}$	gluino	$\tilde{g}$	gluino
$W^\pm$	W-boson	$\tilde{W}^\pm$	wino		
H^-	Higgs boson	$\tilde{H}_1^-$	higgsino	$\left.\right\}$ $\tilde{\chi}_{1,2}^\pm$	chargino
H^+	Higgs boson	$\tilde{H}_2^+$	higgsino		
B	B-field	$\tilde{B}$	bino		
W^3	W^3-field	$\tilde{W}^3$	wino		
H_1^0	Higgs boson			$\left.\right\}$ $\tilde{\chi}_{1,2,3,4}^0$	neutralino
H_2^0	Higgs boson	$\tilde{H}_1^0$	higgsino		
A^0	Higgs boson	$\tilde{H}_2^0$	higgsino		

NOTE ADDED

A preliminary combination of standard model Higgs searches with the ATLAS and CMS experiments was presented today, December 13, 2011.

Per ATLAS reporting: In a dataset corresponding to an integrated luminosity of up to 4.9 fb^{-1} of pp collisions collected at $\sqrt{s} = 7$ TeV, an excess of events is being observed for a Higgs boson mass hypothesis close to $m_H = 126$ GeV. The maximum local significance of this excess is 3.6σ above the expected standard model background, while the global probability of such a fluctuation to happen anywhere in the full explored Higgs mass domain is estimated to be approximately 1%, corresponding to a global significance of 2.3σ. The three most sensitive channels in this mass range, $H \to \gamma\gamma$, $H \to ZZ^{(*)} \to \ell^+\ell^-\ell^+\ell^-$ and $H \to WW^{(*)} \to \ell^+\nu\ell^-\overline{\nu}$, contribute individual local significances of 2.8σ, 2.1σ and 1.4σ, respectively, to the excess.[6]

Per CMS reporting: The combination of results of searches for a standard model Higgs boson in five decay modes (gg, bb, tt, WW, and ZZ) yields a 2.4σ significance at $m_H = 124$ GeV. The data correspond to an integrated total luminosity of up to 4.7 fb^{-1} of pp collisions at $\sqrt{s} = 7$ TeV.[7]

---

[6] ATLAS Collaboration, ATLAS-CONF-2011-163.
[7] CMS Collaboration, CMS PAS HIG-11-032.